Dynamic Modeling of Vehicular Platoons: Highlighting The Effects of Communication Topologies on Safety, Robustness, and Scalability

by

Amir Zakerimanesh

A thesis submitted in partial fulfillment of the requirements for the degree of

Doctor of Philosophy

in

Control Systems

Department of Electrical and Computer Engineering
University of Alberta

Abstract

Recent advancements in information and communication technologies have accelerated the development of intelligent transportation systems. Among these, platooning technology involves the coordinated movement of a lead vehicle and multiple followers at specified inter-vehicle distances and synchronized speeds. Beyond its transformative potential in industries such as commercial transportation and traffic management, intelligent vehicle platooning holds promise for enhancing safety, optimizing infrastructure utilization, increasing highway capacity, reducing aerodynamic drag and fuel consumption, mitigating road traffic accidents, and stimulating economic growth.

However, realizing these benefits presents challenges. Factors such as transient distance variations from desired values, limitations of individual vehicle speeds and accelerations, effect of communication topologies, the effect of parity and disparity between vehicles, and the identification of appropriate control gains must be addressed to prevent potential collisions and avoid impractical accelerations and decelerations. Additionally, the ability to decouple the proper control-gains identifications from the leader vehicle's speed is of paramount importance, providing the consideration of various scenarios, including those with constant and varying speeds for the lead vehicle during steady-state.

This research explores distributed linear controllers and transitioning from distinctions between follower-leader states to variations among neighboring vehicles, we have unearthed the dynamics governing deviations in state from their target values. Our findings demonstrate that these dynamics operate independently of the leader vehicle's state, enabling the assurance of desired distances and synchronized speeds

even when the leader vehicle's speed fluctuates during platoon's steady-state. These dynamics are presented for typical and non-typical communication topologies, regardless of the number of vehicles, and under identical and nonidentical control gain feedback.

Moreover, this study elucidates the profound influence of initial conditions on the evolution of vehicle states and elucidates the intricate relationship between these initial conditions and transient deviations, all within the context of communication topologies, vehicle attributes, and control parameters. It strategically incorporates collision and safe distance constraints, as well as feasible-velocity limitations, producing graphical pattern outputs based on varying control gains specific to each communication topology. This approach allows for a comprehensive exploration of the diverse effects of different communication structures. Additionally, it delves into the dynamics of heterogeneous platoons and emphasizes the crucial role of broadcasting the leader vehicle's state in enhancing platoon scalability and robustness, offering valuable insights into these two fundamental aspects of this complex domain.

In summary, this work offers valuable insights into the dynamics governing deviations in states from their desired values and the influence of communication topologies, initial conditions, vehicle features, and control parameters.

Preface

The ultimate goal of this research is to pave the way for more efficient and safe transportation systems by harnessing the power of effective communication and control strategies in vehicular platoons. This thesis was mentored and led by Dr. Mahdi Tavakoli (principal investigator) at the Department of Electrical and Computer Engineering, University of Alberta and Dr. Tony Z. Qiu at the Department of Civil and Environmental Engineering. All of the work presented in this thesis was conducted in the Telerobotic and Biorobotic Systems Lab and the Centre for Smart Transportation group at the University of Alberta. I was responsible for theoretical development, results analysis and verification, simulation, and the manuscript preparation.

Chapter 1 presents the motivation and objectives of this project and summarized the thesis organization and contributions.

Chapter 2 of this thesis is dedicated to literature review and preliminaries.

Chapter 3 of this thesis has been published as: Amir Zakerimanesh, Tony Z. Qiu, Mahdi Tavakoli, Heterogeneous Vehicular Platooning With Stable Decentralized Linear Feedback Control, IEEE International Conference on Autonomous Systems, 2021. The aim of this chapter was to highlight the complexity of stability analysis of heterogeneous vehicular platoons.

Chapter 4 of this thesis, which is the revised version of a reviewed initial manuscript, has been submitted to IEEE Transactions on Control Systems Technology as: Amir Zakerimanesh, Tony Z. Qiu, Mahdi Tavakoli, Stability and Intervehicle Distance Analysis of Homogeneous Vehicular Platoons: Highlighting the Impact of Bidirectional Communication Topologies. This chapter introduces a novel closed-loop dynamic

model for platoon, suitable for the analysis of deviations of relative states from their desired values. The focus of this chapter is on typical bidirectional communication topologies.

Chapter 5 of this thesis is under review in IEEE Transactions on Control of Network Systems as: Amir Zakerimanesh, Tony Z. Qiu, Mahdi Tavakoli, Impact of Communication Topologies on Stability and Intervehicle Distances: Homogeneous Vehicular Platoons. This chapter takes a step further and reformulates the previous chapter, tailoring the problem for any type of communication topologies.

Chapter 6 of this thesis is under review in IEEE Transactions on Cybernetics as: Amir Zakerimanesh, Tony Z. Qiu, Mahdi Tavakoli, Stability and Distance Analysis: Heterogeneous Platoons under Look-Ahead Topologies. This Chapter, unlike chapters 4-5, incorporates the heterogeneity of vehicles and control feedback gains into account. The focus of this chapter is on look-ahead communication topologies.

Chapter 7 of this thesis is under review in IEEE Transactions on Intelligent Transportation Systems as: Amir Zakerimanesh, Tony Z. Qiu, Mahdi Tavakoli, Effects of Communication on Inter-Vehicle Distance and Scalability in Heterogeneous Vehicular Platoon Control: Considering Comprehensive Initial States. This chapter, unlike the Chapter 6, adds the full initial conditions into problem development and solves the previous problem for any type of communication topologies. This chapter highlights also the effect of communication topologies on robustness and scalability of the platoon.

Acknowledgements

I wish to extend my sincere appreciation to the University of Alberta, which provided an exceptional environment for the pursuit of my Ph.D. studies. This institution's commitment to academic excellence, cutting-edge research, and unwavering support has been instrumental in shaping my academic journey. The resources and opportunities offered by the University have played a vital role in my growth as a researcher.

In addition, I am profoundly grateful for the invaluable guidance and support provided by my esteemed supervisors, Dr. Mahdi Tavakoli and Dr. Tony Z. Qiu. Their expertise, dedication, and insightful feedback have not only enhanced the quality of my work but have also been a source of inspiration throughout the entire thesis-writing process. Their mentorship has pushed me to strive for excellence, and I am truly indebted to them for their unwavering commitment to my academic and professional development.

I also wish to express my heartfelt thanks to my colleagues and friends in the TBS (Telerobotics and Biorobotics Systems) and CTS (Centre for Smart Transportation) groups. Their camaraderie, thought-provoking discussions, and shared experiences have added a layer of enrichment to my research endeavors. Their support, collaboration, and continuous motivation have made this journey not only intellectually stimulating but also enjoyable.

My deepest gratitude extends to my beloved family, whose unwavering love, encouragement, and unwavering belief in my abilities have been my cornerstone. Their support, understanding, and countless sacrifices have been instrumental in enabling me to pursue my academic goals. I am profoundly thankful to my parents, and I hold

my father, now resting in peace, forever in my heart as a source of endless motivation. My siblings and extended family have also been a pillar of strength, and their constant presence in my life is a treasure that I hold dear.

To everyone who has played a part in my journey, whether through substantial contributions or small acts of support, your presence and assistance have been indispensable. I am deeply grateful for the network of individuals who have touched my life and helped me along the way.

Table of Contents

List of Tables

List of Figures

List of Symbols

D_i^{i+1} Real distance between vehicles i and $i+1$

L_i Length of the i^{th} vehicle

$\Delta\ddot{x}_{i+1}^{j} = \ddot{x}_{i+1} - \ddot{x}_j$

$\Delta\dot{x}_{i+1}^{j} = \dot{x}_{i+1} - \dot{x}_j$

$\Delta\tilde{a}_i^{i+1} = \ddot{\tilde{x}}_i - \ddot{\tilde{x}}_{i+1}$

$\Delta\tilde{v}_i^{i+1} = \dot{\tilde{x}}_i - \dot{\tilde{x}}_{i+1}$

$\Delta x_{i+1}^{j} = x_{i+1} - x_j$

$\Delta\tilde{\mathbb{P}} = [\Delta\tilde{p}_0^1;\ \Delta\tilde{p}_1^2;\ \ldots;\ \Delta\tilde{p}_{n-1}^n]$

$\Delta\tilde{\mathbf{X}}_t = [\Delta\tilde{\mathbf{X}}_0^1;\ \Delta\tilde{\mathbf{X}}_1^2; \ldots;\ \Delta\tilde{\mathbf{X}}_{n-1}^n]$

$\Delta\tilde{p}_{i,zi}^{i+1}$ TIDE of neighboring vehicles i and $i+1$ from initial conditions (zero input)

$\Delta\tilde{p}_{i,zs}^{i+1}$ TIDE of neighboring vehicles i and $i+1$ when $\Delta\tilde{p}_i^{i+1}(0) = 0$ (zero state)

$\Delta\dddot{x}_{i+1}^{j} = \dddot{x}_{i+1} - \dddot{x}_j$

$\Delta\dot{\tilde{\mathbf{X}}}_i^{i+1} = [\Delta\tilde{v}_i^{i+1};\ \Delta\tilde{a}_i^{i+1};\ \Delta\tilde{\mathbf{J}}_i^{i+1}]$

$\Delta\tilde{\mathbf{J}}_i^{i+1} = \dddot{\tilde{x}}_i - \dddot{\tilde{x}}_{i+1}$

$\Delta\tilde{\mathbf{X}}_i^{i+1} = [\Delta\tilde{p}_i^{i+1};\ \Delta\tilde{v}_i^{i+1};\ \Delta\tilde{a}_i^{i+1}]$

$\Delta\tilde{p}_i^{i+1} = \tilde{x}_i - \tilde{x}_{i+1}$

$\Delta\tilde{u}_i^{i+1}$ Input signal for coupled dynamics of neighboring vehicles i and $i+1$

Ψ_i TIDE of neighboring vehicles i and $i+1$ from initial conditions

$\tilde{\mathbf{A}}_{\Delta t}$ Closed-loop system matrix with $\Delta\tilde{\mathbf{X}}_t$ as the platoon's total state vector

$\tilde{\mathbf{A}}_t$ Closed-loop system matrix with $\tilde{\mathbf{X}}_t$ as the platoon's total state vector

$\tilde{\mathbf{X}}_t = [\tilde{\mathbf{X}}_1;\ \tilde{\mathbf{X}}_2; \ldots;\ \tilde{\mathbf{X}}_n]$

α_i Vehicles ahead providing info to i^{th} follower in pair $(i, i+1)$

$\approx$	Approximately equal to
β_i	Vehicles behind providing info to $(i+1)^{th}$ follower in pair $(i, i+1)$
$\dddot{\tilde{x}}_{i+1}$	$=\dddot{x}_{i+1} - \dddot{x}^*_{i+1}$
$\dddot{x}_{i+1}$	Jerk ($\beth_{i+1}$) of the $(i+1)^{th}$ vehicle
$\ddot{\tilde{x}}_{i+1}$	$=\ddot{x}_{i+1} - \ddot{x}^*_{i+1}$
$\ddot{x}^*_{i+1}$	Desired acceleration of the $(i+1)^{th}$ vehicle
$\ddot{x}_{i+1}$	Acceleration (a_{i+1}) of the $(i+1)^{th}$ vehicle
$\dot{\mathbf{X}}_{i+1}$	$=[\dot{x}_{i+1}; \ddot{x}_{i+1}; \dddot{x}_{i+1}]$
$\dot{\tilde{x}}_{i+1}$	$=\dot{x}_{i+1} - \dot{x}^*_{i+1}$
$\dot{x}^*_{i+1}$	Desired velocity of the $(i+1)^{th}$ vehicle
$\dot{x}_{i+1}$	Velocity (v_{i+1}) of the $(i+1)^{th}$ vehicle
ϵ_{i+1}	$= -\frac{1}{\tau}a_0 - \dot{a}_0$, a_0 is leader acceleration
$\mathbb{I}_{i+1}$	Set of vehicles from which the $(i+1)^{th}$ follower gets information
$\mathbb{K}$	$=[k, b, 1+h]$
$\mathbb{K}_{i+1}$	$=[\mathbf{k}_{i+1},\ \mathbf{b}_{i+1},\ \mathbf{h}_{i+1}]$
$\mathbb{R}_{i+1}$	$= \mathbb{I}_{i+1} - \{i\}$
$\mathbb{R}_i$	$= \mathbb{I}_i - \{i+1\}$
$\mathbf{A}_i^{i+1}$	System matrix for coupled dynamics of neighboring vehicles
$\mathbf{B}_i$	Vehicles behind $(j \geq i+1)$ providing info to i^{th} follower in pair $(i, i+1)$
$\mathbf{J}_i$	Union of $\mathbf{M}_i$ and $\mathbf{B}_i$
$\mathbf{K}$	$=[k,\ b,\ h]$
$\mathbf{M}_i$	Vehicles ahead $(j \leq i)$ providing info to $(i+1)^{th}$ follower in pair $(i, i+1)$
$\mathbf{Q}$	Matrix mapping initial conditions to TIDEs: $\Delta\tilde{\mathbb{P}} = \mathbf{Q}^{-1}\mathbf{\Psi}$
$\mathbf{X}_{i+1}$	$=[x_{i+1}; \dot{x}_{i+1}; \ddot{x}_{i+1}]$
$\mathbf{\Psi}$	$=[\Psi_0^1;\ \Psi_1^2;\ \ldots;\ \Psi_{n-1}^n]$
$\boldsymbol{\epsilon}_{i+1}$	$= [0; 0; \epsilon_{i+1}]$
μ	$=\Delta\tilde{p}_i^{i+1}(0)$
ω_i^{i+1}	$L_i + d_i^{i+1}$
$\otimes$	Kronecker product

τ Engine time-constant of vehicles

Vec(.) Concatenates its arguments vertically

$\tilde{\mathbf{X}}_{i+1}$ $=[\tilde{x}_{i+1};\ \dot{\tilde{x}}_{i+1};\ \ddot{\tilde{x}}_{i+1}]$

$\tilde{x}_{i+1}$ $=x_{i+1} - x^*_{i+1}$

$\triangleq$ Equal to by definition

b Coefficient of velocity errors in the distributed controller

$d_{i+1,j}$ Desired position difference between vehicles $i+1$ and j

$d^s_{i,i+1}$ Safe distance between neighboring vehicles

d^{i+1}_i Desired distance between vehicles i and $i+1$

h Coefficient of acceleration errors in the distributed controller

k Coefficient of position errors in the distributed controller

x^*_{i+1} Desired position of the $(i+1)^{th}$ vehicle

x_{i+1} Position of the $(i+1)^{th}$ vehicle

$z^i_{i+1} = 0$ Indicates vehicle $i+1$ does not receive information from vehicle i

$z^i_{i+1} = 1$ Indicates vehicle $i+1$ receives information from vehicle i

sgn Sign function

Abbreviations

BD Bidirectional topology.

BDL Bidirectional-Leader topology.

CV Connected Vehicles.

DLFC Distributed Linear Feedback Control.

DP Distance Policy.

FL Feedback Linearization.

IFT Information Flow Topology.

ITS Intelligent Transportation System.

LFC Linear Feedback Control.

MPF Multiple-Predecessor Following topology.

PF Predecessor Following topology.

PLF Predecessor-Leader Following topology.

SPTF Single-Predecessor-Two-Following topology.

TPF Two-Predecessor Following topology.

TPLF Two-Predecessor-Leader Following topology.

TPSF Two-Predecessor-Single-Following topology.

V2V Vehicle-to-Vehicle communication.

Chapter 1

Introduction

In recent times, autonomous vehicles have garnered remarkable attention, widespread acceptability, and growing popularity. This surge of interest has prompted automotive manufacturers to invest heavily in this promising technology, striving to gain a competitive edge in the automotive market. As a testament to the significance of this industry shift, billions of dollars have been allocated for research and development. ABI Research[1] has even forecasted that by 2025, eight million autonomous or semi-autonomous vehicles, equipped with SAE[2] (Society of Automotive Engineers) levels of automation including 3, 4 or 5, will be sold.

For decades, vehicles have served primarily as a medium for radio entertainment and, more recently, as connected platforms offering enhanced features like navigation and streaming services. However, there is a growing realization among automakers that advanced communication technology is becoming integral to vehicle operation. This technology is seen as a means to enhance road safety, improve fuel efficiency, increase driver and passenger comfort, and, ultimately, foster economic growth and customer satisfaction.

One pivotal technology in this domain is Vehicle-to-Vehicle (V2V) communication. V2V technology enables vehicles to wirelessly exchange critical information about their state, including speed, acceleration, location, and heading. Operating on a

[1] https://www.abiresearch.com/pages/about-us/
[2] https://www.sae.org/

short-range broadcast model, V2V technology allows vehicles to broadcast and receive omnidirectional messages from neighboring vehicles at a frequency of up to 10 Hz. For instance, V2V technology can establish a 360-degree "awareness" of other vehicles, providing early warnings to drivers in the event of potential accidents. Another application of this technology is vehicle platooning, which is an intelligent transportation system (ITS) aiming to connect multiple vehicles in a convoy while automatically setting and maintaining close-proximity following distances, particularly on highways. In a platoon, the leading vehicle sets the pace, while the following vehicles adapt to its movements. However, it's essential to note that full autonomy for the follower vehicles in platooning is still an emerging technology. Regulatory and safety concerns mean that, for now, drivers must remain actively engaged in the control loop.

Recent advancements in information and communication technologies have accelerated the development of platooning technology. Intelligent vehicle platooning holds promise for enhancing safety, optimizing infrastructure utilization, increasing highway capacity, reducing aerodynamic drag and fuel consumption, mitigating road traffic accidents, and stimulating economic growth.

Vehicle platooning is poised to make road transport safer, cleaner, and more efficient in the future. It achieves this through:

1. Enhanced Safety: Platooning improves safety by enabling automatic and immediate braking, significantly reducing reaction time compared to human drivers.

2. Lowered Fuel Consumption and Emissions: The close proximity of platooning vehicles decreases air-drag friction, leading to lower fuel consumption and reduced CO2 emissions.

3. Increased Efficiency: Platooning optimizes transport by using roads more effectively, enabling faster goods delivery and reducing traffic congestion. It also provides drivers with the flexibility to perform other tasks, such as administrative work or making calls.

In summary, intelligent vehicle platooning not only fosters innovation and effi-

ciency in industries like commercial transportation but also offers improved safety for drivers and pedestrians, greater infrastructure efficiency, increased highway capacity, reduced drag and fuel consumption, and ultimately contributes to economic growth. It represents a significant advancement in the automotive industry and holds great potential for a safer, cleaner, and more efficient future of road transport.

1.1 Motivation

The motivation for this research stems from the critical need to address various challenges associated with the implementation of distributed linear controllers in vehicular platooning systems. In the quest to unlock the numerous benefits that these systems can offer, we recognize several key hurdles that must be overcome.

One of the primary challenges lies in dealing with transient distance variations from desired values. The limitations of individual vehicle speeds and accelerations further compound the complexity of the problem. Additionally, the influence of communication topologies, the effects of parity and disparity between vehicles, and the identification of appropriate control gains all present formidable obstacles that demand our attention. The overarching goal here is to prevent potential collisions and avoid impractical accelerations and decelerations in platooning scenarios. Also, we recognize that the ability to decouple the determination of proper control gains from the leader vehicle's speed is of paramount importance. This requirement ensures that our approach is adaptable to a wide range of scenarios, including those involving constant and varying speeds for the lead vehicle during steady-state platooning.

1.2 Thesis Objectives

The primary objective of this research is to address the substantial challenges encountered within the domain of vehicular platooning systems. We are motivated by the imperative to enhance the performance, safety, and adaptability of these systems,

which drives our investigation. To attain this overarching goal, we have delineated specific objectives that serve as guiding principles for our research.

Our foremost objective is to shift our focus away from the traditional follower-leader state differences and redirect it towards the disparities in states among neighboring vehicles. This strategic shift in our research is aimed at uncovering the underlying dynamics governing deviations in state differences between neighboring vehicles and their target values. This marks a pivotal contribution, as it paves the way for the identification of control gains necessary to achieve the desired transient behaviors of these states before they stabilize at their intended values. To illustrate, the transformed state coordinate, particularly in terms of position, assumes a critical role in quantifying the deviation in intervehicle distances from their desired values. By imposing constraints on these deviations, we can ensure the attainment of appropriate transient distances, thus preventing them from falling below safe distances for adjacent vehicles.

Another vital objective is to establish that the deviation dynamics remain entirely independent of the leader vehicle's state. This independence is instrumental in providing analytical guarantees for the maintenance of desired distances and synchronized speeds within the platoon. This is especially important in scenarios where the leader vehicle's speed undergoes changes during steady-state operation. By achieving this independence, the dynamics become solely reliant on constant parameters associated with the platoon's structure, such as vehicle characteristics and communication topology. Also, we aim to ensure that our findings and solutions have broad applicability, regardless of the number of vehicles, variations in vehicle capabilities, the use of identical or non-identical control gains, and the type of communication topology.

Moreover, we investigate the impact of initial conditions on the evolution of vehicle states. Our objective is to map these initial conditions to transient deviations based on communication topology, vehicle characteristics, and control parameters. This endeavor provides insights into the influence of platoon structure on this mapping.

1.3 Thesis Outline

The subsequent chapters in this dissertation are structured as follows. In Chapter 2, a comprehensive review of existing literature is presented, covering the fundamentals of vehicle dynamics, controller systems, and communication topologies. This chapter lays the theoretical groundwork for the subsequent analytical and experimental work. Chapter 3 introduces innovative stability analysis techniques for heterogeneous platoons, employing decentralized linear feedback controllers with non-identical gains and various Information Flow Topologies (IFTs). It emphasizes the significance of communication and the benefits of incorporating leader feedback into follower controllers. In Chapter 4, the focus shifts to homogeneous platoons, introducing a closed-loop distance dynamic model. This model facilitates a detailed investigation of inter-vehicle distances (IDs) and discusses the impact of different Communication Topologies (CTs) on platoon performance. Chapter 5 delves into achieving internal stability and favorable transient dynamics in inter-vehicle distances. It scrutinizes the strengths and weaknesses of bidirectional communication topologies (BDCTs) and the significance of leader information dissemination. Chapter 6 extends the research beyond internal stability considerations, emphasizing a coupled distance dynamic model. It examines how control parameters and initial conditions impact platoon stability and distance errors, validated through high-fidelity simulations. In Chapter 7, the impact of communication topologies on inter-vehicle distances in larger platoons is explored. It highlights the potential for scalability while maintaining efficiency and emphasizes the critical role of leader information dissemination. The subsequent chapters in this dissertation are structured as follows. In Chapter 2, a comprehensive review of existing literature is presented, covering the fundamentals of vehicle dynamics, controller systems, and communication topologies. This chapter lays the theoretical groundwork for the subsequent analytical and experimental work. Chapter 3 introduces innovative stability analysis techniques for heterogeneous platoons, em-

ploying decentralized linear feedback controllers with non-identical gains and various Information Flow Topologies (IFTs). It emphasizes the significance of communication and the benefits of incorporating leader feedback into follower controllers. In Chapter 4, the focus shifts to homogeneous platoons, introducing a closed-loop distance dynamic model. This model facilitates a detailed investigation of inter-vehicle distances (IDs) and discusses the impact of different Communication Topologies (CTs) on platoon performance. Chapter 5 delves into achieving internal stability and favorable transient dynamics in inter-vehicle distances. It scrutinizes the strengths and weaknesses of bidirectional communication topologies (BDCTs) and the significance of leader information dissemination. Chapter 6 extends the research beyond internal stability considerations, emphasizing a coupled distance dynamic model. It examines how control parameters and initial conditions impact platoon stability and distance errors, validated through high-fidelity simulations. In Chapter 7, the impact of communication topologies on inter-vehicle distances in larger platoons is explored. It highlights the potential for scalability while maintaining efficiency and emphasizes the critical role of leader information dissemination. Chapter 8 serves as the conclusion, summarizing key findings and outlining future research directions. It underlines the importance of communication strategies and leader information in enhancing platoon performance and positions the research as a foundation for further innovation in the field.

Chapter 2

Literature Review and Preliminaries

2.1 Literature Review

Platooning is a convoy of vehicles, typically consisting of one leader and several followers, traveling in close formation along a designated track. The primary objective of platooning is to maintain a desired spacing between the vehicles and ensure that the followers track the leader vehicle's velocity and acceleration. This coordinated movement results in a reduction in aerodynamic drag between the vehicles, leading to decreased fuel consumption [1, 2]. Additionally, the use of smaller spacing between vehicles can increase the capacity of highways and improve safety and energy efficiency by enabling rapid reactions when necessary [3–7]. Safety and energy constraints can also be integrated into the platoon control system to enhance overall performance [8, 9].

2.1.1 Platoon Structure

Vehicles in platoons can be broadly categorized into two primary groups: homogeneous [10, 11] and heterogeneous [12, 13]. In homogeneous platoons, all vehicles share similar characteristics, including size and degree of automation, resulting in a uniform and standardized fleet. In contrast, heterogeneous platoons consist of vehicles with differences in size or automation levels, leading to a diverse mix of vehicle

types within the platoon. The desired inter-vehicle distances in a platoon can be maintained through various spacing policies, which can be either constant or varying [14–16]. Two common spacing policies are the Constant Distance (CD) policy, which aims to keep a fixed distance between consecutive vehicles, and the Constant Time Headway (CTH) policy, where the spacing depends on the leader's velocity and, therefore, varies with time [14–16]. Other policies, such as the nonlinear distance policy [17] and the delay-based distance policy [18], offer different approaches to maintaining inter-vehicle distances. Evaluating these spacing policies involves assessing two key criteria: individual vehicle stability, which focuses on the convergence of vehicle velocities and inter-vehicle distances to desired values, and string stability, which examines the dissipation of small perturbations along the platoon [19–22]. For a comprehensive overview of string stability definitions, please refer to [20, 23].

When considering only the longitudinal dynamics of vehicles in a platoon, the system can be characterized by four main components: vehicles' longitudinal motion, information flow topology (IFT), distributed controllers, and the chosen spacing policy [22, 24]. The IFT, also referred to as communication topology (CT), defines how information is exchanged between vehicles, specifying whether they receive data from vehicles ahead, behind, or both [22, 24]. Examples of typical IFTs include PF (Predecessor Following), MPF (Multiple-Predecessor Following), TPLF (Two-Predecessor-Leader Following), PLF (Predecessor-Leader Following), TPF (Two-Predecessor Following), BDL (Bidirectional-Leader), BD (Bidirectional), TBPF (Two-Bidirectional Predecessor Following), TPSF (Two-Predecessor-Single-Following), and SPTF (Single-Predecessor-Two-Following) [22, 24]. The structure of these IFTs is visually represented in Figure 2.1. Additionally, distributed controllers must be designed effectively to achieve the platoon's objectives [23, 25–28].

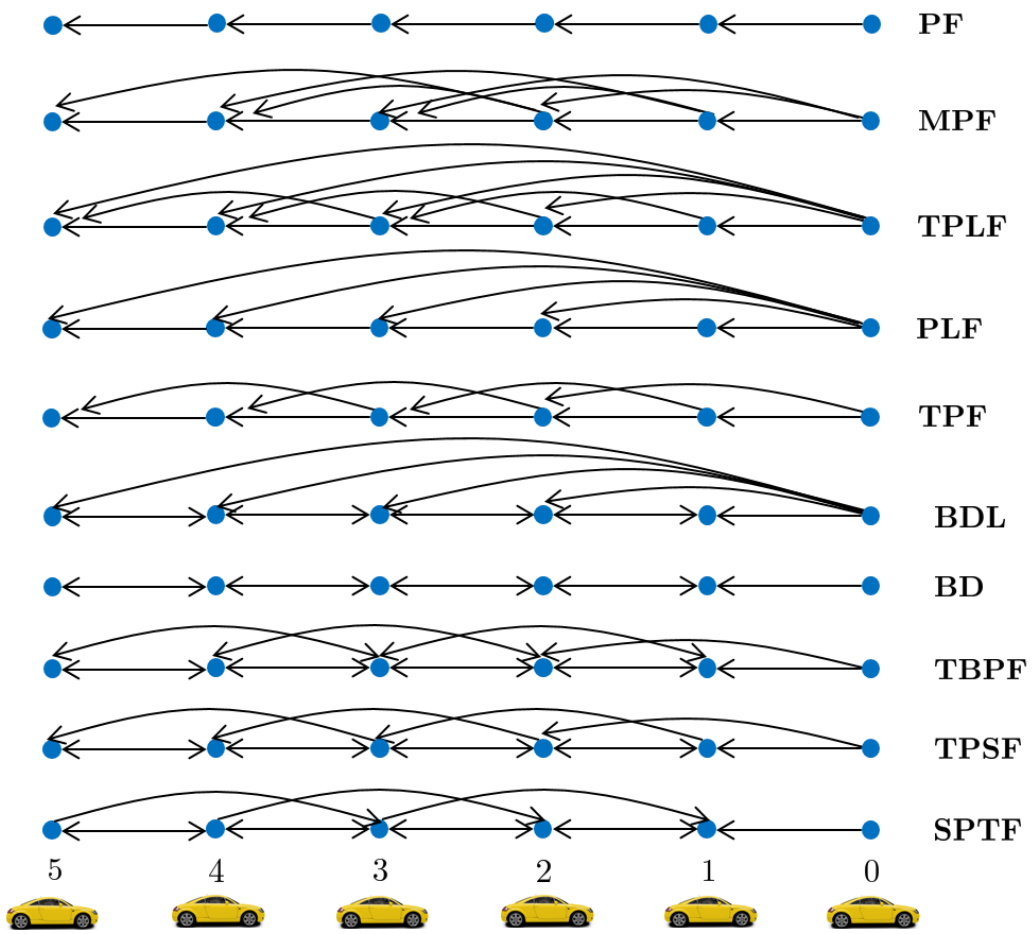

Figure 2.1: Various communication topologies (CTs) between vehicles in the platoon.

2.1.2 Longitudinal Control

The term "longitudinal controller" typically denotes any control system responsible for managing the vehicle's longitudinal motion, including factors like longitudinal velocity, acceleration, or its distance from a preceding vehicle in the same highway lane [29]. Longitudinal control is executed through actuators, namely the throttle and brakes. A common illustration of longitudinal control is the standard cruise control system found in most vehicles today. In this system, the driver sets a constant desired speed for the vehicle. The cruise control system then autonomously adjusts the throttle to maintain the specified speed. It remains the driver's responsibility to ensure that the chosen speed is safe for highway travel. If a preceding vehicle traveling at a slower speed or closely following the ego vehicle appears on the highway, the driver

must intervene and, if necessary, apply the brakes. Brake application automatically disengages the cruise control system, restoring control of the throttle to the driver.

2.1.3 Distributed Control of Vehicular Platoon

In large-scale systems with interconnected processors, distributed estimation and/or control algorithms are commonly used. The algorithm is divided into parts, each of which is operated independently with limited information. Due to these characteristics and to redeem computational complexity, rather than using central control architecture, distributed algorithms are suitable to operate connected vehicles.

The platoon's vehicle control module is divided into longitudinal and lateral control components. Longitudinal control focuses on maintaining a pre-established distance among platoon vehicles, ensuring uniform speed, and upholding the string stability of the platoon against disturbances. On the other hand, lateral control governs the platoon's lateral motion during maneuvers, such as joining or leaving the formation. The focus of this research is on longitudinal control.

Distributed longitudinal control of vehicular platoons has been extensively studied in literature such that various techniques based on model predictive control [30–34], sliding mode control [12, 13, 35], consensus-based control [36–39], event-triggered control [40–43], adaptive control [44–46], observer-based control [47–50], robust control [13, 51], reinforcement learning-based control [52], and linear feedback control (LFC) [27, 53–57] are utilized for coordination of platoon vehicles.

2.1.4 Safety Incorporation

Apart from stability and tracking performance, safety and collision analysis are crucial aspects of platooning. In the realm of control systems, the significance of transient performance equals that of steady-state performance. In certain dynamic systems, transient performance takes precedence over steady-state performance. The efficacy of Prescribed Performance Control [58] has been demonstrated as a formidable tool,

ensuring that control system outputs/errors exhibit the desired transient performance alongside steady-state performance [59]. In [60], a robust distributed control is suggested for large platoons of vehicles with second-order uncertain nonlinear dynamics under PF and BD topologies. Designer-specified performance functions guide transient and steady-state responses, preventing connectivity breaks and intervehicular collisions arising from sensor limitations. In [61], a prescribed performance (PP) platoon formation control is proposed for unmanned surface vehicles with input saturation and dead zone. Prescribed performance constraints on line-of-sight range and angular errors ensure both transient and steady-state performance, achieving collision avoidance and connectivity maintenance. In [62] and [63], adaptive finite-time PP control schemes are devised for vehicular platoons with dead-zone and saturation, such that, for the former, PP is achieved irrespective of the initial state.

Other than prescribed performance control, safety and collision have been considered in other control methods as well. In [64], a Distributed Model Predictive Control has been used to address collision-free properties by employing coupled state constraints and terminal sets. In [65], a proposed nonlinear adaptive cruise controller for vehicular platoons under PF topology utilizes feedback controllers constructed as nonlinear functions of the distance between successive vehicles and their speeds. Safety (collision avoidance) and bounded vehicle speeds are achieved by explicitly characterizing the set of allowable inputs. In [66], bilateral inequality constraints on the spacing error between adjacent vehicles are formulated and integrated into an adaptive controller to attain collision avoidance and compact formation performance. In [67], a controller design is introduced with collision avoidance (CA) functionality to ensure safety. The nominal controller is applied in a safe operational region, designed independently of the CA function. If the nominal controller cannot ensure safety, a predefined gradual braking strategy is implemented. In [68], conditions are established for ensuring collision avoidance based on vehicle dynamics. It is demonstrated that achieving these control objectives requires the controlled vehicles to be externally

positive in both velocity and distance output, which is both necessary and sufficient. In [69], an adaptive control architecture is devised with both emergency and nominal controllers to guarantee safety and comfort. Safety is maintained through the switching between the nominal controller, utilizing model predictive control to compute optimal inputs for maintaining a safe distance, and the emergency controller, which analytically determines the braking distance based on the host vehicle's deceleration profile, assuming the leading vehicle can fully brake at each time step. In [70], an adaptive platoon control is suggested for nonlinear vehicular systems with asymmetric nonlinear input deadzone and inter-vehicular spacing constraints. To prevent collisions between consecutive vehicles and maintain connectivity amid limited sensing capabilities, a symmetric barrier Lyapunov function is utilized. Subsequently, a neural-network-based terminal sliding mode control scheme with minimal learning parameters is devised to simultaneously uphold inter-vehicle connectivity and avoid collisions. In [71], a mathematical transformation scheme is introduced to limit the spacing error. Building on this, a distributed control algorithm is developed to ensure the boundedness of the spacing error. In [72], the paper addresses a secure and safe distributed cooperative control problem involving multiple platoons of automated vehicles amidst unknown data falsification attacks on driving commands.

Control Barrier Function (CBF) analysis provides a robust framework to ensure safety and performance assurances in intricate systems such as platoons. This method utilizes barrier functions to establish safe operating zones, directing control design to proactively prevent state trajectories from surpassing these boundaries, thus ensuring effective collision avoidance. In [73], an innovative distributed adaptive backstepping control scheme is presented utilizing barrier functions. This approach not only takes into account third-order nonlinear vehicle models but also dynamically identifies uncertain parameters in real-time. The control strategy guarantees the preservation of full-state constraints while effectively accomplishing tracking control objectives. In [74], utilizing fuzzy logic systems, the unknown nonlinear functions are approxi-

mated. It introduces a control scheme featuring an auxiliary design system to tackle input saturation. Notably, the design incorporates barrier Lyapunov functions to enforce distance restrictions, ensuring collision avoidance and sustaining communication connections among vehicles. In [75], a novel prescribed time performance recovery fault-tolerant control method is introduced to maintain nominal platoon performance despite multiple faults, encompassing actuator faults with deferred backup actuator switching and leader-follower link faults. The key innovation lies in a barrier function-based prescribed time sliding mode controller, designed to ensure platoon consensus errors and convergence time within specified constraints under normal conditions.

2.1.5 Communication Effect

In recent years, there has been a notable surge in research addressing concerns about the performance and resilience of distributed platooning algorithms, particularly in the face of faults and adversarial behaviors [40, 76, 77]. Beyond traditional systems and control tools, researchers have leveraged networks and graph theory to model various structures of connected vehicles. The intersection of network science and systems and control, inherent in networked control systems, has been a dynamic area of investigation [78, 79]. This interdisciplinary exploration involves advancements in applied mathematics and systems theory, such as algebraic graph theory and structured systems theory. Researchers have actively redefined system-theoretic notions from a network perspective. Noteworthy concepts introduced in this direction include network coherence [79, 80], providing a system-norm interpretation of a networked control system, and network robustness [81], which evaluates a network's ability to navigate adversarial conditions during the operation of distributed algorithms.

Recently some works have delved into the impact of platoon topologies on cooperative adaptive cruise control algorithms. For example, [27, 82] investigated how the platoon topology affects the stability and string stability of a vehicle platoon formation. In [83], researchers explored the influence of directed and bidirectional topologies

on the robustness of platoons to communication disturbances. Proposed methods to address communication delays in homogeneous cooperative adaptive cruise control systems are outlined in [84]. Moreover, in [85], the impact of topology on robustness to time delay is studied, revealing a trade-off between making the platoon robust to time delays and disturbances or additive faults.

Communication topology plays a central role in determining platoon stability and performance by governing how vehicles exchange critical information, such as position, velocity, and acceleration. Although existing research has extensively examined stability and performance within specific CTs, limited attention has been given to differentiating the impact of CTs on platoon performance. Recent studies have started to address this gap. In [86], a graph theory framework is applied to explore the impact of connectivity measures within CTs on the performance of distributed algorithms. This investigation assesses the ability of these algorithms to mitigate communication disruptions, detect cyber-attacks, and uphold resilience against such challenges. Additionally, [87] delves into the distinctions among three unidirectional communication topologies and their implications on stability, robustness, safety, and emissions within vehicle platoons. In terms of safety analysis, this study relies on two metrics, maximum time to collision (MTTC) and deceleration rate to avoid a crash (DRAC), to assess and contrast the security performance of platoons operating under the influence of three different UCTs. It is worth mentioning that in UCTs, vehicles only receive data from vehicles ahead of them. The transient behavior of inter-vehicle distances, a critical factor closely linked to platoon safety, is an aspect that has received limited attention in existing literature.

2.2 Preliminaries

This research centers on Distributed Linear Feedback Controllers (DLFCs). While existing literature has predominantly focused on the internal stability of platoons and steady-state convergence for position, velocity, and acceleration, it has overlooked the

transient behavior of inter-vehicle distances. To address this gap, we formulate the coupled dynamics of neighboring vehicles, providing analytical expressions for inter-vehicle distances and their derivatives. Our study encompasses both homogeneous and heterogeneous platoons, considering various communication scenarios among vehicles. We also comprehensively analyze initial conditions for platoons of any size. Additionally, we introduce an analytical tool to differentiate between communication topologies and assess their impact on safety, scalability and the robustness of platoons. Our analysis sets the stage for investigating how communication topologies influence the robustness of platoon performance in the presence of time delays.

In this Thesis, time-dependent signals will only be included if they enhance clarity. To differentiate between elements within vertical and horizontal vectors, we will utilize the semicolon and colon symbols, respectively. For instance, a 3-by-1 vector is symbolized as $[.;.;.]$, while a 1-by-3 vector takes the form of $[.,.,.]$. This notation will be consistently employed throughout the document to improve lucidity and ease of reading.

2.2.1 Platoon Longitudinal Framework

Figure 2.2 shows a platoon that has $n+1$ vehicles such that the one designated by 0 is the leader vehicle and the others labeled by $1,\ldots,i,i+1,\ldots,n-1,n$ are the followers. The real and desired distance between consecutive vehicles i and $i+1$ are denoted by D_i^{i+1} and d_i^{i+1}, respectively. Also, L_i presents the length of the i^{th} vehicle, and the x axis shows the position of the vehicles during their movement such that x_0 and x_i are the positions of the leader vehicle and the i^{th} follower vehicle, respectively. Furthermore, the notation $p_i^{i+1} \triangleq x_i - x_{i+1}$ is unitized for positions difference between consecutive vehicles.

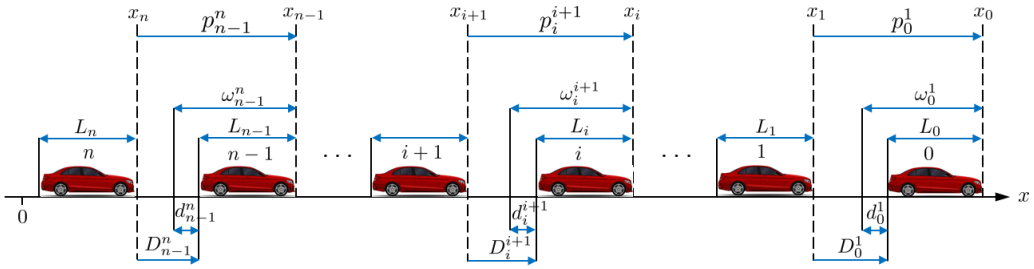

Figure 2.2: A platoon divided to consecutive-pairwise vehicles.

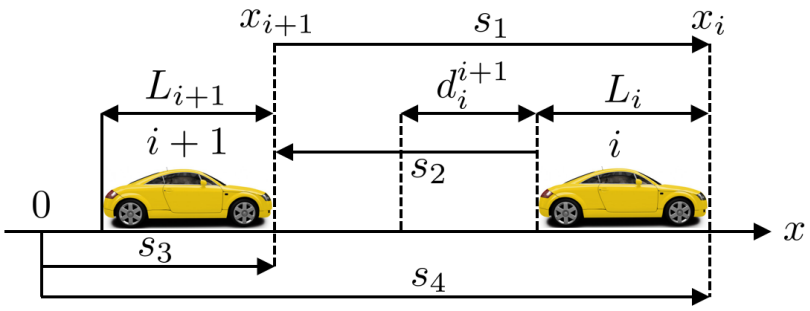

Figure 2.3: Illustrating adjacent vehicles: Vehicle $i+1$ as the follower and vehicle i as the predecessor, showing constant and changing distances.

2.2.2 Representation of Constant and Changing Distances

Considering Figure 2.2, we use a left-to-right direction for vehicle movement, designated as $\rightarrow$ for positive direction, and $\leftarrow$ for negative direction. Constant lengths or distances are represented by $\leftrightarrow$. To clarify this issue, in Figure 2.3 for instance, L_i and L_{i+1} indicate vehicle lengths, while d_i^{i+1} represents the desired constant gap between them. Arbitrary defined variable distances s_1, s_2, s_3, and s_4 follow the formulas: $s_1 = x_i - x_{i+1}$, $s_2 = x_{i+1} - (x_i - L_i)$, $s_3 = x_{i+1}$, and $s_4 = x_i$. Here, x_i and x_{i+1} refer to the front-side positions of the vehicles.

2.2.3 Control Structure

Generally speaking, longitudinal control of a platoon consists of two parts. First is the inner force/acceleration feedback linearization (FL) control, compensating for the vehicles' nonlinear dynamics. Second, an outer intervehicle distance control loop is

responsible for enforcing the desired spacing between the neighboring vehicles. The FL control is based on the assumption that the vehicle dynamics and its parameters are fully known which means that a perfect nonlinear dynamics cancellation can be achieved. We assume that the FL part has already canceled the dynamics nonlinearities and therefore we only focus on the inter-vehicle distance control loop. Consider that for platooning, and as far as the leader vehicle is concerned, we only need its position, velocity and acceleration, and it does not undergo any control process.

2.2.4 Vehicle Dynamics

Let the following formulation characterize the dynamics of the i^{th} follower vehicle [55, 88]:

$$\dot{a}_i = f_i\left(v_i, a_i\right) + g_i\left(v_i\right) c_i \qquad i = 1, \ldots, n \tag{2.1}$$

in which v_i and a_i are the velocity and acceleration of the i^{th} follower, and $f_i\left(v_i, a_i\right)$ and $g_i\left(v_i\right)$ are according to

$$\begin{cases} f_i\left(v_i, a_i\right) = -\frac{1}{\tau_i}\left(a_i + \frac{\sigma_i A_i C_{di} v_i^2}{2m_i} + \frac{d_{mi}}{m_i}\right) - \frac{\sigma_i A_i C_{di} v_i a_i}{m_i} \\ g_i\left(v_i\right) = \frac{1}{\tau_i m_i} \end{cases} \tag{2.2}$$

where c_i is the engine input. The parameters $\sigma_i,\ A_i,\ C_{di},\ d_{mi}, m_i,\ \tau_i$ are specific mass of air, and vehicles' cross sectional area, drag coefficient, mechanical drag, mass, and engine time constant, respectively. Let the engine input c_i be governed by following FL controller [55]:

$$c_i = u_i m_i + 0.5\sigma_i A_i C_{di} v_i^2 + d_{mi} + \tau_i \sigma_i A_i C_{di} v_i a_i \tag{2.3}$$

substituting which into (2.1) results in [27, 31, 43, 46–48, 53, 54, 56, 57] a third-order linear model mathematically describing each following vehicle's behavior within the platoon as follows.

$$\begin{cases} \dot{x}_i = v_i \\ \dot{v}_i = a_i \\ \dot{a}_i = -\frac{1}{\tau_i} a_i + \frac{1}{\tau_i} u_i \end{cases} \tag{2.4}$$

in which u_i is the input signal to be designed properly. Therefore, the FL transforms the mathematical description of the nonlinear system into a simplified linear system.

State-Space Presentation

Let $\mathbf{X}_i \triangleq [x_i;\ \dot{x}_i;\ \ddot{x}_i]$ denote the state of the i^{th} follower where $\dot{x}_i = v_i$ and $\ddot{x}_i = a_i$. Thus, for $i = 1, \ldots, n$ and given (2.4), the state-space model for the i^{th} follower can be written as

$$\dot{\mathbf{X}}_i = \mathbf{A}_i \mathbf{X}_i + \mathbf{B}_i u_i = \begin{bmatrix} 0 & 1 & 0 \\ 0 & 0 & 1 \\ 0 & 0 & -\frac{1}{\tau_i} \end{bmatrix} \mathbf{X}_i + \begin{bmatrix} 0 \\ 0 \\ \frac{1}{\tau_i} \end{bmatrix} u_i \tag{2.5}$$

2.2.5 Desired Distances: Constant Distance Policy

Assuming a constant distance policy for the platoon, the objective of designing the controller u_i is to guarantee that the followers' velocities/accelerations reach to the leader's velocity/acceleration while desired constant inter-vehicle distances ($\triangleq d_i^{i+1}$) are maintained between back-to-back vehicles. In other words, the aim is to have

$$\begin{cases} v_i(t) = v_0(t); \quad i = 1, \ldots n \\ x_\kappa - x_{\kappa+1} = L_\kappa + d_\kappa^{\kappa+1}; \quad \kappa = 0, \ldots, n-1 \end{cases} \tag{2.6}$$

in which $v_0(t)$ is the leader vehicle's velocity.

2.2.6 Distributed Controller

To ensure the accomplishment of the aims mentioned in (2.6), the following distributed linear controller [89] is utilized:

$$\begin{cases} u_i = -\sum_{j \in \mathbb{I}_i} \left[k\left(x_i - x_j - d_{ij}\right) + b\left(\dot{x}_i - \dot{x}_j\right) + h\left(\ddot{x}_i - \ddot{x}_j\right) \right] \\ d_{ij} \triangleq -sgn(i-j) \sum_{\kappa=\min(i,j)}^{\max(i,j)-1} \omega_\kappa^{\kappa+1}; \quad \omega_k^{\kappa+1} \triangleq L_\kappa + d_\kappa^{\kappa+1} \end{cases} \tag{2.7}$$

in which the notation $\triangleq$ is utilized for definition, and $\mathbb{I}_i \subset \{\{0, 1, \ldots, n\} - \{i\}\}$ indicates all the vehicles from which the i^{th} vehicle receives information. For connections between vehicles, let $z_i^j = 0$ denote the case in which the i^{th} vehicle does not receive information from the j^{th} vehicle, and $z_i^j = 1$ if the other way around.

Chapter 3

Heterogeneous Vehicular Platooning With Stable Decentralized Linear Feedback Control[1]

In this chapter, a dynamic representation for platoons is established using linearized longitudinal dynamic models for individual vehicles. A constant distance policy is adopted, a distributed linear feedback controller is employed, and differences in dynamic models and feedback information across the vehicles are considered. The chapter focuses on providing platoon stability analysis, with a particular emphasis on highlighting the challenges associated with analyzing large platoons. As a case study, a platoon with one leader and two followers is investigated through the proposed strategy, with the stability conditions provided. The chapter also includes numerical simulations to explore the stability range of control gains and discuss the effect of different information flow topologies (IFTs) on the platoon's performance.

3.1 Vehicle Model and Problem Formulation

Figure 3.1 depicts a platoon consisting of $N + 1$ vehicles, where the leader vehicle is designated as 0 and the subsequent vehicles are labeled from 1 to N. The distance

[1]A version of this chapter has been published as Amir Zakerimanesh, Tony Z. Qiu, Mahdi Tavakoli, *Heterogeneous Vehicular Platooning With Stable Decentralized Linear Feedback Control*, IEEE International Conference on Autonomous Systems, 2021.

between consecutive vehicles, denoted as D_i^{i+1}, and the length of the i^{th} follower vehicle, represented by L_i, are illustrated on the x-axis. This axis reflects the positions of the vehicles during their movement, with x_0 denoting the leader vehicle's position and x_i indicating the position of the i^{th} follower.

Broadly, the longitudinal control of this platoon involves two key components. First, there's an inner force/acceleration control loop known as feedback linearization (FL) control, designed to compensate for the nonlinear dynamics of the vehicles. Second, an outer control loop manages inter-vehicle distances, ensuring that the platoon maintains the desired spacing as per the spacing policy.

The FL control operates under the assumption that both the vehicle dynamics and its parameters are entirely known, allowing for the perfect cancellation of nonlinear dynamics. This discussion will primarily focus on the inter-vehicle distance control loop, as we assume that the FL component has already addressed the dynamics' nonlinearities.

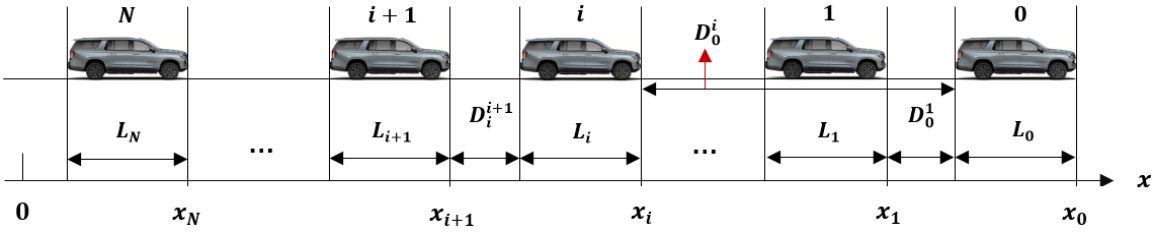

Figure 3.1: A platoon with constant inter-vehicle spacing.

Each following vehicle's behavior within the platoon is described mathematically using a third-order linear model as

$$\tau_i \dot{a}_i + a_i = u_i \tag{3.1}$$

in which u_i is an auxiliary input signal associated with the outer control loop to be designed. Let $\mathbf{X}_i \triangleq [x_i,\ \dot{x}_i,\ \ddot{x}_i]$ denote the states of the i^{th} follower where $\dot{x}_i = v_i$ and $\ddot{x}_i = a_i$. Thus, given (3.1), the state-space model for the i^{th} follower can be written

as

$$\dot{\mathbf{X}}_i = \mathbf{A}_i\mathbf{X}_i + \mathbf{B}_i u_i = \begin{bmatrix} 0 & 1 & 0 \\ 0 & 0 & 1 \\ 0 & 0 & -\frac{1}{\tau_i} \end{bmatrix} \mathbf{X}_i + \begin{bmatrix} 0 \\ 0 \\ \frac{1}{\tau_i} \end{bmatrix} u_i \tag{3.2}$$

where both the vehicles' feedback-linearized dynamics (characterized by $\mathbf{A}_i$, $\mathbf{B}_i$ and τ_i) and the platoon's controllers (characterized by u_i) are nonidentical, meaning that they are not the same for all follower vehicles, constituting a heterogeneous platoon. Therefore, the problem formulation and stability analysis would be developed with taking account of heterogeneity in the dynamic models and feedback information to the vehicles.

In this chapter, the objective of designing the controller u_i is to guarantee that when the leader has a constant steady velocity ($\triangleq v_0^s$), the followers' velocities track that leading velocity while desired constant distances ($\triangleq d_i^{i+1}$) are maintained between any two back-to-back vehicles within the platoon. In other words, for $\kappa = 1, \ldots, N-1$, the aim is to have

$$\begin{aligned} & v_i(t) = v_0^s(t) \\ & x_\kappa - x_{\kappa+1} = L_\kappa + d_\kappa^{\kappa+1} \qquad \equiv \qquad D_\kappa^{\kappa+1} = d_\kappa^{\kappa+1} \end{aligned} \tag{3.3}$$

and to ensure which, we design a distributed controller with non-identical gains as

$$u_i = -\sum_{j \in \mathbb{I}_i} \left[k_i \left(x_i - x_j - d_{ij} \right) + b_i \left(\dot{x}_i - \dot{x}_j \right) + h_i \left(\ddot{x}_i - \ddot{x}_j \right) \right] \tag{3.4}$$

where

$$d_{ij} \triangleq -sgn(i-j) \sum_{\kappa=\min(i,j)}^{\max(i,j)-1} \left[l_\kappa + d_\kappa^{\kappa+1} \right] \tag{3.5}$$

and $\mathbb{I}_i \subset \{\{0, 1, \ldots, N\} - \{i\}\}$ indicates the vehicles from which the vehicle i receives information. Please note that the intention is to develop the platoon formulation regardless of the type of communications between the vehicles such that any IFTs can suit properly in the problem development. Having d_i^{i+1} as the desired spacing between the consecutive vehicles and x_0 as the position of the leader vehicle, the

desired position and velocity of the i^{th} follower can be defined accordingly as

$$x_i^* \triangleq x_0 - \sum_{\kappa=0}^{i-1} \left[l_\kappa + d_\kappa^{\kappa+1} \right], \qquad \dot{x}_i^* = v_0^s = \dot{x}_0^s \tag{3.6}$$

For conciseness in presentation and ease in later analysis, the state error of the i^{th} follower is defined as $\tilde{x}_i = x_i - x_i^*$ utilizing which readily results in $x_i - x_j = \tilde{x}_i - \tilde{x}_j + d_{ij}$, and subsequently substituting which into the controller (3.4) gives

$$u_i = -\sum_{j \in \mathbb{I}_i} \left[k_i \left(\tilde{x}_i - \tilde{x}_j \right) + b_i \left(\dot{\tilde{x}}_i - \dot{\tilde{x}}_j \right) + h_i \left(\ddot{\tilde{x}}_i - \ddot{\tilde{x}}_j \right) \right] \tag{3.7}$$

and plugging (3.7) in (3.1) yields

$$\dddot{\tilde{x}}_i = -\frac{|\mathbb{I}_i|\, k_i}{\tau_i} \tilde{x}_i - \frac{|\mathbb{I}_i|\, b_i}{\tau_i} \dot{\tilde{x}}_i - \frac{1 + |\mathbb{I}_i|\, h_i}{\tau_i} \ddot{\tilde{x}}_i + \frac{k_i}{\tau_i} \sum_{j \in \mathbb{I}_i} \tilde{x}_j + \frac{b_i}{\tau_i} \sum_{j \in \mathbb{I}_i} \dot{\tilde{x}}_j + \frac{h_i}{\tau_i} \sum_{j \in \mathbb{I}_i} \ddot{\tilde{x}}_j \tag{3.8}$$

which obtained using the facts that $\ddot{x}_i = \ddot{\tilde{x}}_i$ and $\dddot{x}_i = \dddot{\tilde{x}}_i$. Note that $|\mathbb{I}_i|$ is the cardinality of the set $\mathbb{I}_i$. Considering (3.8), knowing $\tilde{x}_0 = \dot{\tilde{x}}_0 = \ddot{\tilde{x}}_0 = 0$, and defining the i^{th} vehicle control gains as $\mathbf{K}_i = [k_i\, , b_i,\ h_i]$ and platoon state error as $\tilde{\mathbf{X}}_N \triangleq \left[\tilde{x}_1;\ \dot{\tilde{x}}_1;\ \ddot{\tilde{x}}_1; \ldots; \tilde{x}_N;\ \dot{\tilde{x}}_N;\ \ddot{\tilde{x}}_N \right]$, the platoon closed-loop state-space dynamics model can be characterized by

$$\dot{\tilde{\mathbf{X}}}_N = \tilde{\mathbf{A}}_N \tilde{\mathbf{X}}_N = \begin{bmatrix} \mathbf{A}_{11}^* & \mathbf{A}_{12}^* & \ldots & \mathbf{A}_{1N}^* \\ \\ \mathbf{A}_{21}^* & \mathbf{A}_{22}^* & \ldots & \mathbf{A}_{2N}^* \\ \vdots & \ldots & \ddots & \vdots \\ \mathbf{A}_{N1}^* & \mathbf{A}_{N2}^* & \ldots & \mathbf{A}_{NN}^* \end{bmatrix} \tilde{\mathbf{X}}_N \tag{3.9}$$

where $\tilde{\mathbf{A}}_N$ is overall closed-loop system matrix such that for a given follower i, we have $\mathbf{A}_{ii}^* \triangleq \mathbf{A}_i - |\mathbb{I}_i|\, \mathbf{B}_i \mathbf{K}_i$ and $\mathbf{A}_{ij}^* \triangleq \mathbf{B}_i \mathbf{K}_i$. Using $\tilde{\mathbf{A}}_N$, the determinant of the block matrix $s\mathbf{I}_N - \tilde{\mathbf{A}}_N$, which can be obtained analytically [90], will provide the characteristic polynomial of the platoon, using which the stability conditions with respect to the control gains can be obtained. Note that $\mathbf{I}_N$ is the identity matrix of size N, and the closed-loop system would be stable if all the eigenvalues of $\tilde{\mathbf{A}}_N$ are negative. In the rest of this chapter, we will consider stability conditions for an two-followers platoon.

3.1.1 Case Study: Stability Analysis For $N = 2$.

Considering $N = 2$, (3.9) can be written as

$$\dot{\tilde{\mathbf{X}}}_2 = \tilde{\mathbf{A}}_2\tilde{\mathbf{X}}_2 = \begin{bmatrix} \mathbf{A}_1 - |\mathbb{I}_1|\,\mathbf{B}_1\mathbf{K}_1 & \mathbf{B}_1\mathbf{K}_1 \\ \mathbf{B}_2\mathbf{K}_2 & \mathbf{A}_2 - |\mathbb{I}_2|\,\mathbf{B}_2\mathbf{K}_2 \end{bmatrix} \tilde{\mathbf{X}}_2 \tag{3.10}$$

where the platoon would be asymptotically stable if and only if all the eigenvalues of the matrix $\tilde{\mathbf{A}}_2$ are negative. In this respect, the characteristic polynomial of matrix $\tilde{\mathbf{A}}_2$ can be derived by the following determinant:

$$\left| \begin{bmatrix} s\mathbf{I}_3 - \mathbf{A}^*_{11} & -\mathbf{A}^*_{12} \\ -\mathbf{A}^*_{21} & s\mathbf{I}_3 - \mathbf{A}^*_{22} \end{bmatrix} \right| = |s\mathbf{I}_3 - \mathbf{A}^*_{11}| \left| (s\mathbf{I}_3 - \mathbf{A}^*_{22}) - \mathbf{A}^*_{21}\,(s\mathbf{I}_3 - \mathbf{A}^*_{11})^{-1}\,\mathbf{A}^*_{12} \right| \tag{3.11}$$

deriving which presents the characteristic polynomial $as^6+bs^5+cs^4+ds^3+es^2+fs^1+g$ in which the coefficients are according to the following formulas.

$$\begin{aligned}
a &= \tau_1\tau_2 \\
b &= \tau_1\,(1 + h_2\,|\mathbb{I}_2|) + \tau_2\,(1 + h_1\,|\mathbb{I}_1|) \\
c &= \tau_1 b_2\,|\mathbb{I}_2| + (1 + h_1\,|\mathbb{I}_1|)\,(1 + h_2\,|\mathbb{I}_2|) + \tau_2 b_1\,|\mathbb{I}_1| - h_1h_2 \\
d &= \tau_1 k_2\,|\mathbb{I}_2| + b_2\,|\mathbb{I}_2|\,(1 + h_1\,|\mathbb{I}_1|) + b_1\,|\mathbb{I}_1|\,(1 + h_2\,|\mathbb{I}_2|) + \tau_2 k_1\,|\mathbb{I}_1| - b_1h_2 - b_2h_1 \\
e &= k_2\,|\mathbb{I}_2|\,(1 + h_1\,|\mathbb{I}_1|) + b_1\,|\mathbb{I}_1|\,b_2\,|\mathbb{I}_2| + k_1\,|\mathbb{I}_1|\,(1 + h_2\,|\mathbb{I}_2|) - k_2h_1 - b_1b_2 - h_2k_1 \\
f &= b_1\,|\mathbb{I}_1|\,k_2\,|\mathbb{I}_2| + k_1\,|\mathbb{I}_1|\,b_2\,|\mathbb{I}|_2 - k_2b_1 - b_2k_1 \\
g &= k_1\,|\mathbb{I}_1|\,k_2\,|\mathbb{I}_2| - k_1k_2
\end{aligned} \tag{3.12}$$

and if the first follower does not receive information from the second follower, or vice versa, then we will have $\mathbf{A}^*_{12} = 0$ or $\mathbf{A}^*_{21} = 0$, respectively. Thus, the coefficients

would be

$$
\begin{aligned}
a &= \tau_1\tau_2 \\
b &= \tau_1\left(1+h_2\left|\mathbb{I}_2\right|\right)+\tau_2\left(1+h_1\left|\mathbb{I}_1\right|\right) \\
c &= \tau_1 b_2\left|\mathbb{I}_2\right|+\tau_2 b_1\left|\mathbb{I}_1\right|+\tau_1\left(1+h_2\left|\mathbb{I}_2\right|\right)+\tau_2\left(1+h_1\left|\mathbb{I}_1\right|\right) \\
d &= \tau_1 k_2\left|\mathbb{I}_2\right|+b_2\left|\mathbb{I}_2\right|\left(1+h_1\left|\mathbb{I}_1\right|\right)+b_1\left|\mathbb{I}_1\right|\left(1+h_2\left|\mathbb{I}_2\right|\right)+\tau_2 k_1\left|\mathbb{I}_1\right| \\
e &= k_2\left|\mathbb{I}_2\right|\left(1+h_1\left|\mathbb{I}_1\right|\right)+b_1\left|\mathbb{I}_1\right| b_2\left|\mathbb{I}_2\right|+k_1\left|\mathbb{I}_1\right|\left(1+h_2\left|\mathbb{I}_2\right|\right) \\
f &= b_1\left|\mathbb{I}_1\right| k_2\left|\mathbb{I}_2\right|+k_1\left|\mathbb{I}_1\right| b_2\left|\mathbb{I}\right|_2 \\
g &= k_1\left|\mathbb{I}_1\right| k_2\left|\mathbb{I}_2\right|
\end{aligned}
\tag{3.13}
$$

Now, having (3.12)-(3.13) and using Routh–Hurwitz criterion, the stability conditions can be obtained as follows.

$$
\begin{aligned}
&1.\ a,b,c,d,e,f,g>0 \\
&2.\ ad-bc\le 0 \\
&3.\ d\left(ad-bc\right)\le b\left(af-be\right) \\
&4.\ \left(ad-bc\right)\left[b^2g+f\left(ad-bc\right)\right]\le\left(af-be\right)\left[d\left(ad-bc\right)-b\left(af-be\right)\right] \\
&5.\ \left(b^2g+f\left(ad-bc\right)\right)\left[\left(ad-bc\right)\left[b^2g+f\left(ad-bc\right)\right]\right. \\
&\quad\left.-\left(af-be\right)\left[d\left(ad-bc\right)-b\left(af-be\right)\right]\right]\ge bg\left[d\left(ad-bc\right)-b\left(af-be\right)\right]^2
\end{aligned}
\tag{3.14}
$$

3.2 Simulation Results

In this section, simulation results are provided to evaluate the stability conditions for different IFTs that are depicted in Fig. (3.2). For simulations, we consider a velocity trajectory for the leader vehicle (see Fig. 3.4) and choose the vehicles' initial velocities and accelerations equal to zero. Also, the vehicles' length are the same and equal to $4m$, and vehicles' initial positions are selected as $x_0(0)=0m$, $x_1(0)=-10m$, and $x_2(0)=-20m$. As you can see in the Fig. 3.4, the steady-state velocities (v_0^s) for the leader vehicle are $30m/s$ (its maximum value) persisting for $12s$, and $0m/s$ that is associated with the time the leader vehicle brakes and stands still. Furthermore, we choose $d_i^{i+1}=10m$ as the desired spacing between the vehicles.

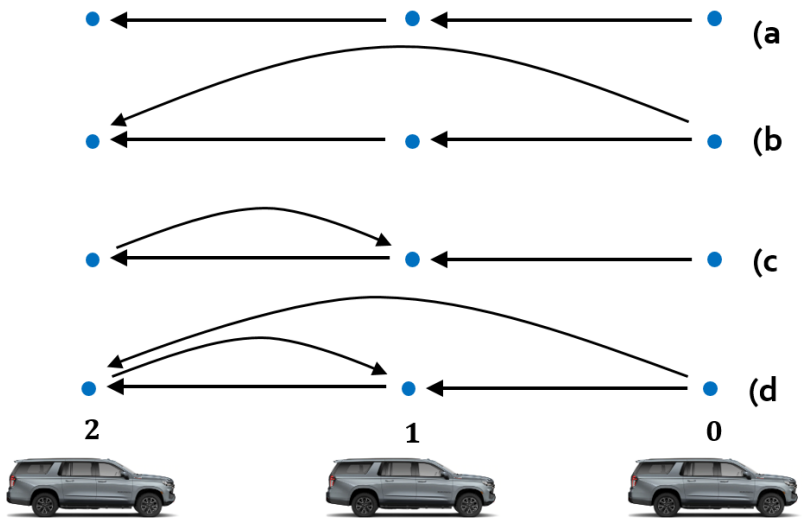

Figure 3.2: Schematic of different IFTs between the vehicles in the one-leader-two-follower platoon.

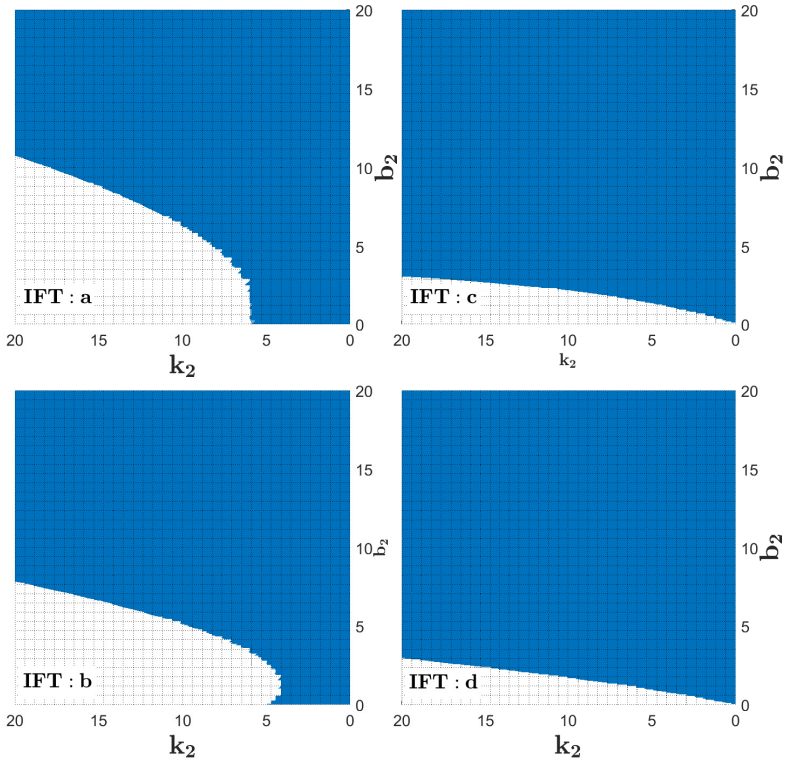

Figure 3.3: The stability area (the blue area) with respect to the control gains k_2 and b_2 for different IFTs sketched in Fig. 3.2.

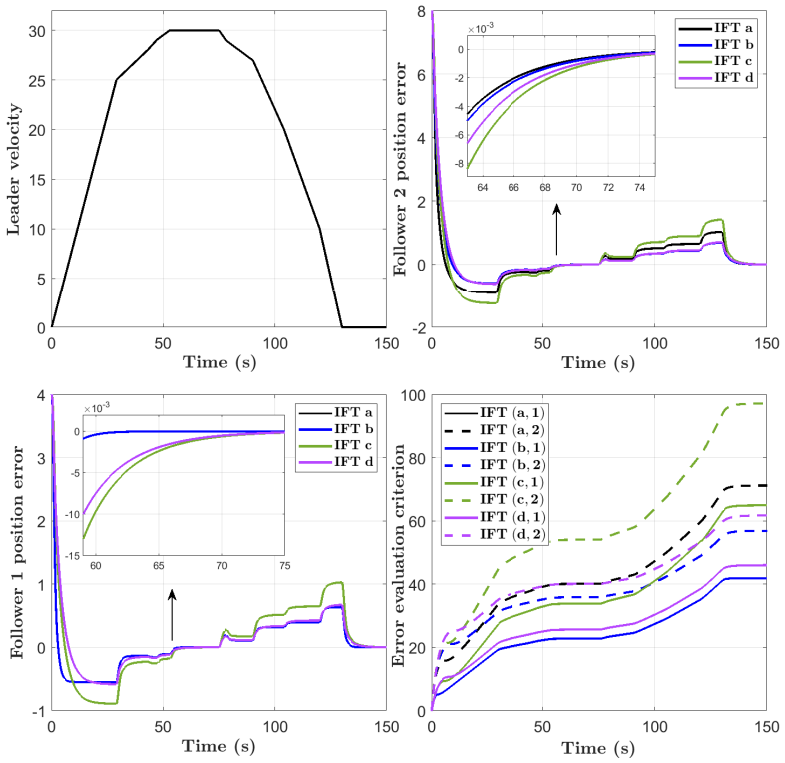

Figure 3.4: Error signals of the followers for the different IFTs.

First, we assume that $\tau_1 = \tau_2 = 0.5$ s, and the controller gains of all the vehicles are the same, i.e., $k_1 = k_2$, $b_1 = b_2$ and $h_1 = h_2 = 1$. Based upon the stability conditions given in the work [27] and for IFT c illustrated in Fig. 3.2, we assign $k_1 = k_2 = 3$, $b_1 = b_2 = 5$, and $h_1 = h_2 = 1$. Having k_1, b_1, h_1, we choose $h_2 = h_1$ and let k_2 and b_2 to be selected within the stability conditions given in (3.14). Regarding (3.12)-(3.13), this time we will find stability conditions with respect to the control gains k_2 and b_2 and for the four IFTs in Fig. 3.2. The results for the different IFTs are depicted in Fig. 3.3. The stability areas are shown in Fig. 3.3. As you can see, by comparing the stability areas of IFTs a and b, or IFTs c and d, or IFTs a and c, and or IFTs b and d, an additional communication channel between the vehicles makes the stability area larger. The IFT a has the smallest stability area and the IFT d has the largest stability area.

In order to draw an analogy between the controller performances in different IFTs, using root locus analysis for a given plausible k_2 or b_2 that belongs to all the stability areas of Fig. 3.3, we assign $k_2 = 2.5$ and $b_2 = 10$. Therefore, the control gains become $k_1 = 3$, $k_2 = 2.5$, $b_1 = 5$, $b_2 = 10$, and $h_1 = h_2 = 1$. Note here $\tau_1 = 0.5$ and $\tau_2 = 0.5$ are chosen for engines time constants. So, using this controller, the results for the different IFTs are shown in Fig. 3.4 in which, for instance, IFT $(a, 2)$ indicates the position error for the second follower and implies that the controller is utilized within the IFT of case a represented in Fig. 3.2. Note that the position error for the i^{th} follower is defined as $e_i(t) = x_i(t) - x_i^*(t)$. Investigating the simulation results for the different IFTs, we can see that when the leader has a constant steady velocity, the followers' position errors asymptotically converge to zero. Also, in IFTs b and d, in which both the first and second followers receive information from the leader, the error signal exhibits better damping behavior that can come in handy when, for instance, we want to enforce small desired spacing between the vehicles. To shed more light on the damping behavior, let the following formula be defined as the *error evaluation*

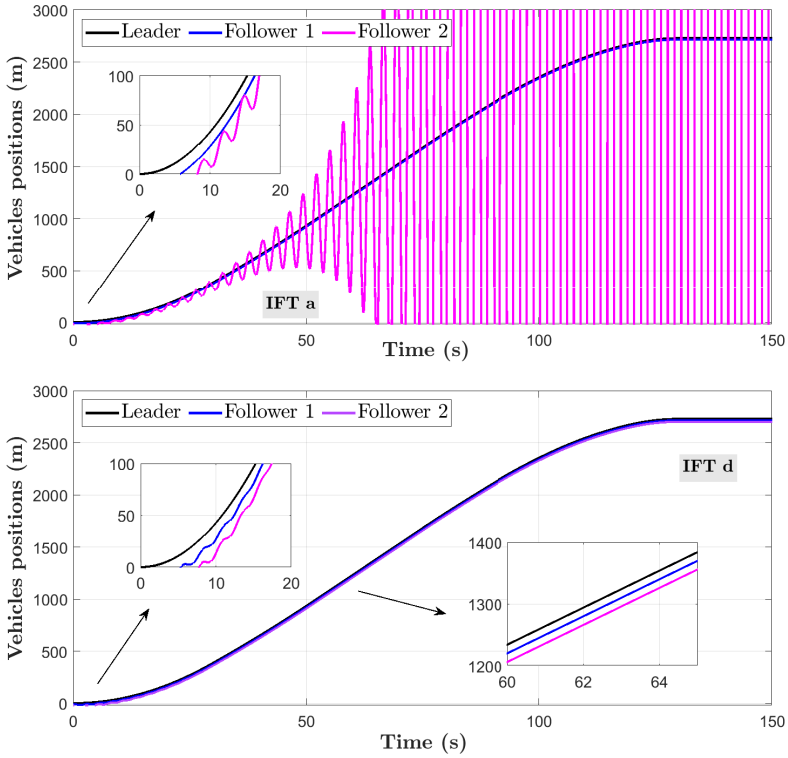

Figure 3.5: Vehicles' positions using control gains $k_1 = 3$, $b_1 = 5$, $h_1 = 1$, $k_2 = 10$, $b_2 = 2$, and $h_2 = 1$, and IFTs a and d.

criterion (EEC) for the transient behavior of the error signals of the followers.

$$EEC_i \triangleq \int_0^t |e_i(t)|\, dt \tag{3.15}$$

regarding which the results for the followers within the given IFTs are shown in Fig. 3.4. It is possible to see that the IFTs b and d provide better performance for the platoon respecting EEC measure. Moreover, making a comparison between the IFTs b and d, we can see that the communication from the second follower to the first follower has increased the settling time and so the convergence occurs slower.

Fig. 3.5 shows the positions of the vehicles for the given velocity of the leader and for the two IFTs a and d. As obvious from Fig. 3.3, for $k_2 = 10$ and $b_2 = 2$, the platoon of the IFT a would be unstable and the platoon of the IFT d would be stable. Accordingly, in Fig. 3.5, using the IFT d, the desired distances between the vehicles are maintained, however, in the IFT a the system is unstable and numerous collisions

occur.

3.3 Conclusion

In conclusion, the aim of this chapter was to illustrate the complexity of stability analysis for heterogeneous platoons. By employing a decentralized linear feedback controller with non-identical gains and accommodating various Information Flow Topologies (IFTs), we developed a state-space model for these diverse platoons. This approach allowed us to determine stability conditions using the Routh–Hurwitz criterion for platoons of any size. As a case study, we presented simulation results for a two-followers platoon and discussed the influence of different IFTs on system performance. Our findings underscored the notion that increased inter-vehicle communication, as facilitated by various IFTs, affords greater flexibility in selecting control gains that meet stability criteria. Furthermore, it was evident that incorporating feedback signals from the leader into both followers' controllers can significantly enhance the overall performance of the platoon.

Chapter 4

Stability and Intervehicle Distance Analysis of Homogeneous Vehicular Platoons: Highlighting the Impact of Bidirectional Communication Topologies[1]

Vehicular platooning, a configuration comprising a leading vehicle and multiple follower vehicles (FVs) seeks to achieve and maintain specific intervehicle distances (IDs) while synchronizing FVs with the velocity and acceleration of the leading vehicle. Prior to attaining a desired stable state, the IDs may undergo transient fluctuations. While the attainment of internal stability is pivotal for realizing the intended spacing between vehicles, it does not inherently guarantee that these transient fluctuations remain within safe thresholds, thereby mitigating the risk of collisions. Communication between vehicles has a critical role in vehicular platooning and significantly influences these transient distance fluctuations. Consequently, we present a mapping a between the initial conditions and these transient fluctuations which hinges on the communication topology, as well as the control parameters, and independent of the state of the leading vehicle. Specifically, our focus is directed towards bidirectional

[1]A version of this chapter has been submitted as Amir Zakerimanesh, Tony Z. Qiu, Mahdi Tavakoli, *Stability and Intervehicle Distance Analysis of Homogeneous Vehicular Platoons: Highlighting the Impact of Bidirectional Communication Topologies*, IEEE Transactions on Control Systems Technology.

communication topologies (BDCTs), wherein FVs possess the capability to communicate both with preceding and subsequent vehicles within the platoon. Investigation of these mappings illuminates the advantages and disadvantages of various BDCTs. Notably, we discern that within BDCTs, the receipt of information from a greater number of vehicles situated behind may at times hinder the overall performance of the platoon, resulting in larger deviations from the desired intervehicle distances or the velocity and acceleration of the leading vehicle. In contrast, information derived from vehicles located ahead, particularly the leading vehicle itself, serves to enhance intervehicle distances and thereby contributes significantly to the safety of the platoon. In conclusion, our theoretical insights are substantiated through a series of simulations.

A group of vehicles, led by one primary vehicle and followed by several others, forms what is known as a vehicular platoon. The primary objective of platooning is twofold: firstly, to attain and maintain the desired intervehicle distances (IDs), and secondly, to ensure that the follower vehicles (FVs) closely mirror the speed and acceleration of the lead vehicle. This collaborative formation brings several advantages. Firstly, due to the reduced space between vehicles, there is a significant decrease in aerodynamic drag between them, resulting in a substantial reduction in fuel consumption [1, 2]. Furthermore, the tight spacing of vehicles in a platoon allows for the accommodation of more vehicles on the road, thus enhancing highway capacity. Additionally, platooning systems are designed to enable automated and rapid responses by follower vehicles to the lead vehicle's actions, thereby contributing to the overall safety of drivers [3, 4]. To achieve these objectives, various spacing policies have been utilized, including constant time headway [16], nonlinear [17], delay-based [18], and constant distance [14, 15] policies. This work focuses on the constant distance policy, which seeks to establish and sustain fixed distances between adjacent vehicles. Platoon dynamics encompass considerations of vehicle dynamics, communication topology (CT), distributed controllers, and spacing policies [22, 24]. In this study, the emphasis is

placed on the longitudinal motion of vehicles and the utilization of distributed linear controllers [27, 53, 55].

Communication topology, which governs how vehicles exchange essential information such as position, velocity, and acceleration, holds a central position in determining platoon stability and performance. While existing literature extensively examines the stability and performance of vehicle platoons within specific CTs, there is a limited focus on differentiating the impact of CTs on platoon performance. Recent studies have started addressing this gap. In [86], a general graph theory framework is applied to explore the impact of connectivity measures within CTs on the performance of distributed algorithms. This investigation assesses the ability of these algorithms to mitigate communication disruptions, detect cyber-attacks, and uphold resilience against such challenges. Additionally, [87] delves into the distinctions among three unidirectional communication topologies (UCTs) and their implications on stability, robustness, safety, and emissions within vehicle platoons. In terms of safety analysis, this study relies on two metrics, maximum time to collision (MTTC) and deceleration rate to avoid a crash (DRAC), to assess and contrast the security performance of platoons operating under the influence of three different UCTs. It is worth mentioning that in UCTs, vehicles only receive data from vehicles ahead of them. On the other hand, one aspect of platooning that has received limited attention in the existing literature is the transient behavior of IDs, a critical factor closely linked to platoon safety. It is worth noting that favorable transient behaviors, as well as steady-state conditions, as studied in [60], can significantly contribute to preventing intervehicular collisions and enhancing the overall safety of platooning.

Therefore, in addition to the roles of controllers, vehicle features, and initial conditions, communication structures play a pivotal role in influencing platooning dynamics, particularly their impact on transient distances between vehicles. This study thoroughly explores this critical aspect by focusing on transient intervehicle distance errors (TIDEs). In our definition, TIDEs quantify momentary deviations in spacing

between neighboring vehicles before their distances align with the intended values. Our specific investigation centers on how various bidirectional communication topologies (BDCTs) affect TIDEs, as these transient distances are paramount in determining the safety and collision-free operation of platoons. Notably, unlike unidirectional communication topologies (UCTs), BDCTs enable vehicles following one another to exchange their current state information with both preceding and succeeding vehicles. This chapter's contributions can be summarized as follows:

1. Novel Dynamic Model: We have introduced a novel closed-loop dynamic model for vehicular platoons, shifting our focus from differences between follower-leader states to differences among neighboring vehicles. This approach allows for the relaxation of the requirement for the leader vehicle's velocity to remain constant for intervehicle distance convergence and for followers to reach their desired velocities and accelerations. As a result, the key determinant for the convergence lies solely in achieving internal stability.

2. Analysis of Transient Intervehicle Distances: Our findings indicate that transient intervehicle distances are unaffected by the leader vehicle's state. Instead, they depend on crucial parameters such as initial conditions, control gains, the engine time constants of follower vehicles (FVs), the number of FVs in the platoon, and the communication type employed.

3. Analytical Distance Trajectories: We have developed analytical distance trajectories for each pair of neighboring vehicles, revealing their behavior across different bidirectional communication topologies (BDCTs).

4. Communication Topology Insights 1: We have highlighted the advantages and disadvantages of various BDCTs. Our observations suggest that, within the domain of distributed controllers, the collection of data from a greater number of vehicles ahead, especially the leading vehicle, has the potential to reduce

the likelihood of breaching safe intervehicle distances in BDCTs. Although our focus differs from the study in [87], our findings align with their conclusion, emphasizing that predecessor-leader-following (PLF) and multiple-predecessor-leader-following (MPLF) configurations are notably superior to predecessor-following (PF).

5. Communication Topology Insights 2: Conversely, incorporating information from more vehicles behind can have an adverse impact on intervehicle distances, elevating the risk of breaching the safe spacing between vehicles.

6. Enhanced Platoon Performance: We have demonstrated that broadcasting the leader vehicle's state to other vehicles has the potential to improve overall platoon performance. This leads to smaller deviations from desired values during transient states.

7. Simulation Validation: We have provided simulations to validate our theoretical findings and support our research contributions.

In summary, this chapter emphasizes the importance of studying transient intervehicle distances and their relationship with various bidirectional communication topologies.

4.1 Preliminaries

In this chapter, time-dependent signals will only be included if they enhance clarity. To differentiate between elements within vertical and horizontal vectors, we will utilize the semicolon and colon symbols, respectively. For instance, a 3-by-1 vector is symbolized as $[.;.;.]$, while a 1-by-3 vector takes the form of $[.,.,.]$. This notation will be consistently employed throughout the document to improve lucidity and ease of reading.

4.1.1 Bidirectional Communication Copologies (BDCTs)

Fig. 4.1 displays common BDCTs employed in vehicle platooning. In this context, each follower vehicle (FV) possesses the ability to communicate its state, including position, velocity, and acceleration, with both the vehicles ahead and those behind. This interplay establishes a bidirectional flow of communication across all vehicles. Subsequently, to maintain conciseness, unless specifically stated otherwise, we will collectively denote the state information of each vehicle, comprising its position, velocity, and acceleration, as simply 'information'.

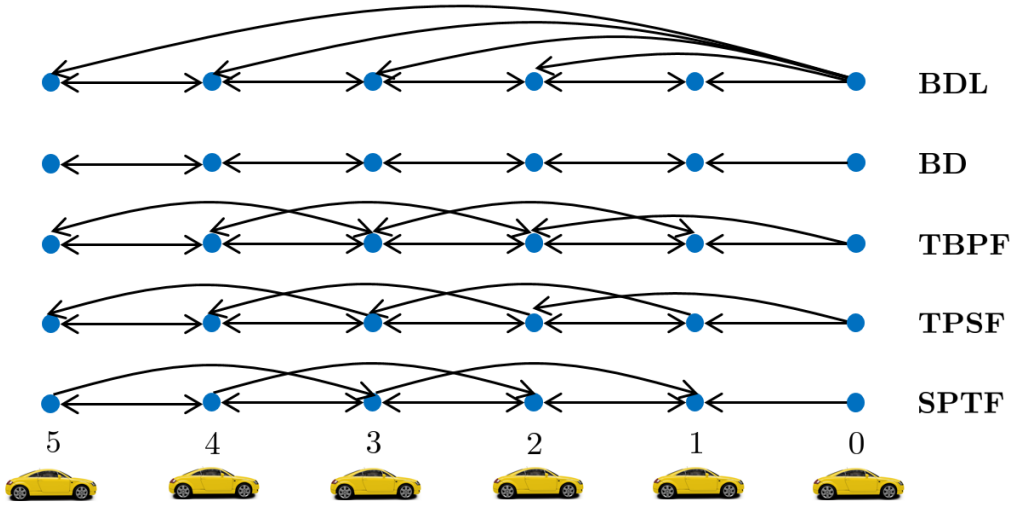

Figure 4.1: Different common BDCTs between vehicles. The leading vehicle (referred to as the leader) is designated as 0, while the FVs are labeled from 1 to 5.

In the depicted bidirectional-leader (BDL) topology in Fig. 4.1, each FV receives information from the leader vehicle. Simultaneously, every FV exchanges information with both its immediate successive and preceding vehicles. Similarly, within the bidirectional (BD) topology, each FV participates in information exchange with both its following and preceding vehicles. In the two-bidirectional-predecessor-following (TBPF) topology, each FV communicates with its two immediate followers and two immediate predecessors. In the two-predecessor-single-following (TPSF) topology, each FV obtains information from its two immediate predecessors and conveys its

own state to its following vehicle. In the single-predecessor-two-following (SPTF) topology, each FV acquires information from its predecessor and shares its state with its two immediate preceding vehicles.

Consider the platoon shown in Fig. 4.1 and, in preparation for later use, let for the pairwise vehicles $(i, i+1)$ where i ranges from 0 to $n-1$ (with $n = 5$ for the showcased platoon), the following sets be defined as:

1. $\mathbb{I}_{i+1}$: Vehicles from which the $(i+1)^{th}$ follower gets information. For example, in TPSF topology for pair (2,3), $\mathbb{I}_3$ is $\{1, 2, 4\}$.

2. $\mathbb{I}_i$: Vehicles from which the i^{th} follower obtains information. In TPSF topology for pair (2,3), $\mathbb{I}_2$ is $\{0, 1, 3\}$.

3. $\mathbb{R}_{i+1}$: Vehicles, excluding vehicle i, providing information to the $(i+1)^{th}$ follower. In SPTF topology for pair (2,3), $\mathbb{R}_3$ is $\{4, 5\}$.

4. $\mathbb{R}_i$: Vehicles, excluding vehicle $i+1$, supplying information to the i^{th} follower. In SPTF topology for pair (2,3), $\mathbb{R}_2$ is $\{1, 4\}$.

We also use z_i^j to represent the information linkage between vehicles i and j, where $z_i^j = 1$ means vehicle i gets information from vehicle j, and $z_i^j = 0$ means it does not. For TPSF topology, examples are $z_3^1 = 1$ and $z_4^1 = 0$ (Figure 4.1).

4.1.2 Representation of Constant and Changing Distances

We use a left-to-right direction for vehicle movement, designated as $\rightarrow$ for positive direction, and $\leftarrow$ for negative direction. Constant lengths or distances are represented by $\leftrightarrow$. In Figure 4.2, L_i and L_{i+1} indicate vehicle lengths, while d_i^{i+1} represents the desired constant gap between them. Variable distances s_1, s_2, s_3, and s_4 follow the formulas: $s_1 = x_i - x_{i+1}$, $s_2 = x_{i+1} - (x_i - L_i)$, $s_3 = x_{i+1}$, and $s_4 = x_i$. Here, x_i and x_{i+1} refer to the front-side positions of the vehicles.

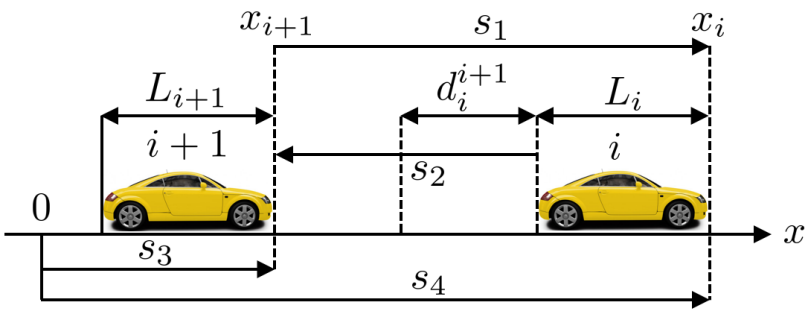

Figure 4.2: Illustrating adjacent vehicles: Vehicle $i+1$ as the follower and vehicle i as the predecessor, showing constant and changing distances.

4.1.3 Vehicles Dynamics and 'Follower-Leader' State Errors

We make the assumption that the leading vehicle does not undergo any control process. Instead, the position, velocity, and acceleration of the leading vehicle are utilized to govern the behavior of the subsequent vehicles. In this context, each following vehicle's behavior within the platoon is described mathematically using a third-order linear model [27, 31, 43, 46–48, 53, 54, 56, 57]. This model is defined as:

$$\begin{cases} \dot{x}_{i+1} = v_{i+1} \\ \dot{v}_{i+1} = a_{i+1} \\ \dot{a}_{i+1} = -\frac{1}{\tau}a_{i+1} + \frac{1}{\tau}u_{i+1} \end{cases} \qquad i = 0, \ldots, n-1 \tag{4.1}$$

Here, a_{i+1}, v_{i+1}, and τ represent the acceleration, velocity, and engine time constant of the $(i+1)^{th}$ follower. Let $\mathbf{X}_{i+1} \triangleq [x_{i+1};\ \dot{x}_{i+1};\ \ddot{x}_{i+1}]$ define the state vector of the $(i+1)^{th}$ follower, where $\dot{x}_{i+1} = v_{i+1}$ and $\ddot{x}_{i+1} = a_{i+1}$. Consequently, for $i = 0, \ldots, n-1$, and given the equation (4.1), the state-space model for the $(i+1)^{th}$ follower can be represented as:

$$\dot{\mathbf{X}}_{i+1} = \underbrace{\begin{bmatrix} 0 & 1 & 0 \\ 0 & 0 & 1 \\ 0 & 0 & -\frac{1}{\tau} \end{bmatrix}}_{\triangleq \mathbf{A}} \mathbf{X}_{i+1} + \underbrace{\begin{bmatrix} 0 \\ 0 \\ \frac{1}{\tau} \end{bmatrix}}_{\triangleq \mathbf{B}} u_{i+1} \tag{4.2}$$

The controller u_{i+1} will be discussed subsequently. For each index $i = 0, \ldots, n-1$, the desired position denoted as x^*_{i+1}, desired velocity denoted as $\dot{x}^*_{i+1}$, and desired

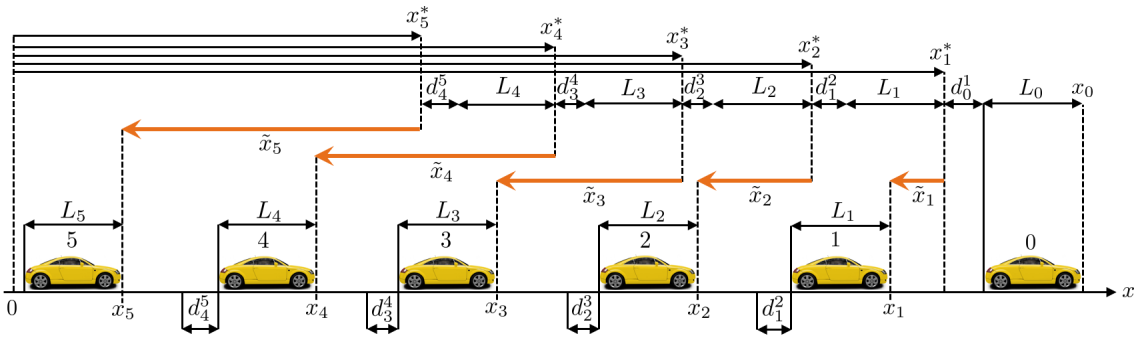

Figure 4.3: Desired positions and 'follower-leader' position errors of the follower vehicles.

acceleration denoted as $\ddot{x}_{i+1}^*$ of the $(i+1)^{th}$ follower with respect to the state of the leader vehicle are defined as follows:

$$x_{i+1}^* \triangleq x_0 - \sum_{\kappa=0}^{i}(L_\kappa + d_\kappa^{\kappa+1}), \quad \dot{x}_{i+1}^* = v_0, \text{ and } \ddot{x}_{i+1}^* = a_0 \tag{4.3}$$

regarding which let the desired state vector of the $(i+1)^{th}$ follower be denoted as $\mathbf{X}_{i+1}^* \triangleq [x_{i+1}^*;\ \dot{x}_{i+1}^*;\ \ddot{x}_{i+1}^*]$. It is important to observe that our specified reference values in (4.3) are in contrast to those presented in [27, 53, 54], where $\ddot{x}_{i+1}^*$ was set to 0. Through these considerations, the desired state of the followers are calculated with respect to the state of the leader vehicle. Therefore, let 'follower-leader' state error of the $(i+1)^{th}$ follower be defined as $\tilde{\mathbf{X}}_{i+1} \triangleq \mathbf{X}_{i+1} - \mathbf{X}_{i+1}^* = [\tilde{x}_{i+1};\ \dot{\tilde{x}}_{i+1};\ \ddot{\tilde{x}}_{i+1}]$ where $\tilde{x}_{i+1} = x_{i+1} - x_{i+1}^*$, $\dot{\tilde{x}}_{i+1} = \dot{x}_{i+1} - \dot{x}_{i+1}^*$, and $\ddot{\tilde{x}}_{i+1} = \ddot{x}_{i+1} - \ddot{x}_{i+1}^*$.

Illustrated in Fig. 4.3 is a vehicular platoon, where the desired positions and the 'follower-leader' position errors, denoted as $\tilde{x}_{i+1}$, are showcased for each follower. This presentation spans the range of $i = 0, \ldots, n-1$ (with $n = 5$ in this instance). Since state errors are calculated relative to the leading vehicle, we have $\tilde{x}_0 = \dot{\tilde{x}}_0 = \ddot{\tilde{x}}_0 = 0$.

4.1.4 Platoon Targeted-Kinematics, and Controllers

The primary goal of the controller u_{i+1} in (4.2) is to achieve synchronization between the velocities and accelerations of the follower vehicles and those of the leading vehicle. Additionally, it aims to maintain desired distances between adjacent vehicles, denoted

as d_i^{i+1}. To put it more straightforwardly, for each value of index i within the range from 0 to $n-1$, the controller has two main aims: firstly, to eliminate the 'follower-leader' state errors, and secondly, to align the velocity v_{i+1} and acceleration a_{i+1} with the velocity and acceleration of the leading vehicle, indicated as v_0 and a_0, respectively. To accomplish this dual objective, a distributed linear control law [89] is utilized. The control law can be expressed using the following equations:

$$\begin{cases} u_{i+1} = -\sum\limits_{j\in\mathbb{I}_{i+1}} k(\Delta x_{i+1}^j - d_{i+1,j}) + b\Delta\dot{x}_{i+1}^j + \Delta h\ddot{x}_{i+1}^j \\ d_{i+1,j} \triangleq -sgn(i+1-j)\sum\limits_{\kappa=\min(i+1,j)}^{\max(i+1,j)-1} l_\kappa + d_\kappa^{\kappa+1} \end{cases} \tag{4.4}$$

where $\Delta x_{i+1}^j \triangleq x_{i+1} - x_j$, $\Delta\dot{x}_{i+1}^j \triangleq \dot{x}_{i+1} - \dot{x}_j$, and $\Delta\ddot{x}_{i+1}^j \triangleq \ddot{x}_{i+1} - \ddot{x}_j$. Considering that $x_{i+1} - x_j - d_{i+1,j} = \tilde{x}_{i+1} - \tilde{x}_j$, $\dot{x}_{i+1} - \dot{x}_j = \dot{\tilde{x}}_{i+1} - \dot{\tilde{x}}_j$, and $\ddot{x}_{i+1} - \ddot{x}_j = \ddot{\tilde{x}}_{i+1} - \ddot{\tilde{x}}_j$, the controller (4.4) can be reformulated as:

$$u_{i+1} = -\sum_{j\in\mathbb{I}_{i+1}} \mathbf{K}\left(\tilde{\mathbf{X}}_{i+1} - \tilde{\mathbf{X}}_j\right) = -\sum_{j\in\mathbb{I}_{i+1}} \mathbf{K}\Delta\tilde{\mathbf{X}}_{i+1}^j \tag{4.5}$$

in which $\Delta\tilde{\mathbf{X}}_{i+1}^j \triangleq \tilde{\mathbf{X}}_{i+1} - \tilde{\mathbf{X}}_j$ and the vector $\mathbf{K} \triangleq [k,\ b,\ h]$ is introduced as the control-gain vector, which quantifies the impact of relative measurements between the $(i+1)^{th}$ follower and the vehicles transmitting information to it.

4.1.5 Platoon Dynamics, and Internal Stability

To find the platoon closed-loop dynamics, first noting that $\ddot{x}_{i+1} = \ddot{\tilde{x}}_{i+1} + a_0$ and $\dddot{x}_{i+1} = \dddot{\tilde{x}}_{i+1} + \dot{a}_0$, and plugging (4.5) in (4.1), for $i = 0, \ldots, n-1$, yields (See Appendix B)

$$\dddot{\tilde{x}}_{i+1} = -\frac{1}{\tau}\mathbb{K}_{i+1}\tilde{\mathbf{X}}_{i+1} + \sum_{j\in\mathbb{I}_{i+1}} \frac{1}{\tau}\mathbf{K}\tilde{\mathbf{X}}_j + \epsilon_{i+1} \tag{4.6}$$

in which $\epsilon_{i+1} \triangleq -\frac{1}{\tau}a_0(t) - \dot{a}_0(t)$ and $\mathbb{K}_{i+1} \triangleq [\mathbf{k}_{i+1},\ \mathbf{b}_{i+1},\ \mathbf{h}_{i+1}]$ such that

$$\mathbf{k}_{i+1} \triangleq |\mathbb{I}_{i+1}|k,\ \ \mathbf{b}_{i+1} \triangleq |\mathbb{I}_{i+1}|b,\ \ \mathbf{h}_{i+1} \triangleq 1 + |\mathbb{I}_{i+1}|h \tag{4.7}$$

where $|\mathbb{I}_{i+1}|$ denotes the cardinality of the set $\mathbb{I}_{i+1}$. Now, considering (4.6), knowing $\tilde{x}_0 = \dot{\tilde{x}}_0 = \ddot{\tilde{x}}_0 = 0$, and defining the platoon's total 'follower-leader' state-error vector by $\tilde{\mathbf{X}}_t \triangleq [\tilde{\mathbf{X}}_1;\ \tilde{\mathbf{X}}_2; \ldots,\ \tilde{\mathbf{X}}_n]$, then the platoon's closed-loop state-space dynamic model can be compactly characterized by

$$\dot{\tilde{\mathbf{X}}}_t = \underbrace{[\mathbf{I}_n \otimes \mathbf{A} - \mathbf{P} \otimes \mathbf{BK}]}_{\mathbf{A}_t} \tilde{\mathbf{X}}_t + \underbrace{\mathbf{I}_{3n}}_{\triangleq \mathbf{B}_t} \underbrace{\mathbf{Vec}(\boldsymbol{\epsilon}_1, \boldsymbol{\epsilon}_2, \ldots, \boldsymbol{\epsilon}_n)}_{\triangleq \mathbf{u}_t} \tag{4.8}$$

in which $\mathbf{Vec}(\boldsymbol{\epsilon}_1, \boldsymbol{\epsilon}_2, \ldots, \boldsymbol{\epsilon}_n) = [\boldsymbol{\epsilon}_1; \boldsymbol{\epsilon}_2, \ldots; \boldsymbol{\epsilon}_n]$ where for $i = 0, \ldots, n-1$, $\boldsymbol{\epsilon}_{i+1} \triangleq [0; 0; \epsilon_{i+1}]$, $\mathbf{I}_{3n}$ is the identity matrix of size $3n$, and $\mathbf{P} \in R^{n \times n}$ whose elements $p_{\kappa j}$ are according to

$$p_{\kappa j} = \begin{cases} |\mathbb{I}_\kappa| & \text{if} \quad \kappa = j \\ 0 & \text{if} \quad z_\kappa^j = 0 \\ -1 & \text{if} \quad z_\kappa^j = 1 \end{cases} \tag{4.9}$$

where $\kappa, j = 1, \ldots, n$ and $|\mathbb{I}_\kappa|$ shows the cardinality of the set $\mathbb{I}_\kappa$.

Remark 1 *Given* (4.9) *and Fig. 4.1, for BDCTs: BDL, BD and TBPF, since the communication between followers is undirected, i.e.,* $j \in \mathbb{I}_i \iff i \in \mathbb{I}_j$, $i, j = 1, \ldots, n-1$, *then the matrix* $\mathbf{P}$ *has only real eigenvalues* (λ_i, $i = 1, \ldots, n$) *[27]. Also, for BDCTs: TPSF and SPTF, the matrix* $\mathbf{P}$ *has combination of real* ($\bar{\lambda}_i$, $i = 1, \ldots, l$) *and conjugate complex* ($\sigma_i \pm j\omega_i$, $i = 1, \ldots, \frac{n-l}{2}$) *eigenvalues [53].*

Remark 2 *For those BDCTs in which the matrix* $\mathbf{P}$ *has only real eigenvalues, the platoon dynamics* (4.8) *would be asymptotically stable if and only if the resultant matrices*

$$\mathbf{A} - \lambda_i \mathbf{BK} \tag{4.10}$$

are all Hurwitz, i.e., their eigenvalues are all negative [27]. Note that λ_i; $i = 1, \ldots, n-1$, *denote the eigenvalues of the matrix* $\mathbf{P}$. *Given that* $k, b, h > 0$, *using Routh-Hurwitz stability criterion, the following condition can be found for the internal stability of the platoon:*

$$b > \frac{k\tau}{1 + \lambda_{min} h} \tag{4.11}$$

where $\lambda_{min} = \min_i\{\lambda_i\}$.

Remark 3 *For those BDCTs in which the eigenvalues of the matrix* $\mathbf{P}$ *are combination of real and conjugate complex values, the platoon dynamics* (4.8) *would be asymptotically stable if and only if the following resultant matrices*

$$\begin{cases} 1)\mathbf{A} - \bar{\lambda}_i \mathbf{BK} & i = 1, \ldots, l \\ 2)\mathbf{I}_2 \otimes \mathbf{A} - \begin{bmatrix} \sigma_i & \omega_i \\ \omega_i & \sigma_i \end{bmatrix} \otimes \mathbf{BK} & i = 1, \ldots, \frac{n-l}{2} \end{cases} \tag{4.12}$$

are all Hurwitz, i.e., their eigenvalues are all negative [53]. Note that in (4.12)*, the second matrix would result in a characteristic polynomial of degree six.*

Remark 4 *Internal stability in platooning ensures that vehicle states (positions, velocities, and accelerations) remain bounded over time for any bounded input. However, it does not guarantee collision-free distances between vehicles, as we will show with examples. Meeting internal stability conditions is crucial for stable platoon behavior but does not always prevent collisions or unsafe distances caused by control gains that meet these conditions. In simpler terms, relying solely on an internally stable platoon will not guarantee favorable transient spacing between vehicles or even transient speeds and accelerations of the FVs. To reiterate, 'transient' simply pertains to the duration of trajectories before they reach their desired values.*

Remark 5 *Considering* (4.8)*, when* $a_0(t) = 0$*, we arrive at* $\dot{\tilde{\mathbf{X}}}_t = \mathbf{A}_t \tilde{\mathbf{X}}_t$*. Ensuring the internal stability conditions are met will lead to* $\tilde{\mathbf{X}}_t$ *converging to zero in a steady state, which implies that* $x_{i+1}(t) = x^*_{i+1}(t)$*,* $\dot{x}_{i+1}(t) = \dot{x}^*_{i+1}(t)$*, and* $\ddot{x}_{i+1}(t) = \ddot{x}^*_{i+1}(t)$ *for* $i = 0, \ldots, n-1$*. However, if* $a_0 \neq 0$ *in a steady state, the control input* $\mathbf{u}_t$ *will impact the convergence of IDs as well as the follower's velocities and accelerations toward their desired values. Nevertheless, we will demonstrate that by employing a state coordinate transformation, the new states become independent of the leader vehicle's acceleration and jerk trajectories. Consequently, even if* $a_0 \neq 0$ *in a steady state, satisfying the internal stability conditions will still be sufficient for achieving convergence of IDs, velocities, and accelerations to their desired values.*

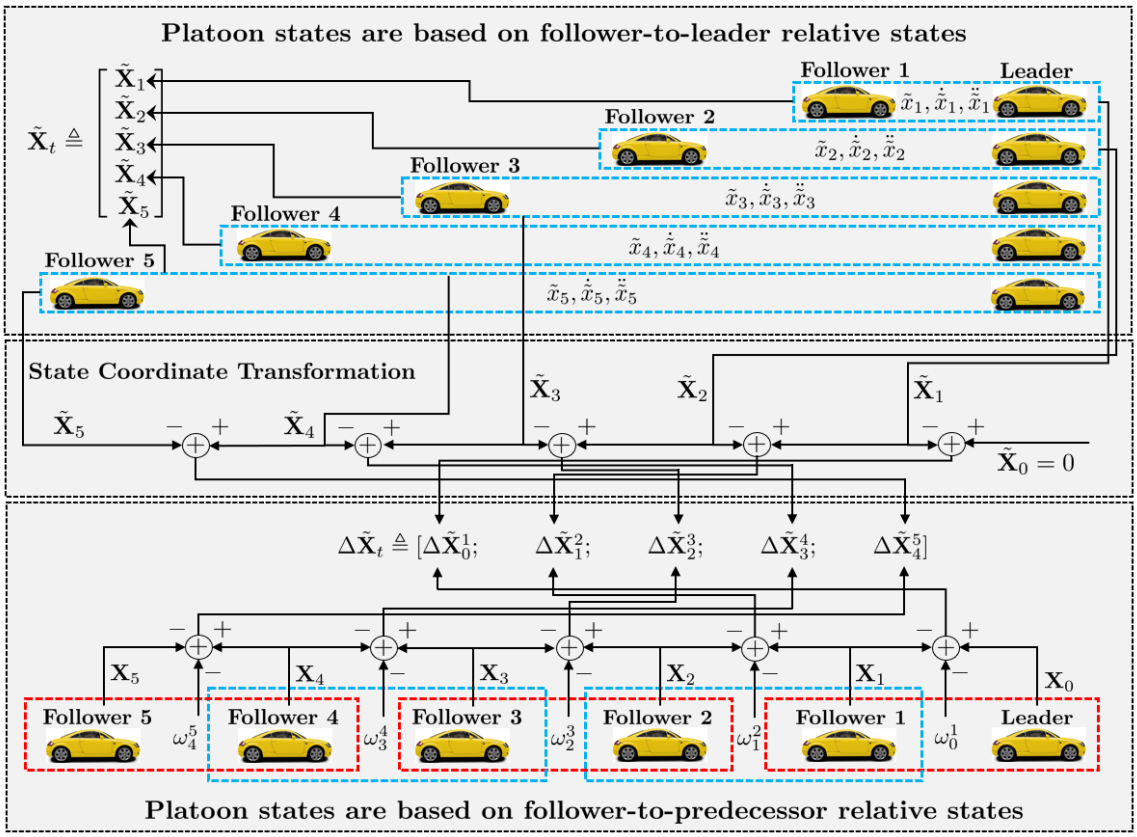

Figure 4.4: State coordinate transformation from 'follower-leader' errors to 'follower-predecessor' errors.

4.2 State Coordinate Transformation

Highlighting the platoon's dynamics, the closed-loop dynamics (4.8) emerges through the incorporation of established state errors between the 'follower' and 'leader' units. These errors are denoted as $\tilde{\mathbf{X}}_{i+1}$ where $i = 0, \ldots, n-1$, and their visual representation can be observed in Fig. 4.3. Nevertheless, achieving internal stability does not inherently safeguard against momentary variable distances among neighboring vehicles dropping below a safe threshold before attaining a desired intervehicle spacing. On the other hand, the 'follower-leader' state errors do not provide direct information about the state differences between adjacent vehicles. As such and as far as safety and collision concerned, we need to have a direct formulation for distance between every neighboring vehicles.

Adding to this, the visual representation of 'follower-leader' position errors, as evident in Fig. 4.3, not only lacks an intuitive portrayal of distances between adjacent vehicles but also inadequately facilitates direct analysis of transient intervehicle distances (TIDs). To establish a comprehensive framework surpassing internal stability considerations and fostering an intuitive TIDs examination, we undertake a transformation of previous state coordinates from 'follower-leader' errors to 'follower-predecessor' errors. This transformation yields 'follower-predecessor' errors derived from consecutive 'follower-leader' errors, exemplified in Fig. 4.4. An instance of this is the 'follower-predecessor' error between followers 1 and 2, derived from the 'follower#1-leader' and 'follower#2-leader' pairs.

According to this coordinate transformation, we introduce coupled position, velocity, acceleration, and jerk errors between neighboring vehicles i and $i+1$ as follows: 1. Coupled position error: Denoted as $\Delta\tilde{p}_i^{i+1} \triangleq \tilde{x}_i - \tilde{x}_{i+1}$, representing the difference in position errors. 2. Coupled velocity error: Denoted as $\Delta\tilde{v}_i^{i+1} \triangleq \dot{\tilde{x}}_i - \dot{\tilde{x}}_{i+1}$, signifying the difference in velocity errors. 3. Coupled acceleration error: Denoted as $\Delta\tilde{a}_i^{i+1} \triangleq \ddot{\tilde{x}}_i - \ddot{\tilde{x}}_{i+1}$, representing the difference in acceleration errors. 4. Coupled jerk error: Denoted as $\Delta\tilde{\jmath}_i^{i+1} \triangleq \dddot{\tilde{x}}_i - \dddot{\tilde{x}}_{i+1}$, indicating the difference in jerk errors. With these formulations, the 'follower-predecessor' state error and its derivative for neighboring vehicles i and $i+1$ can be expressed as follows:

$$\begin{aligned} \Delta\tilde{\mathbf{X}}_i^{i+1} &\triangleq \tilde{\mathbf{X}}_i - \tilde{\mathbf{X}}_{i+1} \triangleq \left[\Delta\tilde{p}_i^{i+1}; \Delta\tilde{v}_i^{i+1}; \Delta\tilde{a}_i^{i+1}\right] \\ \Delta\dot{\tilde{\mathbf{X}}}_i^{i+1} &\triangleq \dot{\tilde{\mathbf{X}}}_i - \dot{\tilde{\mathbf{X}}}_{i+1} \triangleq \left[\Delta\tilde{v}_i^{i+1}; \Delta\tilde{a}_i^{i+1}; \Delta\tilde{\jmath}_i^{i+1}\right] \end{aligned} \tag{4.13}$$

Using these error terms, we derive the coupled distance dynamics governing neighboring vehicles in BDCTs. We will refer to $\Delta\tilde{p}_i^{i+1}(.)$ as the transient intervehicle distance error (TIDE) between vehicles i and $i+1$ in both the time and Laplace domains. Importantly, 'follower-predecessor' state errors between vehicles i and j (where $j > i$) can be expressed as $\Delta\tilde{\mathbf{X}}_i^j \triangleq \tilde{\mathbf{X}}_i - \tilde{\mathbf{X}}_j$.

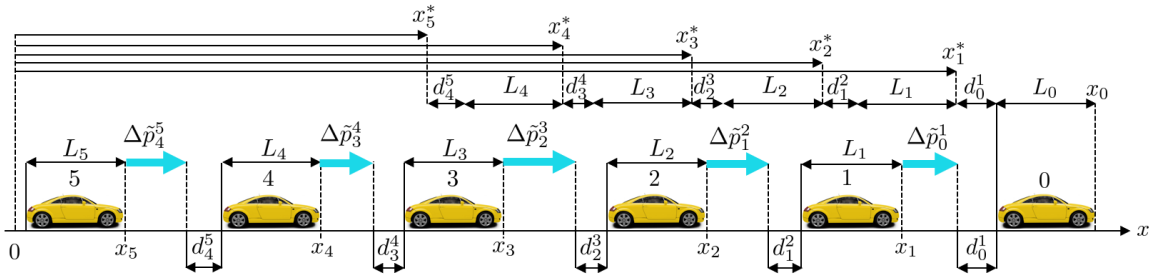

Figure 4.5: Desired positions and 'follower-leader' position errors of the follower vehicles.

4.3 Platoon Distance Dynamic model

In this section, we present an alternative dynamic model based on (4.8), sharing the previously mentioned internal stability conditions (Remarks 2-3). This model enables the examination of TIDEs and the determination of control gains to prevent collisions and maintain safe spacing between vehicles. To extract the dynamics governing neighboring vehicles' behavior under BDCTs (as shown in Fig. 4.1), we consider a small sampling time $0 < \Delta t \ll 1$ and apply the Euler method, yielding:

$$\frac{\Delta\tilde{\mathbf{X}}_i^{i+1}(t+\Delta t) - \Delta\tilde{\mathbf{X}}_i^{i+1}(t)}{\Delta t} \approx \Delta\dot{\tilde{\mathbf{X}}}_i^{i+1}(t) \tag{4.14}$$

To find the coupled dynamics of pairwise neighboring vehicles i and $i+1$, we need $\Delta\tilde{\mathbb{J}}_i^{i+1}$ for $i = 0, 1, \ldots, n-1$.

Theorem 6 *For $i = 0, \ldots, n-1$, the coupled jerk error between neighboring vehicles i and $i+1$ under BDCTs (Fig. 4.3) is given by:*

$$\Delta\tilde{\mathbb{J}}_i^{i+1} = -\frac{1}{\tau}\mathbb{J}_i\Delta\tilde{\mathbf{X}}_i^{i+1} + \frac{1}{\tau}\mathbf{K}\sum_{j\in\alpha_i}\sum_{\kappa=j}^{i-1}\Delta\tilde{\mathbf{X}}_\kappa^{\kappa+1} + \frac{1}{\tau}\mathbf{K}\sum_{j\in\beta_i}\sum_{\kappa=i+1}^{j-1}\Delta\tilde{\mathbf{X}}_\kappa^{\kappa+1} \tag{4.15}$$

In this equation, $\mathbb{J}_i$ is defined as $[|\mathbf{J}_i|k,\ |\mathbf{J}_i|b,\ 1+|\mathbf{J}_i|h]$, where $|\mathbf{J}_i|$ is determined as follows:

$$|\mathbf{J}_i| = \begin{cases} |\mathbb{I}_i| & \text{if} \quad \beta_i = \emptyset \ \& \ i \neq 0 \\ 1 & \text{if} \quad i = 0 \\ |\mathbb{I}_{i+1}| & \text{if} \quad \beta_i \neq \emptyset \ \& \ i \neq 0 \end{cases} \tag{4.16}$$

The sets α_i and β_i are defined as $\alpha_i \triangleq \{j \in \mathbb{R}_i \mid z_i^j = 1 \,\&\, z_{i+1}^j = 0 \,\&\, j < i\}$ and $\beta_i \triangleq \{j \in \mathbb{R}_{i+1} \mid z_{i+1}^j = 1 \,\&\, z_i^j = 0 \,\&\, j > i+1\}$, respectively. Refer to Table 4.1 for sets α_i, β_i, and $|\mathbb{I}_{i+1}|$ values for the platoon under BDCTs (Fig. 4.1).

Proof. For $i = 1, \ldots, n-1$, using (4.6), we have

$$\begin{cases} \dddot{\tilde{x}}_i = -\frac{1}{\tau}\mathbb{K}_i\tilde{\mathbf{X}}_i + \frac{1}{\tau}\sum_{j\in\mathbb{I}_i}\mathbf{K}\tilde{\mathbf{X}}_j + \boldsymbol{\epsilon}_i \\ \dddot{\tilde{x}}_{i+1} = -\frac{1}{\tau}\mathbb{K}_{i+1}\tilde{\mathbf{X}}_{i+1} + \frac{1}{\tau}\sum_{j\in\mathbb{I}_{i+1}}\mathbf{K}\tilde{\mathbf{X}}_j + \boldsymbol{\epsilon}_{i+1} \end{cases} \tag{4.17}$$

Therefore, given $\boldsymbol{\epsilon}_i = \boldsymbol{\epsilon}_{i+1}$ and $\Delta\tilde{\mathbf{J}}_i^{i+1} \triangleq \dddot{\tilde{x}}_i - \dddot{\tilde{x}}_{i+1}$, we get

$$\Delta\tilde{\mathbf{J}}_i^{i+1} = -\frac{1}{\tau}\mathbb{K}_i\Delta\tilde{\mathbf{X}}_i^{i+1} - \frac{1}{\tau}\left(\mathbb{K}_i - \mathbb{K}_{i+1}\right)\tilde{\mathbf{X}}_{i+1} + \sum_{j\in\mathbb{I}_i}\frac{1}{\tau}\mathbf{K}\tilde{\mathbf{X}}_j - \sum_{j\in\mathbb{I}_{i+1}}\frac{1}{\tau}\mathbf{K}\tilde{\mathbf{X}}_j \tag{4.18}$$

Since $-\frac{1}{\tau}\left(\mathbb{K}_i - \mathbb{K}_{i+1}\right) = \sum_{j\in\mathbb{I}_{i+1}}\frac{1}{\tau}\mathbf{K} - \sum_{j\in\mathbb{I}_i}\frac{1}{\tau}\mathbf{K}$ then (4.18) can be rewritten as

$$\Delta\tilde{\mathbf{J}}_i^{i+1} = -\frac{1}{\tau}\mathbb{K}_i\Delta\tilde{\mathbf{X}}_i^{i+1} + \sum_{j\in\mathbb{I}_i}\frac{1}{\tau}\mathbf{K}\Delta\tilde{\mathbf{X}}_j^{i+1} - \sum_{j\in\mathbb{I}_{i+1}}\frac{1}{\tau}\mathbf{K}\Delta\tilde{\mathbf{X}}_j^{i+1} \tag{4.19}$$

Also, as $\tilde{\mathbf{X}}_j - \tilde{\mathbf{X}}_{i+1} = \tilde{\mathbf{X}}_j - \tilde{\mathbf{X}}_i + \tilde{\mathbf{X}}_i - \tilde{\mathbf{X}}_{i+1}$, (4.19) can be reformulated as

Table 4.1: Sets α_i and β_i, and values of $|\mathbb{I}_{i+1}|$ and $|\mathbf{J}_i|$ for the platoon and BDCTs given in Fig. 4.1.

Pairs:	$(0,1)$	$(1,2)$	$(2,3)$	$(3,4)$	$(4,5)$
	$\{\alpha_0,\beta_0\}$ & $\lvert\mathbb{I}_1\rvert$ & $\lvert\mathbf{J}_0\rvert$	$\{\alpha_1,\beta_1\}$ & $\lvert\mathbb{I}_2\rvert$ & $\lvert\mathbf{J}_1\rvert$	$\{\alpha_2,\beta_2\}$ & $\lvert\mathbb{I}_3\rvert$ & $\lvert\mathbf{J}_2\rvert$	$\{\alpha_3,\beta_3\}$ & $\lvert\mathbb{I}_4\rvert$ & $\lvert\mathbf{J}_3\rvert$	$\{\alpha_4,\beta_4\}$ & $\lvert\mathbb{I}_5\rvert$ & $\lvert\mathbf{J}_4\rvert$
BDL	$\{\emptyset,\{2\}\}$ & 2 & 1	$\{\emptyset,\{3\}\}$ & 3 & 3	$\{\{1\},\{4\}\}$ & 3 & 3	$\{\{2\},\{5\}\}$ & 3 & 3	$\{\{3\},\emptyset\}$ & 2 & 3
BD	$\{\emptyset,\{2\}\}$ & 2 & 1	$\{\{0\},\{3\}\}$ & 2 & 2	$\{\{1\},\{4\}\}$ & 2 & 2	$\{\{2\},\{5\}\}$ & 2 & 2	$\{\{3\},\emptyset\}$ & 1 & 2
TBPF	$\{\emptyset,\{2,3\}\}$ & 3 & 1	$\{\emptyset,\{4\}\}$ & 4 & 4	$\{\{0\},\{5\}\}$ & 4 & 4	$\{\{1\},\emptyset\}$ & 3 & 4	$\{\{2\},\emptyset\}$ & 2 & 3
TPSF	$\{\emptyset,\{2\}\}$ & 2 & 1	$\{\emptyset,\{3\}\}$ & 3 & 3	$\{\{0\},\{4\}\}$ & 3 & 3	$\{\{1\},\{5\}\}$ & 3 & 3	$\{\{2\},\emptyset\}$ & 2 & 3
SPTF	$\{\emptyset,\{2,3\}\}$ & 3 & 1	$\{\{0\},\{4\}\}$ & 3 & 3	$\{\{1\},\{5\}\}$ & 3 & 3	$\{\{2\},\emptyset\}$ & 2 & 3	$\{\{3\},\emptyset\}$ & 1 & 2

$$\Delta\tilde{\mathbf{J}}_i^{i+1} = \frac{1}{\tau}\left(-\left(\mathbb{K}_i + \mathbf{K}\right) + \sum_{j\in\mathbb{R}_i}\mathbf{K} - \sum_{j\in\mathbb{R}_{i+1}}\mathbf{K}\right)\Delta\tilde{\mathbf{X}}_i^{i+1} + \sum_{j\in\mathbb{R}_i}\frac{1}{\tau}\mathbf{K}\Delta\tilde{\mathbf{X}}_j^{i} - \sum_{j\in\mathbb{R}_{i+1}}\frac{1}{\tau}\mathbf{K}\Delta\tilde{\mathbf{X}}_j^{i} \tag{4.20}$$

Note that for the given BDCTs we have $\mathbb{I}_i = \mathbb{R}_i \cup \{i+1\}$ and $\mathbb{I}_{i+1} = \mathbb{R}_{i+1} \cup \{i\}$. Splitting $j \in \mathbb{R}_i$ and $j \in \mathbb{R}_{i+1}$ in two parts, i.e., $j < i$ and $j > i+1$, and using the

fact that for part $j > i+1$, we have $\mathbf{X}_j - \tilde{\mathbf{X}}_i = \mathbf{X}_j - \tilde{\mathbf{X}}_{i+1} - \left(\tilde{\mathbf{X}}_i - \tilde{\mathbf{X}}_{i+1}\right)$, (4.20) can be reformulated as

$$\begin{aligned}\Delta\tilde{\mathbb{J}}_i^{i+1} =& \frac{1}{\tau}\left(-\left(\mathbb{K}_i + \mathbf{K}\right) + \sum_{j\in\mathbb{R}_i<i}\mathbf{K} - \sum_{j\in\mathbb{R}_{i+1}<i}\mathbf{K}\right)\Delta\tilde{\mathbf{X}}_i^{i+1} + \sum_{j\in\mathbb{R}_i<i}\frac{1}{\tau}\mathbf{K}\Delta\tilde{\mathbf{X}}_j^{i} - \\ & \sum_{j\in\mathbb{R}_{i+1}<i}\frac{1}{\tau}\mathbf{K}\Delta\tilde{\mathbf{X}}_j^{i} + \sum_{j\in\mathbb{R}_{i+1}>i+1}\frac{1}{\tau}\mathbf{K}\Delta\tilde{\mathbf{X}}_{i+1}^{j} - \sum_{j\in\mathbb{R}_i>i+1}\frac{1}{\tau}\mathbf{K}\Delta\tilde{\mathbf{X}}_{i+1}^{j}\end{aligned} \tag{4.21}$$

Remark 7 *In the context of the provided BDCTs, when we examine any pair $(i, i+1)$, one of the following conditions holds: 1. Both the i^{th} and $(i+1)^{th}$ vehicles receive information from vehicles either ahead or behind them. 2. Only the i^{th} vehicle receives information from specific vehicles ahead, while the $(i+1)^{th}$ vehicle does not. 3. Only the $(i+1)^{th}$ vehicle acquires information from specific vehicles behind, while the i^{th} vehicle does not.*

Given Remark 7, and sets α_i and β_i, (4.21) can be simplified to

$$\Delta\tilde{\mathbb{J}}_i^{i+1} = \frac{1}{\tau}\left(-\left(\mathbb{K}_i + \mathbf{K}\right) + \sum_{j\in\alpha_i}\mathbf{K}\right)\Delta\tilde{\mathbf{X}}_i^{i+1} + \sum_{j\in\alpha_i}\frac{1}{\tau}\mathbf{K}\Delta\tilde{\mathbf{X}}_j^{i} + \sum_{j\in\beta_i}\frac{1}{\tau}\mathbf{K}\Delta\tilde{\mathbf{X}}_{i+1}^{j} \tag{4.22}$$

Having $|\alpha_i|$ as the cardinality of the set α_i, (4.22) can be reformulated as

$$\Delta\tilde{\mathbb{J}}_i^{i+1} = -\frac{1}{\tau}\left(\mathbb{K}_i + \mathbf{K} - |\alpha_i|\mathbf{K}\right)\Delta\tilde{\mathbf{X}}_i^{i+1} + \sum_{j\in\alpha_i}\frac{1}{\tau}\mathbf{K}\Delta\tilde{\mathbf{X}}_j^{i} + \sum_{j\in\beta_i}\frac{1}{\tau}\mathbf{K}\Delta\tilde{\mathbf{X}}_{i+1}^{j} \tag{4.23}$$

On the other hand, for $i = 1, \ldots, n-1$ and BDCTs, we have

$$\begin{cases}|\mathbb{I}_{i+1}| = |\mathbb{I}_i| - 1 \;\&\; |\alpha_i| = 1 \text{if} \quad \beta_i = \emptyset \\ |\mathbb{I}_{i+1}| = |\mathbb{I}_i| + (1 - |\alpha_i|) \;\&\; |\beta_i| = 1 \text{if} \quad \beta_i \neq \emptyset\end{cases} \tag{4.24}$$

which implies that

$$\mathbb{K}_i + \mathbf{K} - |\alpha_i|\mathbf{K} = \begin{cases}\mathbb{K}_i & \text{if} \quad \beta_i = \emptyset \\ \mathbb{K}_{i+1} & \text{if} \quad \beta_i \neq \emptyset\end{cases} \tag{4.25}$$

Therefore, given (4.24), (4.23) can be rewritten as

$$\Delta\tilde{\mathbb{J}}_i^{i+1} = \begin{cases}-\frac{1}{\tau}\mathbb{K}_i\Delta\tilde{\mathbf{X}}_i^{i+1} + \sum_{j\in\alpha_i}\frac{1}{\tau}\mathbf{K}\Delta\tilde{\mathbf{X}}_j^{i}; \beta_i = \emptyset \\ -\frac{1}{\tau}\mathbb{K}_{i+1}\Delta\tilde{\mathbf{X}}_i^{i+1} + \sum_{j\in\alpha_i}\frac{1}{\tau}\mathbf{K}\Delta\tilde{\mathbf{X}}_j^{i} + \sum_{j\in\beta_i}\frac{1}{\tau}\mathbf{K}\Delta\tilde{\mathbf{X}}_{i+1}^{j}; \beta_i \neq \emptyset\end{cases} \tag{4.26}$$

Now, given that for the pair $(i, i+1)$, $\Delta\tilde{\mathbf{X}}_j^i$ and $\Delta\tilde{\mathbf{X}}_{i+1}^j$ can be rewritten in the following form:

$$\begin{cases} \Delta\tilde{\mathbf{X}}_j^i = \sum_{\kappa=j}^{i-1} \Delta\tilde{\mathbf{X}}_\kappa^{\kappa+1}; & j < i \\ \Delta\tilde{\mathbf{X}}_{i+1}^j = \sum_{\kappa=i+1}^{j-1} \Delta\tilde{\mathbf{X}}_\kappa^{\kappa+1}; & j > i+1 \end{cases} \tag{4.27}$$

then substituting (4.27) into (4.26) yields

$$\Delta\tilde{\mathbb{J}}_i^{i+1} = \begin{cases} -\frac{1}{\tau}\mathbb{K}_i\Delta\tilde{\mathbf{X}}_i^{i+1} + \frac{1}{\tau}\mathbf{K}\sum_{j\in\alpha_i}\sum_{\kappa=j}^{i-1}\Delta\tilde{\mathbf{X}}_\kappa^{\kappa+1}; \beta_i = \emptyset \\ -\frac{1}{\tau}\mathbb{K}_{i+1}\Delta\tilde{\mathbf{X}}_i^{i+1} + \frac{1}{\tau}\mathbf{K}\sum_{j\in\alpha_i}\sum_{\kappa=j}^{i-1}\Delta\tilde{\mathbf{X}}_\kappa^{\kappa+1} + \frac{1}{\tau}\mathbf{K}\sum_{j\in\beta_i}\sum_{\kappa=i+1}^{j-1}\Delta\tilde{\mathbf{X}}_\kappa^{\kappa+1}; \beta_i \neq \emptyset \end{cases} \tag{4.28}$$

Now, let us study the pair $(0, 1)$. For the given BDCTs, given that $\tilde{\mathbf{X}}_0 = 0$ we have

$$\begin{aligned} \Delta\tilde{\mathbb{J}}_0^1 &= -\frac{1}{\tau}\mathbb{K}_1\Delta\tilde{\mathbf{X}}_0^1 - \frac{1}{\tau}\sum_{j\in\mathbb{R}_1}\mathbf{K}\tilde{\mathbf{X}}_j = -\frac{1}{\tau}\mathbb{K}_1\Delta\tilde{\mathbf{X}}_0^1 + \frac{1}{\tau}\sum_{j\in\mathbb{R}_1\geq 2}\mathbf{K}\left(\Delta\tilde{\mathbf{X}}_0^1 + \Delta\tilde{\mathbf{X}}_1^j\right) \\ &= -\frac{1}{\tau}\left(\mathbb{K}_1 - |\beta_0|\mathbf{K}\right)\Delta\tilde{\mathbf{X}}_0^1 + \frac{1}{\tau}\sum_{j\in\beta_0}\mathbf{K}\Delta\tilde{\mathbf{X}}_1^j \end{aligned} \tag{4.29}$$

where $\beta_0 \triangleq \{j \in \mathbb{R}_1 | j \geq 2\}$. Also, for the pair $(0, 1)$, since $|\beta_0| = |\mathbb{I}_1| - (1 - |\alpha_0|)$, then $\mathbb{K}_1 - |\beta_0|\mathbf{K} = \mathbb{K}$, where $\mathbb{K} \triangleq [k,\ b,\ 1+h]$. Therefore, (4.29) can be rewritten as

$$\Delta\tilde{\mathbb{J}}_0^1 = -\frac{1}{\tau}\mathbb{K}\Delta\tilde{\mathbf{X}}_0^1 + \frac{1}{\tau}\mathbf{K}\sum_{j\in\beta_0}\sum_{\kappa=1}^{j-1}\Delta\tilde{\mathbf{X}}_\kappa^{\kappa+1} \tag{4.30}$$

Subsequently (4.28) and (4.30) can be unified as a single formula. Let the set $\mathbf{J}_i$ be defined as $\mathbf{J}_i \triangleq \{j \mid j \leq i\ \&\ z_{i+1}^j = 1\} \cup \{j \mid j \geq i+1\ \&\ z_i^j = 1\}$; $i = 0, \ldots, n-1$. For $i = 1, \ldots, n-1$, first we split the set $\mathbf{J}_i$ in two sets: $\mathbf{M}_i \triangleq \{j \mid j \leq i\ \&\ z_{i+1}^j = 1\}$ and $\mathbf{B}_i \triangleq \{j \mid j \geq i+1\ \&\ z_i^j = 1\}$, such that $\mathbf{J}_i = \mathbf{M}_i \cup \mathbf{B}_i$. Figs. 4.6a-4.6b depicts these sets, respectively. Regarding the definition $\beta_i \triangleq \{j \in \mathbb{R}_{i+1} \mid z_{i+1}^j = 1\ \&\ z_i^j = 0\ \&\ j > i+1\}$, we have two cases for the pair $(i, i+1)$; $i = 1, \ldots, n-1$:

Case 1: $\beta_i = \emptyset$

Having $\beta_i = \emptyset$ implies that the followers behind from which the $(i+1)^{th}$ follower receives information (the followers $\mathbb{I}_{i+1} - \mathbf{M}_i$, see Fig. 4.6a), also send information

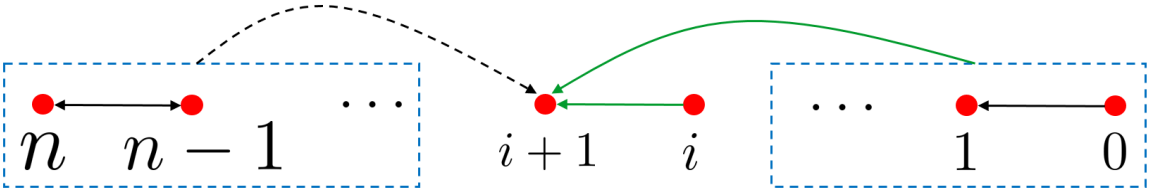

(a) $\mathbf{M}_i \triangleq \{j \mid j \leq i \;\&\; z_{i+1}^j = 1\}$ which is depicted with solid green arrows. The dashed black arrow represents the followers $\mathbb{I}_{i+1} - \mathbf{M}_i$ from which the $(i+1)^{th}$ follower receives information.

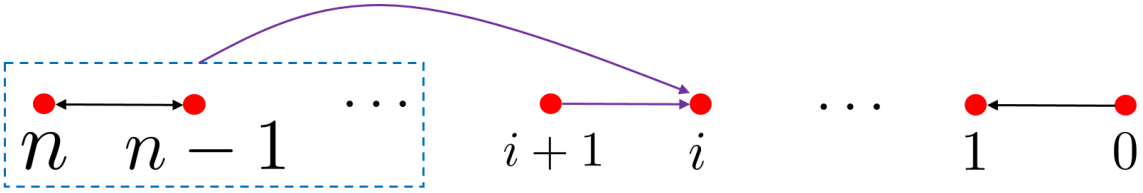

(b) $\mathbf{B}_i \triangleq \{j \mid j \geq i+1 \;\&\; z_i^j = 1\}$ which is depicted with solid purple arrows.

Figure 4.6: Illustration of sets $\mathbf{M}_i$ and $\mathbf{B}_i$

to the i^{th} follower. Therefore, the set $\mathbf{B}_i$ (see Fig. 4.6b) can be obtained as $\mathbf{B}_i = \{i+1\} \cup (\mathbb{I}_{i+1} - \mathbf{M}_i)$. It is clear that $|\mathbf{J}_i| = |\mathbf{M}_i| + |\mathbf{B}_i|$ in which $|.|$ denotes the cardinality of the sets. As such, we have $|\mathbf{B}_i| = 1 + |\mathbb{I}_{i+1}| - |\mathbf{M}_i|$ and, therefore, $|\mathbf{J}_i| = 1 + |\mathbb{I}_{i+1}| = |\mathbb{I}_i|$ (see (4.24)).

Case 2: $\beta_i \neq \emptyset$

Having $\beta_i \neq \emptyset$ implies that the followers behind (other than the $(i+1)^{th}$ follower) from which the i^{th} follower receives information are only $\mathbb{I}_{i+1} - \mathbf{M}_i - \beta_i$. Therefore, $\mathbf{B}_i = \{i+1\} \cup (\mathbb{I}_{i+1} - \mathbf{M}_i - \beta_i)$, and thus $|\mathbf{B}_i| = 1 + |\mathbb{I}_{i+1}| - |\mathbf{M}_i| - |\beta_i|$ and $|\mathbf{J}_i| = |\mathbf{M}_i| + |\mathbf{B}_i| = 1 + |\mathbb{I}_{i+1}| - |\beta_i| = |\mathbb{I}_{i+1}|$ (see (4.24)).

Finally, given the definition of the set $\mathbf{J}_i$, we always have $\mathbf{J}_0 = \{0\}$ and therefore $|\mathbf{J}_0| = 1$. Thus, for $i = 0, \ldots, n-1$, (4.28) and (4.30) can be unified and the unified coupled jerk error between the neighboring vehicles i and $i+1$ under the BDCTs given in Fig. 7.1 would be according to (4.15). Therefore, the proof completed. ■

Theorem 8 *The state errors of 'follower-leader' pairs and the state errors of neighboring 'follower-predecessor' pairs are governed by a shared internal stability condition.*

Proof. Considering (4.15), regarding the facts that $d/dt\{\Delta\tilde{p}_i^{i+1}\} = \Delta\tilde{v}_i^{i+1}$ and $d/dt\{\Delta\tilde{v}_i^{i+1}\} = \Delta\tilde{a}_i^{i+1}$, assuming $\Delta\tilde{y}_i^{i+1} = \Delta\tilde{p}_i^{i+1}$ as the output of the pairs coupled dynamics, then for $i = 0, \ldots, n-1$, the state-space model for the pair $(i, i+1)$ can be presented as

$$\begin{cases} \Delta\dot{\tilde{\mathbf{X}}}_i^{i+1} = \mathbf{A}_i^{i+1}\Delta\tilde{\mathbf{X}}_i^{i+1} + \mathbf{B}_i^{i+1}\Delta\tilde{u}_i^{i+1} \\ \Delta\tilde{y}_i^{i+1} = \mathbf{C}_i^{i+1}\Delta\tilde{\mathbf{X}}_i^{i+1} \end{cases} \tag{4.31}$$

where $\mathbf{C}_i^{i+1} = [1,\ 0,\ 0]$, $\mathbf{B}_i^{i+1} = \mathbf{B}$, and $\mathbf{A}_i^{i+1} \in R^{3\times 3}$ and $\tilde{u}_i^{i+1} \in R$ are

$$\mathbf{A}_i^{i+1} = \begin{bmatrix} 0 & 1 & 0 \\ 0 & 0 & 1 \\ -\frac{|\mathbf{J}_i|k}{\tau} & -\frac{|\mathbf{J}_i|b}{\tau} & -\frac{1+|\mathbf{J}_i|h}{\tau} \end{bmatrix} \tag{4.32}$$

and

$$\Delta\tilde{u}_i^{i+1} = \mathbf{K}\sum_{j\in\alpha_i}\sum_{\kappa=j}^{i-1}\Delta\tilde{\mathbf{X}}_\kappa^{\kappa+1} + \mathbf{K}\sum_{j\in\beta_i}\sum_{\kappa=i+1}^{j-1}\Delta\tilde{\mathbf{X}}_\kappa^{\kappa+1} \tag{4.33}$$

respectively. Note that that the sets $\mathbf{J}_i$, α_i and β_i are mutually disjoint, i.e., $\mathbf{J}_i \cap \alpha_i = \emptyset$, $\mathbf{J}_i \cap \beta_i = \emptyset$ and $\alpha_i \cap \beta_i = \emptyset$. Also, always $\alpha_0 = \emptyset$ and $\beta_{n-1} = \emptyset$. Defining $\Delta\tilde{\mathbf{X}}_t \in R^{3n\times 1} = [\Delta\tilde{\mathbf{X}}_0^1;\ \Delta\tilde{\mathbf{X}}_1^2;\ \ldots,\ \Delta\tilde{\mathbf{X}}_{n-1}^n]$, applying $i = 0, \ldots, n-1$ to the first relation in (4.31), the stacked resultant relations can be compactly shown as

$$\Delta\dot{\tilde{\mathbf{X}}}_t = \tilde{\mathbf{A}}_{t\Delta}\Delta\tilde{\mathbf{X}}_t = \left[\mathbf{I}_n \otimes \mathbf{A} - \bar{\mathbf{P}} \otimes \mathbf{BK}\right]\Delta\tilde{\mathbf{X}}_t \tag{4.34}$$

where $\tilde{\mathbf{A}}_{t\Delta} = \mathbf{I}_n \otimes \mathbf{A} - \bar{\mathbf{P}} \otimes \mathbf{BK}$, and $\bar{\mathbf{P}} \in R^{n\times n}$ whose elements $\bar{p}_{ij}$ would be according to

$$\bar{p}_{ij} = \begin{cases} -|\mathbb{S}_j \cap \alpha_{i-1}| & \text{if} \quad j < i \\ |\mathbf{J}_{i-1}| & \text{if} \quad j = i \\ -|\mathbb{V}_j \cap \beta_{i-1}| & \text{if} \quad j > i \end{cases} \tag{4.35}$$

where $|.|$ denotes the cardinality of the relevant sets, $\mathbb{S}_j \triangleq \{j-1, j-2, \ldots, 0\}$ and $\mathbb{V}_j \triangleq \{j, j+1, \ldots, n\}$. Also, $\bar{p}_{ij} = 0$ in case of $\mathbb{S}_j \cap \alpha_{i-1} = \emptyset$ or $\mathbb{V}_j \cap \beta_{i-1} = \emptyset$. Fig. 4.7, illustrates the platoon dynamics (4.8) which has been developed by using the 'follower-leader' state errors, and the alternative dynamics (4.34) which obtained after state coordinate transformation and utilizing neighboring 'follower-predecessor' state errors.

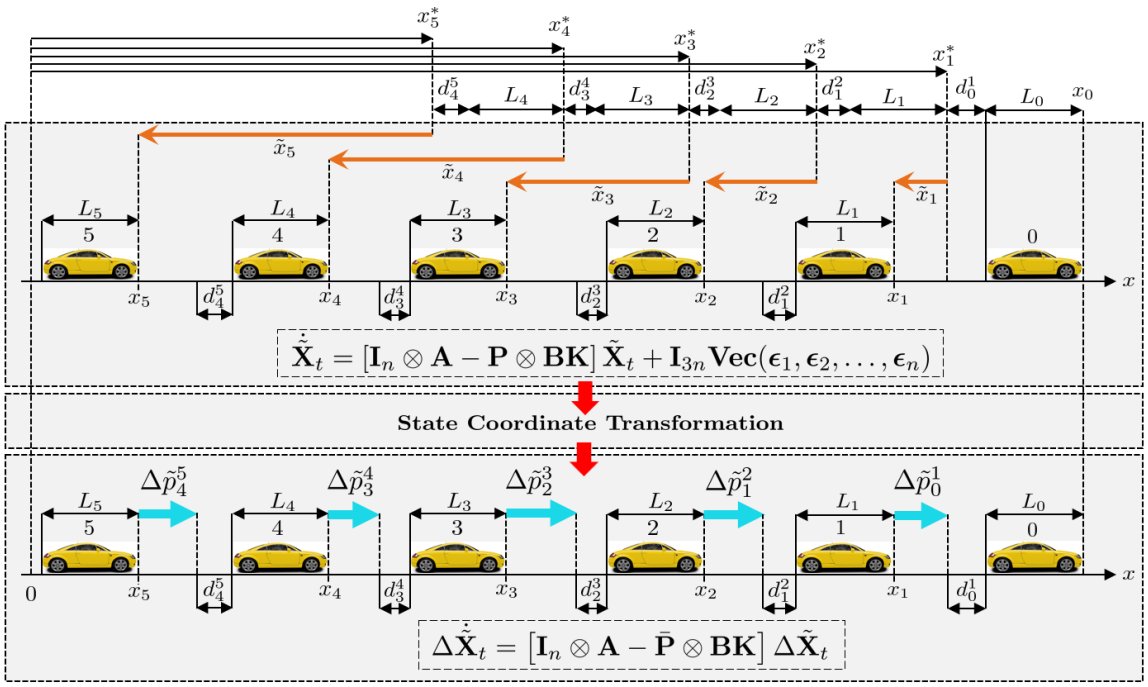

Figure 4.7: Illustration of platoon dynamics with 'follower-leader' and neighboring 'follower-predecessor' state errors.

Following (4.9) and (4.35), for any BDCT depicted in Fig. 4.1, the eigenvalues of the matrices $\mathbf{P}$ and $\bar{\mathbf{P}}$ are identical. For instance, for the case of having five followers and using TBPF topology, the matrices are

$$\mathbf{P} = \begin{bmatrix} 1 & -2 & -1 & 0 & 0 \\ 0 & 4 & -1 & -1 & 0 \\ -1 & -1 & 4 & -1 & -1 \\ 0 & -1 & -1 & 4 & 0 \\ 0 & 0 & -1 & -1 & 3 \end{bmatrix}, \quad \mathbf{P} = \begin{bmatrix} 3 & -1 & -1 & 0 & 0 \\ -1 & 4 & -1 & -1 & 0 \\ -1 & -1 & 4 & -1 & -1 \\ 0 & -1 & -1 & 3 & -1 \\ 0 & 0 & -1 & -1 & 2 \end{bmatrix} \tag{4.36}$$

both of which have eigenvalues: 0.2935, 2.1324, 3.3900, 5.0000 and 5.1841 and thus are similar matrices. Please check Link for matrices $\mathbf{P}$ and $\bar{\mathbf{P}}$ of the other BDCTs. Considering (4.8) and (4.34), since the system matrices $\tilde{\mathbf{A}}_t$ and $\tilde{\mathbf{A}}_{t\Delta}$ are in similar formats as

$$\tilde{\mathbf{A}}_t = [\mathbf{I}_n \otimes \mathbf{A} - \mathbf{P} \otimes \mathbf{BK}] \tag{4.37a}$$

$$\tilde{\mathbf{A}}_{t\Delta} = [\mathbf{I}_n \otimes \mathbf{A} - \bar{\mathbf{P}} \otimes \mathbf{BK}] \tag{4.37b}$$

and regarding the property that $\mathbf{P}$ and $\bar{\mathbf{P}}$ are similar, dynamics (4.34) can be utilized

instead of (4.8) for internal stability analysis. Therefore, the two cases mentioned earlier in the Remarks 2-3 are valid for the matrix $\bar{\mathbf{P}}$ as well. Thus the proof completed.

■

4.4 Transient Intervehicle Distance Errors (TIDEs)

Given (4.15) and BDCTs in Fig. 4.1, there is a coupling between the pair $(i, i+1)$ and the pairs in the set $\left(\cup_{j\in\alpha_i}\cup_{\kappa=j}^{i-1}\zeta_\kappa\right)\cup\left(\cup_{j\in\beta_i}\cup_{\kappa=i+1}^{j-1}\zeta_\kappa\right)$ in which the set ζ_κ is defined as $\zeta_\kappa \triangleq \{(\kappa,\kappa+1)\}$. Note that the sets α_i and β_i are not empty sets at the same time. For $i=0,\ldots,n-1$, assuming $\Delta\tilde{v}_i^{i+1}(0)=\Delta\tilde{a}_i^{i+1}(0)=0$, and all initial TIDEs are equal to μ, i.e., $\Delta\tilde{p}_i^{i+1}(0)=\mu$, in Laplacian domain we have

$$\Delta\tilde{\mathbf{X}}_i^{i+1}(s)=\mathbf{T}_1\Delta\tilde{p}_i^{i+1}(s)-\mathbf{T}_2\mu \tag{4.38}$$

where $\mathbf{T}_1 \triangleq [1;\ s;\ s^2]$ and $\mathbf{T}_2 \triangleq [0;\ 1;\ s]$. Given (4.31), $\Delta\tilde{p}_i^{i+1}(s)$, for $i=0,\ldots,n-1$, would be the summation of zero-state ($\Delta\tilde{\mathbf{X}}_i^{i+1}(0)=0$) response and zero-input ($\Delta\tilde{u}_i^{i+1}=0$) response.

Theorem 9 *Given* (4.31) *and* (4.38)*, TIDE between neighboring vehicles would be according to*

$$\Delta\tilde{p}_i^{i+1}(s)=\Psi_i(s)+H_i(s)\sum_{j\in\alpha_i}\sum_{\kappa=j}^{i-1}\Delta\tilde{p}_\kappa^{\kappa+1}(s)+H_i(s)\sum_{j\in\beta_i}\sum_{\kappa=i+1}^{j-1}\Delta\tilde{p}_\kappa^{\kappa+1}(s) \tag{4.39}$$

where

$$H_i(s)=\frac{\frac{h}{\tau}s^2+\frac{b}{\tau}s+\frac{k}{\tau}}{s^3+\bar{h}_is^2+\bar{b}_is+\bar{k}_i};\quad \alpha_i\neq\emptyset\ \textit{or}\ \beta_i\neq\emptyset \tag{4.40}$$

and

$$\Psi_i(s)=\frac{\mu\left(s^2+\frac{1+(|\mathbf{J}_i|-\gamma_i)h}{\tau}s+\frac{(|\mathbf{J}_i|-\gamma_i)b}{\tau}\right)}{s^3+\bar{h}_is^2+\bar{b}_is+\bar{k}_i};\ \ i=0,\ldots,n-1 \tag{4.41}$$

in which $\bar{h}_i=\frac{1+|\mathbf{J}_i|h}{\tau}$, $\bar{b}_i=\frac{|\mathbf{J}_i|b}{\tau}$, $\bar{k}_i=\frac{|\mathbf{J}_i|k}{\tau}$, *and* $\gamma_i=\sum_{j\in\alpha_i}(i-j)+\sum_{j\in\beta_i}(j-i-1)$.

Proof. Given (4.31), the zero-input response, let be defined as $\Delta\tilde{p}_{i,zi}^{i+1}(s)$, would be according to

$$\Delta\tilde{p}_{i,zi}^{i+1}(s)=\mathbf{C}_i^{i+1}\left(s\mathbf{I}_3-\mathbf{A}_i^{i+1}\right)^{-1}\Delta\tilde{\mathbf{X}}_i^{i+1}(0)=\frac{\mu\left(s^2+\bar{h}_is+\bar{b}_i\right)}{s^3+\bar{h}_is^2+\bar{b}_is+\bar{k}_i} \tag{4.42}$$

where $\mathbf{I}_3$ is the identity matrix of size 3. Also, the zero-state response, let be defined as $\Delta\tilde{p}_{i,zs}^{i+1}(s)$, would be

$$\Delta\tilde{p}_{i,zs}^{i+1}(s) = \mathbf{G}_i^{i+1}(s)\Delta\tilde{u}_i^{i+1}(s) \tag{4.43}$$

in which given (4.33) and (4.38) we have $\mathbf{G}_i^{i+1}(s) = \mathbf{C}_i^{i+1}\left(s\mathbf{I}_3 - \mathbf{A}_i^{i+1}\right)^{-1}\mathbf{B}$ and

$$\begin{aligned}\Delta\tilde{u}_i^{i+1}(s) = \mathbf{K}\mathbf{T}_1 \sum_{j\in\alpha_i}\sum_{\kappa=j}^{i-1}\Delta\tilde{p}_\kappa^{\kappa+1}(s) - \mathbf{K}\mathbf{T}_2 \sum_{j\in\alpha_i}\sum_{\kappa=j}^{i-1}\mu \\ + \mathbf{K}\mathbf{T}_1 \sum_{j\in\beta_i}\sum_{\kappa=i+1}^{j-1}\Delta\tilde{p}_\kappa^{\kappa+1}(s) - \mathbf{K}\mathbf{T}_2 \sum_{j\in\beta_i}\sum_{\kappa=i+1}^{j-1}\mu\end{aligned} \tag{4.44}$$

Simplifying (4.44) results in $\mathbf{G}_i^{i+1}(s) = \frac{1}{\tau\left(s^3+\bar{h}_i s^2+\bar{b}_i s+\bar{k}_i\right)}$ and

$$\begin{aligned}\Delta\tilde{u}_i^{i+1}(s) = \left(hs^2+bs+k\right)\times\left(\sum_{j\in\alpha_i}\sum_{\kappa=j}^{i-1}\Delta\tilde{p}_\kappa^{\kappa+1}(s) + \sum_{j\in\beta_i}\sum_{\kappa=i+1}^{j-1}\Delta\tilde{p}_\kappa^{\kappa+1}(s)\right) \\ - (hs+b)\left(\sum_{j\in\alpha_i}\sum_{\kappa=j}^{i-1}\mu + \sum_{j\in\beta_i}\sum_{\kappa=i+1}^{j-1}\mu\right)\end{aligned} \tag{4.45}$$

substituting which into (4.43) yields

$$\begin{aligned}\Delta\tilde{p}_{i,zs}^{i+1}(s) = \frac{\frac{h}{\tau}s^2+\frac{b}{\tau}s+\frac{k}{\tau}}{s^3+\bar{h}_i s^2+\bar{b}_i s+\bar{k}_i}\times\left(\sum_{j\in\alpha_i}\sum_{\kappa=j}^{i-1}\Delta\tilde{p}_\kappa^{\kappa+1}(s) + \sum_{j\in\beta_i}\sum_{\kappa=i+1}^{j-1}\Delta\tilde{p}_\kappa^{\kappa+1}(s)\right) \\ - \frac{\mu\left(\sum_{j\in\alpha_i}(i-j)+\sum_{j\in\beta_i}(j-i-1)\right)\left(\frac{h}{\tau}s+\frac{b}{\tau}\right)}{s^3+\bar{h}_i s^2+\bar{b}_i s+\bar{k}_i}\end{aligned} \tag{4.46}$$

Therefore, given (4.42) and (4.46) we have $\Delta\tilde{p}_i^{i+1}(s) = \Delta\tilde{p}_{i,zi}^{i+1}(s) + \Delta\tilde{p}_{i,zs}^{i+1}(s)$ which would be equal to (4.39). Therefore, the proof completed. ■

4.4.1 Mapping Between TIDEs and Initial Conditions

Calculating (4.39) for $i = 0, \ldots, n-1$ and stacking them together, after some mathematical manipulation, it is possible to reformulate (4.39) in the following compact form:

$$\Delta\tilde{\mathbb{P}}(s) = \mathbf{Q}^{-1}(s)\mathbf{\Psi}(s) \tag{4.47}$$

such that $\Delta\tilde{\mathbb{P}}(s) \triangleq \left[\Delta\tilde{p}_0^1(s);\ \Delta\tilde{p}_1^2(s);\ \ldots;\ \Delta\tilde{p}_{n-1}^n(s)\right]$, $\mathbf{\Psi}(s) \triangleq [\Psi_0(s);\ \Psi_1(s);\ \ldots;\ \Psi_{n-1}(s)]$, and $\mathbf{Q}(s) \in \mathbb{C}^{n\times n}$ whose elements are defined as

$$q_{ij}(s) = \begin{cases} 1 & \text{if} \quad i = j \\ \bar{p}_{ij} H_{i-1}(s) & \text{if} \quad i \neq j \end{cases} \tag{4.48}$$

where $\bar{p}_{ij}$ are defined in (4.35). Therefore, if we define the elements of $\mathbf{Q}^{-1}(s)$ as $Q^{-1}_{(i+1)j}(s)$, then exploring (4.47) yields

$$\Delta\tilde{p}_i^{i+1}(s) = \sum_{j=1}^{n} Q^{-1}_{(i+1)j}(s)\Psi_{j-1}(s); \quad i = 0, \ldots, n-1 \tag{4.49}$$

4.4.2 Different Scenarios for TIDEs

Given (4.49), it follows that $\Delta\tilde{p}_i^{i+1}(t)$ represents the impulse response of $\Delta\tilde{p}_i^{i+1}(s)$, or equivalently the inverse Laplace transform of $\Delta\tilde{p}_i^{i+1}(s)$. Consequently, for a given $\mathbf{K} = [k, b, h]$, the appropriate control gains necessary to ensure safe and collision-free distances can be determined based on the relationship between TIDEs, safe and desired IDs. The different scenario are illustrated in Fig. 4.8. If $\Delta\tilde{p}_i^{i+1}(t) > -(d_i^{i+1} - d_{i,i+1}^s)$ holds during the travel time (TT), it leads to a stable-safe distance over TT (cases **a** and **b**). Similarly, when $\Delta\tilde{p}_i^{i+1}(t) > -d_i^{i+1}$ holds within the TT, and $\Delta\tilde{p}_i^{i+1}(t) < -(d_i^{i+1} - d_{i,i+1}^s)$ occurs during TT, it results in a stable-unsafe distance over TT (case **c**). Conversely, if $\Delta\tilde{p}_i^{i+1}(t) \leq -d_i^{i+1}$ takes place over the TT, it leads to a stable-collision occurrence within platoon (case **d**). Note that, in Fig. 4.8, $D_i^{i+1}(t) = x_i(t) - x_{i+1}(t) - L_i = \Delta\tilde{p}_i^{i+1}(t) + d_i^{i+1}$ exhibits the real distance between neighboring vehicles i and $i+1$. Please observe that when $\Delta\tilde{p}_i^{i+1}(t)$ converges to zero, signifying a stable platoon, the actual distance between adjacent vehicles will also converge to the desired values.

4.5 Simulations and Results

In this section, we present simulation results that serve to validate the theoretical findings. To do so, we consider a platoon comprising one leader and five followers,

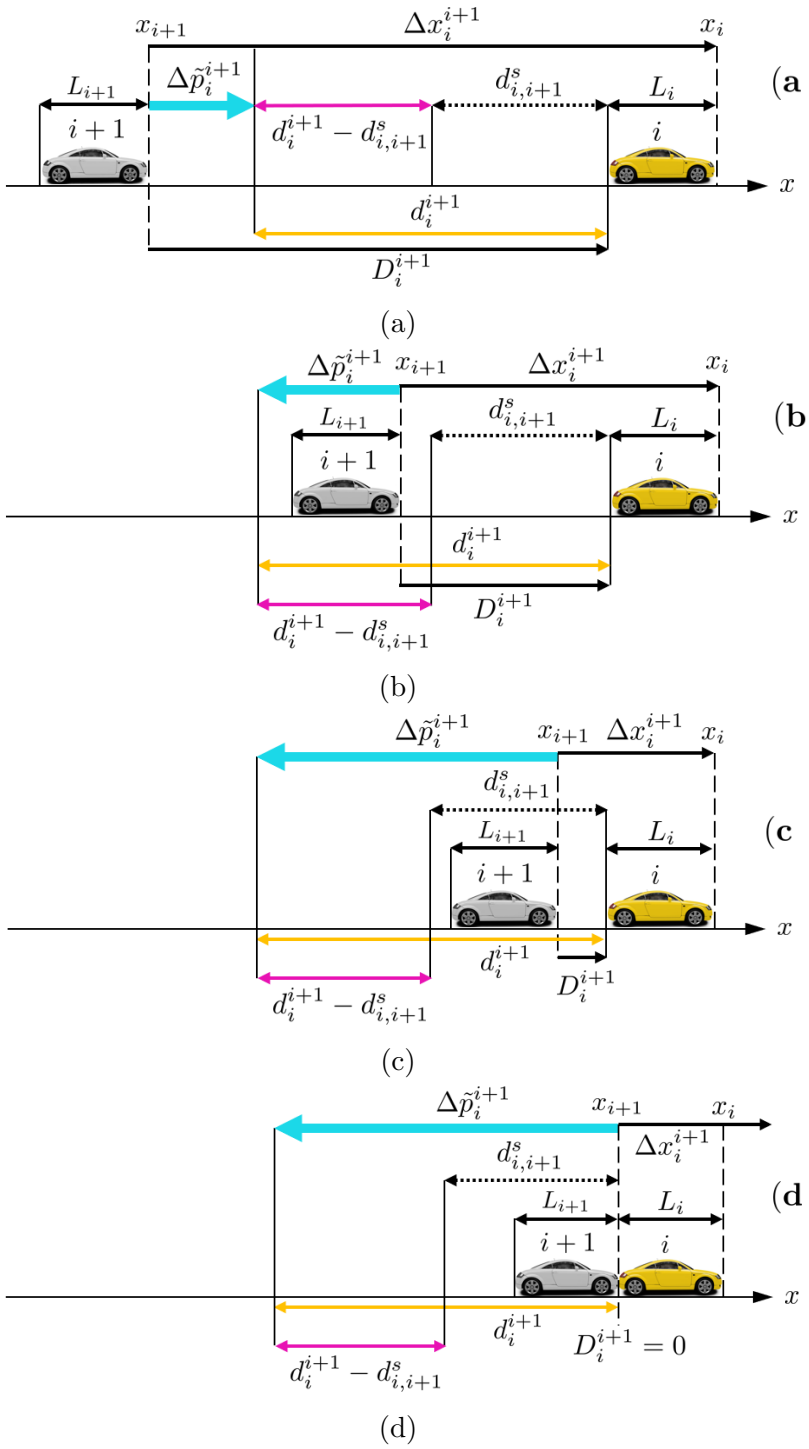

Figure 4.8: Portraying different situations featuring transient intervehicle distance errors (TIDEs) among neighboring vehicles.

with a constant distance policy set at $5m$. Within the simulations, all vehicles begin with initial velocities and accelerations set to zero. Their lengths are uniform at $4m$.

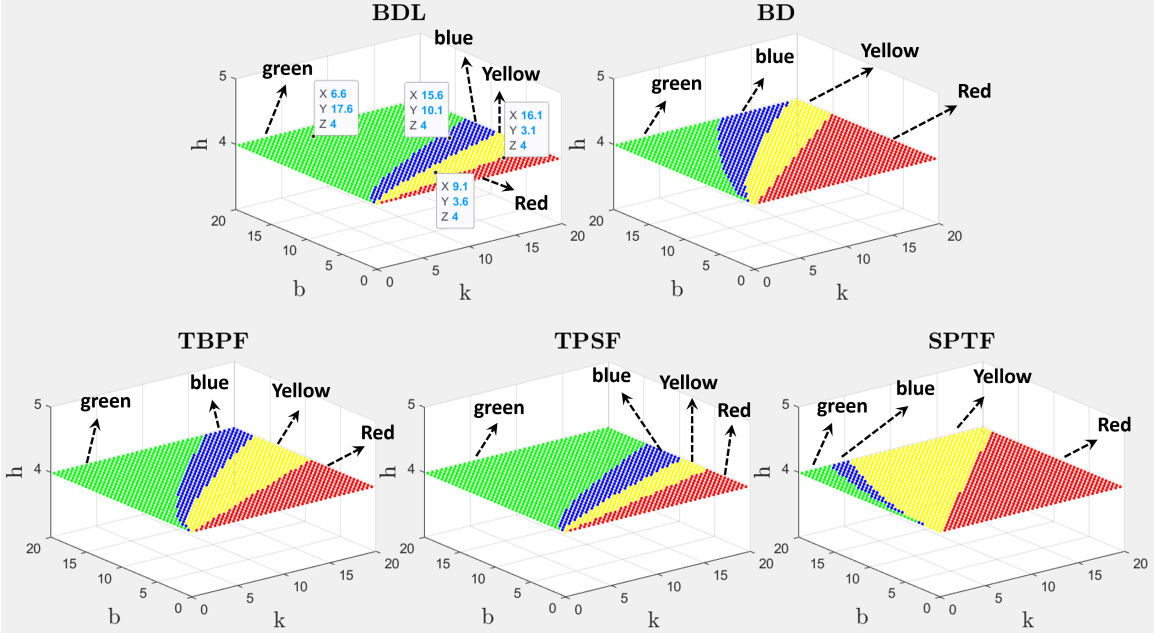

Figure 4.9: Control Gain Categories: Unstable (red), Stable-Collision (yellow), Stable-Unsafe (blue), and Stable-Safe (green). Desired and safe distances between neighboring vehicles: $5m$ and $3m$, respectively.

Additionally, we employ a sampling time of $0.01s$. The simulation time is established as $100s$, though for the sake of clarity in presentation, results may be shown for time intervals less than $100s$. Furthermore, the safe distance between vehicles is set at $3m$, denoted as $d^s_{i,i+1} = 3m$.

4.5.1 Comparing BDCTs Based on TIDE Performance

In the provided BDCTs (see Fig. 4.1), stability analysis reveals that BDL, BD, and TBPF topologies exhibit real eigenvalues in their matrices $\mathbf{P}$ and $\bar{\mathbf{P}}$ (defined in (4.9) and (4.35)), while TPSF and SPTF topologies feature a mix of real and conjugate complex eigenvalues. Control gains k and b vary between 0.1 and 19.6 (with 0.5 increments), under the assumptions of $\tau = 1$ and $h = 4$. Unstable control gains are identified when stability conditions are not met, while stable control gains are those satisfying the conditions.

Further analysis, using (4.49) and the approach detailed in the 'Different Scenarios

for TIDEs' subsection of the previous section, reveals which control gains lead to unstable, stable-collision, stable-unsafe, or stable-safe distances between neighboring vehicles. These findings are visually represented in Fig. 4.9, with red indicating unstable, yellow for stable-collision, blue for stable-unsafe, and green for stable-safe gains. Referring to Fig. 4.9, several noteworthy conclusions can be made:

1. **BDL Reigns Supreme**: BDL topology emerges as the front-runner, boasting larger stable and stable-safe areas, indicating its superior performance in platoon control.

2. **Leader Broadcasting**: Broadcasting the leader's state, as demonstrated in the BDL topology, significantly elevates platoon performance compared to the conventional BD topology.

3. **SPTF's Limitations**: SPTF displays limitations, with the smallest stable area and the largest stable-collision area, suggesting challenges in maintaining platoon stability.

4. **BD vs. SPTF**: Despite SPTF providing more information from vehicles behind, BD outperforms it, highlighting the impact of information sources on performance.

5. **TPSF's Advantage**: TPSF outperforms TBPF, even though TBPF offers additional information from vehicles behind, emphasizing the significance of information exchange with vehicles ahead.

6. **Information from Rear Impacts Performance**: The introduction of extra information from vehicles behind, beyond the immediate follower, is associated with a degradation in platoon performance.

7. **BD, TPSF, SPTF Comparison**: TPSF, with additional information from vehicles ahead, enhances performance compared to BD. Conversely, SPTF, with

extra rearward information, diminishes performance.

8. **BDL vs. TPSF Parity**: BDL and TPSF exhibit comparable performance levels. However, it appears that performance could further improve if the additional information from vehicles ahead originates from the leader vehicle.

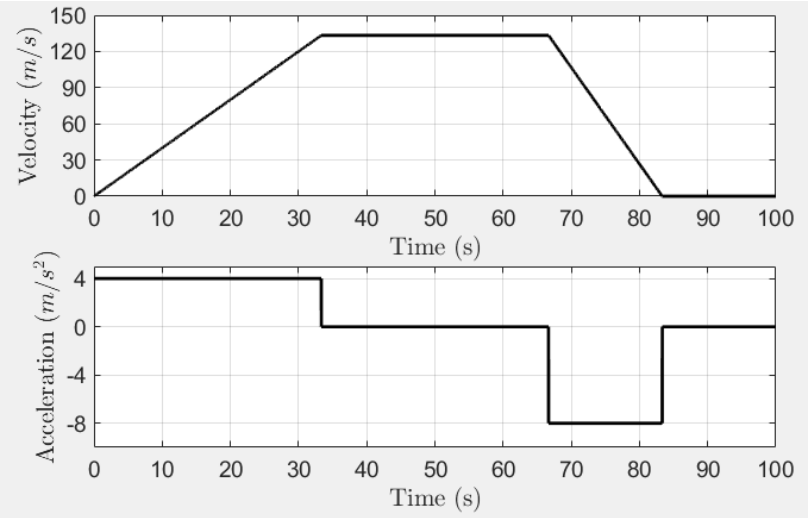

Figure 4.10: Leader's velocity and acceleration.

4.5.2 Analysis Validation for TIDE Study

Consider time interval $t_i^1 \leq t_i < t_i^2$ during which the leader vehicle's acceleration remains constant at a_i^0. Therefore, for each time interval we can apply basic physics principles to find its velocity (v_i^0) and position (x_i^0):

$$\begin{aligned} v_i^0(t) &= a_i^0(t - t_i^1) + v_i^0(t_i^1) \\ x_i^0(t) &= \frac{1}{2}a_i^0(t - t_i^1)^2 + v_i^0(t - t_i^1) + x_i^0(t_i^1) \end{aligned} \tag{4.50}$$

Fig. 6.4 depicts an arbitrary acceleration and the associated velocity trajectories we have considered for the leader vehicle for the simulations. Considering (4.8), and assuming a sampling time of Δt, we can calculate the updated $\tilde{\mathbf{X}}_t(t + \Delta t)$ as follows:

$$\tilde{\mathbf{X}}_t(t + \Delta t) = \left(\mathbf{I}_{3n} + \tilde{\mathbf{A}}_t \Delta t\right) \tilde{\mathbf{X}}_t(t) + \Delta t \mathbf{Vec}(\boldsymbol{\epsilon}_1, \boldsymbol{\epsilon}_2, \ldots, \boldsymbol{\epsilon}_n) \tag{4.51}$$

Here, $\mathbf{I}_{3n}$ is the identity matrix of size $3n$. Now, Given the acceleration trajectory of leader vehicle, using (4.3), and noting that $\tilde{\mathbf{X}}_{i+1}(t) = \mathbf{X}_{i+1}(t) - \mathbf{X}^*_{i+1}(t)$, other than TIDEs, we can find the follower vehicles' position, velocity and acceleration trajectories. The communication topology is considered to be the BDL topology, and the initial positions are selected as $x_i(0) = -17 \times i \ m$, $i = 0, 1, \ldots, 5$, where given $d_i^{i+1} = 5m$, and $d_{i,s}^{i+1} = 3m$, the initial TIDE between neghboring vehicles would be $\Delta\tilde{p}_i^{i+1}(0) = 8m$.

Associated TIDE trajectories of selected points from the BDL topology (Fig. 4.9) are illustrated in Fig. 4.11:

1. $\mathbf{K} = [16.1, 3.1, 4]$ (from the unstable area), error trajectories diverge, rendering the platoon unstable.

2. $\mathbf{K} = [9.1, 3.6, 4]$ (from the stable-collision area) results in converging error trajectories, but some cross the red-dashed line ($-5m$ error), indicating collisions.

3. $\mathbf{K} = [15.6, 10.1, 4]$ (from the stable-unsafe area) leads to converging error trajectories, with some crossing the blue-red line ($-2m$ error), signifying violations of the safe distance.

4. $\mathbf{K} = [6.6, 17.6, 4]$ (from the stable-safe area) results in converging trajectories that do not cross the red-dashed (collision) or blue-dashed (safe distance) lines, ensuring the maintenance of a safe distance between vehicles.

Therefore, the error trajectories validate the identified unstable, stable-collision, stable-unsafe, and stable-safe areas from the provided analysis elaborated on in Section VII.

4.5.3 Tracking Performance

Platooning aims to achieve two vital objectives: 1) aligning followers with the leader's velocity and acceleration, and 2) ensuring IDs converge to preset values, assumed here

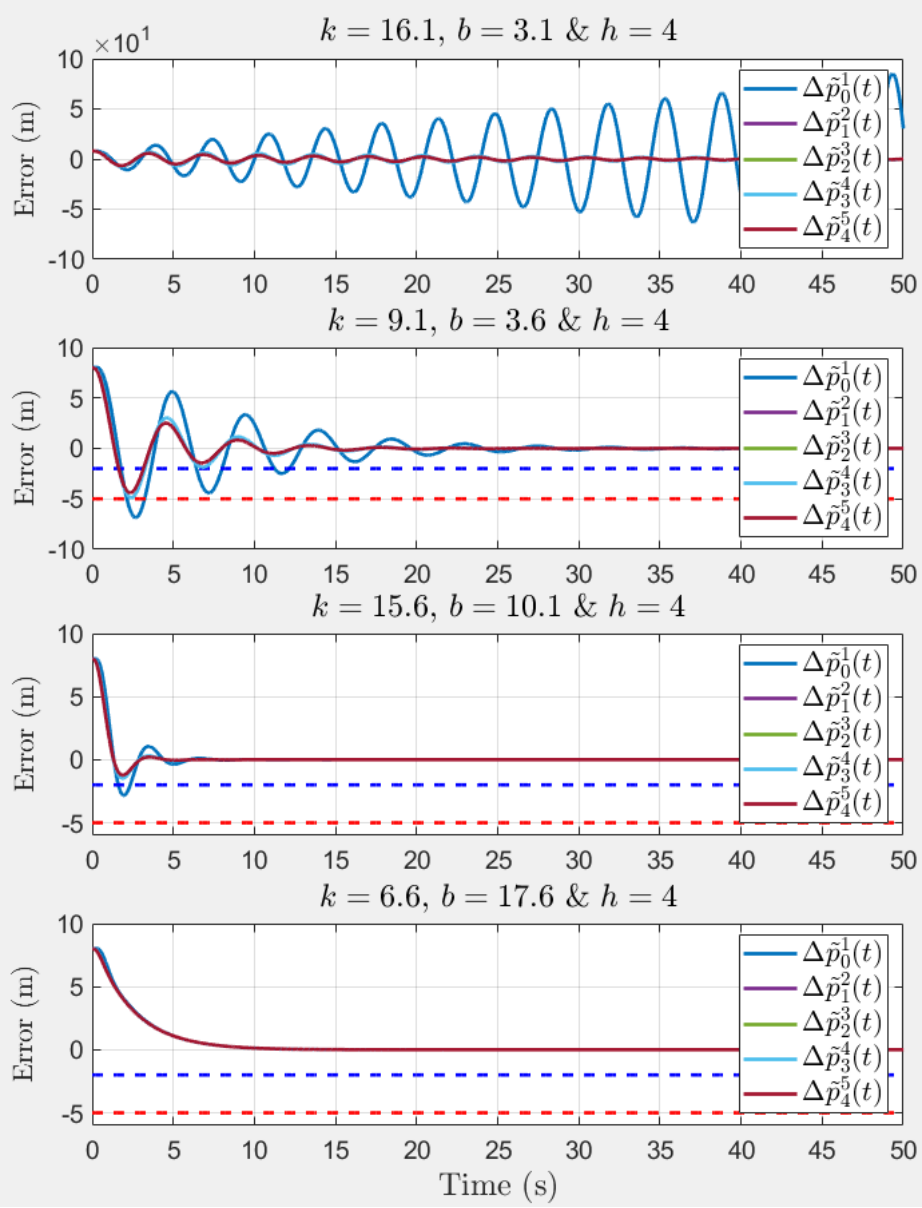

Figure 4.11: $\Delta\tilde{p}_i^{i+1}(t)$ trajectories of selected points from the BDL topology (see Fig. 4.9).

to be $5m$. In our demonstration within the BDL topology, we have chosen representative $\mathbf{K}$ points from each stability region (see Fig. 4.9). Fig. 4.12 displays position, velocity, and acceleration trajectories for $i = 1, \ldots, 5$ at these selected points. Within stable regions (yellow, blue, and green areas), we observe velocities and accelerations converging to match the leader's values. The convergence times vary among points,

with the stable-safe point showing the quickest convergence and the stable-collision point the slowest.

In line with our explanation in the 'Verifying the Validity of the Areas' section, selected points within stable regions demonstrate error convergence to zero, ensuring attainment of the predefined desired distances between neighboring vehicles.

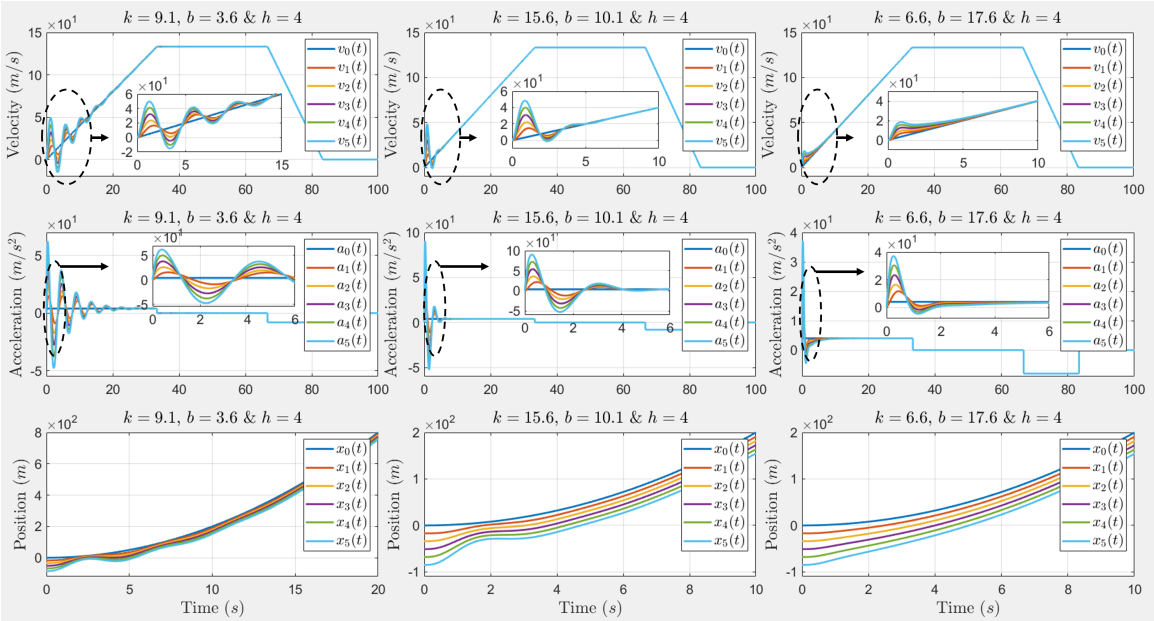

Figure 4.12: Velocity, acceleration and position trajectories for BDL topology under control gains $\mathbf{K} = [9.1, 3.6, 4]$ (stable-collision), $\mathbf{K} = [15.6, 10.1, 4]$ (stable-unsafe) and $\mathbf{K} = [6.6, 17.6, 4]$ (stable-safe), respectively.

4.5.4 High-Fidelity Simulation of Truck Platooning

We have assessed the controller's performance and communication topologies in realistic vehicle platooning using MATLAB's Vehicle Dynamics Blockset for simulation, employing both BDL and BD communications. Each vehicle's dynamics in the platooning setup encompassed key aspects, including vehicle geometry, suspension, tire, powertrain, and steering/braking systems. The platooning controller governed acceleration input for each vehicle, maintaining a fixed steering angle of zero degrees, focusing on longitudinal control.

In addition to the intricate components of vehicle dynamics modeling, the platooning scenario also integrates vehicle-to-vehicle (V2V) communication for deployment. In the realm of communication modeling, each vehicle within the platoon is equipped with V2V transmitters and receivers. Specifically, we configure the communication model to utilize BDL and BD communication protocols. The transmitters are responsible for transmitting basic safety messages (BSMs) containing pose information, while the receivers within the platoon's followers intercept and extract this valuable data from the BSMs. Subsequently, the information obtained by the receivers of the platoon followers is employed by their respective controllers to compute the necessary acceleration for maintaining the desired following distance from the lead vehicle and effectively tracking its movements.

The platooning setup includes one leader and four followers. Each follower has a platooning controller (specified in (4.4)) that regulates longitudinal controls to maintain a constant spacing from the preceding vehicle while following the lead vehicle. The inbuilt vehicle dynamics are modeled using a six degrees of freedom tractor-trailer system, representing a three-axle tractor towing a three-axle trailer through a hitch. Both the tractor and trailer have individual models for their vehicle body, wheels, and suspension. The vehicle lengths are set at $17.2m$, and the safe and desired intervehicle spacing are established at $7m$ and $3m$. Identical control gains are applied to each follower vehicle, defined as $\mathbf{K} = [20, 25, 4]$. Additionally, the initial positions for the trucks are initialized as $x_i(0) = -32 \times i$ for $i = 0$ to 4.

Figs.4.13a and 4.13b illustrate the vehicle velocities under BDL and BD topologies. This simulation emphasizes the substantial enhancement in velocity tracking for follower vehicles achieved through the broadcast of the leader vehicle's state. Additionally, in Figs. 4.14a and 4.14b, the desired and safe distances between vehicles, as well as the actual distances between adjacent vehicles in the platoon, are presented. This simulation outcome further underscores the improved platoon performance in coordinating vehicles with the desired intervehicle distances, resulting from the broadcast

of the leader vehicle's state. It is noteworthy that in the BDL topology, the distances between vehicles consistently remain above the safe distance threshold, while in the BD topology, the distance between the leader and the first follower has breached the safe distance threshold. Fig. 4.15 shows the corresponding truck platooning at times $t = 0s$ and $t = 50s$. Please note that an associated simulation video accompanies these results as pointed out to in Fig. 4.15.

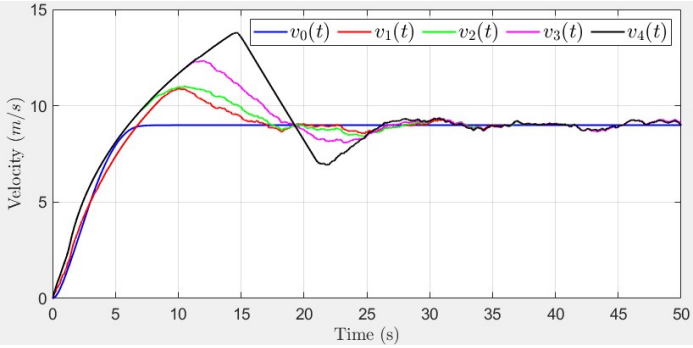

(a) Vehicles' velocities under BDL topology

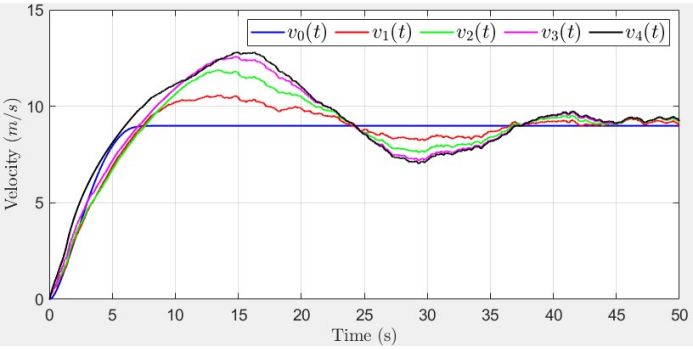

(b) Vehicles' velocities under BD topology

Figure 4.13: Illustrating the beneficial impact of broadcasting the state of the leader vehicle to FVs.

4.6 Conclusion

In conclusion, this chapter addressed the complexities of achieving not only internal stability but also favorable transient dynamics in the intervehicle distances among adjacent vehicles within a platoon. We accomplished this by introducing a novel closed-loop distance dynamic model that shifted our focus from follower-leader state

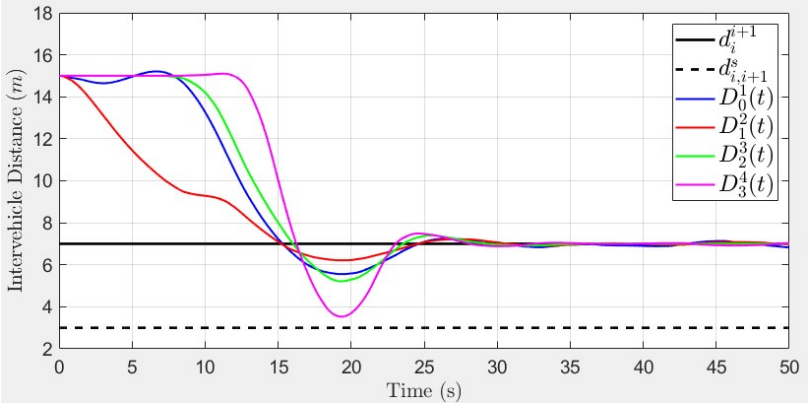

(a) Distance between trucks under BDL topology

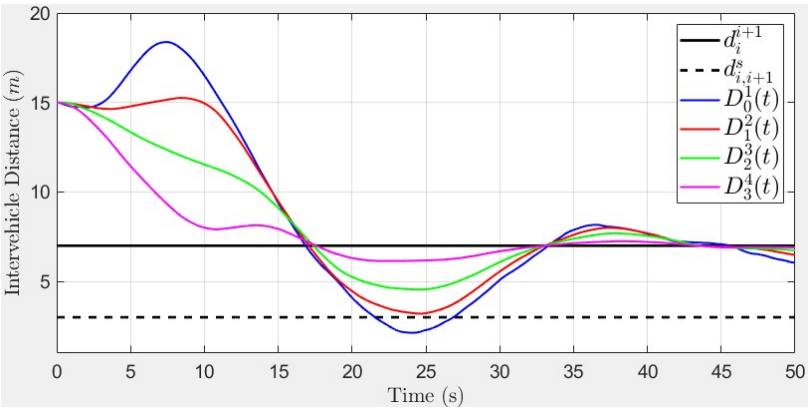

(b) Distance between trucks under BD topology

Figure 4.14: Illustrating the beneficial impact of broadcasting the state of the leader vehicle to FVs.

differences to neighboring-vehicle state differences.

Through this innovative dynamic model, we delved into both system stability and transient intervehicle distance analysis. Regardless of the leader vehicle's state, relying solely on initial conditions, engine time constants, the number of vehicles, and communication type, we analytically determined distance trajectories between adjacent vehicles. As part of our investigation, we explored various control gains, allowing us to scrutinize distance trajectories across different bidirectional communication topologies (BDCTs).

These investigations shed light on the strengths and weaknesses of different BDCTs. Our findings revealed that, within BDCTs and with a given control gain, receiving information from vehicles further behind could potentially hinder platoon performance.

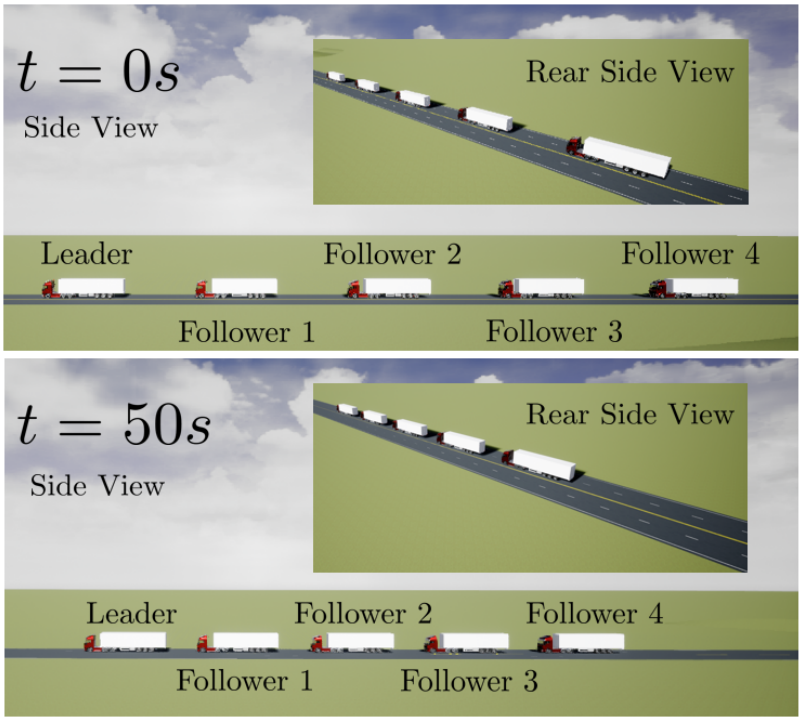

Figure 4.15: Truck Platooning under BDL topology. States of platoon at $t = 0s$ and $t = 50s$. Please check the link https://youtu.be/rxQ-XsYFaEM?si=uJITOoELSiFWvoEH to watch the simulation video for BDL case.

Conversely, obtaining information from vehicles further ahead enhanced transient intervehicle distances, ensuring they remained within a safe range. Furthermore, we demonstrated that broadcasting the leader vehicle's state to other vehicles had the potential to elevate the overall performance of the platoon. Finally, to substantiate our theoretical findings, we provided comprehensive simulations, illustrating the practical implications of our research.

Chapter 5

Impact of Communication Topologies on Stability and Intervehicle Distances: Homogeneous Vehicular Platoons[1]

As a promising intelligent transportation technology, vehicle platooning has the potential to improve highway capacity and throughput, fuel consumption, exhaust emission rate, transportation efficiency, and traffic safety [91–96]. Platooning refers to coordinating a group of vehicles with a leader and several followers to travel at desired intervehicle (IDs) distances and harmonious speeds. Based on some developed spacing policies, IDs can be according to constant distance policy [27, 45, 49, 50, 97, 98], constant time headway policy [33, 99–102], nonlinear headway policy [103, 104], delay-based distance policy [18], and energy-oriented spacing policy [9].

Distributed longitudinal control of vehicular platoons has been extensively studied in literature such that various techniques based on model predictive control [30–34], sliding mode control [12, 13, 35], consensus-based control [36–39], event-triggered control [40–43], adaptive control [44–46], observer-based control [47–50], robust control [13, 51], reinforcement learning-based control [52], and linear feedback control [27, 53–57] are utilized for coordination of platoon vehicles.

[1]A version of this chapter has been submitted as Amir Zakerimanesh, Tony Z. Qiu, Mahdi Tavakoli, *Impact of Communication Topologies on Stability and Intervehicle Distances: Homogeneous Vehicular Platoons*, IEEE Transactions on Control of Network Systems.

The communication topology (CT), which determines the structure of information exchange between vehicles, plays a crucial role in the performance of the platoon. The control and stability of vehicle platoons for topologies with complex eigenvalues [53], real eigenvalues [12], dynamic communication [105], undirected communication [54, 106], and switching communication [32, 46, 57, 107] have been properly investigated in the literature. Switching in topologies may occur because of varying information flow in the vehicular ad hoc network (VANET) [108]. As CTs goes, dynamic communication topology is a solution to partial failures in the network due to packet loss, signal blocking, or damage to vehicle communication module hardware which can render the platoon unstable.

Though the literature has extensively studied the stability and performance of vehicle platoons for individual CTs, enough attention and work have yet to devote to the differentiation of the effect of CTs on vehicle platoons' performance. Recently, some papers have studied/differentiated the impact of communication topologies on the vehicular platoon. The work in [86] has studied the effect of CTs on the performance of platoons and shown that some topologies exhibit resilience to adversarial actions in different distributed estimation and control algorithms. Also, in [87], the effect differences of various CTs in stability region, robustness, safety, and emission on vehicle platoons have been explored.

In this chapter, the study delves into the examination of the distinctions among communication topologies (CTs) and their consequential effects on vehicular platoon performance. The primary considerations revolve around aspects of stability and transient intervehicle distances (IDs), all within the context of a distributed linear feedback control scheme and the constant distance policy governing vehicle spacing. A noteworthy observation is that the mere presence of internal stability does not guarantee the absence of collisions within the platoon, as exemplified by counterexamples. Therefore, investigating the impact of various CTs on transient IDs emerges as a pivotal endeavor.

To facilitate this examination, the focus shifts from follower-leader state differences to the concept of neighboring-vehicles state differences. Consequently, a novel closed-loop distance dynamic model is introduced to enable internal stability analysis. This model, utilizing neighboring-vehicles state differences, allows for the establishment of a coupled dynamic model for adjacent vehicles, which, in turn, provides insights into the variation in distances between consecutive vehicles.

With this closed-loop dynamic model in place, a correspondence between IDs and initial position differences is established. Furthermore, followers' velocities are derived based on their IDs and the leader's velocity. This information forms the basis for determining control gains by setting collision and safe distance limits on IDs and feasible-velocity constraints on follower velocities. These insights lead to valuable conclusions regarding platoon performance under diverse CTs. The scope of this study encompasses all static communication topologies, and the theoretical findings are substantiated through extensive simulations.

5.1 Problem formulation and Preliminaries

Figure 5.1 depicts a platoon including $n+1$ vehicles in which the leader vehicle is designated by 0 and the follower ones are labeled by $1, \ldots, i, i+1, \ldots, n-1, n$. The x axis shows the position of the vehicles during their travel such that x_0 and x_i are the positions of the leader and the i^{th} follower, respectively. The real and desired intervehicle distances (IDs) between vehicles i and $i+1$ are denoted by D_i^{i+1} and d_i^{i+1}, respectively. Also, L_i shows the length of the i^{th} vehicle. Furthermore, the notation $p_i^{i+1} \triangleq x_i - x_{i+1}$ is unitized for positions difference between consecutive vehicles. Longitudinal control of a platoon generally consists of 1) inner force/acceleration control loop, the feedback linearization (FL) control that compensates for the nonlinear dynamics of the vehicles, and 2) an outer ID control loop that is responsible for setting a desired distance between consecutive vehicles. Let us take it for granted that the FL part has already canceled the dynamics nonlinearities which makes it conducive

to focus only on the ID control loop. For platooning, the leader does not undergo any

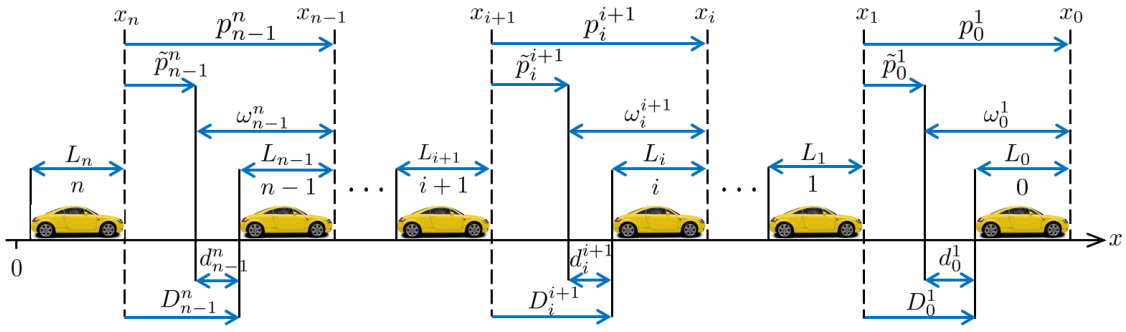

Figure 5.1: A platoon divided into consecutive-pairwise vehicles.

control process but its position, velocity and acceleration are utilized to control the other vehicles. As such, the behavior of each follower vehicle (FV) within the platoon is mathematically described by a third-order linear model [27, 31, 43, 46–48, 53, 54, 56, 57] as follows.

$$\begin{cases} \dot{x}_i = v_i \\ \dot{v}_i = a_i \\ \dot{a}_i = -\frac{1}{\tau} a_i + \frac{1}{\tau} u_i \end{cases} \tag{5.1}$$

in which a_i and v_i are the acceleration and velocity of the i^{th} follower, τ is the engine time constant, and u_i is control signal to be designed properly. Let $\mathbf{X}_i \in R^{3\times 1}$ be defined as $\mathbf{X}_i \triangleq [x_i;\ \dot{x}_i;\ \ddot{x}_i]$ which describes the states of the i^{th} follower such that $\dot{x}_i = v_i$ and $\ddot{x}_i = a_i$. Thus, for $i = 1, \ldots, n$ and given (5.1), the state-space model for the i^{th} follower can be presented as

$$\dot{\mathbf{X}}_i = \mathbf{A}\mathbf{X}_i + \mathbf{B}u_i = \begin{bmatrix} 0 & 1 & 0 \\ 0 & 0 & 1 \\ 0 & 0 & -\frac{1}{\tau} \end{bmatrix} \mathbf{X}_i + \begin{bmatrix} 0 \\ 0 \\ \frac{1}{\tau} \end{bmatrix} u_i \tag{5.2}$$

Assuming a constant distance policy for the platoon, the objective of designing the controller u_i is to guarantee that the followers' velocities/accelerations reach to the leader's velocity/acceleration while desired constant IDs ($\triangleq d_i^{i+1}$) are maintained

between back-to-back vehicles. In other words, the aim is to have

$$\begin{cases} v_i(t) = v_0(t); & i = 1, \dots n \\ x_\kappa - x_{\kappa+1} = L_\kappa + d_\kappa^{\kappa+1}; & \kappa = 0, \dots, n-1 \end{cases} \tag{5.3}$$

and to ensure which, we use the following distributed linear controller:

$$u_i = -\sum_{j \in \mathbb{I}_i} \left[k\left(x_i - x_j - d_{ij}\right) + b\left(\dot{x}_i - \dot{x}_j\right) + h\left(\ddot{x}_i - \ddot{x}_j\right) \right] \tag{5.4}$$

in which the set $\mathbb{I}_i \subset \{\{0, 1, \dots, n\} - \{i\}\}$ indicates all vehicles from which the i^{th} vehicle receives information and

$$d_{ij} \triangleq -sgn(i-j) \sum_{\kappa=\min(i,j)}^{\max(i,j)-1} \omega_\kappa^{\kappa+1}; \quad \omega_k^{\kappa+1} \triangleq L_\kappa + d_\kappa^{\kappa+1} \tag{5.5}$$

where the notation $\triangleq$ is utilized for definition. For later usage, let the notation $z_i^j = 0$ be used to show that the i^{th} vehicle does not receive information from the j^{th} vehicle, and $z_i^j = 1$ if the other way around. Having d_i^{i+1} as the desired ID and x_0 as the position of the leader vehicle, the desired position (x_i^*), velocity ($\dot{x}_i^*$) and acceleration ($\ddot{x}_i^*$) of the i^{th} follower is defined as

$$x_i^* \triangleq x_0 - \sum_{\kappa=0}^{i-1} \omega_\kappa^{\kappa+1}, \quad \dot{x}_i^* = v_0 = \dot{x}_0, \quad \ddot{x}_i^* = 0 \tag{5.6}$$

where $\omega_\kappa^{\kappa+1}$ is already defined in (5.5). Now, the state error of the i^{th} follower can be defined as $\tilde{x}_i \triangleq x_i - x_i^*$ utilizing which readily results in $x_i - x_j = \tilde{x}_i - \tilde{x}_j + d_{ij}$, and substituting which into the controller (5.4) gives

$$u_i = -\sum_{j \in \mathbb{I}_i} \left[k\left(\tilde{x}_i - \tilde{x}_j\right) + b\left(\dot{\tilde{x}}_i - \dot{\tilde{x}}_j\right) + h\left(\ddot{\tilde{x}}_i - \ddot{\tilde{x}}_j\right) \right] \tag{5.7}$$

Now, defining $\tilde{\mathbf{X}}_i \in R^{3\times 1}$ where $\tilde{\mathbf{X}}_i \triangleq \left[\tilde{x}_i;\ \dot{\tilde{x}}_i;\ \ddot{\tilde{x}}_i\right]$ and plugging (5.7) in (5.1) yields

$$\dddot{\tilde{x}}_i = -\frac{1}{\tau}\mathbb{K}_i\tilde{\mathbf{X}}_i + \sum_{j \in \mathbb{I}_i} \frac{1}{\tau}\mathbf{K}\tilde{\mathbf{X}}_j \tag{5.8}$$

where $\mathbf{K} \triangleq [k,\ b,\ h]$ is defined as the control-gain vector of the measurements transmitted from the j^{th} vehicle to the i^{th} vehicle, and $\mathbb{K}_i \triangleq [\mathbf{k}_i,\ \mathbf{b}_i,\ \mathbf{h}_i]$ in which $\mathbf{k}_i \triangleq |\mathbb{I}_i|k$,

$\mathbf{b}_i \triangleq |\mathbb{I}_i|b$ and $\mathbf{h}_i \triangleq 1+|\mathbb{I}_i|h$ where $|\mathbb{I}_i|$ denotes the cardinality of the set $\mathbb{I}_i$. Please note that (5.8) has been obtained using the facts that $\ddot{x}_i = \ddot{\tilde{x}}_i$ and $\dddot{x}_i = \dddot{\tilde{x}}_i$. Now, we go over formulating the closed-loop dynamic model of the platoon. To this end, first, we briefly explain the conventional method as Approach 1, and secondly, we elaborate on our developed novel distance dynamic model for the platoon as Approach 2.

Approach 1: Like [27, 53, 54], the followers-leader state differences are considered as the states of the platoon. Therefore, considering (5.8), knowing $\tilde{x}_0 = \dot{\tilde{x}}_0 = \ddot{\tilde{x}}_0 = 0$, and defining the platoon's total state-error vector ($\tilde{\mathbf{X}}_t \in R^{3n\times 1}$) by $\tilde{\mathbf{X}}_t \triangleq \Big[\tilde{\mathbf{X}}_1,\ \tilde{\mathbf{X}}_2, \ldots,\ \tilde{\mathbf{X}}_n\Big]$, then the platoon's closed-loop state-space dynamic model can be compactly characterized by

$$\dddot{\tilde{\mathbf{X}}}_t = \tilde{\mathbf{A}}_t\tilde{\mathbf{X}}_t = [\mathbf{I}_n \otimes \mathbf{A} - \mathbf{P} \otimes \mathbf{BK}]\,\tilde{\mathbf{X}}_t \tag{5.9}$$

in which $\mathbf{P} \in R^{n\times n}$ whose elements P_{ij} are according to

$$P_{ij} = \begin{cases} |\mathbb{I}_i| & \text{if} \quad i = j \\ 0 & \text{if} \quad z_i^j = 0 \\ -1 & \text{if} \quad z_i^j = 1 \end{cases} \tag{5.10}$$

Remark 10 *Figs. 5.2 and 5.3 show typical unidirectional and bidirectional CTs between vehicles. In unidirectional communication topologies (UCTs), all followers receive information only from vehicles ahead, and in bidirectional communication topologies (BCTs), followers also receive information from vehicles behind. In typical CTs, the communication between vehicles are according to some certain disciplines. Having that said, Fig. 5.4 depicts some arbitrary nontypical CTs that do not follow any certain practice in their communications.*

Remark 11 *Given* (5.10) *and Figs. 5.2-5.4, for typical CTs: PF, MPF, TPLF, PLF, TPF, BDL, BD and TBPF, and nontypical CTs:* **a** *and* **d**, *since the communications between vehicles are either undirected, i.e.,* $j \in \mathbb{I}_i \iff i \in \mathbb{I}_j$, $i, j = 1, \ldots, n-1$,

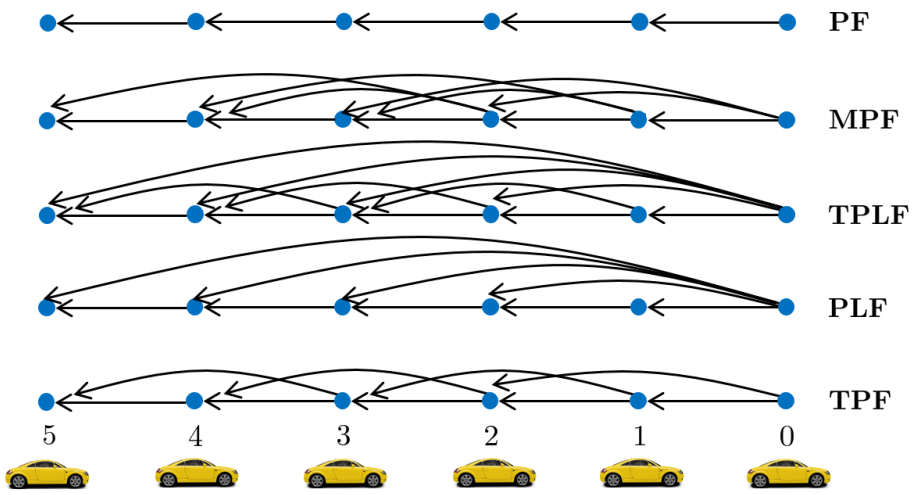

Figure 5.2: Some typical UCTs between vehicles.

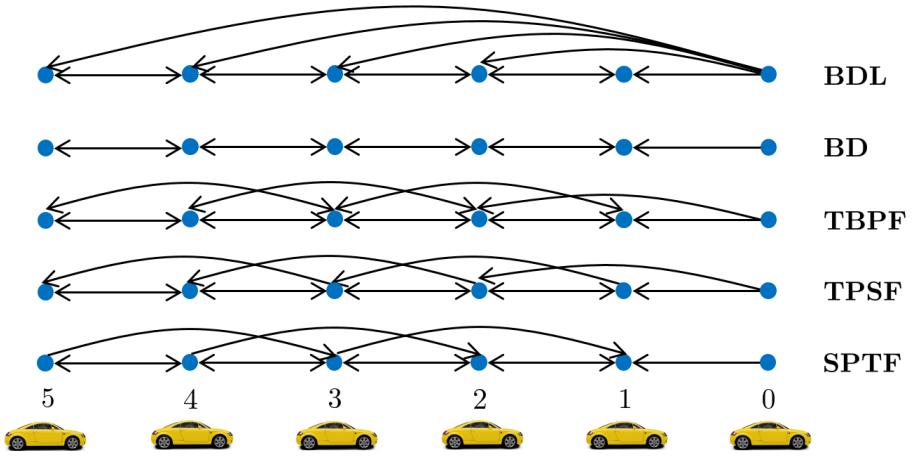

Figure 5.3: Some typical BCTs between vehicles.

or the followers receive information only from vehicles ahead, then their associated matrix $\mathbf{P}$ *has only real eigenvalues* (λ_i, $i = 1, \ldots, n$) *[27]. Also, for CTs: TPSF and SPTF, the matrix* $\mathbf{P}$ *has combination of real* ($\bar{\lambda}_i$, $i = 1, \ldots, l$) *and conjugate complex* ($\sigma_i \pm j\omega_i$, $i = 1, \ldots, \frac{n-l}{2}$) *eigenvalues [53].*

Remark 12 *For those CTs in which the matrix* $\mathbf{P}$ *has only real eigenvalues, the platoon dynamics* (5.9) *would be asymptotically stable if and only if the resultant matrices*

$$\mathbf{A} - \lambda_i \mathbf{B}\mathbf{K} \tag{5.11}$$

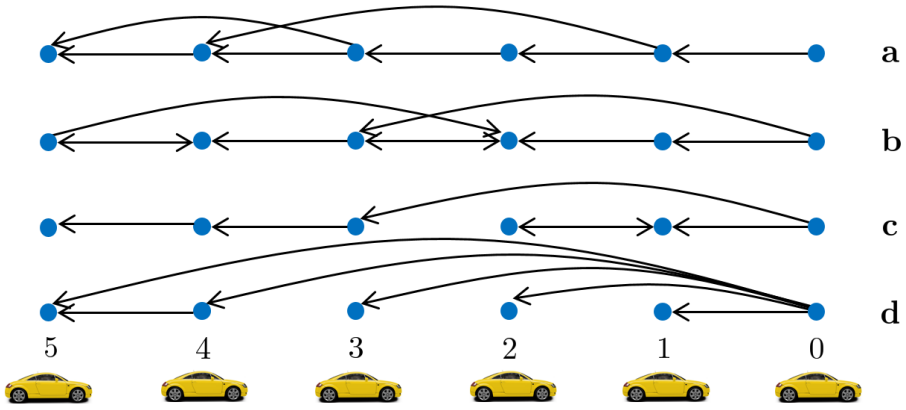

Figure 5.4: Some arbitrary nontypical CTs.

are all Hurwitz, i.e., their eigenvalues are all negative [27]. Note that λ_i*;* $i = 1, \ldots, n-1$*, denote the eigenvalues of the matrix* $\mathbf{P}$*. Given that* $k, b, h > 0$*, using Routh-Hurwitz stability criterion, the following condition can be found for the internal stability of the platoon:* $b > \frac{k\tau}{1+\lambda_{min}h}$ *where* $\lambda_{min} = \min_i\{\lambda_i\}$*.*

Remark 13 *For those CTs in which the eigenvalues of the matrix* $\mathbf{P}$ *are combination of real and conjugate complex values, the platoon dynamics* (5.9) *would be asymptotically stable if and only if the following resultant matrices*

$$\begin{cases} 1)\mathbf{A} - \bar{\lambda}_i\mathbf{BK} & i = 1, \ldots, l \\ 2)\mathbf{I}_2 \otimes \mathbf{A} - \begin{bmatrix} \sigma_i & \omega_i \\ \omega_i & \sigma_i \end{bmatrix} \otimes \mathbf{BK} & i = 1, \ldots, \frac{n-l}{2} \end{cases} \tag{5.12}$$

are all Hurwitz, i.e., their eigenvalues are all negative [53]. Note that in (5.12)*, the second matrix would result in a characteristic polynomial of degree six.*

Approach 2: Instead of using followers-leader state differences, we define neighboring-vehicles state differences as the states of the platoon. Given (5.9) and having internal stability conditions satisfied, one can guarantee that the error signals (i.e., $\tilde{\mathbf{X}}_t$) will become finally zero (steady-state behavior). Thus, IDs will converge to their desired values, and the followers will reach the leader vehicle's velocity. However, internal stability analysis does not provide information about the transient behavior of distances

between neighboring vehicles and whether they reduce below a non-collision safety threshold. Also, for given initial conditions, it is possible to show with a counterexample that the internal stability does not necessarily lead to a non-colliding platoon. Therefore, it entails developing an alternative dynamic model through which besides stability analysis it can offer a proper way to describe the transient behavior of the IDs. In this chapter, presenting an approach to readily describe the IDs, we spot the performance differences of the platoon under different CTs. Next section is dedicated to finding the above-mentioned novel dynamic model for the platoon.

5.2 Novel Dynamic Model for the Platoon Using Neighboring-Vehicles State Differences

In this section, we introduce an alternative dynamic model for (5.9) which results in the same internal stability conditions (Remarks 12-13) but can be exploited to study the transient IDs. To this end, we first extract the dynamics of pairwise consecutive vehicles under any (typical/nontypical) CTs. As such, let the position, velocity, acceleration and jerk errors between the consecutive vehicles characterize by

$$\begin{aligned}\tilde{\mathbf{X}}_i^{i+1} &\triangleq \tilde{\mathbf{X}}_i - \tilde{\mathbf{X}}_{i+1} \triangleq \left[\tilde{p}_i^{i+1},\ \tilde{v}_i^{i+1},\ \tilde{a}_i^{i+1}\right] \\ \dot{\tilde{\mathbf{X}}}_i^{i+1} &\triangleq \dot{\tilde{\mathbf{X}}}_i - \dot{\tilde{\mathbf{X}}}_{i+1} \triangleq \left[\tilde{v}_i^{i+1},\ \tilde{a}_i^{i+1},\ \tilde{\jmath}_i^{i+1}\right]\end{aligned} \tag{5.13}$$

In other words, $\tilde{p}_i^{i+1} \triangleq \tilde{x}_i - \tilde{x}_{i+1}$, $\tilde{v}_i^{i+1} \triangleq \dot{\tilde{x}}_i - \dot{\tilde{x}}_{i+1}$, $\tilde{a}_i^{i+1} \triangleq \ddot{\tilde{x}}_i - \ddot{\tilde{x}}_{i+1}$ and $\tilde{\jmath}_i^{i+1} \triangleq \dddot{\tilde{x}}_i - \dddot{\tilde{x}}_{i+1}$. Furthermore, for $j \in \{i, i+1\}$ and having $0 < \Delta t \ll 1$ as a quite small sampling-time, we will have $\tilde{\mathbf{X}}_j(t + \Delta t) = \tilde{\mathbf{X}}_j(t) + \Delta t \dot{\tilde{\mathbf{X}}}_j(t)$, using which and (5.13), it is obvious that

$$\frac{\tilde{\mathbf{X}}_i^{i+1}(t + \Delta t) - \tilde{\mathbf{X}}_i^{i+1}(t)}{\Delta t} = \dot{\tilde{\mathbf{X}}}_i^{i+1}(t) \tag{5.14}$$

Fig. 5.5 shows the possible connection types between adjacent vehicles, using which

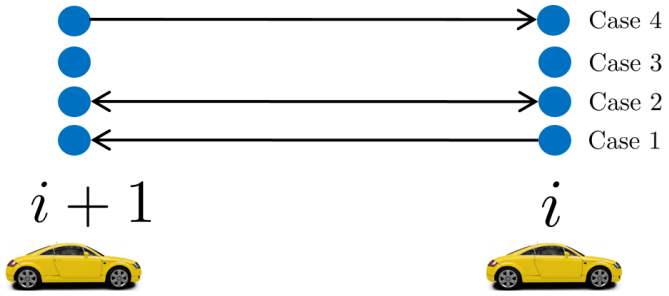

Figure 5.5: Connection types between neighboring vehicles.

we define the parameter ζ_i^{i+1} as

$$\zeta_i^{i+1} = \begin{cases} 1 & \text{if} \quad z_{i+1}^i = 1 \text{ and } z_i^{i+1} = 0 \\ 1 & \text{if} \quad z_i^{i+1} = 1 \text{ and } z_{i+1}^i = 1 \\ 0 & \text{if} \quad z_i^{i+1} = 0 \text{ and } z_{i+1}^i = 0 \\ 0 & \text{if} \quad z_i^{i+1} = 1 \text{ and } z_{i+1}^i = 0 \end{cases} \tag{5.15}$$

in which, for instance, $z_i^{i+1} = 1$ denotes that the i^{th} vehicle receives information from the $(i+1)^{th}$ vehicle, and $z_i^{i+1} = 0$ denotes that the i^{th} vehicle does not receive information from the $(i+1)^{th}$ vehicle. Now using (5.15) and (5.8), $\tilde{\mathfrak{I}}_i^{i+1}$ for $i = 0, 1, \ldots, n-1$ can be obtained as

$$\begin{aligned} \Delta\tilde{\mathfrak{I}}_i^{i+1} = &-\frac{1}{\tau}\mathbb{N}_i\tilde{\mathbf{X}}_i^{i+1} + \frac{1}{\tau}\mathbf{K}\sum_{j\in\alpha_i}\sum_{\kappa=j}^{i-1}\tilde{\mathbf{X}}_\kappa^{\kappa+1} + \frac{1}{\tau}\mathbf{K}\sum_{j\in\beta_i}\sum_{\kappa=i+1}^{j-1}\tilde{\mathbf{X}}_\kappa^{\kappa+1} \\ &- \frac{1}{\tau}\mathbf{K}\sum_{j\in\bar{\alpha}_i}\sum_{\kappa=i+1}^{j-1}\tilde{\mathbf{X}}_\kappa^{\kappa+1} - \frac{1}{\tau}\mathbf{K}\sum_{j\in\bar{\beta}_i}\sum_{\kappa=j}^{i-1}\tilde{\mathbf{X}}_\kappa^{\kappa+1} \end{aligned} \tag{5.16}$$

in which $\mathbb{N}_i = [|\mathbf{N}_i|k,\ |\mathbf{N}_i|b,\ 1+|\mathbf{N}_i|h]$ and $|\mathbf{N}_i|$ denotes the cardinality of set $\mathbf{N}_i$ which is defined as $\mathbf{N}_i \triangleq \{\zeta_i^{i+1} i\} \cup \big(\mathbb{I}_i \cup \bar{\beta}_i - \alpha_i\big)$. Also, sets α_i, β_i, $\bar{\beta}_i$, and $\bar{\alpha}_i$ are defined as $\alpha_i \triangleq \{j \in \mathbb{R}_i \mid z_i^j = 1 \,\&\, z_{i+1}^j = 0 \,\&\, j < i\}$, $\beta_i \triangleq \{j \in \mathbb{R}_{i+1} \mid z_{i+1}^j = 1 \,\&\, z_i^j = 0 \,\&\, j > i+1\}$, $\bar{\beta}_i \triangleq \{j \in \mathbb{R}_{i+1} \mid z_{i+1}^j = 1 \,\&\, z_i^j = 0 \,\&\, j < i\}$, and $\bar{\alpha}_i \triangleq \{j \in \mathbb{R}_i \mid z_i^j = 1 \,\&\, z_{i+1}^j = 0 \,\&\, j > i+1\}$, respectively. For the cases 1, 2, 3 and 4 in (5.15), we have defined and utilized $\mathbb{R}_i = \mathbb{I}_i$ and $\mathbb{R}_{i+1} = \mathbb{I}_{i+1} - \{i\}$, $\mathbb{R}_i = \mathbb{I}_i - \{i+1\}$ and $\mathbb{R}_{i+1} = \mathbb{I}_{i+1} - \{i\}$, $\mathbb{R}_i = \mathbb{I}_i$ and $\mathbb{R}_{i+1} = \mathbb{I}_{i+1}$, and $\mathbb{R}_i = \mathbb{I}_i - \{i+1\}$ and $\mathbb{R}_{i+1} = \mathbb{I}_{i+1}$, respectively.

Proof. First, let define $\tilde{\mathbf{X}}_i^{i+1} \triangleq \tilde{\mathbf{X}}_i - \tilde{\mathbf{X}}_{i+1}$, $\tilde{\mathbf{X}}_j^i \triangleq \tilde{\mathbf{X}}_j - \tilde{\mathbf{X}}_i$ and $\tilde{\mathbf{X}}_{i+1}^j \triangleq \tilde{\mathbf{X}}_{i+1} - \tilde{\mathbf{X}}_j$. Now, for $i = 1, \ldots, n-1$ and using (5.8), we have

$$\begin{cases} \dddot{\tilde{x}}_i = -\frac{1}{\tau}\mathbb{K}_i\tilde{\mathbf{X}}_i + \frac{1}{\tau}\sum_{j\in\mathbb{I}_i}\mathbf{K}\tilde{\mathbf{X}}_j \\ \dddot{\tilde{x}}_{i+1} = -\frac{1}{\tau}\mathbb{K}_{i+1}\tilde{\mathbf{X}}_{i+1} + \frac{1}{\tau}\sum_{j\in\mathbb{I}_{i+1}}\mathbf{K}\tilde{\mathbf{X}}_j \end{cases} \tag{5.17}$$

Therefore, for $\tilde{\mathfrak{J}}_i^{i+1} \triangleq \dddot{\tilde{x}}_i - \dddot{\tilde{x}}_{i+1}$, we get

$$\tilde{\mathfrak{J}}_i^{i+1} = -\frac{1}{\tau}\mathbb{K}_i\tilde{\mathbf{X}}_i^{i+1} - \frac{1}{\tau}\left(\mathbb{K}_i - \mathbb{K}_{i+1}\right)\tilde{\mathbf{X}}_{i+1} + \sum_{j\in\mathbb{I}_i}\frac{1}{\tau}\mathbf{K}\tilde{\mathbf{X}}_j - \sum_{j\in\mathbb{I}_{i+1}}\frac{1}{\tau}\mathbf{K}\tilde{\mathbf{X}}_j \tag{5.18}$$

Since $-\frac{1}{\tau}\left(\mathbb{K}_i - \mathbb{K}_{i+1}\right) = \sum_{j\in\mathbb{I}_{i+1}}\frac{1}{\tau}\mathbf{K} - \sum_{j\in\mathbb{I}_i}\frac{1}{\tau}\mathbf{K}$, then (5.18) can be rewritten as

$$\tilde{\mathfrak{J}}_i^{i+1} = -\frac{1}{\tau}\mathbb{K}_i\tilde{\mathbf{X}}_i^{i+1} + \sum_{j\in\mathbb{I}_i}\frac{1}{\tau}\mathbf{K}\tilde{\mathbf{X}}_j^{i+1} - \sum_{j\in\mathbb{I}_{i+1}}\frac{1}{\tau}\mathbf{K}\tilde{\mathbf{X}}_j^{i+1} \tag{5.19}$$

Now, having $\tilde{\mathbf{X}}_j - \tilde{\mathbf{X}}_{i+1} = \tilde{\mathbf{X}}_j - \tilde{\mathbf{X}}_i + \tilde{\mathbf{X}}_i - \tilde{\mathbf{X}}_{i+1}$, (5.19) is equal to

$$\tilde{\mathfrak{J}}_i^{i+1} = \frac{1}{\tau}\left(-\mathbb{K}_i + \sum_{j\in\mathbb{I}_i}\mathbf{K} - \sum_{j\in\mathbb{I}_{i+1}}\mathbf{K}\right)\tilde{\mathbf{X}}_i^{i+1} + \sum_{j\in\mathbb{I}_i}\frac{1}{\tau}\mathbf{K}\tilde{\mathbf{X}}_j^i - \sum_{j\in\mathbb{I}_{i+1}}\frac{1}{\tau}\mathbf{K}\tilde{\mathbf{X}}_j^i \tag{5.20}$$

which depending on how the connection is between the neighboring vehicles it can be reformulated as

$$\tilde{\mathfrak{J}}_i^{i+1} = -\frac{1}{\tau}\left(\mathbb{K}_i + \zeta_i^{i+1}\mathbf{K} - \sum_{j\in\mathbb{R}_i}\mathbf{K} + \sum_{j\in\mathbb{R}_{i+1}}\mathbf{K}\right)\tilde{\mathbf{X}}_i^{i+1} + \sum_{j\in\mathbb{R}_i}\frac{1}{\tau}\mathbf{K}\tilde{\mathbf{X}}_j^i - \sum_{j\in\mathbb{R}_{i+1}}\frac{1}{\tau}\mathbf{K}\tilde{\mathbf{X}}_j^i \tag{5.21}$$

where ζ_i^{i+1} is defined in (5.15). Splitting $j \in \mathbb{R}_i$ and $j \in \mathbb{R}_{i+1}$ in parts $j < i$ and $j > i+1$, and using the fact that for part $j > i+1$, we have $\mathbf{X}_j - \tilde{\mathbf{X}}_i = \mathbf{X}_j - \tilde{\mathbf{X}}_{i+1} - \left(\tilde{\mathbf{X}}_i - \tilde{\mathbf{X}}_{i+1}\right)$, then (5.21) can be reformulated as

$$\tilde{\mathfrak{J}}_i^{i+1} = -\frac{1}{\tau}\left(\mathbb{K}_i + \zeta_i^{i+1}\mathbf{K} - \sum_{j\in\mathbb{R}_i^{<i}}\mathbf{K} + \sum_{j\in\mathbb{R}_{i+1}^{<i}}\mathbf{K}\right)\tilde{\mathbf{X}}_i^{i+1} + Z \tag{5.22}$$

where $Z = \frac{1}{\tau}\sum_{j\in\mathbb{R}_i^{<i}}\mathbf{K}\tilde{\mathbf{X}}_j^i - \frac{1}{\tau}\sum_{j\in\mathbb{R}_{i+1}^{<i}}\mathbf{K}\tilde{\mathbf{X}}_j^i + \frac{1}{\tau}\sum_{j\in\mathbb{R}_{i+1}^{>i+1}}\mathbf{K}\tilde{\mathbf{X}}_{i+1}^j - \frac{1}{\tau}\sum_{j\in\mathbb{R}_i^{>i+1}}\mathbf{K}\tilde{\mathbf{X}}_{i+1}^j$. It is apparent that for $\{j \mid j \in \mathbb{R}_i \,\&\, j \in \mathbb{R}_{i+1}\}$ we have $Z = 0$. Therefore, depending

on how the pair $(i, i+1)$ receives information from the other vehicles, the overall connection types leading to $Z \neq 0$ can be as the following:

a) The i^{th} follower receives information from some vehicles ahead, from which the $(i+1)^{th}$ follower does not receive. Let the set be defined as $\alpha_i \triangleq \{j \in \mathbb{R}_i \mid z_i^j = 1 \,\&\, z_{i+1}^j = 0 \,\&\, j < i\}$.

b) The $(i+1)^{th}$ follower receives information from some vehicles behind, from which the i^{th} follower does not receive. Let the set be defined as $\beta_i \triangleq \{j \in \mathbb{R}_{i+1} \mid z_{i+1}^j = 1 \,\&\, z_i^j = 0 \,\&\, j > i+1\}$.

c) The $(i+1)^{th}$ follower receives information from some vehicles ahead, from which the i^{th} follower does not receive. Let the set be defined as $\bar{\beta}_i \triangleq \{j \in \mathbb{R}_{i+1} \mid z_{i+1}^j = 1 \,\&\, z_i^j = 0 \,\&\, j < i\}$.

d) The i^{th} follower receives information from some vehicles behind, from which the $(i+1)^{th}$ follower does not receive. Let the set be defined as $\bar{\alpha}_i \triangleq \{j \in \mathbb{R}_i \mid z_i^j = 1 \,\&\, z_{i+1}^j = 0 \,\&\, j > i+1\}$.

Therefore, $Z \neq 0$ can be rewritten as

$$Z = \sum_{j\in\alpha_i} \frac{1}{\tau}\mathbf{K}\tilde{\mathbf{X}}_j^i + \sum_{j\in\beta_i} \frac{1}{\tau}\mathbf{K}\tilde{\mathbf{X}}_{i+1}^j - \sum_{j\in\bar{\alpha}_i} \frac{1}{\tau}\mathbf{K}\tilde{\mathbf{X}}_{i+1}^j - \sum_{j\in\bar{\beta}_i} \frac{1}{\tau}\mathbf{K}\tilde{\mathbf{X}}_j^i \tag{5.23}$$

where substituting $-\sum_{j\in\bar{\alpha}_i} \frac{1}{\tau}\mathbf{K}\tilde{\mathbf{X}}_{i+1}^j = \sum_{j\in\bar{\alpha}_i} \frac{1}{\tau}\mathbf{K}\left(\tilde{\mathbf{X}}_j^i + \tilde{\mathbf{X}}_i^{i+1}\right)$ and $-\sum_{j\in\bar{\beta}_i} \frac{1}{\tau}\mathbf{K}\tilde{\mathbf{X}}_j^i = -\sum_{j\in\bar{\beta}_i} \frac{1}{\tau}\mathbf{K}\left(\tilde{\mathbf{X}}_j^{i+1} - \tilde{\mathbf{X}}_i^{i+1}\right)$ into (5.23), and subsequently the updated (5.23) into (5.22), and using the fact that $\tilde{\mathbf{X}}_j^i$ and $\tilde{\mathbf{X}}_{i+1}^j$ can be rewritten in the following form:

$$\begin{cases} \tilde{\mathbf{X}}_j^i = \sum_{\kappa=j}^{i-1} \tilde{\mathbf{X}}_\kappa^{\kappa+1}; & j < i \\ \tilde{\mathbf{X}}_j^i = -\sum_{\kappa=i}^{j-1} \tilde{\mathbf{X}}_\kappa^{\kappa+1}; & j > i+1 \\ \tilde{\mathbf{X}}_{i+1}^j = \sum_{\kappa=i+1}^{j-1} \tilde{\mathbf{X}}_\kappa^{\kappa+1}; & j > i+1 \\ \tilde{\mathbf{X}}_{i+1}^j = -\sum_{\kappa=j}^{i} \tilde{\mathbf{X}}_\kappa^{\kappa+1}; & j < i \end{cases} \tag{5.24}$$

yields

$$\tilde{\mathfrak{J}}_i^{i+1} = -\frac{1}{\tau}\left(\mathbb{K}_i + \left(\zeta_i^{i+1} + |\bar{\beta}_i| - |\alpha_i|\right)\mathbf{K}\right)\tilde{\mathbf{X}}_i^{i+1} + \frac{1}{\tau}\mathbf{K}\sum_{j\in\alpha_i}\sum_{\kappa=j}^{i-1}\tilde{\mathbf{X}}_\kappa^{\kappa+1} + \frac{1}{\tau}\mathbf{K}\sum_{j\in\beta_i}\sum_{\kappa=i+1}^{j-1}\tilde{\mathbf{X}}_\kappa^{\kappa+1} - \frac{1}{\tau}\mathbf{K}\sum_{j\in\bar{\alpha}_i}\sum_{\kappa=i+1}^{j-1}\tilde{\mathbf{X}}_\kappa^{\kappa+1} - \frac{1}{\tau}\mathbf{K}\sum_{j\in\bar{\beta}_i}\sum_{\kappa=j}^{i-1}\tilde{\mathbf{X}}_\kappa^{\kappa+1} \tag{5.25}$$

Now, let us study for $i = 0$ or to be exact for the pair $(0, 1)$. For typical/nontypical CTs, we have $\bar{\alpha}_0 = \bar{\beta}_0 = \emptyset$ and given that $\tilde{\mathbf{X}}_0 = 0$, using (5.17) yields

$$\tilde{\mathfrak{J}}_0^1 = -\frac{1}{\tau}\mathbb{K}_1\tilde{\mathbf{X}}_0^1 + \frac{1}{\tau}\sum_{j\in\mathbb{R}_1^{\geq 2}}\mathbf{K}\left(\tilde{\mathbf{X}}_0^1 + \tilde{\mathbf{X}}_1^j\right) = -\frac{1}{\tau}\left(\mathbb{K}_1 - |\beta_0|\mathbf{K}\right)\tilde{\mathbf{X}}_0^1 + \frac{1}{\tau}\sum_{j\in\beta_0}\mathbf{K}\tilde{\mathbf{X}}_1^j \tag{5.26}$$

where $\beta_0 \triangleq \{j \in \mathbb{R}_1 | j \geq 2\}$. Also, for the pair $(0, 1)$, since $|\beta_0| = |\mathbb{I}_1| - (1 - |\alpha_0|)$, then $\mathbb{K}_1 - |\beta_0|\mathbf{K} = \mathbb{K}$, where $\mathbb{K} \triangleq [k,\ b,\ 1 + h]$. Therefore, (5.26) can be rewritten as

$$\tilde{\mathfrak{J}}_0^1 = -\frac{1}{\tau}\left(\mathbb{K}_0 + \zeta_0^1\mathbf{K}\right)\tilde{\mathbf{X}}_0^1 + \frac{1}{\tau}\mathbf{K}\sum_{j\in\beta_0}\sum_{\kappa=1}^{j-1}\tilde{\mathbf{X}}_\kappa^{\kappa+1} \tag{5.27}$$

in which we define $\mathbb{K}_0 \triangleq [0,\ 0,\ 1]$. Also, $\zeta_0^1 = 1$ as we suppose that the first follower always receives information from the leader. Please note that $\alpha_0 = \bar{\alpha}_0 = \emptyset$. Therefore, for $i = 0, \ldots, n-1$ and any communication topology, (5.25) holds true. Note that for unidirectional CTs, we have $\bar{\alpha}_i = \bar{\beta}_i = \emptyset$. Now, let define $\mathbb{N}_i \triangleq \mathbb{K}_i + \left(\zeta_i^{i+1} + |\bar{\beta}_i| - |\alpha_i|\right)\mathbf{K}$ such that $\mathbb{N}_i = [|\mathbf{N}_i|k,\ |\mathbf{N}_i|b,\ 1 + |\mathbf{N}_i|h]$ which holds true by defining $\mathbf{N}_i$ as $\mathbf{N}_i \triangleq \{\zeta_i^{i+1} i\} \cup \left(\mathbb{I}_i \cup \bar{\beta}_i - \alpha_i\right)$. Thus, the proof completed. ■

Considering (5.16), regarding the facts that $d/dt\{\tilde{p}_i^{i+1}\} = \tilde{v}_i^{i+1}$ and $d/dt\{\tilde{v}_i^{i+1}\} = \tilde{a}_i^{i+1}$, defining $\tilde{y}_i^{i+1} = \tilde{p}_i^{i+1}$ as the output of the closed-loop dynamics of the neighboring vehicles i and $i+1$, then for $i = 0, \ldots, n-1$, the state-space model for the pair $(i, i+1)$ can be presented as (see (5.2))

$$\begin{cases} \dot{\tilde{\mathbf{X}}}_i^{i+1} = \mathbf{A}_i^{i+1}\tilde{\mathbf{X}}_i^{i+1} + \mathbf{B}\tilde{u}_i^{i+1} \\ \tilde{y}_i^{i+1} = \mathbf{C}\tilde{\mathbf{X}}_i^{i+1} \end{cases} \tag{5.28}$$

Table 5.1: Sets α_i and β_i, and values of $|\mathbb{I}_{i+1}|$ and $|\mathbf{N}_i|$ for the pair $(i, i+1)$ of a platoon with five FVs within different typical communication topologies given in Fig. 5.2-5.3. For the topologies of Figs. 5.2-5.3, the sets $\bar{\alpha}_i$ and $\bar{\beta}_i$ are empty sets, i.e., $\bar{\alpha}_i = \bar{\beta}_i = \emptyset$.

Pairs:	$(0,1)$	$(1,2)$	$(2,3)$	$(3,4)$	$(4,5)$
	$\{\alpha_0, \beta_0\}$ & $\|\mathbb{I}_1\|$ & $\|\mathbf{N}_0\|$	$\{\alpha_1, \beta_1\}$ & $\|\mathbb{I}_2\|$ & $\|\mathbf{N}_1\|$	$\{\alpha_2, \beta_2\}$ & $\|\mathbb{I}_3\|$ & $\|\mathbf{N}_2\|$	$\{\alpha_3, \beta_3\}$ & $\|\mathbb{I}_4\|$ & $\|\mathbf{N}_3\|$	$\{\alpha_4, \beta_4\}$ & $\|\mathbb{I}_5\|$ & $\|\mathbf{N}_4\|$
PF	$\{\emptyset, \emptyset\}$ & 1 & 1	$\{\{0\}, \emptyset\}$ & 1 & 1	$\{\{1\}, \emptyset\}$ & 1 & 1	$\{\{2\}, \emptyset\}$ & 1 & 1	$\{\{3\}, \emptyset\}$ & 1 & 1
MPF	$\{\emptyset, \emptyset\}$ & 1 & 1	$\{\emptyset, \emptyset\}$ & 2 & 2	$\{\emptyset, \emptyset\}$ & 3 & 3	$\{\{0\}, \emptyset\}$ & 3 & 3	$\{\{1\}, \emptyset\}$ & 3 & 3
TPLF	$\{\emptyset, \emptyset\}$ & 1 & 1	$\{\emptyset, \emptyset\}$ & 2 & 2	$\{\emptyset, \emptyset\}$ & 3 & 3	$\{\{1\}, \emptyset\}$ & 3 & 3	$\{\{2\}, \emptyset\}$ & 3 & 3
PLF	$\{\emptyset, \emptyset\}$ & 1 & 1	$\{\emptyset, \emptyset\}$ & 2 & 2	$\{\{1\}, \emptyset\}$ & 2 & 2	$\{\{2\}, \emptyset\}$ & 2 & 2	$\{\{3\}, \emptyset\}$ & 2 & 2
TPF	$\{\emptyset, \emptyset\}$ & 1 & 1	$\{\emptyset, \emptyset\}$ & 2 & 2	$\{\{0\}, \emptyset\}$ & 2 & 2	$\{\{1\}, \emptyset\}$ & 2 & 2	$\{\{2\}, \emptyset\}$ & 2 & 2
BDL	$\{\emptyset, \{2\}\}$ & 2 & 1	$\{\emptyset, \{3\}\}$ & 3 & 3	$\{\{1\}, \{4\}\}$ & 3 & 3	$\{\{2\}, \{5\}\}$ & 3 & 3	$\{\{3\}, \emptyset\}$ & 2 & 3
BD	$\{\emptyset, \{2\}\}$ & 2 & 1	$\{\{0\}, \{3\}\}$ & 2 & 2	$\{\{1\}, \{4\}\}$ & 2 & 2	$\{\{2\}, \{5\}\}$ & 2 & 2	$\{\{3\}, \emptyset\}$ & 1 & 2
TBPF	$\{\emptyset, \{2,3\}\}$ & 3 & 1	$\{\emptyset, \{4\}\}$ & 4 & 4	$\{\{0\}, \{5\}\}$ & 4 & 4	$\{\{1\}, \emptyset\}$ & 3 & 4	$\{\{2\}, \emptyset\}$ & 2 & 3
TPSF	$\{\emptyset, \{2\}\}$ & 2 & 1	$\{\emptyset, \{3\}\}$ & 3 & 3	$\{\{0\}, \{4\}\}$ & 3 & 3	$\{\{1\}, \{5\}\}$ & 3 & 3	$\{\{2\}, \emptyset\}$ & 2 & 3
SPTF	$\{\emptyset, \{2,3\}\}$ & 3 & 1	$\{\{0\}, \{4\}\}$ & 3 & 3	$\{\{1\}, \{5\}\}$ & 3 & 3	$\{\{2\}, \emptyset\}$ & 2 & 3	$\{\{3\}, \emptyset\}$ & 1 & 2

where $\mathbf{C} = [1,\ 0,\ 0]$, and $\mathbf{A}_i^{i+1} \in R^{3\times 3}$ and $\tilde{u}_i^{i+1} \in R$ are

$$\mathbf{A}_i^{i+1} = \begin{bmatrix} 0 & 1 & 0 \\ 0 & 0 & 1 \\ -\frac{|\mathbf{N}_i|k}{\tau} & -\frac{|\mathbf{N}_i|b}{\tau} & -\frac{1+|\mathbf{N}_i|h}{\tau} \end{bmatrix} \tag{5.29}$$

and

$$\tilde{u}_i^{i+1} = \mathbf{K}\sum_{j\in\alpha_i}\sum_{\kappa=j}^{i-1}\tilde{\mathbf{X}}_\kappa^{\kappa+1} + \mathbf{K}\sum_{j\in\beta_i}\sum_{\kappa=i+1}^{j-1}\tilde{\mathbf{X}}_\kappa^{\kappa+1} - \mathbf{K}\sum_{j\in\bar{\alpha}_i}\sum_{\kappa=i}^{j-1}\tilde{\mathbf{X}}_\kappa^{\kappa+1} - \mathbf{K}\sum_{j\in\bar{\beta}_i}\sum_{\kappa=j}^{i}\tilde{\mathbf{X}}_\kappa^{\kappa+1} \tag{5.30}$$

respectively. It is apparent that for a platoon with n followers, $\alpha_0 = \bar{\alpha}_0 = \bar{\beta}_0 = \emptyset$ and $\beta_{n-1} = \bar{\alpha}_{n-1} = \emptyset$ in which the notation $\emptyset$ shows an empty set. Furthermore, for unidirectional CTs we have $\beta_i = \bar{\alpha}_i = \emptyset$, and for typical CTs shown in Figs 5.2-5.3, we have $\bar{\alpha}_i = \bar{\beta}_i = \emptyset$.

Tables (5.1)-(5.2) are prepared to provide an insight about the mentioned sets and values for a platoon with one leader and five followers under CTs given in Figs. 5.2-5.4. Note that the sets α_i and $\bar{\alpha}_i$ show the vehicles ahead/behind from which the i^{th} follower receives information but the $(i+1)^{th}$ follower does not. Also, the sets β_i

Table 5.2: Sets α_i, β_i, $\bar{\alpha}_i$, and $\bar{\beta}_i$, and also values of $|\mathbb{I}_{i+1}|$ and $|\mathbf{N}_i|$ for the pair $(i, i+1)$ of a platoon with five FVs within different nontypical communication topologies given in Fig. 5.4.

Pairs:	$(0,1)$	$(1,2)$	$(2,3)$	$(3,4)$	$(4,5)$
	$\{\alpha_0, \beta_0, \bar{\alpha}_0, \bar{\beta}_0, \lvert\mathbb{I}_1\rvert, \lvert\mathbf{N}_0\rvert\}$	$\{\alpha_1, \beta_1, \bar{\alpha}_1, \bar{\beta}_1, \lvert\mathbb{I}_2\rvert, \lvert\mathbf{N}_1\rvert\}$	$\{\alpha_2, \beta_2, \bar{\alpha}_2, \bar{\beta}_2, \lvert\mathbb{I}_3\rvert, \lvert\mathbf{N}_2\rvert\}$	$\{\alpha_3, \beta_3, \bar{\alpha}_3, \bar{\beta}_3, \lvert\mathbb{I}_4\rvert, \lvert\mathbf{N}_3\rvert\}$	$\{\alpha_4, \beta_4, \bar{\alpha}_4, \bar{\beta}_4, \lvert\mathbb{I}_5\rvert, \lvert\mathbf{N}_4\rvert\}$
a)	$\{\emptyset, \emptyset, \emptyset, \emptyset, 1, 1\}$	$\{\{0\}, \emptyset, \emptyset, \emptyset, 1, 1\}$	$\{\{1\}, \emptyset, \emptyset, \emptyset, 1, 1\}$	$\{\{2\}, \emptyset, \emptyset, \{1\}, 2, 2\}$	$\{\{1\}, \emptyset, \emptyset, \emptyset, 2, 2\}$
b)	$\{\emptyset, \emptyset, \emptyset, \emptyset, 1, 1\}$	$\{\{0\}, \{3,5\}, \emptyset, \emptyset, 3, 1\}$	$\{\{1\}, \emptyset, \{5\}, \{0\}, 2, 4\}$	$\{\{0,2\}, \{5\}, \emptyset, \emptyset, 2, 1\}$	$\{\{3\}, \emptyset, \emptyset, \emptyset, 1, 2\}$
c)	$\{\emptyset, \{2\}, \emptyset, \emptyset, 2, 1\}$	$\{\{0\}, \emptyset, \emptyset, \emptyset, 1, 2\}$	$\{\{1\}, \emptyset, \emptyset, \{0\}, 1, 1\}$	$\{\{0\}, \emptyset, \emptyset, \emptyset, 1, 1\}$	$\{\{3\}, \emptyset, \emptyset, \emptyset, 1, 1\}$
d)	$\{\emptyset, \emptyset, \emptyset, \emptyset, 1, 1\}$	$\{\emptyset, \emptyset, \emptyset, \emptyset, 1, 1\}$	$\{\emptyset, \emptyset, \emptyset, \emptyset, 1, 1\}$	$\{\emptyset, \emptyset, \emptyset, \emptyset, 1, 1\}$	$\{\emptyset, \emptyset, \emptyset, \emptyset, 2, 2\}$

and $\bar{\beta}_i$ indicate the vehicles behind/ahead from which the $(i+1)^{th}$ follower receives information but the i^{th} follower does not.

Defining $\tilde{\mathbf{X}}_t^{\Delta} \in R^{3n\times 1} = \left[\tilde{\mathbf{X}}_0^1;\ \tilde{\mathbf{X}}_1^2;\ \ldots;\ \tilde{\mathbf{X}}_{n-1}^n\right]$, applying $i = 0, \ldots, n-1$ to the first relation in (5.28), the stacked resultant relations is compactly shown as

$$\dot{\tilde{\mathbf{X}}}_t^{\Delta} = \tilde{\mathbf{A}}_t^{\Delta}\tilde{\mathbf{X}}_t^{\Delta} = \left[\mathbf{I}_n \otimes \mathbf{A} - \bar{\mathbf{P}} \otimes \mathbf{BK}\right] \tilde{\mathbf{X}}_t^{\Delta} \tag{5.31}$$

where $\tilde{\mathbf{A}}_t^{\Delta} \in R^{3n\times 3n}$. Also, $\bar{P}_{ij}$ as the elements of $\bar{\mathbf{P}} \in R^{n\times n}$ are according to

$$\bar{P}_{ij} = \begin{cases} \left|\mathbb{S}_j \cap \bar{\beta}_{i-1}\right| - \left|\mathbb{S}_j \cap \alpha_{i-1}\right| & \text{if } j < i \\ \left|\mathbf{N}_{i-1}\right| & \text{if } j = i \\ \left|\mathbb{V}_j \cap \bar{\alpha}_{i-1}\right| - \left|\mathbb{V}_j \cap \beta_{i-1}\right| & \text{if } j > i \end{cases} \tag{5.32}$$

in which the sets $\mathbb{S}_j$ and $\mathbb{V}_j$ are defined as $\mathbb{S}_j \triangleq \{j-1, j-2, \ldots, 0\}$ and $\mathbb{V}_j \triangleq \{j, j+1, \ldots, n\}$, respectively. Note that $|.|$ denotes the cardinality of the relevant sets.

Remark 14 *Given the dynamic model* (5.9) *and the novel one* (5.31)*, there is a key property through which we can use* (5.31) *instead of* (5.9) *to study the internal stability of the platoon. Following* (5.10) *and* (5.32)*, for any CT (including the ones in Figs. 5.2-5.4), the eigenvalues of the matrices* $\mathbf{P}$ *and* $\bar{\mathbf{P}}$ *are identical. For instance, for the case of having five followers and using TBPF topology, the matrices are*

$$\mathbf{P}_{TBPF} = \begin{bmatrix} 1 & -2 & -1 & 0 & 0 \\ 0 & 4 & -1 & -1 & 0 \\ -1 & -1 & 4 & -1 & -1 \\ 0 & -1 & -1 & 4 & 0 \\ 0 & 0 & -1 & -1 & 3 \end{bmatrix}, \quad \mathbf{P}_{TBPF} = \begin{bmatrix} 3 & -1 & -1 & 0 & 0 \\ -1 & 4 & -1 & -1 & 0 \\ -1 & -1 & 4 & -1 & -1 \\ 0 & -1 & -1 & 3 & -1 \\ 0 & 0 & -1 & -1 & 2 \end{bmatrix} \tag{5.33}$$

both of which have eigenvalues: 0.2935, 2.1324, 3.3900, 5.0000 *and* 5.1841. *Please check link for matrices* $\mathbf{P}$ *and* $\bar{\mathbf{P}}$ *of the other CTs.*

Remark 15 *Considering* (5.9) *and* (5.31)*, since the system matrices* $\tilde{\mathbf{A}}_t$ *and* $\tilde{\mathbf{A}}_t^{\Delta}$ *are in similar formats as*

$$\tilde{\mathbf{A}}_t = [\mathbf{I}_n \otimes \mathbf{A} - \mathbf{P} \otimes \mathbf{BK}] \tag{5.34a}$$

$$\tilde{\mathbf{A}}_t^{\Delta} = \left[\mathbf{I}_n \otimes \mathbf{A} - \bar{\mathbf{P}} \otimes \mathbf{BK}\right] \tag{5.34b}$$

and regarding the property mentioned in Remark 14, it is clear that one can use dynamics (5.34b) *instead of* (5.34a) *for internal stability analysis. Therefore, the two cases mentioned earlier in the Remarks 12-13 are valid for the matrix* $\bar{\mathbf{P}}$ *as well.*

The next section formulates the transient IDs which then utilized to find the vehicles velocities.

5.3 Description of the Transient Intervehicle Distances Based on the Matrix $\bar{\mathbf{P}}$

For the sake of simplicity, assuming $\tilde{v}_i^{i+1}(0) = \tilde{a}_i^{i+1}(0) = 0$ and all initial position-differences are equal to β, i.e., $\tilde{p}_i^{i+1}(0) = \beta$, for $i = 0, \ldots, n-1$, we have

$$\tilde{\mathbf{X}}_i^{i+1}(s) = \left[1; s; s^2\right] \tilde{p}_i^{i+1}(s) - \left[0; 1; s\right] \beta \tag{5.35}$$

Therefore, given (5.28) and (5.35), we get the following formula for intervehicle-distances error

$$\begin{aligned} \tilde{p}_i^{i+1}(s) = \Psi_i(s) + \mathbf{H}_i(s) \Bigg[& \sum_{j \in \alpha_i} \sum_{\kappa=j}^{i-1} \tilde{p}_\kappa^{\kappa+1}(s) - \sum_{j \in \bar{\beta}_i} \sum_{\kappa=j}^{i-1} \tilde{p}_\kappa^{\kappa+1}(s) \\ & + \sum_{j \in \beta_i} \sum_{\kappa=i+1}^{j-1} \tilde{p}_\kappa^{\kappa+1}(s) - \sum_{j \in \bar{\alpha}_i} \sum_{\kappa=i+1}^{j-1} \tilde{p}_\kappa^{\kappa+1}(s) \Bigg] \end{aligned} \tag{5.36}$$

in which

$$\mathbf{H}_i(s) = \frac{\frac{h}{\tau}s^2 + \frac{b}{\tau}s + \frac{k}{\tau}}{s^3 + \bar{h}_i s^2 + \bar{b}_i s + \bar{k}_i} \tag{5.37}$$

where $\bar{h}_i = \frac{1+|\mathbf{N}_i|h}{\tau}$, $\bar{b}_i = \frac{|\mathbf{N}_i|b}{\tau}$, $\bar{k}_i = \frac{|\mathbf{N}_i|k}{\tau}$, and $|\mathbf{N}_i|$ denotes the cardinality of the set $\mathbf{N}_i$. Also,

$$\Psi_i(s) = \frac{\beta\left(s^2 + \frac{1+(|\mathbf{N}_i|-\gamma_i)h}{\tau}s + \frac{(|\mathbf{N}_i|-\gamma_i)b}{\tau}\right)}{s^3 + \bar{h}_i s^2 + \bar{b}_i s + \bar{k}_i};\ \ i = 0, \ldots, n-1 \tag{5.38}$$

where $\gamma_i \triangleq \sum_{j\in\alpha_i}(i-j) + \sum_{j\in\beta_i}(j-i-1) - \sum_{j\in\bar{\beta}_i}(i-j) - \sum_{j\in\bar{\alpha}_i}(j-i-1)$.

Proof. Given (5.28), the $\tilde{p}_i^{i+1}(s)$, for $i = 0, \ldots, n-1$, would be the summation of zero-state ($\tilde{\mathbf{X}}_i^{i+1}(0) = 0$) response and zero-input ($\tilde{u}_i^{i+1} = 0$) response. Therefore, given (5.28), the zero-input response would be according to

$$\tilde{p}_{i,zi}^{i+1}(s) = \mathbf{C}\left(s\mathbf{I}_3 - \mathbf{A}_i^{i+1}\right)^{-1}\tilde{\mathbf{X}}_i^{i+1}(0) = \frac{\beta\left(s^2 + \bar{h}_i s + \bar{b}_i\right)}{s^3 + \bar{h}_i s^2 + \bar{b}_i s + \bar{k}_i} \tag{5.39}$$

where $\bar{h}_i = \frac{1+|\mathbf{N}_i|h}{\tau}$, $\bar{b}_i = \frac{|\mathbf{N}_i|b}{\tau}$ and $\bar{k}_i = \frac{|\mathbf{N}_i|k}{\tau}$, and $\mathbf{I}_3$ is the identity matrix of size 3. Also, the zero-state response would be

$$\tilde{p}_{i,zs}^{i+1}(s) = \mathbf{G}_i^{i+1}(s)\tilde{u}_i^{i+1}(s) \tag{5.40}$$

in which given (5.30) and (5.35) we have $\mathbf{G}_i^{i+1}(s) = \mathbf{C}\left(s\mathbf{I}_3 - \mathbf{A}_i^{i+1}\right)^{-1}\mathbf{B}$ and

$$\begin{aligned}
\tilde{u}_i^{i+1}(s) =& \mathbf{K}\mathbf{T}_1 \sum_{j\in\alpha_i}\sum_{\kappa=j}^{i-1}\tilde{p}_\kappa^{\kappa+1}(s) - \mathbf{K}\mathbf{T}_2\sum_{j\in\alpha_i}\sum_{\kappa=j}^{i-1}\beta \\
&+ \mathbf{K}\mathbf{T}_1 \sum_{j\in\beta_i}\sum_{\kappa=i+1}^{j-1}\tilde{p}_\kappa^{\kappa+1}(s) - \mathbf{K}\mathbf{T}_2\sum_{j\in\beta_i}\sum_{\kappa=i+1}^{j-1}\beta \\
&- \mathbf{K}\mathbf{T}_1 \sum_{j\in\bar{\alpha}_i}\sum_{\kappa=i+1}^{j-1}\tilde{p}_\kappa^{\kappa+1}(s) + \mathbf{K}\mathbf{T}_2\sum_{j\in\bar{\alpha}_i}\sum_{\kappa=i+1}^{j-1}\beta \\
&- \mathbf{K}\mathbf{T}_1 \sum_{j\in\bar{\beta}_i}\sum_{\kappa=j}^{i-1}\tilde{p}_\kappa^{\kappa+1}(s) + \mathbf{K}\mathbf{T}_2\sum_{j\in\bar{\beta}_i}\sum_{\kappa=j}^{i-1}\beta
\end{aligned} \tag{5.41}$$

where $\mathbf{T}_1, \mathbf{T}_2 \in R^{3\times 1}$ are as $\mathbf{T}_1 \triangleq [1;\ s;\ s^2]$ and $\mathbf{T}_2 \triangleq [0;\ 1;\ s]$. Simplifying (5.41)

results in $\mathbf{G}_i^{i+1}(s) = \frac{1}{\tau\left(s^3+\bar{h}_i s^2+\bar{b}_i s+\bar{k}_i\right)}$ and

$$\begin{aligned}\tilde{u}_i^{i+1}(s) = \left(hs^2+bs+k\right) \times \Bigg[&\sum_{j\in\alpha_i}\sum_{\kappa=j}^{i-1}\tilde{p}_\kappa^{\kappa+1}(s) \\ &+\sum_{j\in\beta_i}\sum_{\kappa=i+1}^{j-1}\tilde{p}_\kappa^{\kappa+1}(s)-\sum_{j\in\bar{\alpha}_i}\sum_{\kappa=i+1}^{j-1}\tilde{p}_\kappa^{\kappa+1}(s)-\sum_{j\in\bar{\beta}_i}\sum_{\kappa=j}^{i-1}\tilde{p}_\kappa^{\kappa+1}(s)\Bigg] \\ -(hs+b)\Bigg[&\sum_{j\in\alpha_i}\sum_{\kappa=j}^{i-1}\beta+\sum_{j\in\beta_i}\sum_{\kappa=i+1}^{j-1}\beta-\sum_{j\in\bar{\alpha}_i}\sum_{\kappa=i+1}^{j-1}\beta-\sum_{j\in\bar{\beta}_i}\sum_{\kappa=j}^{i-1}\beta\Bigg]\end{aligned} \tag{5.42}$$

substituting which into (5.40) yields

$$\begin{aligned}\tilde{p}_{i,zs}^{i+1}(s) = &\frac{\frac{h}{\tau}s^2+\frac{b}{\tau}s+\frac{k}{\tau}}{s^3+\bar{h}_i s^2+\bar{b}_i s+\bar{k}_i} \times \Bigg[\sum_{j\in\alpha_i}\sum_{\kappa=j}^{i-1}\tilde{p}_\kappa^{\kappa+1}(s) \\ &+\sum_{j\in\beta_i}\sum_{\kappa=i+1}^{j-1}\tilde{p}_\kappa^{\kappa+1}(s)-\sum_{j\in\bar{\alpha}_i}\sum_{\kappa=i+1}^{j-1}\tilde{p}_\kappa^{\kappa+1}(s)-\sum_{j\in\bar{\beta}_i}\sum_{\kappa=j}^{i-1}\tilde{p}_\kappa^{\kappa+1}(s)\Bigg] \\ &-\beta\left[\sum_{j\in\alpha_i}(i-j)+\sum_{j\in\beta_i}(j-i-1)-\sum_{j\in\bar{\beta}_i}(i-j)-\sum_{j\in\bar{\alpha}_i}(j-i-1)\right] \\ &\times\frac{\frac{h}{\tau}s+\frac{b}{\tau}}{s^3+\bar{h}_i s^2+\bar{b}_i s+\bar{k}_i}\end{aligned} \tag{5.43}$$

Therefore, given (5.39) and (5.43) we have $\tilde{p}_i^{i+1}(s) = \tilde{p}_{i,zi}^{i+1}(s) + \tilde{p}_{i,zs}^{i+1}(s)$ which results in

$$\begin{aligned}\tilde{p}_i^{i+1}(s) = &\frac{\frac{h}{\tau}s^2+\frac{b}{\tau}s+\frac{k}{\tau}}{s^3+\bar{h}_i s^2+\bar{b}_i s+\bar{k}_i} \times \Bigg[\sum_{j\in\alpha_i}\sum_{\kappa=j}^{i-1}\tilde{p}_\kappa^{\kappa+1}(s) \\ &+\sum_{j\in\beta_i}\sum_{\kappa=i+1}^{j-1}\tilde{p}_\kappa^{\kappa+1}(s)-\sum_{j\in\bar{\alpha}_i}\sum_{\kappa=i+1}^{j-1}\tilde{p}_\kappa^{\kappa+1}(s)-\sum_{j\in\bar{\beta}_i}\sum_{\kappa=j}^{i-1}\tilde{p}_\kappa^{\kappa+1}(s)\Bigg] \\ &+\frac{\beta\left(s^2+\frac{1+(|\mathbf{N}_i|-\gamma_i)h}{\tau}s+\frac{(|\mathbf{N}_i|-\gamma_i)b}{\tau}\right)}{s^3+\bar{h}_i s^2+\bar{b}_i s+\bar{k}_i}\end{aligned} \tag{5.44}$$

where $\gamma_i \triangleq \sum_{j\in\alpha_i}(i-j) + \sum_{j\in\beta_i}(j-i-1) - \sum_{j\in\bar{\beta}_i}(i-j) - \sum_{j\in\bar{\alpha}_i}(j-i-1)$. Therefore, the proof of (5.36) has been completed. ■

Calculating (5.36) for $i = 0, \ldots, n-1$ and stacking them together, it is possible to formulate a mapping between initial conditions and IDs errors as the following

compact form:

$$\tilde{\mathbf{P}}(s) = \mathbf{Q}^{-1}(s)\mathbf{\Psi}(s) \tag{5.45}$$

where $\tilde{\mathbf{P}}(s) \triangleq \left[\tilde{p}_0^1(s);\ \tilde{p}_1^2(s);\ \ldots;\ \tilde{p}_{n-1}^n(s)\right]$; $\mathbf{\Psi}(s) \triangleq [\Psi_0(s);\ \Psi_1(s);\ \ldots;\ \Psi_{n-1}(s)]$, and $\mathbf{Q}(s) \in \mathbb{C}^{n\times n}$ whose elements are defined as

$$Q_{ij}(s) = \begin{cases} 1 & \text{if} \quad i = j \\ \bar{P}_{ij}\mathbf{H}_{i-1}(s) & \text{if} \quad i \neq j \end{cases} \tag{5.46}$$

Therefore, if $\bar{\mathbf{Q}}(s) \triangleq \mathbf{Q}^{-1}(s)$, then one can conclude that

$$\tilde{p}_i^{i+1}(s) = \sum_{j=1}^{n} \bar{Q}_{(i+1)j}(s)\Psi_{j-1}(s); \quad i = 0, \ldots, n-1 \tag{5.47}$$

which implies that $\tilde{p}_i^{i+1}(t)$ would be the impulse response of $\tilde{p}_i^{i+1}(s)$. Therefore, relation (7.42) maps the initial position errors to IDs such that for any given $\mathbf{K} = [k, b, h]$, if $\tilde{p}_i^{i+1}(t) > -d_i^{i+1}$; $i = 0, 1, \ldots, n-1$ then we would have a non-colliding platoon. Similarly, if $\tilde{p}_i^{i+1}(t) > -\left(d_i^{i+1} - d_{i,s}^{i+1}\right)$ in which $d_{i,s}^{i+1}$ is considered to be a preset safe-distance between neighboring vehicles, then the distance between consecutive vehicles would be always higher than $d_{i,s}^{i+1}$. Note that, in control theory, the impulse response represents a system's reaction to a 'Dirac delta input'. This concept holds great significance in the analysis of dynamic systems. The Laplace transform of the delta function yields a value of 1, which means that the impulse response can be regarded as the inverse Laplace transform of the system's transfer function. Thus, the impulse response of $\tilde{p}_i^{i+1}(s)$ (take it as a transfer function) would present $\tilde{p}_i^{i+1}(t)$.

Remark 16 *Considering* (5.36)*, for stable* $\mathbf{K} = [k, b, h]$*, and based on the final value theorem of Laplace transform we have* $\lim_{t\to\infty} \tilde{p}_i^{i+1}(t) = \lim_{s\to 0} s\tilde{p}_i^{i+1}(s) = 0$ *and since* $D_i^{i+1}(t) = \tilde{p}_i^{i+1}(t) + d_i^{i+1}$ *then we get* $D_i^{i+1}(t) = d_i^{i+1}$*;* $i = 0, 1, \ldots, n-1$ *which implies that all IDs finally reach to the desired constant intervehicle distances* d_i^{i+1}*.*

We know that to have a feasible vehicular platoon, other than stability and safety concerns, vehicles need to have positive velocities (in line with the leader's velocity)

throughout the travel time. To study this, given that $\tilde{v}_i^{i+1}(t) = \frac{d}{dt}\left(\tilde{p}_i^{i+1}(t)\right)$, then for $i = 0, \ldots, n-1$ it is possible to conclude that

$$v_{i+1}(t) = v_i(t) - \mathcal{L}^{-1}\left\{s\tilde{p}_i^{i+1}(s)\right\} + \tilde{p}_i^{i+1}(0)\delta(t) \tag{5.48}$$

where $\mathcal{L}^{-1}$ signifies the inverse Laplace transform operator and $\delta(t)$ is delta function such that $\mathcal{L}^{-1}\left\{\tilde{p}_i^{i+1}(0)\right\} = \tilde{p}_i^{i+1}(0)\delta(t)$. Now, using (5.48) and assuming that $\tilde{p}_i^{i+1}(0) = \beta$, the velocity of the i^{th} follower can be obtained according to

$$v_i(t) = v_0(t) - \mathcal{L}^{-1}\left\{s\sum_{\kappa=0}^{i-1}\tilde{p}_\kappa^{\kappa+1}(s)\right\} + i\beta\delta(t) \tag{5.49}$$

Now, substituting (5.47) into (5.49) yields

$$v_i(t) = v_0(t) - \mathcal{L}^{-1}\left\{s\sum_{\kappa=0}^{i-1}\sum_{j=1}^{n}\bar{Q}_{(\kappa+1)j}(s)\Psi_{j-1}(s)\right\} + i\beta\delta(t) \tag{5.50}$$

Therefore, for any given $\mathbf{K} = [k, b, h]$, if $v_i(t) > 0$; $i = 1, \ldots, n$ then in terms of vehicles' velocities the platoon would be feasible. In a similar way that explained in Remark 16, one can conclude that $\lim_{t\to\infty} v_i(t) = v_0(t)$; $i = 1, \ldots, n$.

5.4 Simulations and Results

For simulations, we consider a platoon with one leader and five followers and constant distance policy equal to $5m$. In the simulations, the initial velocities and accelerations of the vehicles are all set to zero. The vehicles' lengths are identical and equal to 4 m. Moreover, the simulations are done with sampling time equal to 0.01 s. Also, let $h = 4$ and $\tau = 1$, and the control gains k and b vary between 0.1 and 19.6 by 0.5 incremental. Note that in simulations, the simulation time for all trajectories is equal to $100s$. However, for the sake of clarity in presentation, results may provided for times less than $100s$. Also, the safe distance between vehicles is considered to be equal to $3m$, i.e. $d_{i,s}^{i+1} = 3m$. In the following, the simulations results are provided separately for typical and nontypical communication topologies (CTs).

5.4.1 Intervehicle Distances and Vehicle Velocities

Based on what explained in Section 6.5, we can find intervehicle distances (IDs) and the velocity of vehicles for different $\mathbf{K} = [k, b, 4]$ and CTs between vehicles.

Typical CTs

In this part, we study the IDs and vehicles velocities for typical CTs (Figs 5.2-5.3):

Intervehicle Distances: Bases on Remarks 11-13, it is possible to find stable and unstable control gains. As such, in (5.7), let $h = 4$ and control gains k and b vary between values 0.1 and 19.6 by 0.5 incremental. Any $\mathbf{K} = [k, b, 4]$ that does not satisfy stability conditions is considered as an unstable control gain, otherwise a stable $\mathbf{K}$. Thus, for $i = 0, \ldots, n-1$ and a given stable $\mathbf{K}$, using (5.47), if $-5m < \tilde{p}_i^{i+1}(t) < -2m$ then $\mathbf{K}$ is a stable-non-collision control gain. Similarly, if $\tilde{p}_i^{i+1}(t) < -5m$, then we name $\mathbf{K}$ a stable-collision control gain. Furthermore, if $\tilde{p}_i^{i+1}(t) > -2m$, then $\mathbf{K}$ is named a stable-safe control gain which implies that the IDs are always larger than $3m$ which is assumed as the safe distance between neighboring vehicles. The results using the mentioned scenarios are provided in Fig. 5.6 in which unstable, stable-collision, stable-non-collision, and stable-safe gains are presented with red, yellow, blue, and green colors, respectively.

Vehicles Velocities: For studying the feasibility of velocities under different typical CTs, let the leader has a velocity trajectory. As such, we assume that it starts with zero velocity and gradually increases its velocity with the acceleration of 4 m/s^2 till the one-third of simulation time, which afterwards the velocity becomes constant till the two-thirds of the simulation time. After that the leader vehicle starts to decelerate with the acceleration of -8 m/s^2 till its velocity becomes zero and the leader vehicle stops (see Fig. 5.7). The simulations are done for two time intervals:
1) $[0, \frac{2}{3}$simulation-time] during which the leader starts with zero velocity, accelerate till the one third of the simulation-time and then reaches a constant velocity which persists till two third of the simulation-time. The stable control gains $\mathbf{K} = [k, b, 4]$

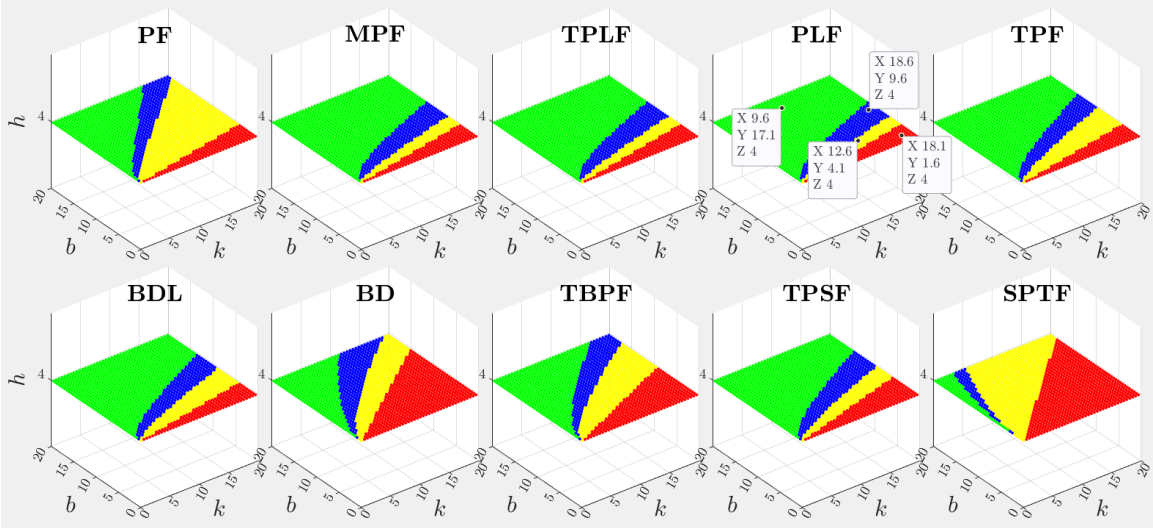

Figure 5.6: (a): Unstable (red), stable-collision (yellow), stable-non-collision (blue) and stable-safe (green) control gains $\mathbf{K} = [k, b, 4]$. The collision distance is $5m$, therefore the control gains that result in $\tilde{p}_i^{i+1}(t) > -5m$ are called stable-non-collision gains. Also, the safe distance is $3m$, thus the control gains that result in $\tilde{p}_i^{i+1}(t) > -2m$ are called stable-safe gains.

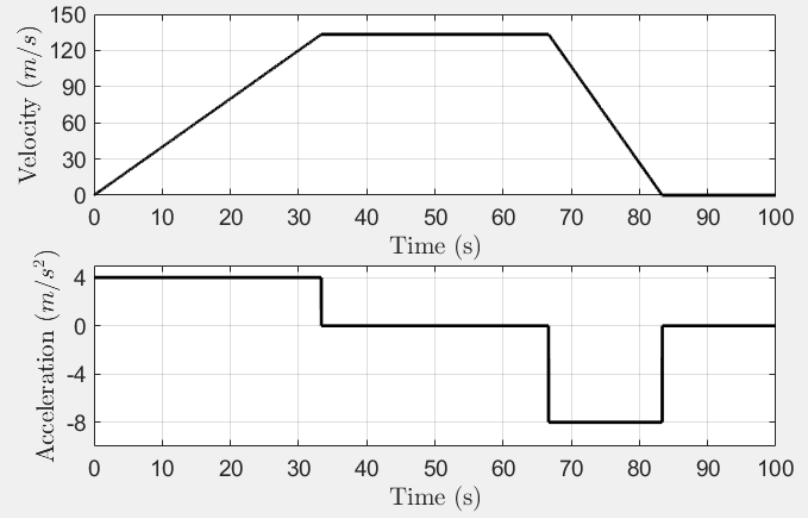

Figure 5.7: Leader's velocity and acceleration.

using which all vehicles during the mentioned time interval have positive velocities are depicted in Fig. 5.8 with cyan dots.

2) $[0, \text{simulation-time}]$ during which the leader starts with zero velocity, accelerate till the one third of the simulation-time and then reaches a constant velocity which

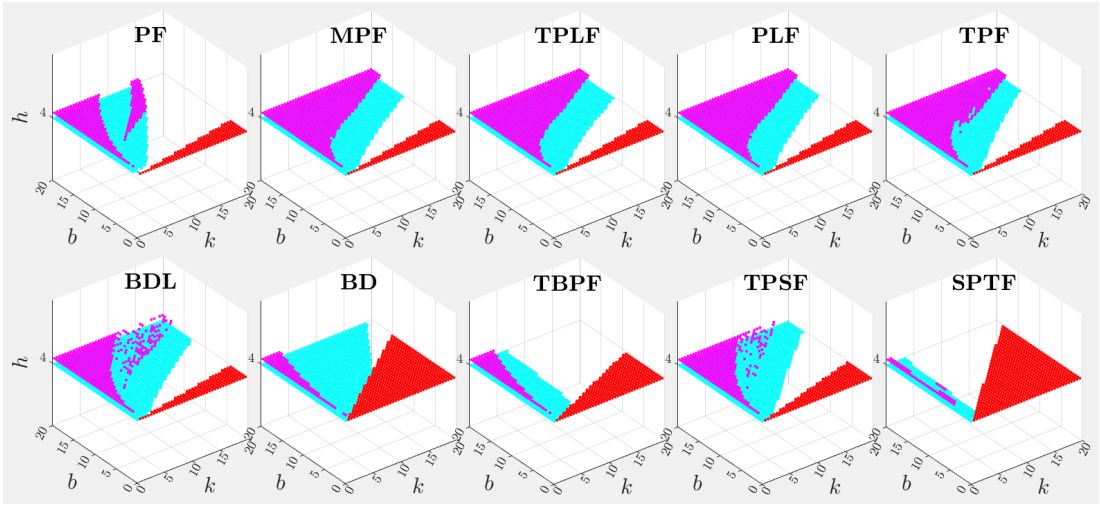

Figure 5.8: (a): Red dots depict unstable control gains $\mathbf{K} = [k, b, 4]$. Cyan dots show $\mathbf{K} = [k, b, 4]$ under which $v_i(t) > 0$; $i = 1, \ldots, n$ for the time interval $[0, \frac{2}{3}$simulation-time$]$. Magenta dots illustrate $\mathbf{K} = [k, b, 4]$ using which $v_i(t) > 0$; $i = 1, \ldots, n$ for the time interval $[0,$ simulation-time$]$.

persists till two third of the simulation-time. Then it decelerates and finally the velocity becomes zero. The stable control gains $\mathbf{K} = [k, b, 4]$ using which all vehicles during the mentioned time interval have positive velocities are depicted in Fig. 5.8 with magenta dots. Note that in Fig. 5.8, magenta dots are plotted over the cyan dots.

Remark 17 *In Fig. 5.8 magenta dots imply that under the associated control gains* $\mathbf{K} = [k, b, 4]$*, whenever the leader's velocity becomes zero, the followers simultaneously stand still and their velocity becomes zero. Accordingly, for cyan dots that do not overlap with the magenta dots, whenever the leader's velocity becomes zero, the follower velocities may fluctuate a little bit around zero. Also, one can notice that in terms of vehicle's velocities, TPLF, MPF, PLF and TPF topologies have better performance.*

Nontypical CTs

Using the same approach and scenarios utilized for typical CTs, for the nontypical CTs given in Fig. 5.4, the simulation results are provided in Fig. 5.9.

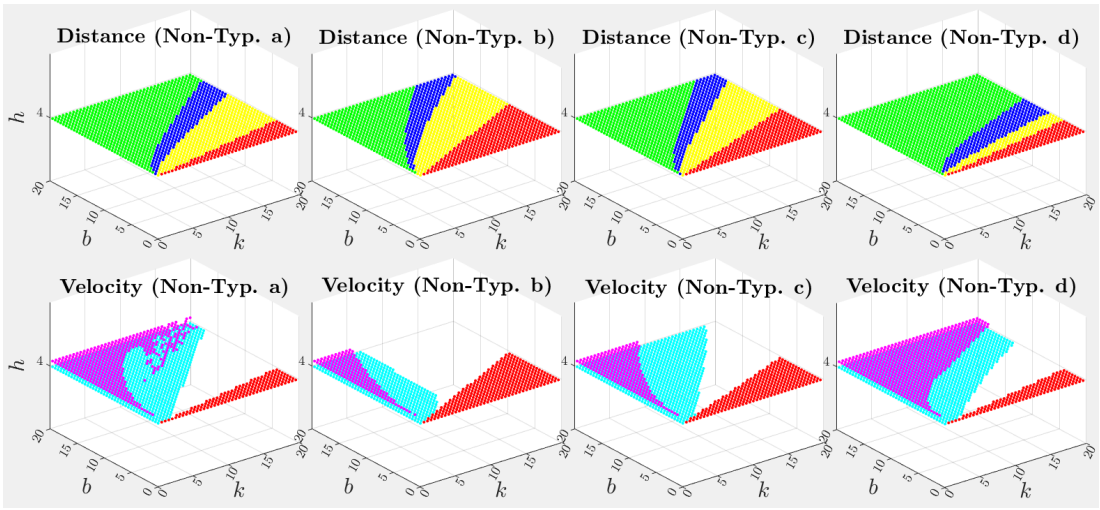

Figure 5.9: (a): Unstable (red), stable-collision (yellow), stable-non-collision (blue) and stable-safe (green) control gains $\mathbf{K} = [k, b, 4]$. Cyan dots show $\mathbf{K} = [k, b, 4]$ under which $v_i(t) > 0$; $i = 1, \ldots, n$ for the time interval $[0, \frac{2}{3}$simulation-time$]$. Magenta dots illustrate $\mathbf{K} = [k, b, 4]$ using which $v_i(t) > 0$; $i = 1, \ldots, n$ for the time interval $[0,$ simulation-time$]$.

5.4.2 Settling Time for Intervehicle Distances Errors

To have a better understanding of the effect of CTs on the performance of vehicles, other than IDs and vehicles velocities, we also have studied the settling time (t_s^i) for $\tilde{p}_i^{i+1}(t) \to 0$ under different typical CTs. The results are shown in Fig. 5.10. Investigation the results, we notice that SPTF, BD and TBPF are the first three CTs with the weakest performance. Conversely, PLF, TPLF, MPF are the first three CTs with the best performance.

5.4.3 Discussion on Communication Topologies

In this part, we study the impact of the CTs on the platoon performance. To this end, we take three criteria into account: 1) intervehicle-distances such that those control gains that lead to stable-non-collision and stable-safe distances, then the control gains are favorable, 2) The feasibility of the velocities such that those control gains that result in $v_i(t) > 0$ are our favorable $\mathbf{K}$, and 3) settling times for IDs errors such that those control gains that lead to the smaller settling times, then considered as better

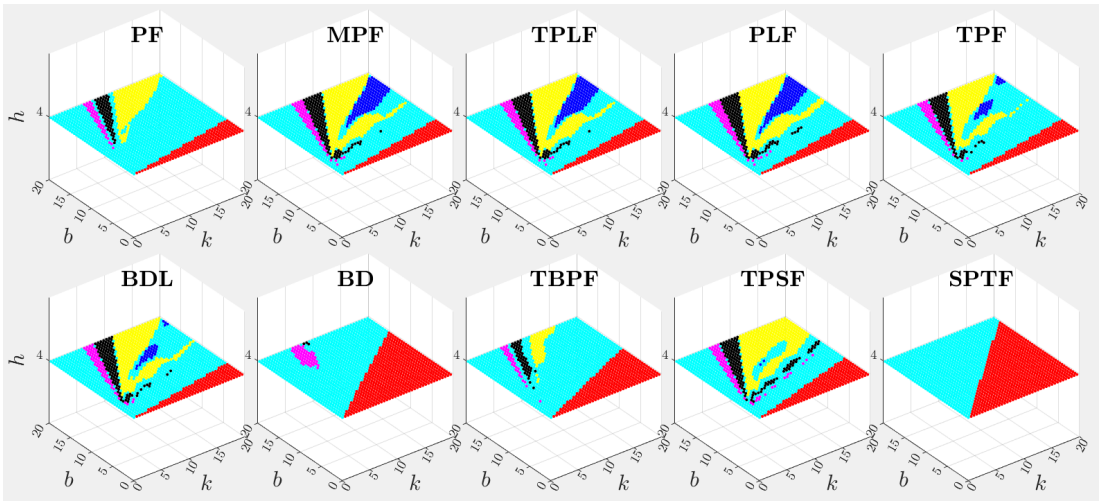

Figure 5.10: Settling time (t_s^i) for $\tilde{p}_i^{i+1}(t)$; $i = 0, 1, \ldots, n-1$. Those $\mathbf{K} = [k, b, 4]$ that result in $t_s^i \leq 3$, $3 < t_s^i \leq 6$, $6 < t_s^i \leq 9$, $9 < t_s^i \leq 12$ and $t_s^i > 12$ are depicted with blue, yellow, black, magenta, and cyan colors, respectively.

K.

From Figs. 5.6 and 5.8-5.10, some important implications can be drawn as follows:

1. The TPLF, MPF, and PLF topologies surpass others in terms of the size of the stable and stable-safe areas, the size of positive-velocity areas, and the size of smaller-settling-times areas.

2. Comparing BD/BDL, PF/PLF and TPF/TPLF topologies: it is apparent that broadcasting the leader's state to the follower vehicles has starkly improved the performance of the platoon.

3. SPTF has the smallest stable area, the smallest stable-safe area, the biggest stable-collision area, the smallest positive-velocity area, and the biggest larger-settling-time area.

4. Comparing PF/BD, and BD/SPTF topologies: under BD and SPTF topologies and in comparison with PF and BD topologies respectively, the followers receive information from one more vehicle behind which degrades the performance of the platoon under BD and SPTF topologies when compared to those of PF and BD topologies, respectively.

5. Comparing BD/TPSF, and SPTF/TBPF topologies: under BD/SPTF topologies, follower vehicles receive information from one/two vehicles behind and one/one vehicle ahead respectively, and under TPSF/TBPF they receive from one/two vehicles behind and two/two vehicles ahead. Getting more information from vehicles ahead improves the platoon performance under TPSF/TBPF with respect to those of BD/SPTF topologies, respectively.

6. Comparing PLF/TPF, and BDL/TPSF topologies: the performance of PLF and BDL are comparable to those of TPF and TPSF, respectively. However, it sounds that if the additional information from vehicles ahead is actually from the leader vehicle, then the performance would be slightly better.

7. Comparing TPLF, PLF, and nontypical CT d: there are subtle differences between performances which imply that when followers are of "look-ahead" type, and receive information from the leader, the leader's data outweighs those of the other followers. In other words, the information followers receive from other non-leader vehicles may be redundant which can be exploited to accomplished some other performance specifications. This issue needs more reseach.

Investigating the simulation results, it seems that generally for a given CT, the larger the difference between the number of cars ahead and behind from which each follower receives information, the better the performance of the platoon would be. Also, if for two CTs the differences are the same, then for the one under which the followers receive information from larger number of vehicles ahead, then its performance would be better. Comparing the typical CTs, Fig. 5.11 shows the performance-comparison of platoon under typical CTs. As we can see, TPLF, MPF and PLF topologies lead to better performance for the platoon. The numbers in the Fig. 5.11 show the number of vehicles ahead or behind from which each follower receives information.

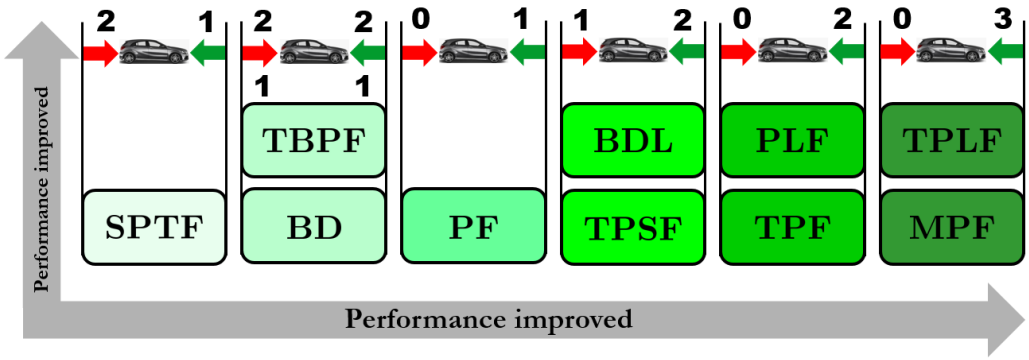

Figure 5.11: The schematic of platoon performance under different typical CTs given in Figs. 5.2-5.3.

5.4.4 Tracking Performance and Areas based on IDs: Validation

Our analysis on IDs and vehicles velocities led to formulations (5.47) and (5.50), respectively. Based on these formulations and mathematical analysis we found unstable, stable-collision, stable-non-collision, stable-safe and positive-velocity areas. Now, we examine the validity of the theoretical finding for one of the CTs. To this end, we assume that the platoon works under PLF topology and vehicles' initial-positions are selected as $x_i(0) = -17 \times i \ m, \ i = 0, 1, \ldots, 5$, i.e., $\tilde{p}_{i,i+1}(0) = 8m$. Let assume that the acceleration of the leader for the time interval $t_1 \leq t < t_2$ is $a_0(t) = a_0$ then based of Physics its velocity and position would be $v_0(t) = a_0 t + v_0(0)$ and $x_0(t) = \frac{1}{2} a_0 t^2 + v_0(0)t + x_0(0)$, respectively. Assuming sampling time equal to $\Delta t = 0.01s$, it is possible to get

$$\tilde{\mathbf{X}}_t(t + \Delta t) = \left(\mathbf{I}_{3n} + \tilde{\mathbf{A}}_t \Delta t\right) \tilde{\mathbf{X}}_t(t) \tag{5.51}$$

and reminding that $\tilde{\mathbf{X}}_i(t) = \mathbf{X}_i(t) - \mathbf{X}_i^*(t)$, we have found and simulated the inter-vehicle distances and vehicles velocities given the provided velocity and acceleration trajectory for the leader in Fig. 5.7. For selected points from PLF topology (see Fig. 5.6), the simulation results are depicted in Fig. 5.12. As we can see, for $\mathbf{K} = [18.1, 1.6, 4]$ which is picked up from unstable area, the error trajectories have

diverged and so the platoon is unstable. For $\mathbf{K} = [12.6, 4.1, 4]$ which is selected from stable-collision area, the error trajectories have converged to zero, however, some have crossed the dashed-red line (error $= -5m$) which indicates that we have collision occurrence in the platoon. Also, for $\mathbf{K} = [18.6, 9.6, 4]$ which is chosen from stable-non-collision area, the error trajectories have converged to zero and we do not have a collision occurrence. However, some trajectories have crossed the dashed-blue line (error $= -2m$) which indicates that some IDs violated the safe distance. Finally, for $\mathbf{K} = [9.6, 17.1, 4]$ which is taken from stable-safe area, the trajectories have converged to zero, and they neither have crossed the red-dashed line (collision distance) nor blue-dashed line (safe distance). Therefore, always the safe distance between vehicles is maintained. Simulation results shows that what we have spotted as unstable, stable-collision, stable-non-collision, and stable-safe areas, through the analysis provided in the paper, are all valid.

To show the tracking performance of the platoon - followers reach to the leader's velocity and acceleration - under PLF topology, we choose $\mathbf{K} = [9.6, 17.1, 4]$ from the stable-safe area. The selected point is designated in Fig. 5.6. Under the selected control gain, Fig. 5.13 shows the simulation results for the velocity and accelerations of the vehicles, i.e., $v_i(t)$ and $a_i(t)$; $i = 0, 1, \ldots, 5$. As we can see, the velocity and accelerations of the followers have converged to the leader's velocity and acceleration. Also, all follower velocities are positive that matches with the simulation results shown in Fig. 5.8 which we obtained from the provided analysis.

5.5 Conclusion

In summary, this chapter introduced a novel approach to platoon stability analysis by utilizing neighboring-vehicles state differences in a closed-loop distance dynamic model. The focus shifted from follower-leader state differences to explore the dynamics of a homogeneous platoon. The derived coupled dynamic model for adjacent vehicles allowed for a detailed investigation of intervehicle distances (IDs). Notably, it

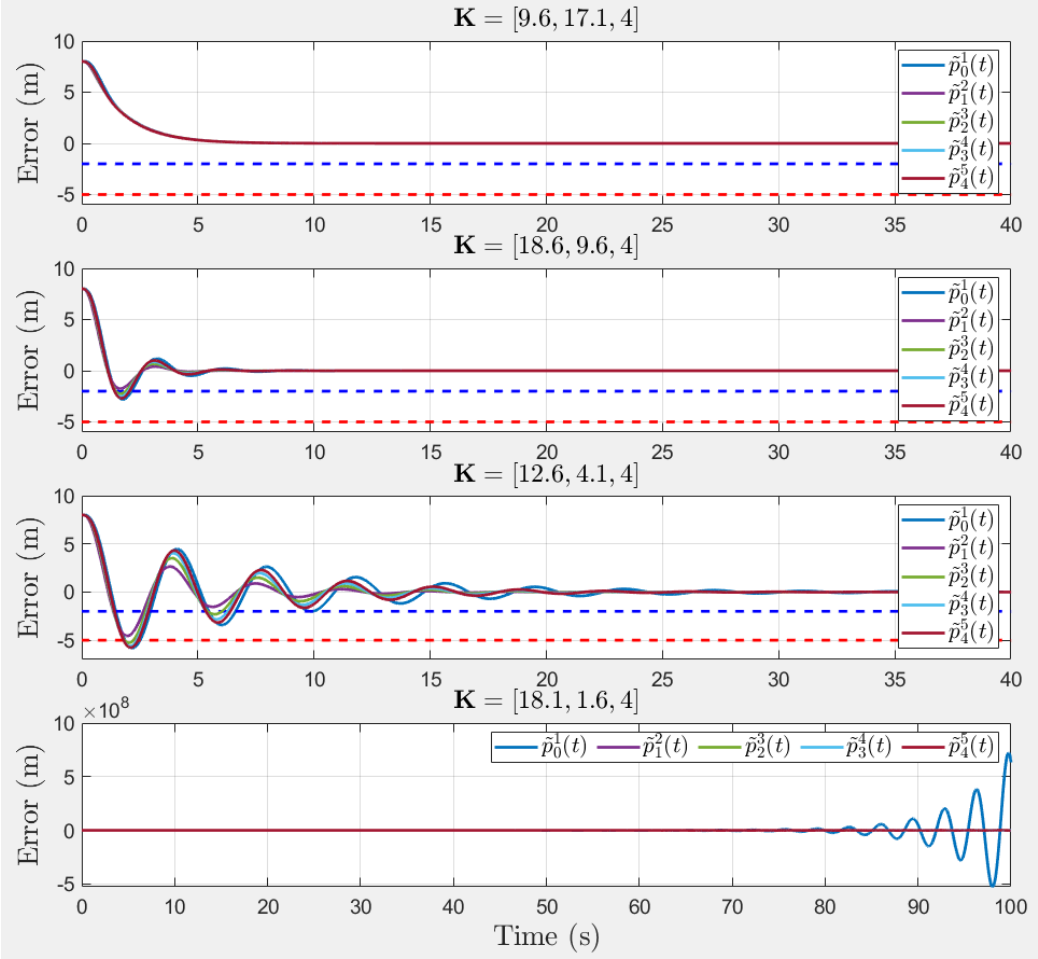

Figure 5.12: $\tilde{p}_i^{i+1}(t)$ trajectories for PLF topology under control gains $\mathbf{K} = [9.6, 17.1, 4]$ (stable-safe), $\mathbf{K} = [18.6, 9.6, 4]$ (stable-non-collision), $\mathbf{K} = [12.6, 4.1, 4]$ (stable-collision) and $\mathbf{K} = [18.1, 1.6, 4]$ (unstable), respectively. Blue-dashed and red-dashed lines indicate thresholds for safe and collision distances, i.e., $\tilde{p}_i^{i+1}(t) = -2m$ and $\Delta\tilde{p}_i^{i+1}(t) = -5m$, respectively.

was demonstrated that the closed-loop dynamics enabled the derivation of IDs from initial conditions, providing valuable insights into platoon behavior. Furthermore, the velocity of each follower was determined using IDs and the leader's velocity. By imposing constraints on collision and safe distance limits for IDs, as well as feasible-velocity limits for the followers, the chapter comprehensively examined the platoon's performance under various Communication Topologies (CTs). It is important to note that the focus of this chapter was on the analysis of a homogeneous platoon, and the

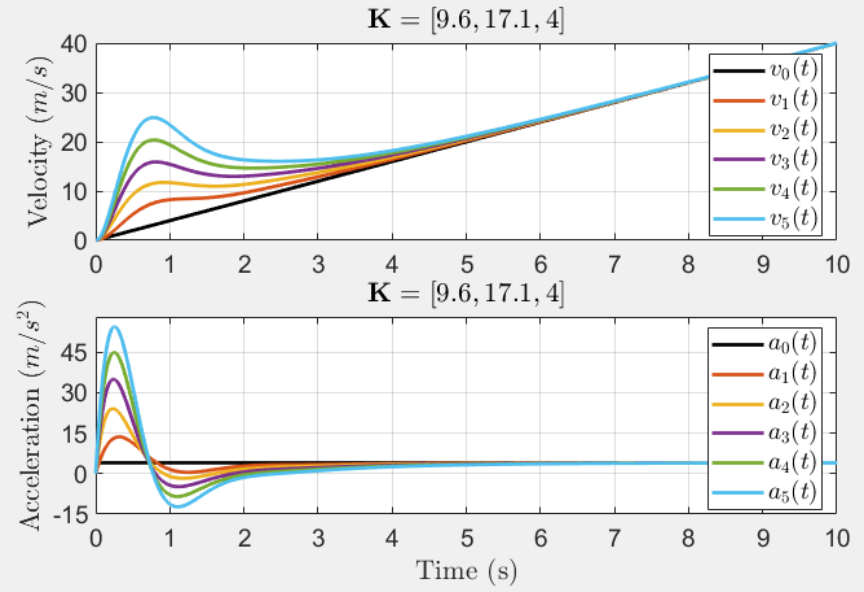

Figure 5.13: Tracking the velocity/acceleration of the leader under PLF communication topology and $\mathbf{K} = [9.6, 17.1, 4]$.

results obtained were substantiated through comprehensive simulations, thereby contributing to a deeper understanding of platoon dynamics and behavior.

Chapter 6

Stability and Distance Analysis: Heterogeneous Platoons under Look-Ahead Topologies[1]

This chapter presents a comprehensive investigation into the stability and intervehicle distances (IDs) of heterogeneous platoons operating under look-ahead topologies, considering disparities in control gains for position, velocity, and acceleration feedback. Ensuring transient intervehicle spacing within a non-colliding distance is a challenge, as internal stability alone may not guarantee safe distances between neighboring vehicles. Therefore, this study formulates the behavior of IDs during platoon travel and numerically identifies suitable control gains that promote stable and collision-free platoon operations. To address the issue, we divide the platoon into successive pairs of vehicles and analyze the distance dynamics between neighboring vehicles. The look-ahead structure of the platoon necessitates successive stable distance dynamics for overall platoon stability. By imposing collision and safe distance limits on the formulated IDs, appropriate control gains are determined to achieve a non-colliding platoon configuration. The formulated approach is demonstrated through simulation results, validating the theoretical findings.

The integration of vehicle platooning as an intelligent transportation technology

[1]A version of this chapter has been submitted as Amir Zakerimanesh, Tony Z. Qiu, Mahdi Tavakoli, *Stability and Distance Analysis: Heterogeneous Platoons under Look-Ahead Topologies*, IEEE Transactions on Cybernetics.

holds significant promise in enhancing various aspects of highway operations, such as capacity, fuel efficiency, emissions, transportation efficiency, and traffic safety [96]. Platooning involves a coordinated group of vehicles, led by one vehicle and followed by others, traveling at harmonized speeds and maintaining desired intervehicle distances (IDs). Different spacing policies, such as constant distance policy [49], constant time headway policy [102, 109], nonlinear headway policy [104], delay-based distance policy [18], and energy-oriented spacing policy [9], have been developed for managing these IDs.

In the literature, substantial attention has been devoted to the study of distributed longitudinal control techniques for vehicular platoons, encompassing various approaches based on model predictive control [31, 32], sliding mode control [12, 13, 110], consensus-based control [38, 39], event-triggered control [41, 43, 111], adaptive control [44–46], observer-based control [48, 49], robust control [10, 13, 112], reinforcement learning-based control [52], cross-coupling strategy [113], and linear feedback control [27, 53–57] for platoon coordination.

The communication topology (CT), which governs the information exchange structure among vehicles, significantly impacts platoon performance. Researchers have explored the control and stability of vehicle platoons under various CTs, such as those with complex eigenvalues [53], real eigenvalues [12], dynamic communication [105], undirected communication [106], and switching communication [32, 46, 107, 114]. Switching communication is particularly relevant to address partial failures in the vehicular ad hoc network (VANET) [108], ensuring platoon stability despite varying information flow.

Besides stability and tracking performance, safety and collision analysis are of paramount importance in platooning. Analyzing transient IDs is crucial to ensure collision-free operations. However, previous works [27, 53–57] have often overlooked this aspect, leaving a gap in the literature. In this paper, we address this void and provide a comprehensive analysis of transient distances between platoon vehi-

cles, even considering non-identical control gains. Incorporating non-identical control gains offers greater flexibility in achieving stability and desired transient behavior, particularly when small control gains are required.

In this chapter, we study the stability and ID of heterogeneous platoons operating under look-ahead topologies, utilizing a distributed linear feedback control scheme and a constant distance policy between vehicles. While internal stability has been widely studied, it is demonstrated with a counterexample that it may not guarantee a non-colliding platoon. Hence, to address collision concerns effectively, transient IDs are examined. Instead of considering follower-leader state differences, neighboring-vehicles state differences are used to develop a coupled dynamic model for adjacent vehicles. By analyzing this model, stability conditions and ID variations are derived. Consequently, collision and safe distance limits are imposed on IDs, leading to the identification of proper control gains for a non-colliding and safe platoon. Thorough simulations are performed to validate and provide further insights into the theoretical findings.

6.1 Problem formulation: Preliminaries

Throughout this chapter, unless necessary for clarity, we omit explicit time-dependent signals. We will use semicolon and colon symbols to differentiate elements of vertical and horizontal vectors, respectively. For example, $[.;.;.]$ represents a 3-by-1 vector, and $[.,.,.]$ represents a 1-by-3 vector. This notation will be employed consistently throughout the paper for better clarity and readability. In Figure 6.1, we illustrate a platoon comprising a leader vehicle labeled as 0 and n followers denoted as $1, \ldots, i, i+1, \ldots, n-1, n$. The real intervehicle distance (ID) between neighboring vehicles i and $i+1$ is denoted by D_i^{i+1}, while d_i^{i+1} represents the desired ID. The length of the i^{th} vehicle is indicated as L_i, and the positions of the leader vehicle and the i^{th} follower are represented by x_0 and x_i, respectively. Additionally, $p_i^{i+1} = x_i - x_{i+1}$ denotes the position difference between front sides of vehicles i and $i+1$.

Regarding linear control, the longitudinal control of the platoon consists of two main components: 1) Feedback linearization (FL) control, serving as the inner force/acceleration control loop, where dynamics nonlinearities are already cancelled, and 2) An ID control loop responsible for achieving the desired spacing between consecutive vehicles. In this chapter, we concentrate on the ID control loop, assuming that the FL control has already addressed the cancellation of nonlinearities in the dynamics. Please note that FL transforms nonlinear systems into linear equivalents using variable adjustments and feedback control. This simplifies control design by mimicking the more manageable behavior of linear systems. That being stated, this enables us to direct our analysis towards attaining the designated IDs within the platoon.

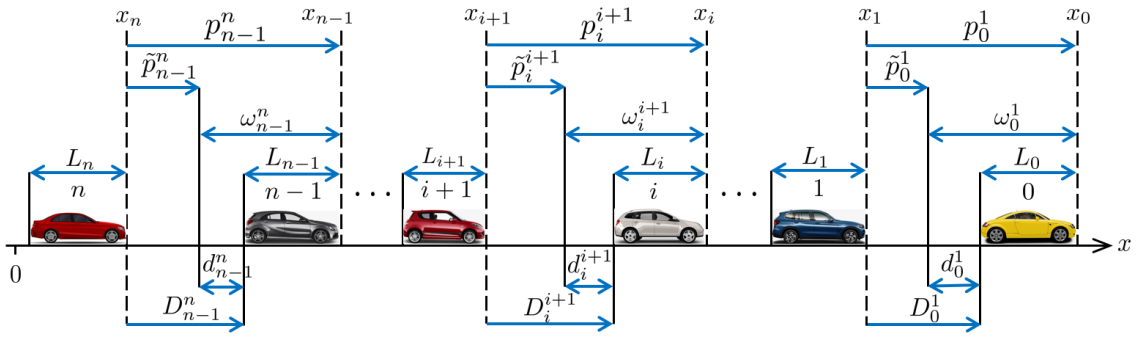

Figure 6.1: A heterogeneous platoon: Kinematics of pairwise vehicles, i.e., the pairs $(0,1)$, $(1,2)$, $\ldots$, and $(n-1,n)$. Note that, throughout the paper, $\tilde{p}_i^{i+1}$ is mentioned as intervehicle distance error (IDE) between neighboring vehicles.

6.1.1 Vehicles dynamics

We consider that the leader vehicle does not undergo any control procedure. Instead, its position, velocity, and acceleration are used to control the following vehicles within the platoon. Consequently, the dynamics of the follower vehicles are modeled by the following third-order linear model [46, 48, 56]:

$$\begin{cases} \dot{x}_{i+1} = v_{i+1} \\ \dot{v}_{i+1} = a_{i+1} \\ \dot{a}_{i+1} = -\frac{1}{\tau_{i+1}} a_{i+1} + \frac{1}{\tau_{i+1}} u_{i+1} \end{cases} \qquad i = 0, \ldots, n-1 \tag{6.1}$$

in which v_{i+1}, a_{i+1}, and τ_{i+1} are velocity, acceleration, and engine-time-constant of the $(i+1)^{th}$ follower. Also, u_{i+1} is the input signal of the $(i+1)^{th}$ follower to be designed properly. Let $\mathbf{X}_{i+1} \triangleq [x_{i+1};\ \dot{x}_{i+1};\ \ddot{x}_{i+1}]$ denote the state of the $(i+1)^{th}$ follower such that $\dot{x}_{i+1} = v_{i+1}$ and $\ddot{x}_{i+1} = a_{i+1}$. Thus, given (6.1) and for $i = 0, \ldots, n-1$, the state-space presentation of the $(i+1)^{th}$ follower would be according to

$$\dot{\mathbf{X}}_{i+1} = \underbrace{\begin{bmatrix} 0 & 1 & 0 \\ 0 & 0 & 1 \\ 0 & 0 & -\frac{1}{\tau_{i+1}} \end{bmatrix}}_{\mathbf{A}_{i+1}} \mathbf{X}_{i+1} + \underbrace{\begin{bmatrix} 0 \\ 0 \\ \frac{1}{\tau_{i+1}} \end{bmatrix}}_{\mathbf{B}_{i+1}} u_{i+1} \tag{6.2}$$

6.1.2 Aim and Controller

The objective of the controller u_{i+1} is to synchronize the velocities and accelerations of the follower vehicles with those of the leader vehicle and also ensure that the distances between adjacent vehicles in the platoon match the desired values, i.e., d_i^{i+1}. In essence, the controller aims to achieve velocity/acceleration tracking and ID regulation to maintain the desired platoon formation. In other words, for $i = 0, \ldots, n-1$, the aim is to have

$$\begin{cases} v_{i+1} = v_0 \\ x_i - x_{i+1} = L_i + d_i^{i+1} \end{cases} \quad \equiv \quad D_i^{i+1} = d_i^{i+1} \tag{6.3}$$

where $\equiv$ denotes equivalence. To accomplish the mentioned aims, we use the following distributed linear feedback control law [89] $(i = 0, \ldots, n-1)$

$$\begin{cases} u_{i+1} = -\sum\limits_{j \in \mathbb{I}_{i+1}} \mathbf{K}_{i+1}^{j} \left[x_{i+1} - x_j - d_{i+1,j}; \dot{x}_{i+1} - \dot{x}_j; \ddot{x}_{i+1} - \ddot{x}_j \right] \\ d_{i+1,j} \triangleq -sgn(i+1-j) \sum\limits_{\kappa=\min(i+1,j)}^{\max(i+1,j)-1} \omega_{\kappa}^{\kappa+1} \end{cases} \tag{6.4}$$

in which $\omega_k^{\kappa+1} \triangleq L_\kappa + d_\kappa^{\kappa+1}$ and $\mathbf{K}_{i+1}^{j} \triangleq [k_{i+1}^{j},\ b_{i+1}^{j},\ h_{i+1}^{j}]$ is the control-gain vector of the differences between measurements transmitted from the j^{th} vehicle to the $(i+1)^{th}$ follower, and the $(i+1)^{th}$ follower's state. Also, the set $\mathbb{I}_{i+1} \subset \{0, 1, \ldots, i\}$ is associated with the vehicles from which the $(i+1)^{th}$ follower gets information.

6.1.3 Look-Ahead Topology

Figure 6.2 illustrates an arbitrary look-ahead CT employed in vehicle platooning. In this topology, each follower vehicle exclusively receives information from vehicles that are positioned ahead of it within the platoon. This means that communication is unidirectional, with information flow limited to vehicles in the front.

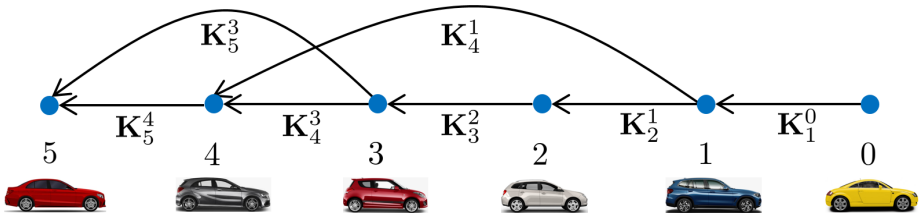

Figure 6.2: A heterogeneous vehicle platoon under an arbitrary look-ahead CT.

6.1.4 The Controller Based on Desired-States of the Followers

For $i = 0, \ldots, n-1$, the desired position (x_{i+1}^*), velocity ($\dot{x}_{i+1}^*$) and acceleration ($\ddot{x}_{i+1}^*$) of the $(i+1)^{th}$ follower with respect to the state of the leader vehicles is defined as

$$x_{i+1}^* \triangleq x_0 - \sum_{\kappa=0}^{i} \omega_\kappa^{\kappa+1}, \quad \dot{x}_{i+1}^* = v_0, \quad \ddot{x}_{i+1}^* = 0 \tag{6.5}$$

Therefore, the position error of the $(i+1)^{th}$ follower can be defined as $\tilde{x}_{i+1} \triangleq x_{i+1} - x_{i+1}^*$, utilizing which readily results in $x_{i+1} - x_j = \tilde{x}_{i+1} - \tilde{x}_j + d_{i+1,j}$, and substituting which into the controller (6.4) gives

$$u_{i+1} = -\sum_{j \in \mathbb{I}_{i+1}} \mathbf{K}_{i+1}^j \left(\tilde{\mathbf{X}}_{i+1} - \tilde{\mathbf{X}}_j \right) \tag{6.6}$$

where $\tilde{\mathbf{X}}_{i+1} \triangleq \left[\tilde{x}_{i+1};\ \dot{\tilde{x}}_{i+1};\ \ddot{\tilde{x}}_{i+1} \right]$ and $\tilde{\mathbf{X}}_j \triangleq \left[\tilde{x}_j;\ \dot{\tilde{x}}_j;\ \ddot{\tilde{x}}_j \right]$ such that $\tilde{\mathbf{X}}_{i+1}$ and $\tilde{\mathbf{X}}_j$ are state errors of $(i+1)^{th}$ and j^{th} vehicles, respectively. Also, for $k \in \{i+1, j\}$, $\dot{\tilde{x}}_k$, $\ddot{\tilde{x}}_k$, and $\dddot{\tilde{x}}_k$ are velocity, acceleration, and jerk errors of the k^{th} vehicle.

6.1.5 State-Space Presentation of the Platoon

Using the facts $\ddot{x}_{i+1} = \ddot{\tilde{x}}_{i+1}$ and $\dddot{x}_{i+1} = \dddot{\tilde{x}}_{i+1}$, and plugging (6.6) in (6.1) yields

$$\dddot{\tilde{x}}_{i+1} = -\frac{1}{\tau_{i+1}}\mathbb{K}_{i+1}\tilde{\mathbf{X}}_{i+1} + \sum_{j\in\mathbb{I}_{i+1}} \frac{1}{\tau_{i+1}}\mathbf{K}_{i+1}^{j}\tilde{\mathbf{X}}_{j} \tag{6.7}$$

in which $\mathbb{K}_{i+1} \triangleq \left[\bar{k}_{i+1},\ \bar{b}_{i+1},\ \bar{h}_{i+1}\right]$ where

$$\bar{k}_{i+1} \triangleq \sum_{j\in\mathbb{I}_{i+1}} k_{i+1}^{j},\ \ \bar{b}_{i+1} \triangleq \sum_{j\in\mathbb{I}_{i+1}} b_{i+1}^{j},\ \ \bar{h}_{i+1} \triangleq 1 + \sum_{j\in\mathbb{I}_{i+1}} h_{i+1}^{j} \tag{6.8}$$

Now, considering (6.7), knowing $\tilde{x}_0 = \dot{\tilde{x}}_0 = \ddot{\tilde{x}}_0 = 0$, and defining the platoon's total state-error vector by $\tilde{\mathbf{X}}_t \triangleq \left[\tilde{\mathbf{X}}_1;\ \tilde{\mathbf{X}}_2; \ldots;\ \tilde{\mathbf{X}}_n\right]$, then the platoon's closed-loop state-space presentation can be characterized by

$$\dot{\tilde{\mathbf{X}}}_t = \tilde{\mathbf{A}}_t\tilde{\mathbf{X}}_t = \begin{bmatrix} \mathbf{A}_{11}^{*} & \mathbf{0}_{3\times3} & \ldots & \mathbf{0}_{3\times3} \\ \\ \mathbf{A}_{21}^{*} & \mathbf{A}_{22}^{*} & \ldots & \mathbf{0}_{3\times3} \\ \vdots & \ldots & \ddots & \vdots \\ \mathbf{A}_{n1}^{*} & \mathbf{A}_{n2}^{*} & \ldots & \mathbf{A}_{nn}^{*} \end{bmatrix} \tilde{\mathbf{X}}_t \tag{6.9}$$

where $\tilde{\mathbf{A}}_t$ is the overall closed-loop system matrix such that for $i = 0, \ldots, n-1$, we have ($\kappa = i + 1$)

$$\mathbf{A}_{\kappa\kappa}^{*} \triangleq \mathbf{A}_{\kappa} - \mathbf{B}_{\kappa}\mathbf{K}_{\kappa}, \qquad \mathbf{A}_{\kappa j}^{*} \triangleq \mathbf{B}_{\kappa}\mathbf{K}_{\kappa}^{j};\quad j < \kappa \tag{6.10}$$

where $\mathbf{K}_{\kappa} \triangleq \sum_{j\in\mathbb{I}_{\kappa}} \mathbf{K}_{\kappa}^{j}$.

6.1.6 Stability of the Platoon

Indeed, the determinant of the block matrix $s\mathbf{I}_n - \tilde{\mathbf{A}}_t$ provides the characteristic polynomial of the platoon. The roots of this polynomial correspond to the eigenvalues of the system matrix $\tilde{\mathbf{A}}_t$. Here, $\mathbf{I}_n$ represents the identity matrix of size n.

The stability of the closed-loop system is determined by the sign of the eigenvalues of $\tilde{\mathbf{A}}_t$. The system is stable if and only if all eigenvalues of $\tilde{\mathbf{A}}_t$ have negative real parts.

In other words, for the platoon to be stable, all eigenvalues of the system matrix $\tilde{\mathbf{A}}_t$ must lie in the left half of the complex plane.

Ensuring stability is a critical aspect in the control of vehicle platoons, as it guarantees that the system will behave in a predictable manner during platoon operations. Analyzing the eigenvalues of the system matrix provides valuable insights into the stability properties of the platoon, enabling the design of control strategies that maintain stability and robustness in various operational scenarios.

Remark 18 *$\tilde{\mathbf{A}}_t$ is a triangular block matrix, then $det(s\mathbf{I}_n - \tilde{\mathbf{A}}_t) = \Pi_{\kappa=1}^{n} det(s\mathbf{I}_3 - \mathbf{A}_{\kappa\kappa}^{*})$ which implies that the eigenvalues of the matrix $\tilde{\mathbf{A}}_t$ constitutes the union of the eigenvalues of the individual matrices $\mathbf{A}_{\kappa\kappa}^{*}$; $\kappa = 1, \ldots, n$. Given the definition of $\mathbf{A}_{\kappa\kappa}^{*}$ in (7.10) and noting (7.2), $\tilde{\mathbf{A}}_t$ would be stable if $\mathbf{A}_{\kappa\kappa}^{*}$; $\kappa = 1, \ldots, n$ are all stable which is true if $\bar{b}_\kappa \bar{h}_\kappa > \tau_\kappa \bar{k}_\kappa$ such that $\bar{k}_\kappa$, $\bar{b}_\kappa$, and $\bar{h}_\kappa$ need to be positive and nonzero.*

6.2 Neighboring Vehicles Coupled Dynamics

In this section, we employ state-error differences between neighboring vehicles to derive coupled distance dynamics between adjacent vehicles under look-ahead topologies. Before proceeding with the analysis, we introduce some preliminary formulations. Specifically, we define coupled position, velocity, acceleration, and jerk errors between neighboring vehicles as follows:

1. coupled position error: the difference between position errors of vehicles i and $i+1$ which we denote as $\tilde{p}_i^{i+1} \triangleq \tilde{x}_i - \tilde{x}_{i+1}$.

2. coupled velocity error: the difference between velocity errors of vehicles i and $i+1$ which we denote as $\tilde{v}_i^{i+1} \triangleq \dot{\tilde{x}}_i - \dot{\tilde{x}}_{i+1}$.

3. coupled acceleration error: the difference between acceleration errors of vehicles i and $i+1$ which we denote as $\tilde{a}_i^{i+1} \triangleq \ddot{\tilde{x}}_i - \ddot{\tilde{x}}_{i+1}$.

4. coupled jerk error: the difference between jerk errors of vehicles i and $i+1$ which we denote as $\tilde{\mathbb{J}}_i^{i+1} \triangleq \dddot{\tilde{x}}_i - \dddot{\tilde{x}}_{i+1}$.

Given the above-mentioned formulas, let define the coupled state-error and its derivative between the neighboring vehicles i and $i+1$ as

$$\begin{aligned} \tilde{\mathbf{X}}_i^{i+1} &\triangleq \tilde{\mathbf{X}}_i - \tilde{\mathbf{X}}_{i+1} \triangleq \left[\tilde{p}_i^{i+1};\ \tilde{v}_i^{i+1};\ \tilde{a}_i^{i+1}\right] \\ \dot{\tilde{\mathbf{X}}}_i^{i+1} &\triangleq \dot{\tilde{\mathbf{X}}}_i - \dot{\tilde{\mathbf{X}}}_{i+1} \triangleq \left[\tilde{v}_i^{i+1};\ \tilde{a}_i^{i+1};\ \tilde{\mathbb{J}}_i^{i+1}\right] \end{aligned} \tag{6.11}$$

These error formulations allow us to capture the differences in position, velocity, acceleration, and jerk between adjacent vehicles in the platoon. Utilizing these error terms, we will proceed to derive the coupled distance dynamics that govern the behavior of neighboring vehicles under the look-ahead CT. Also, from now on, we will refer to $\tilde{p}_i^{i+1}(.)$ (in time-domain or Laplace-domain) as the intervehicle distance error (IDE) between vehicles i and $i+1$.

Assumption 1 *In the look-ahead CT between vehicles, a connection path exists between the leader and all other follower vehicles within the platoon. This means that each follower vehicle can obtain information about the leader's state either directly or indirectly through a sequence of intermediate vehicles. As a result, every follower has access to the leader's state, allowing them to synchronize their movements and maintain the desired IDs.*

Assumption 2 *Under the assumption that the look-ahead CT is satisfied, we use the notation $z_{i+1}^i = 0$ to indicate that vehicle $(i+1)$ does not receive information directly from vehicle i. Conversely, if $z_{i+1}^i = 1$, it indicates that vehicle $(i+1)$ receives information from vehicle i. In other words, $z_{i+1}^i = 1$ signifies that vehicle i directly transmits its state information to vehicle $(i+1)$.*

Assumption 3 *To simplify the analysis without loss of generality, we assume the following initial conditions for $i = 0, \ldots, n-1$:*

1) Initial coupled velocity and acceleration: at time $t = 0$, the velocity error and acceleration error between vehicles i and $i+1$ are set to zero, i.e., $\tilde{v}_i^{i+1}(0) = \tilde{a}_i^{i+1}(0) = 0$.

2) Initial coupled position difference: the initial position difference between vehicles i and $i+1$ is the same for all pairs and equal to $\beta > 0$, i.e., $\tilde{p}_i^{i+1}(0) = \beta$.

With these initial conditions, the initial coupled-state vector for vehicles i and $i+1$ can be represented as $\mathbf{X}_i^{i+1}(0) = [\beta; 0; 0]$. This initial condition vector indicates that at $t = 0$, the position difference between vehicles i and $i+1$ is β, while the velocity and acceleration errors are both zero.

Theorem 19 *With the given equations* (6.1), (6.6), (6.8), *and* (6.11), *and by defining $\tilde{y}_i^{i+1} \triangleq \tilde{p}_i^{i+1}$, for $i = 0, \ldots, n-1$, the coupled state-space representation of vehicles i and $i+1$ based on their state differences is as follows:*

$$\begin{cases} \dot{\tilde{\mathbf{X}}}_i^{i+1} = \underbrace{\begin{bmatrix} 0 & 1 & 0 \\ 0 & 0 & 1 \\ -\frac{\bar{k}_{i+1}}{\tau_{i+1}} & -\frac{\bar{b}_{i+1}}{\tau_{i+1}} & -\frac{\bar{h}_{i+1}}{\tau_{i+1}} \end{bmatrix}}_{\triangleq \mathbf{A}_i^{i+1}} \tilde{\mathbf{X}}_i^{i+1} + \underbrace{\begin{bmatrix} 0 \\ 0 \\ 1 \end{bmatrix}}_{\triangleq \mathbf{B}_i^{i+1}} \tilde{u}_i^{i+1} \\ \tilde{y}_i^{i+1} = \underbrace{\begin{bmatrix} 1 & 0 & 0 \end{bmatrix}}_{\triangleq \mathbf{C}_i^{i+1}} \tilde{\mathbf{X}}_i^{i+1} \end{cases} \tag{6.12}$$

in which $\tilde{u}_i^{i+1}$ is according to

$$\tilde{u}_i^{i+1} = -\frac{1}{\tau_i} \boldsymbol{\tau}_i^{i+1} \sum_{\kappa=0}^{i-1} \tilde{\mathbf{X}}_\kappa^{\kappa+1} + \frac{1}{\tau_i} \sum_{j \in \mathbb{I}_i} \sum_{\kappa=j}^{i-1} \mathbf{K}_i^j \tilde{\mathbf{X}}_\kappa^{\kappa+1} - \frac{1}{\tau_{i+1}} \sum_{j \in \mathbb{R}_{i+1}} \sum_{\kappa=j}^{i-1} \mathbf{K}_{i+1}^j \tilde{\mathbf{X}}_\kappa^{\kappa+1} \tag{6.13}$$

where $\boldsymbol{\tau}_i^{i+1} = \left[0,\ 0,\ \frac{\tau_i - \tau_{i+1}}{\tau_{i+1}}\right]$, and the set $\mathbb{R}_{i+1} \triangleq \mathbb{I}_{i+1} - \{i\}$ if $z_{i+1}^i = 1$, and $\mathbb{R}_{i+1} = \mathbb{I}_{i+1}$ if $z_{i+1}^i = 0$.

Remark 20 *It is crucial, obvious and worth emphasizing that in* (6.12), *the input $\tilde{u}_i^{i+1}$ is totally independent of the coupled state variable $\tilde{\mathbf{X}}_i^{i+1}$. In other words, for the specific input $\tilde{u}_i^{i+1}$ given in* (6.13), *it always holds that $\kappa \neq i$. Also, note that for the pair* $(0, 1)$, *$\tilde{u}_i^{i+1} = 0$.*

Proof. First, for later usage, let define $\tilde{\mathbf{X}}_j^i \triangleq \tilde{\mathbf{X}}_j - \tilde{\mathbf{X}}_i$ and $\tilde{\mathbf{X}}_{i+1}^j \triangleq \tilde{\mathbf{X}}_{i+1} - \tilde{\mathbf{X}}_j$. Now, for $i = 1, \ldots, n-1$ and using (6.7), we have

$$\begin{cases} \ddot{\tilde{x}}_i = -\dfrac{1}{\tau_i}\mathbb{K}_i\tilde{\mathbf{X}}_i + \dfrac{1}{\tau_i}\displaystyle\sum_{j\in\mathbb{I}_i}\mathbf{K}_i^j\tilde{\mathbf{X}}_j \\ \ddot{\tilde{x}}_{i+1} = -\dfrac{1}{\tau_{i+1}}\mathbb{K}_{i+1}\tilde{\mathbf{X}}_{i+1} + \dfrac{1}{\tau_{i+1}}\displaystyle\sum_{j\in\mathbb{I}_{i+1}}\mathbf{K}_{i+1}^j\tilde{\mathbf{X}}_j \end{cases} \tag{6.14}$$

Therefore, for $\tilde{\mathfrak{J}}_i^{i+1} \triangleq \dddot{\tilde{x}}_i - \dddot{\tilde{x}}_{i+1}$, we get

$$\tilde{\mathfrak{J}}_i^{i+1} = -\frac{1}{\tau_i}\mathbb{K}_i\tilde{\mathbf{X}}_i^{i+1} - \left(\frac{1}{\tau_i}\mathbb{K}_i - \frac{1}{\tau_{i+1}}\mathbb{K}_{i+1}\right)\tilde{\mathbf{X}}_{i+1} + \sum_{j\in\mathbb{I}_i}\frac{1}{\tau_i}\mathbf{K}_i^j\tilde{\mathbf{X}}_j - \sum_{j\in\mathbb{I}_{i+1}}\frac{1}{\tau_{i+1}}\mathbf{K}_{i+1}^j\tilde{\mathbf{X}}_j \tag{6.15}$$

Since $-\left(\frac{\mathbb{K}_i}{\tau_i} - \frac{\mathbb{K}_{i+1}}{\tau_{i+1}}\right) = \sum_{j\in\mathbb{I}_{i+1}}\frac{\mathbf{K}_{i+1}^j}{\tau_{i+1}} - \sum_{j\in\mathbb{I}_i}\frac{\mathbf{K}_i^j}{\tau_i} + \frac{\boldsymbol{\tau}_i^{i+1}}{\tau_i}$ then (6.15) can be rewritten as

$$\tilde{\mathfrak{J}}_i^{i+1} = -\frac{1}{\tau_i}\left(\mathbb{K}_i + \boldsymbol{\tau}_i^{i+1}\right)\tilde{\mathbf{X}}_i^{i+1} + \sum_{j\in\mathbb{I}_i}\frac{1}{\tau_i}\mathbf{K}_i^j\tilde{\mathbf{X}}_j^{i+1} - \sum_{j\in\mathbb{I}_{i+1}}\frac{1}{\tau_{i+1}}\mathbf{K}_{i+1}^j\tilde{\mathbf{X}}_j^{i+1} - \frac{1}{\tau_i}\boldsymbol{\tau}_i^{i+1}\sum_{\kappa=0}^{i-1}\tilde{\mathbf{X}}_\kappa^{\kappa+1} \tag{6.16}$$

Now, having $\tilde{\mathbf{X}}_j - \tilde{\mathbf{X}}_{i+1} = \tilde{\mathbf{X}}_j - \tilde{\mathbf{X}}_i + \tilde{\mathbf{X}}_i - \tilde{\mathbf{X}}_{i+1}$, (6.16) is equal to

$$\begin{aligned} \tilde{\mathfrak{J}}_i^{i+1} = &-\left(\bar{\boldsymbol{\tau}}_i^{i+1} + \sum_{j\in\mathbb{I}_{i+1}}\frac{1}{\tau_{i+1}}\mathbf{K}_{i+1}^j\right)\tilde{\mathbf{X}}_i^{i+1} + \sum_{j\in\mathbb{I}_i}\frac{1}{\tau_i}\mathbf{K}_i^j\tilde{\mathbf{X}}_j^i \\ &- \sum_{j\in\mathbb{I}_{i+1}}\frac{1}{\tau_{i+1}}\mathbf{K}_{i+1}^j\tilde{\mathbf{X}}_j^i - \frac{1}{\tau_i}\boldsymbol{\tau}_i^{i+1}\sum_{\kappa=0}^{i-1}\tilde{\mathbf{X}}_\kappa^{\kappa+1} \end{aligned} \tag{6.17}$$

in which $\bar{\boldsymbol{\tau}}_i^{i+1} = \left[0,\ 0,\ \frac{1}{\tau_{i+1}}\right]$ and depending on how the connection is between the neighboring vehicles ($z_i^{i+1} = 1$ or $z_i^{i+1} = 0$), (6.17) can be reformulated as

$$\begin{aligned} \tilde{\mathfrak{J}}_i^{i+1} = &-\left(\bar{\boldsymbol{\tau}}_i^{i+1} + \zeta_i^{i+1} + \sum_{j\in\mathbb{R}_{i+1}}\frac{1}{\tau_{i+1}}\mathbf{K}_{i+1}^j\right)\tilde{\mathbf{X}}_i^{i+1} + \frac{1}{\tau_i}\sum_{j\in\mathbb{I}_i}\mathbf{K}_i^j\tilde{\mathbf{X}}_j^i \\ &- \frac{1}{\tau_{i+1}}\sum_{j\in\mathbb{R}_{i+1}}\mathbf{K}_{i+1}^j\tilde{\mathbf{X}}_j^i - \frac{1}{\tau_i}\boldsymbol{\tau}_i^{i+1}\sum_{\kappa=0}^{i-1}\tilde{\mathbf{X}}_\kappa^{\kappa+1} \end{aligned} \tag{6.18}$$

where $\mathbb{R}_{i+1} = \mathbb{I}_{i+1} - \{i\}$ if $z_{i+1}^i = 1$, $\mathbb{R}_{i+1} = \mathbb{I}_{i+1}$ if $z_{i+1}^i = 0$, and

$$\zeta_i^{i+1} = \begin{cases} \frac{1}{\tau_{i+1}}\mathbf{K}_i^{i+1} & \text{if} \quad z_{i+1}^i = 1 \\ 0 & \text{if} \quad z_{i+1}^i = 0 \end{cases} \tag{6.19}$$

Now, defining $\mathbf{A}_i^{i+1} \triangleq -\bar{\boldsymbol{\tau}}_i^{i+1} - \zeta_i^{i+1} - \sum_{j\in\mathbb{R}_{i+1}} \frac{1}{\tau_{i+1}}\mathbf{K}_{i+1}^j = -\bar{\boldsymbol{\tau}}_i^{i+1} - \sum_{j\in\mathbb{I}_{i+1}} \frac{1}{\tau_{i+1}}\mathbf{K}_{i+1}^j = -\frac{1}{\tau_{i+1}}\mathbb{K}_{i+1}$ (see (6.8)) and given that $\tilde{\mathbf{X}}_j^i = \sum_{\kappa=j}^{i-1} \tilde{\mathbf{X}}_\kappa^{\kappa+1}$; $j < i$, we get

$$\begin{aligned}\tilde{\mathbf{J}}_i^{i+1} =& -\frac{1}{\tau_{i+1}}\mathbb{K}_{i+1}\tilde{\mathbf{X}}_i^{i+1} - \frac{1}{\tau_i}\boldsymbol{\tau}_i^{i+1}\sum_{\kappa=0}^{i-1}\tilde{\mathbf{X}}_\kappa^{\kappa+1} \\ &+ \frac{1}{\tau_i}\sum_{j\in\mathbb{I}_i}\sum_{\kappa=j}^{i-1}\mathbf{K}_i^j\tilde{\mathbf{X}}_\kappa^{\kappa+1} - \frac{1}{\tau_{i+1}}\sum_{j\in\mathbb{R}_{i+1}}\sum_{\kappa=j}^{i-1}\mathbf{K}_{i+1}^j\tilde{\mathbf{X}}_\kappa^{\kappa+1}\end{aligned} \tag{6.20}$$

Now, let study $\tilde{\mathbf{J}}_i^{i+1}$ for $i = 0$ or to be exact for the pair $(0, 1)$. Given the fact that $\tilde{\mathbf{X}}_0 = 0$ and using (6.14) yields $\tilde{\mathbf{J}}_0^1 = -\frac{1}{\tau_1}\mathbb{K}_1^0\tilde{\mathbf{X}}_0^1$ which matches with (6.20). We assume that the first follower always receives the leader vehicle's state. Therefore, for $i = 0, \ldots, n-1$, (6.20) holds true. Given (6.20) and (6.13), it is apparent that $\tilde{\mathbf{J}}_i^{i+1} = -\frac{1}{\tau_{i+1}}\mathbb{K}_{i+1}\tilde{\mathbf{X}}_i^{i+1} + \tilde{u}_i^{i+1}$. Therefore, using (6.20), noting that $d/dt\{\tilde{p}_i^{i+1}\} = \tilde{v}_i^{i+1}$, $d/dt\{\tilde{v}_i^{i+1}\} = \tilde{a}_i^{i+1}$, and $\tilde{y}_i^{i+1} = \tilde{p}_i^{i+1}$, then the state-space presentation (6.12) holds true. ■

Remark 21 *Let's define the following constants to simplify the expression:* $\bar{k}_i^{i+1} \triangleq \frac{\bar{k}_{i+1}}{\tau_{i+1}}$, $\bar{b}_i^{i+1} \triangleq \frac{\bar{b}_{i+1}}{\tau_{i+1}}$ *and* $\bar{h}_i^{i+1} \triangleq \frac{\bar{h}_{i+1}}{\tau_{i+1}}$. *With these definitions, and considering the equation* (6.12)*, the characteristic polynomial of the pair* $(i, i+1)$ *can be represented as:* $\mu_i^{i+1}(s) = s^3 + \bar{h}_i^{i+1}s^2 + \bar{b}_i^{i+1}s + \bar{k}_i^{i+1}$. *For the stability of the coupled dynamics of the pair* $(i, i+1)$*, it is imperative to have* $\bar{b}_i^{i+1}\bar{h}_i^{i+1} > \bar{k}_i^{i+1}$*, or equivalently* $\bar{b}_{i+1}\bar{h}_{i+1} > \tau_{i+1}\bar{k}_{i+1}$. *This condition ensures that the coefficients of the characteristic polynomial are such that the system remains stable. Specifically,* $\bar{k}_{i+1}$, $\bar{b}_{i+1}$, *and* $\bar{h}_{i+1}$ *need to be positive and nonzero to meet this stability requirement. This stability condition is of great significance in the design and analysis of the coupled dynamics between vehicles* i *and* $i+1$*, as it guarantees that the ID regulation remains stable during platoon operations. By satisfying this condition for all vehicle pairs in the platoon, the overall stability of the heterogeneous platoon can be assured.*

Remark 22 *Given* (6.8) *and investigating the stability condition* $\bar{b}_{i+1}\bar{h}_{i+1} > \tau_{i+1}\bar{k}_{i+1}$ *mentioned in Remark 21, one can squarely conclude that, in the CT, there should be at*

least one connection path between the leader and other follower vehicles as mentioned in Assumption 1.

Remark 23 *Noting relation* (6.13)*, we have* $\tilde{\mathbf{X}}_{\kappa}^{\kappa+1}(s) = [1; s; s^2]\tilde{p}_{\kappa}^{\kappa+1}(s) - [0; 1; s]\beta$ *where* s *is the Laplace variable. Thus,* (6.13) *in Laplace domain can be simplified to* $\tilde{u}_i^{i+1}(s) = \tilde{u}_{i,p}^{i+1}(s) + \tilde{u}_{i,\beta}^{i+1}(s)$ *where*

$$\tilde{u}_{i,p}^{i+1}(s) = \sum_{j\in\mathbb{I}_i}\sum_{\kappa=j}^{i-1}\frac{\mathbf{K}_i^j}{\tau_i}\mathbf{T}_1\tilde{p}_{\kappa}^{\kappa+1}(s) - \sum_{\kappa=0}^{i-1}\frac{\boldsymbol{\tau}_i^{i+1}}{\tau_i}\mathbf{T}_1\tilde{p}_{\kappa}^{\kappa+1}(s) - \sum_{j\in\mathbb{R}_{i+1}}\sum_{\kappa=j}^{i-1}\frac{\mathbf{K}_{i+1}^j}{\tau_{i+1}}\mathbf{T}_1\tilde{p}_{\kappa}^{\kappa+1}(s) \tag{6.21}$$

in which $\mathbf{T}_1 \triangleq [1;\ s;\ s^2]$ *and* $\mathbf{T}_2 \triangleq [0;\ 1;\ s]$*. Also,* $\tilde{u}_{i,\beta}^{i+1}(s) = \left(\Theta_i^{i+1}s + \Gamma_i^{i+1}\right)\beta$ *such that* Θ_i^{i+1} *and* Γ_i^{i+1} *are defined as*

$$\begin{cases} \Theta_i^{i+1} \triangleq \dfrac{-1}{\tau_i}\left[\displaystyle\sum_{j\in\mathbb{I}_i}(i-j)\,h_i^j - \frac{i\,(\tau_i-\tau_{i+1})}{\tau_{i+1}}\right] + \displaystyle\sum_{j\in\mathbb{R}_{i+1}}\frac{i-j}{\tau_{i+1}}h_{i+1}^j \\ \Gamma_i^{i+1} \triangleq \dfrac{-1}{\tau_i}\displaystyle\sum_{j\in\mathbb{I}_i}(i-j)\,b_i^j + \displaystyle\sum_{j\in\mathbb{R}_{i+1}}\frac{i-j}{\tau_{i+1}}b_{i+1}^j \end{cases} \tag{6.22}$$

Note that $\tilde{u}_{i,\beta}^{i+1}(s)$ *is the fraction of input signal* $\tilde{u}_i^{i+1}(s)$ *that is just out of the initial conditions related to all neighboring pairs* $(\kappa, \kappa+1)$ *satisfying* (6.13) *(see Remark 20). Also,* $\tilde{u}_{i,p}^{i+1}(s)$ *is the input signal* $\tilde{u}_i^{i+1}(s)$ *when* $\tilde{u}_{i,\beta}^{i+1}(s) = 0$*.*

6.3 Intervehicle Distance Error (IDE) Formulation

In this section, we present the formulation for the IDEs and demonstrate that there exists a mapping between the trajectories of IDEs and the initial conditions. Note that the IDE between vehicles i and $i+1$ was denoted as $\tilde{p}_i^{i+1}$ (see Fig. 6.1).

By analyzing the coupled dynamics, we show that the trajectories of the IDEs can be determined based on the initial conditions of the platoon. The mapping between the ID-error trajectories and the initial conditions highlights the interdependence of the platoon's behavior and its starting configuration. It indicates that the initial conditions play a crucial role in shaping the evolution of IDEs as the platoon operates over time. This knowledge can be leveraged to choose control gains that lead to

desired IDs and ensure stable platoon operations under various scenarios and initial conditions.

6.3.1 IDE Between Vehicles i and $i+1$

First, the Laplace-domain trajectory of the distance error between neighboring vehicles i and $i+1$; $i = 0, \ldots, n-1$, is presented. Analyzing this Laplace-domain equation will allow us to understand the behavior of the distance errors and assess the stability and performance of the platoon under different control gains and initial conditions.

Theorem 24 *Given* (6.12)*, Remarks 20 and 23, let the IDE out of the initial position differences between vehicles i and $i+1$, and all vehicles κ and $\kappa+1$ satisfying* (6.13)*, be defined as $\psi_i^{i+1}(s)$ and according to*

$$\psi_i^{i+1}(s) = \beta \left(s^2 + \left(\bar{h}_i^{i+1} + \Theta_i^{i+1} \right) s + \bar{b}_i^{i+1} + \Gamma_i^{i+1} \right) H_i^{i+1}(s) \tag{6.23}$$

in which $H_i^{i+1}(s)$ specified by

$$H_i^{i+1}(s) = \left(s^3 + \bar{h}_i^{i+1} s^2 + \bar{b}_i^{i+1} s + \bar{k}_i^{i+1} \right)^{-1} \tag{6.24}$$

Proof. Given (6.12)-(6.13), and since the system is linear, $\tilde{p}_i^{i+1}(s)$ is equal to the summation of zero-state response of the pair $(i, i+1)$ ($\tilde{\mathbf{X}}_i^{i+1}(0) = [0; 0; 0]$) and its zero-input response ($\tilde{u}_i^{i+1}(s) = 0$, see Remark 23). Reminding Remark 20, in the zero-state response of the pair $(i, i+1)$, $\tilde{\mathbf{X}}_\kappa^{\kappa+1}(0) = [0; 0; \beta]$ for all pairs $(\kappa, \kappa+1)$ satisfying (6.13) hold true. The zero-input response, let be defined as $\tilde{p}_{i,zi}^{i+1}(s)$, would be according to

$$\tilde{p}_{i,zi}^{i+1}(s) = \mathbf{C}_i^{i+1} \left(s\mathbf{I}_3 - \mathbf{A}_i^{i+1} \right)^{-1} \tilde{\mathbf{X}}_i^{i+1}(0) = \frac{\beta \left(s^2 + \bar{h}_i^{i+1} s + \bar{b}_i^{i+1} \right)}{s^3 + \bar{h}_i^{i+1} s^2 + \bar{b}_i^{i+1} s + \bar{k}_i^{i+1}} \tag{6.25}$$

in which $\mathbf{I}_3$ is the identity matrix of size 3. Also, given Remarks 20 and 23, the zero-state response of the pair $(i, i+1)$ out of the initial conditions related to the pairs $(\kappa, \kappa+1)$ satisfying (6.13), let be defined by $\tilde{p}_{i,zs\beta}^{i+1}(s)$, would be

$$\tilde{p}_{i,zs\beta}^{i+1}(s) = \mathbf{C}_i^{i+1} \left(s\mathbf{I}_3 - \mathbf{A}_i^{i+1} \right)^{-1} \mathbf{B}_i^{i+1} \tilde{u}_{i,\beta}^{i+1}(s) = \frac{\beta \left(\Theta_i^{i+1} s + \Gamma_i^{i+1} \right)}{s^3 + \bar{h}_i^{i+1} s^2 + \bar{b}_i^{i+1} s + \bar{k}_i^{i+1}} \tag{6.26}$$

Therefore, given (6.25) and (6.26), and noting that $\psi_i^{i+1}(s) = \tilde{p}_{i,zi}^{i+1}(s) + \tilde{p}_{i,zs\beta}^{i+1}(s)$, then (6.23) holds true. ■

Theorem 25 *Given Theorem 24, the IDE between vehicles i and $i+1$, independent of all initial conditions, let be defined as $\tilde{p}_{i,zsp}^{i+1}(s)$, is governed by*

$$\begin{aligned}\tilde{p}_{i,zsp}^{i+1}(s) = \Bigg[&\sum_{j\in\mathbb{I}_i}\sum_{\kappa=j}^{i-1}\frac{\mathbf{K}_i^j}{\tau_i}\mathbf{T}_1\tilde{p}_\kappa^{\kappa+1}(s) - \sum_{\kappa=0}^{i-1}\frac{\boldsymbol{\tau}_i^{i+1}}{\tau_i}\mathbf{T}_1\tilde{p}_\kappa^{\kappa+1}(s)\\ &- \sum_{j\in\mathbb{R}_{i+1}}\sum_{\kappa=j}^{i-1}\frac{\mathbf{K}_{i+1}^j}{\tau_{i+1}}\mathbf{T}_1\tilde{p}_\kappa^{\kappa+1}(s)\Bigg] H_i^{i+1}(s)\end{aligned} \tag{6.27}$$

Proof. Independent of all initial conditions conveys the zero-state response of the pair $(i, i+1)$, $\tilde{\mathbf{X}}_i^{i+1} = [0;0;0]$, when all other initial conditions related to pairs $(\kappa, \kappa+1)$ satisfying (6.13) considered to be zero as well. Therefore, given Remark 23, $\tilde{p}_{i,zsp}^{i+1}(s)$ would be

$$\tilde{p}_{i,zsp}^{i+1}(s) = \mathbf{C}_i^{i+1}\left(s\mathbf{I}_3 - \mathbf{A}_i^{i+1}\right)^{-1}\mathbf{B}_i^{i+1}\tilde{u}_{i,p}^{i+1}(s) \tag{6.28}$$

using which and considering (6.21), (6.27) holds true. ■

Thus, given Theorems 19 and 24, the Laplace-domain trajectory of the distance error between vehicles i and $i+1$ can be obtained by $\tilde{p}_i^{i+1}(s) = \tilde{p}_{i,zi}^{i+1}(s) + \tilde{p}_{i,zs\beta}^{i+1}(s) + \tilde{p}_{i,zsp}^{i+1}(s)$ which results in

$$\begin{aligned}\tilde{p}_i^{i+1}(s) = \psi_i^{i+1}(s) + H_i^{i+1}(s)\Bigg[&\sum_{j\in\mathbb{I}_i}\sum_{\kappa=j}^{i-1}\frac{\mathbf{K}_i^j}{\tau_i}\mathbf{T}_1\tilde{p}_\kappa^{\kappa+1}(s)\\ &- \sum_{\kappa=0}^{i-1}\frac{\boldsymbol{\tau}_i^{i+1}}{\tau_i}\mathbf{T}_1\tilde{p}_\kappa^{\kappa+1}(s) - \sum_{j\in\mathbb{R}_{i+1}}\sum_{\kappa=j}^{i-1}\frac{\mathbf{K}_{i+1}^j}{\tau_{i+1}}\mathbf{T}_1\tilde{p}_\kappa^{\kappa+1}(s)\Bigg]\end{aligned} \tag{6.29}$$

6.3.2 Mapping Between IDEs and Initial Conditions

Calculating (6.29) for $i = 0, \ldots, n-1$ and stacking them together, a mapping between initial conditions and the IDEs can be found as follows.

$$\tilde{\mathbf{P}}(s) = \mathbf{Q}^{-1}(s)\boldsymbol{\Psi}(s) \tag{6.30}$$

where $\mathbf{\Psi}(s) \triangleq \left[\psi_0^1(s);\ \psi_1^2(s);\ \ldots;\ \psi_{n-1}^n(s)\right]$ in which all $\psi_i^{i+1}(s)$ can be obtained by (6.23), $\tilde{\mathbf{P}}(s) \triangleq \left[\tilde{p}_0^1(s);\ \tilde{p}_1^2(s);\ \ldots;\ \tilde{p}_{n-1}^n(s)\right]$, and $\mathbf{Q}(s) \in \mathbb{C}^{n\times n}$ whose elements are based on ($i = 0, \ldots, n-1$ and $\kappa = 1, \ldots, n$)

$$Q_{(i+1)\kappa}(s) = \begin{cases} -\mathbf{K}_{i,i+1}^{\kappa}\mathbf{T}_1 H_i^{i+1}(s) & \text{if } \ i+1 > \kappa \\ 1 & \text{if } \ i+1 = \kappa \\ 0 & \text{if } \ i+1 < \kappa \end{cases} \tag{6.31}$$

in which

$$\mathbf{K}_{i,i+1}^{\kappa} \triangleq \frac{1}{\tau_i}\sum_{j_\kappa}\mathbf{K}_i^j - \frac{1}{\tau_{i+1}}\sum_{j_\kappa^+}\mathbf{K}_{i+1}^j - \frac{1}{\tau_i}\boldsymbol{\tau}_i^{i+1} \tag{6.32}$$

where $j_\kappa \triangleq \{j | j \in \mathbb{I}_i \ \&\ j \leq \kappa - 1\}$ and $j_\kappa^+ \triangleq \{j | j \in \mathbb{R}_{i+1} \ \&\ j \leq \kappa - 1\}$. Therefore, if $\bar{\mathbf{Q}}(s) \triangleq \mathbf{Q}^{-1}(s)$, then one can conclude that

$$\tilde{p}_i^{i+1}(s) = \sum_{j=1}^{n}\bar{Q}_{(i+1)j}(s)\psi_{j-1}^j(s); \quad i = 0, \ldots, n-1 \tag{6.33}$$

such that $\bar{Q}_{(i+1)j} = 1$ if $i+1 = j$ and $\bar{Q}_{(i+1)j} = 0$ if $i+1 < j$.

Remark 26 *Noting* (6.23), (6.30) *and* (6.31), *and by having initial conditions and engines' time constants, and for a given CT and control gains, one can form* $\mathbf{\Psi}(s)$, $\mathbf{Q}(s)$, $\bar{\mathbf{Q}}(s)$ *and consequently* $\tilde{\mathbf{P}}(s)$, *and so* $\tilde{p}_i^{i+1}(s)$; $i = 0, \ldots, n-1$.

Remark 27 *Given* (6.33), *to have all* $\tilde{p}_i^{i+1}(s)$ *stable,* $\psi_i^{i+1}(s)$; $i = 0, \ldots, n-1$, *and* $\bar{Q}_{(i+1)j}$; $i+1 > j$, *all need to be stable. Therefore, given* (6.23) *and* (6.31), *and reminding that* $\mathbf{Q}(s)$ *is a lower triangular matrix, it is imperative to have all* $H_i^{i+1}(s)$; $i = 0, \ldots, n-1$ *stable (see* (6.24)*). This entails to have* $\bar{b}_i^{i+1}\bar{h}_i^{i+1} > \bar{k}_i^{i+1}$, *or equivalently* $\bar{b}_{i+1}\bar{h}_{i+1} > \tau_{i+1}\bar{k}_{i+1}$ *such that* $\bar{k}_{i+1}$, $\bar{k}_{i+1}$, *and* $\bar{h}_{i+1}$ *need to be positive and nonzero. This is in line with Remarks 18 and 21 and implies that to have a stable platoon under look-ahead topologies discussed in this work, all coupled dynamics related to pairs* $(i, i+1)$; $i = 0, \ldots, n-1$, *need to be stable.*

Remark 28 *To find* $\tilde{p}_i^{i+1}(t)$, *which is the time-domain trajectory of the IDE between vehicles* i *and* $i+1$, *we need to take the inverse Laplace transform of* $\tilde{p}_i^{i+1}(s)$. *However,*

if we consider $\tilde{p}_i^{i+1}(s)$ *as if it is the transfer function of a system, then* $\tilde{p}_i^{i+1}(t)$ *would the impulse response of the system* $\tilde{p}_i^{i+1}(s)$.

Remark 29 *Given Remark 28, suppose that, for a given stable control gains (see Remark 27), one have found* $\tilde{p}_i^{i+1}(t)$; $i = 0, \ldots, n-1$. *Therefore, if exists* $\tilde{p}_i^{i+1}(t) < -d_i^{i+1}$; $i = 0, \ldots, n-1$, *then, for the given control gains, we would have collision occurrence in the platoon. Similarly, if all* $-d_i^{i+1} < \tilde{p}_i^{i+1}(t) < -\left(d_i^{i+1} - d_{i,s}^{i+1}\right)$ *in which* $d_{i,s}^{i+1}$ *is considered to be a preset safe-distance between neighboring vehicles, then we would have a non-colliding platoon but the distance between consecutive vehicles violate the safe distance. Also, if all* $\tilde{p}_i^{i+1}(t) > -\left(d_i^{i+1} - d_{i,s}^{i+1}\right)$, *then the distances between adjacent vehicles would be always higher than* $d_{i,s}^{i+1}$.

Remark 30 *For stable control gains, according to* (6.29) *and final value theorem of Laplace transform, we have* $\lim_{t\to\infty} \tilde{p}_i^{i+1}(t) = \lim_{s\to 0} s\tilde{p}_i^{i+1}(s) = 0$ *and since* $D_i^{i+1}(t) = \tilde{p}_i^{i+1}(t) + d_i^{i+1}$ *then we get* $D_i^{i+1}(t) = d_i^{i+1}$; $i = 0, 1, \ldots, n-1$ *which implies that all IDs finally converge to their corresponding desired values* d_i^{i+1} *(see Fig. 6.1).*

6.4 Simulation Results

Consider a platoon with one leader and four followers under the communication topology (CT) shown in Fig. A.1.

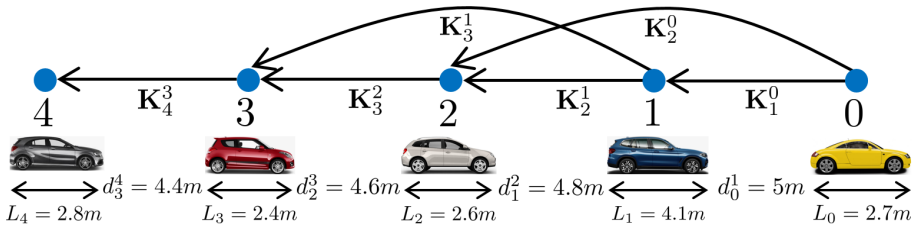

Figure 6.3: The look-ahead CT considered for simulations.

The assumed target distances among vehicles are as follows: $d_0^1 = 5m$, $d_1^2 = 4.8m$, $d_2^3 = 4.6m$, and $d_3^4 = 4.4m$. The lengths of each vehicle are given as $L_0 = 2.7m$,

$L_1 = 4.1m$, $L_2 = 2.6m$, $L_3 = 2.4m$, and $L_4 = 2.8m$, respectively. All initial velocities and accelerations are initialized to zero. Simulations are executed using a sampling interval of 0.01 seconds. The safe distance between vehicles is set at $3m$ and denoted as $d_{i,s}^{i+1} = 3m$. Furthermore, the engine time constants are defined as $\tau_1 = 0.7$, $\tau_2 = 0.6$, $\tau_3 = 1$, and $\tau_4 = 0.9$, respectively.

6.4.1 Platoon Stability and Intervehicle Distances (IDs)

Let's define the total control gain vector of the platoon as $\mathbf{K}_t = [\mathbf{K}_1^0, \mathbf{K}_2^1, \mathbf{K}_2^0, \mathbf{K}_3^2, \mathbf{K}_3^1, \mathbf{K}_4^3]$, where each individual control gain vector is denoted as $\mathbf{K}_i^j = [k_i^j,\ b_i^j,\ h_i^j]$. According to Remark 27, the platoon shown in Figure A.1 will be stable if and only if

1. $b_1^0(1 + h_1^0) > \tau_1 k_1^0$
2. $(b_2^1 + b_2^0)(1 + h_2^1 + h_2^0) > \tau_2(k_2^1 + k_2^0)$
3. $(b_3^2 + b_3^1)(1 + h_3^2 + h_3^1) > \tau_3(k_3^2 + k_3^1)$
4. $b_4^3(1 + h_4^3) > \tau_4 k_4^3$

Referring to equation (6.33) and considering the aforementioned prerequisites for Platoon Stability (PS), Table 6.1 outlines the impact, or lack thereof, of different parameters on both PS and IDs. The symbol ✓ signifies an influence, while the symbol $\times$ denotes the absence of influence by the corresponding parameter. Various distance scenarios have been defined, encompassing the following: Unstable (U), Stable-No-Collision (SNC), Stable-No-Collision-Safe (SNCS), Stable-No-Collision-Not-Safe (SNCNS), and Stable-Collision (SC) IDs. These scenarios are elucidated alongside their respective conditions in Table 6.2. Specifically, the U scenario demonstrates platooning instability, SNC signifies a stable platoon without collisions, SNCS mirrors SNC but ensures that IDs never dip below a safe distance, SNCNS resembles SNC but with some IDs falling below the safe distance, and lastly, SC indicates platoon stability coexisting with collisions during platooning.

In Table 6.2, the symbol ✓ signifies the validity of the respective condition for $i = 0, \ldots, 3$, while the symbol $\times$ indicates the absence of validity for at least one of the pairs. A '-' denotes that the relevant condition is no longer needed to be studied. See Appendix A for a comprehensive explanation elucidating the rationale behind the content presented in Table 6.1.

Table 6.1: The effect of parameters on IDEs and PS.

	$\mathbf{K}_1^0$	$\mathbf{K}_2^1$	$\mathbf{K}_2^0$	$\mathbf{K}_3^2$	$\mathbf{K}_3^1$	$\mathbf{K}_4^3$	τ_1	τ_2	τ_3	τ_4	β
$\tilde{p}_0^1$	✓	×	×	×	×	×	✓	×	×	×	✓
$\tilde{p}_1^2$	✓	✓	✓	×	×	×	✓	✓	×	×	✓
$\tilde{p}_2^3$	✓	✓	✓	✓	✓	×	✓	✓	✓	×	✓
$\tilde{p}_3^4$	✓	✓	✓	✓	✓	✓	✓	✓	✓	✓	✓
PS	✓	✓	✓	✓	✓	✓	✓	✓	✓	✓	×

Table 6.2: Conditions for unstable (U), stable-no-collision (SNC), stable-no-collision-safe (SNCS), stable-no-collision-not-safe (SNCNS), and stable-collision (SC) IDs.

Condition	$\mathbf{K}_t$	$\mathbf{K}_t$	$\mathbf{K}_t$	$\mathbf{K}_t$	$\mathbf{K}_t$
$\bar{b}_{i+1}\bar{h}_{i+1} > \tau_{i+1}\bar{k}_{i+1}$	×	✓	✓	✓	✓
$\tilde{p}_i^{i+1} > -d_i^{i+1}$	-	✓	-	✓	×
$\tilde{p}_i^{i+1} > -(d_i^{i+1} - 3)$	-	-	✓	×	-
Result	U	SNC	SNCS	SNCNS	SC

Based on the information in Table 6.1, the initial conditions (denoted as β) do not have any impact on the stability of the platoon. Stability is determined by other factors such as control parameters and engine time constants. However, the initial conditions do affect all IDEs between the vehicles in the platoon. Moreover,

it is observed that the IDE between the third and fourth followers (the last pair of vehicles) is influenced by all control parameters, engine time constants, and initial conditions. This indicates that the stability and behavior of this specific pair are particularly sensitive to variations in these factors.

6.4.2 Control Gains Selection

For each i ranging from 0 to 3, and for every j belonging to the set of integers $\mathbb{I}_{i+1}$, we make the assumption that h_{i+1}^{j} remains constant at a value of ζ. Additionally, k_{i+1}^{j} and b_{i+1}^{j} are allowed to vary within the range of positive values q_1 to q_2 with incremental changes of ϵ. Utilizing the information from Table 6.2, it is possible to perform a numerical assessment to determine whether a given $\mathbf{K}_t$ corresponds to unstable, colliding, non-colliding, or safe conditions for IDs. As an example, let's take $\zeta = 4$, $q_1 = 0.1$, $q_2 = 4$, and $\epsilon = 1$. Moreover, we select control gains that ensure the time-settling of IDEs are less than 15 seconds for the 'SNC', 'SNCS', and 'SNCNS' cases. It's important to note that the 'SNC' scenario can manifest in either 'SNCS' or 'SNCNS' forms. Consequently, the simulations will present outcomes for the 'SNCS', 'SNCNS', and 'SC' scenarios. The simulations are conducted within three distinct scenarios:

Initial distances are beyond the safe distance ($3m$)

In this case, initial IDEs are uniformly set to $\beta = 8m$. Accordingly, given the vehicles' lengths, and the desired distances illustrated in the Fig. A.1, the initial positions of the vehicles are $x_1(0) = 15.7m$, $x_2(0) = 32.6m$, $x_3(0) = 47.8m$, and $x_4(0) = 62.6m$. These initializations are based on the assumption that $x_0(0) = 0$. Table 6.3, show examples of $\mathbf{K}_t$ found for each distance scenario.

Verification of control gains: If we consider any time interval $0 < t_1 \leq t < t_2$ and assume that the leader vehicle's acceleration, denoted as $a_0(t)$, remains constant

Table 6.3: Selected control gains for each distance scenario.

Category	$\mathbf{K}_t$
SNC	$[1.1, 3.1, 4.0, 1.1, 3.1, 4.0, 1.1, 3.1, 4.0, 0.1, 3.1, 4.0, 1.1, 3.1, 4.0, 1.1, 3.1, 4.0]$
SNCS	$[1.1, 3.1, 4.0, 0.1, 2.1, 4.0, 1.1, 3.1, 4.0, 0.1, 3.1, 4.0, 1.1, 3.1, 4.0, 1.1, 3.1, 4.0]$
SNCNS	$[3.1, 3.1, 4.0, 2.1, 2.1, 4.0, 3.1, 3.1, 4.0, 2.1, 3.1, 4.0, 2.1, 3.1, 4.0, 1.1, 3.1, 4.0]$
SC	$[2.1, 1.1, 4.0, 0.1, 2.1, 4.0, 1.1, 0.1, 4.0, 1.1, 2.1, 4.0, 2.1, 1.1, 4.0, 1.1, 2.1, 4.0]$

with the value a_0 during this period, we can apply principles of Physics to derive its velocity and position as follows:

The velocity of the leader vehicle, denoted as $v_0(t)$, can be expressed as $v_0(t) = a_0 t + v_0(0)$, where $v_0(0)$ represents its initial velocity. Similarly, the position of the leader vehicle, denoted as $x_0(t)$, can be determined using the equation $x_0(t) = \frac{1}{2}a_0 t^2 + v_0(0)t + x_0(0)$, where $x_0(0)$ represents its initial position. Figure 6.4 illustrates the trajectory of the leader vehicle's acceleration and its corresponding velocity.

Given (6.5) and reminding that $\tilde{\mathbf{X}}_i(t) = \mathbf{X}_i(t) - \mathbf{X}_i^*(t)$, using (6.9) and assuming that the sampling time is equal to Δt, it becomes possible to calculate the state vector $\tilde{\mathbf{X}}_t(t + \Delta t)$ as follows:

$$\tilde{\mathbf{X}}_t(t + \Delta t) = \left(\mathbf{I}_{3n} + \tilde{\mathbf{A}}_t \Delta t\right) \tilde{\mathbf{X}}_t(t) \tag{6.34}$$

Here, $\mathbf{I}_{3n}$ represents the identity matrix of size $3n$. Using the expression (6.34), it becomes straightforward to determine both the IDEs and vehicle velocities. The IDEs are visually represented in Fig. 6.5 for the control gains provided in Table 6.3. The results strongly validate the analysis presented. For instance, when employing SC sample control gains, the trajectories $\tilde{p}_0^1(t)$, $\tilde{p}_1^2(t)$, $\tilde{p}_2^3(t)$, and $\tilde{p}_3^4(t)$ intersect with the dashed line, which serves as the threshold for avoiding collisions between vehicles.

Tracking verification: The primary objective of platooning is not only to maintain the desired distances between vehicles but also to achieve synchronization between

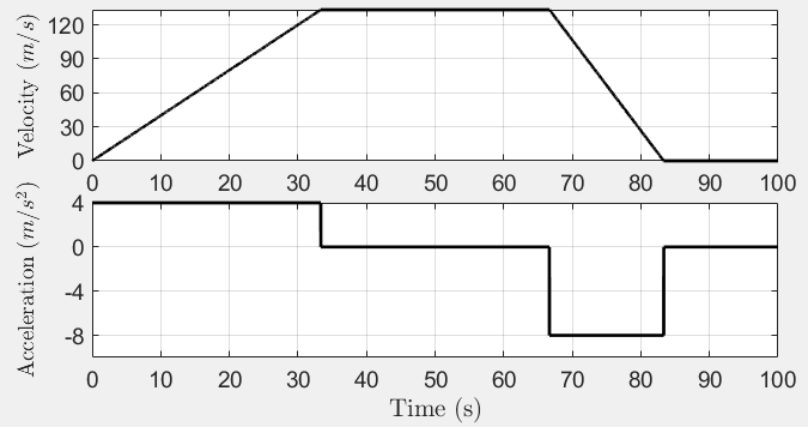

Figure 6.4: Leader's velocity and acceleration.

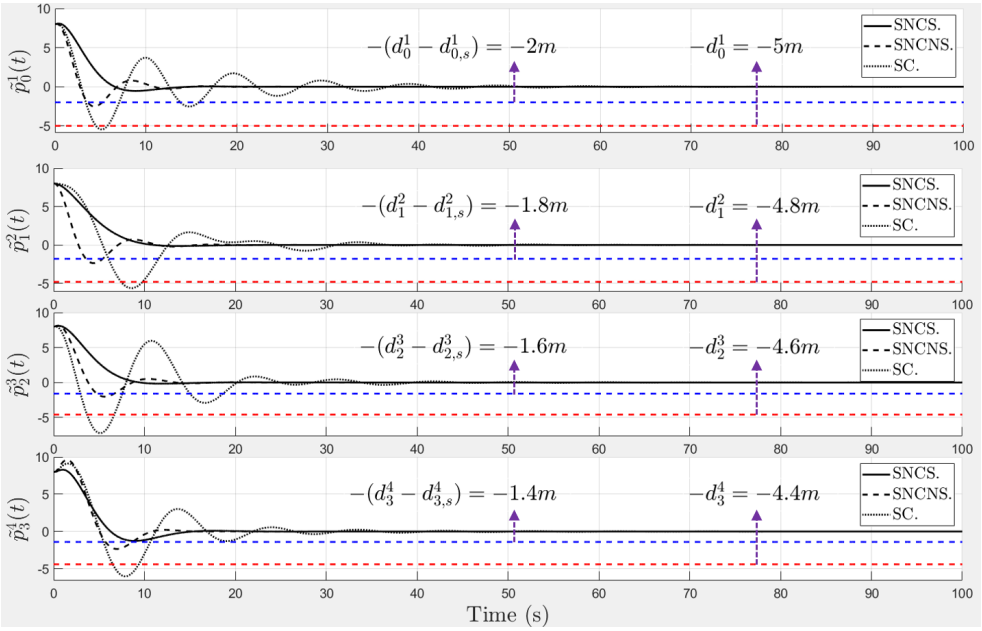

Figure 6.5: IDEs under leader velocity (Fig. 6.4) and sample control gains shown in Table 6.3. Red and blue dashed lines show collision and safe distance thresholds, respectively.

follower vehicles and the leader vehicle. This synchronization entails having the follower vehicles track the velocity and acceleration profiles of the leader vehicle. The follower vehicles aim to replicate the speed and acceleration behavior of the leader to maintain a cohesive and coordinated platoon movement. Figs. 6.6 and 6.7 visually depict the follower vehicles' tracking of the velocity and acceleration of the leader

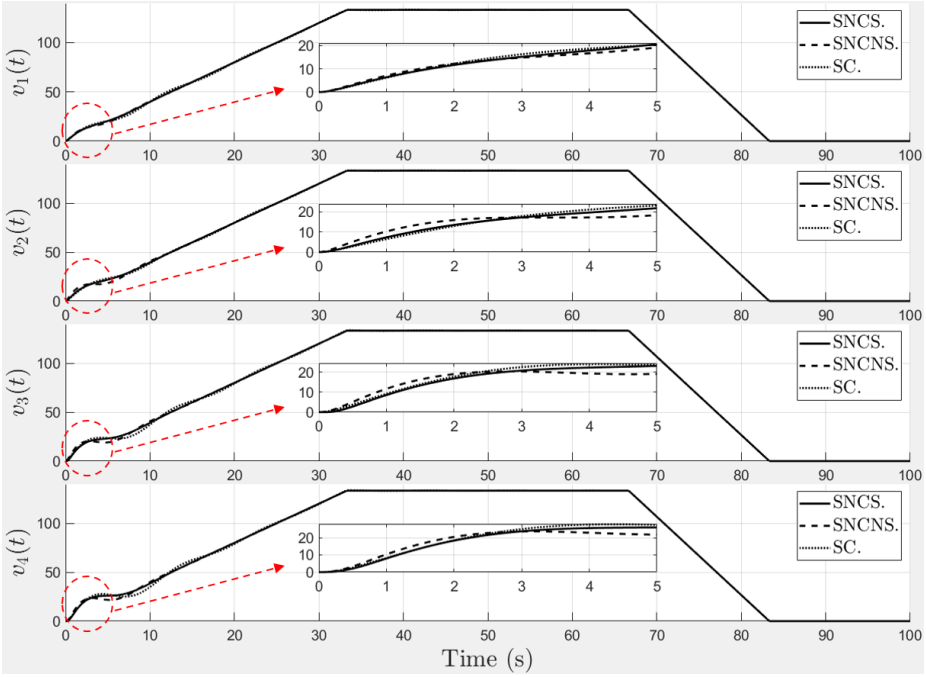

Figure 6.6: Follower vehicles' velocities given leader velocity in Fig. 6.4 and sample control gains shown in Table 6.3.

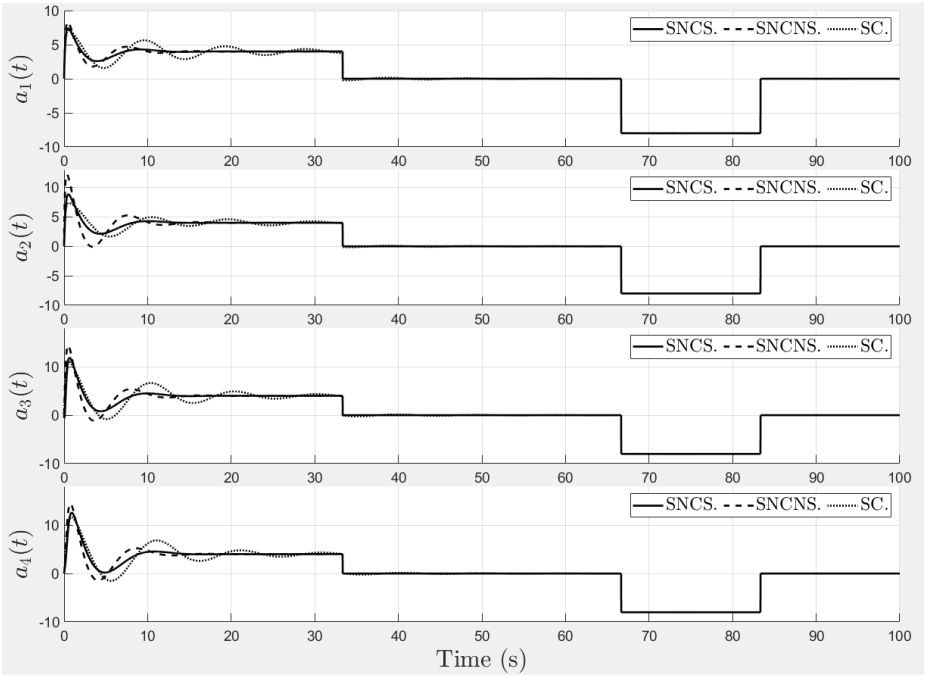

Figure 6.7: Follower vehicles' accelerations given leader velocity in Fig. 6.4 and sample control gains shown in Table 6.3.

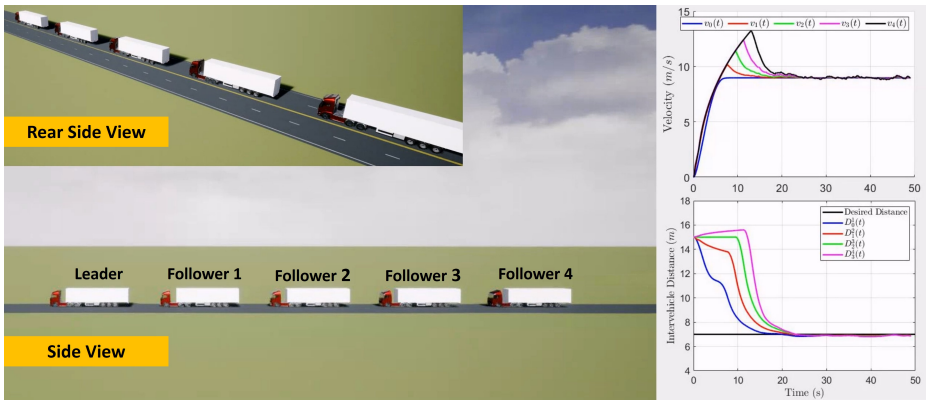

Figure 6.8: Truck platooning using Vehicle Dynamics Blockset under the controller (6.4) and CT given in the Fig. A.1. Click to watch the video: https://youtu.be/JEHl4JLRxKs

vehicle, respectively. These figures illustrate how well the followers are able to replicate the leader's speed and acceleration profiles over time. These figures are crucial in evaluating the effectiveness of the platooning control strategy. If the follower vehicles can accurately track the leader's velocity and acceleration, it indicates that the platoon is well-controlled, and the synchronization objectives are being met. Please check the simulation videos for SNCS[2], SNCNS[3], and SC[4] scenarios, respectively.

Initial distances fall below the safe distance $(3m)$

In the simulations of the previous scenario, the initial conditions were set beyond the safe distance (i.e., $3m$). However, since the provided analysis is general, the same conclusions apply even if some of the initial IDEs are smaller than the safe distance. Therefore, by choosing appropriate control gains based on the provided analysis, the system can effectively coordinate vehicles and guide them back to a safe set from an unsafe situation. In this case, the initial positions of the vehicles are set as follows: $x_1(0) = -6.2m$, $x_2(0) = -13.6m$, $x_3(0) = -19.3m$, and $x_4(0) = -24.6m$, assuming $x_0(0) = 0$. In this case ($\beta = -1.5m$), given the vehicles' lengths, and the desired

[2] https://youtu.be/ExioKt5bMbk
[3] https://youtu.be/jU3IgpfRQOI
[4] https://youtu.be/sxwmQS78fdM

distances illustrated in the Fig. A.1, the initial distance between the vehicles three and four fall below the safe distance. Please check the associated simulation video[5].

High-fidelity simulation of truck platooning

In the last scenario, to analyze the controller's performance in realistic vehicle platooning, we used MATLAB Vehicle Dynamics Blockset for simulation. The platooning setup includes one leader and four followers with vehicle-to-vehicle (V2V) communication, as illustrated in Fig. A.1. Each follower has a platooning controller (specified in (6.4)) that regulates longitudinal controls to maintain a constant spacing from the preceding vehicle while following the lead vehicle. The inbuilt vehicle dynamics are modeled using a six degrees of freedom tractor-trailer system, representing a three-axle tractor towing a three-axle trailer through a hitch. Both the tractor and trailer have individual models for their vehicle body, wheels, and suspension. The platooning controller influences the acceleration input, while the steering angle is maintained at zero. The V2V communication model between the five vehicles incorporates the arbitrary look-ahead CT. Each vehicle in the platoon is equipped with a V2V transmitter and receiver. The transmitter sends basic safety messages (BSMs) containing pose information, and the receivers of the platoon followers receive and extract information from these BSMs. This information is then used by each follower's controller to calculate the appropriate acceleration for maintaining the desired spacing from the preceding vehicle and following the lead vehicle. The lengths of the vehicles are $17.2m$ and control gains are considered to be identical for each follower vehicle such that $\mathbf{K}_1^0 = \mathbf{K}_2^1 = \mathbf{K}_2^0 = \mathbf{K}_3^2 = \mathbf{K}_3^1 = \mathbf{K}_4^3 = [2,\ 10,\ 10]$. Fig. 6.8 shows the visualization of the mentioned truck platooning. Please check the associated high-fidelity simulation video[6]

[5] https://youtu.be/UttMe5b9fg8

[6] https://youtu.be/JEHl4JLRxKs

6.5 Conclusion

In conclusion, this research introduced an innovative approach that goes beyond traditional internal stability considerations. By focusing on neighboring-vehicle state differences and formulating a coupled distance dynamic model, we have advanced our understanding of platoon dynamics. This model not only allows us to derive intervehicle distances but also facilitates the analysis of collision possibilities and the establishment of safe distance limits.

Through the careful setting of appropriate collision and safe distance limits, along with the identification of control gains, our methodology ensures both stable and safe behaviors for vehicles within a platoon. We conducted a comprehensive examination of how control parameters and initial conditions impact platoon stability and intervehicle distance errors, presenting a range of distance scenarios and their associated conditions.

The theoretical findings presented here were rigorously validated through simulations, including high-fidelity truck platooning scenarios in MATLAB Vehicle Dynamics Blockset. These simulations demonstrated the effectiveness of the proposed control strategies in ensuring stability and safety within heterogeneous platoons operating under look-ahead topologies. This research contributes to our ability to optimize platoon performance while prioritizing the safety of all vehicles involved.

Chapter 7

Effects of Communication on Inter-Vehicle Distance and Scalability in Heterogeneous Vehicular Platoon Control: Considering Comprehensive Initial States[1]

This chapter serves as the foundation for exploring the impact of communication topologies (CTs) on the performance of heterogeneous vehicular platoons. It investigates Scalability, stability, and transient intervehicle distances (IDs) under a distributed linear feedback control law, considering full-state initial conditions.

7.1 Preliminaries

Throughout this paper, the argument of time-dependent signals are left out unless they are required for the sake of clarity. Also, we separate elements of vertical and horizontal vectors by semicolon and colon symbols, respectively. For instance, $[.;.;.]$ shows a 3-by-1 vector and $[.,.,.]$ shows a 1-by-3 vector. Figure 7.1 depicts a platoon

[1]A version of this chapter has been submitted as Amir Zakerimanesh, Tony Z. Qiu, Mahdi Tavakoli, *Effects of Communication on Inter-Vehicle Distance and Scalability in Heterogeneous Vehicular Platoon Control: Considering Comprehensive Initial States*, IEEE Transactions on Intelligent Transportation Systems.

including the leader vehicle designated by 0, and the follower vehicles labeled by $1, \ldots, i, i+1, \ldots, n-1, n$. The x axis shows the movement direction of vehicles, and the notations x_0 and x_i indicate the front positions of the leader and the i^{th} follower vehicle, respectively. The real and preset desired intervehicle distances (IDs) between neighboring vehicles i and $i+1$ are denoted by D_i^{i+1} and d_i^{i+1}, respectively. Also, L_i shows the length of the i^{th} vehicle. Furthermore, for $i = 0, \ldots, n-1$, $p_i^{i+1} \triangleq x_i - x_{i+1}$ denotes position difference between the consecutive vehicles. Accordingly, $\tilde{p}_i^{i+1} \triangleq p_i^{i+1} - \omega_i^{i+1}$ in which $\omega_i^{i+1} \triangleq L_i + d_i^{i+1}$. Longitudinal control of a platoon generally consists of 1) inner force/acceleration control loop, the feedback linearization control that compensates for the nonlinear dynamics of the vehicles, and 2) an outer ID control loop that is responsible for maintaining the desired distances between consecutive vehicles. Let dynamics nonlinearities be already canceled by the FL part and, thus, in the following we focus on the ID control loop.

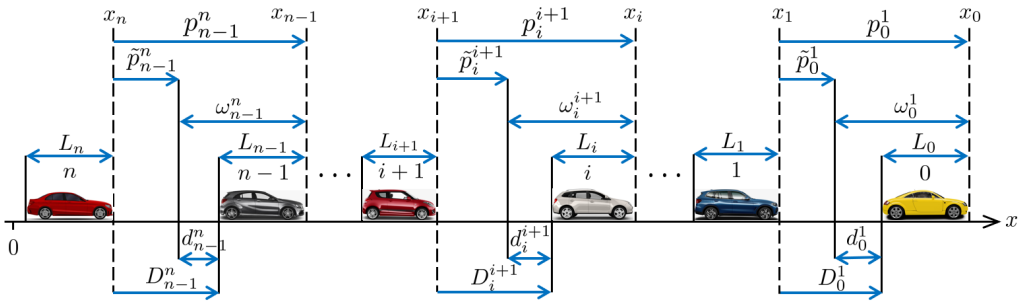

Figure 7.1: A platoon divided into consecutive-pairwise vehicles.

7.1.1 Vehicles Dynamics

We assume that the leader vehicle does not undergo any control process but its position, velocity and acceleration are utilized to control the following vehicles. As such, the behavior of each follower vehicle (FV) within the platoon is mathematically

described by a third-order linear model [27, 31, 43, 46–48, 53, 54, 56, 57] as follows.

$$\begin{cases} \dot{x}_{i+1} = v_{i+1} \\ \dot{v}_{i+1} = a_{i+1} \\ \dot{a}_{i+1} = -\frac{1}{\tau_{i+1}} a_{i+1} + \frac{1}{\tau_{i+1}} u_{i+1} \end{cases} \qquad i = 0, \ldots, n-1 \tag{7.1}$$

in which a_{i+1}, v_{i+1}, and τ_{i+1} are acceleration, velocity, and engine-time-constant of the $(i+1)^{th}$ follower. Also, u_{i+1} is its input signal to be designed properly. Let $\mathbf{X}_{i+1} \in R^{3\times 1}$ be defined as $\mathbf{X}_{i+1} \triangleq [x_{i+1}; \dot{x}_{i+1}; \ddot{x}_{i+1}]$ which describes the states of the $(i+1)^{th}$ follower such that $\dot{x}_{i+1} = v_{i+1}$ and $\ddot{x}_{i+1} = a_{i+1}$. Thus, for $i = 0, \ldots, n-1$ and given (7.1), the state-space model for the $(i+1)^{th}$ follower can be presented as

$$\dot{\mathbf{X}}_{i+1} = \mathbf{A}_{i+1}\mathbf{X}_{i+1} + \mathbf{B}_{i+1}u_{i+1} = \begin{bmatrix} 0 & 1 & 0 \\ 0 & 0 & 1 \\ 0 & 0 & -\frac{1}{\tau_{i+1}} \end{bmatrix} \mathbf{X}_{i+1} + \begin{bmatrix} 0 \\ 0 \\ \frac{1}{\tau_{i+1}} \end{bmatrix} u_{i+1} \tag{7.2}$$

7.1.2 Controller and Kinematics Aims

The controller u_{i+1} requires to make the velocities/accelerations of the follower vehicles reach the leader's ones and the distances between adjacent vehicles meet the desired values (d_i^{i+1}). In other words, for $i = 0, \ldots, n-1$, the aim is to have

$$\begin{cases} v_{i+1} = v_0 \\ x_i - x_{i+1} = \omega_i^{i+1} = L_i + d_i^{i+1} \end{cases} \tag{7.3}$$

and to ensure which, we use the following distributed linear feedback control law [89] $(i = 0, \ldots, n-1)$

$$\begin{cases} u_{i+1} = -\sum\limits_{j \in \mathbb{I}_{i+1}} \mathbf{K} \left[x_{i+1} - x_j - d_{i+1,j}; \dot{x}_{i+1} - \dot{x}_j; \ddot{x}_{i+1} - \ddot{x}_j \right] \\ d_{i+1,j} \triangleq -sgn(i+1-j) \sum\limits_{\kappa=\min(i+1,j)}^{\max(i+1,j)-1} \omega_\kappa^{\kappa+1} \end{cases} \tag{7.4}$$

in which $\mathbf{K} \triangleq [k, b, h]$ is the control-gain vector of measurements transmitted from the j^{th} vehicle to the $(i+1)^{th}$ follower. Also, the set $\mathbb{I}_{i+1} \subset (\{0, 1, \ldots, n\} - \{i+1\})$ shows the vehicles from which the $(i+1)^{th}$ follower gets information.

7.1.3 Desired States of the Followers

According to (7.3), for $i = 0, \dots, n-1$, the desired position (x^*_{i+1}), velocity ($\dot{x}^*_{i+1}$) and acceleration ($\ddot{x}^*_{i+1}$) of the $(i+1)^{th}$ follower with respect to the state of the leader vehicle is defined as

$$x^*_{i+1} \triangleq x_0 - \sum_{\kappa=0}^{i} \omega_\kappa^{\kappa+1}, \quad \dot{x}^*_{i+1} = v_0, \quad \ddot{x}^*_{i+1} = 0 \tag{7.5}$$

Therefore, the state error of the $(i+1)^{th}$ follower can be defined as $\tilde{x}_{i+1} \triangleq x_{i+1} - x^*_{i+1}$, utilizing which readily results in $x_{i+1} - x_j = \tilde{x}_{i+1} - \tilde{x}_j + d_{i+1,j}$, and substituting which into the controller (7.4) gives

$$u_{i+1} = -\sum_{j \in \mathbb{I}_{i+1}} \mathbf{K}\left(\tilde{\mathbf{X}}_{i+1} - \tilde{\mathbf{X}}_j\right) = -\sum_{j \in \mathbb{I}_{i+1}} \mathbf{K}\tilde{\mathbf{X}}^j_{i+1} \tag{7.6}$$

in which $\tilde{\mathbf{X}}^j_{i+1} \triangleq \tilde{\mathbf{X}}_{i+1} - \tilde{\mathbf{X}}_j$ where $\tilde{\mathbf{X}}_{i+1} \triangleq \left[\tilde{x}_{i+1}; \dot{\tilde{x}}_{i+1}; \ddot{\tilde{x}}_{i+1}\right]$ and $\tilde{\mathbf{X}}_j \triangleq \left[\tilde{x}_j; \dot{\tilde{x}}_j; \ddot{\tilde{x}}_j\right]$.

7.1.4 State-Space Presentation of the Platoon

Using the facts $\ddot{x}_{i+1} = \ddot{\tilde{x}}_{i+1}$ and $\dddot{x}_{i+1} = \dddot{\tilde{x}}_{i+1}$, and plugging (7.6) in (7.1) yields

$$\dddot{\tilde{x}}_{i+1} = -\frac{1}{\tau_{i+1}}\mathbb{K}_{i+1}\tilde{\mathbf{X}}_{i+1} + \sum_{j \in \mathbb{I}_{i+1}} \frac{1}{\tau_{i+1}}\mathbf{K}\tilde{\mathbf{X}}_j \tag{7.7}$$

in which $\mathbb{K}_{i+1} \triangleq \left[\bar{k}_{i+1}, \bar{b}_{i+1}, \bar{h}_{i+1}\right]$ such that

$$\bar{k}_{i+1} \triangleq |\mathbb{I}_{i+1}|k, \;\; \bar{b}_{i+1} \triangleq |\mathbb{I}_{i+1}|b, \;\; \bar{h}_{i+1} \triangleq 1 + |\mathbb{I}_{i+1}|h \tag{7.8}$$

where $|\mathbb{I}_{i+1}|$ denotes the cardinality of the set $\mathbb{I}_{i+1}$. Now, considering (7.7), knowing $\tilde{x}_0 = \dot{\tilde{x}}_0 = \ddot{\tilde{x}}_0 = 0$, and defining the platoon's total state-error vector by $\tilde{\mathbf{X}}_t \triangleq \left[\tilde{\mathbf{X}}_1; \tilde{\mathbf{X}}_2; \dots, \tilde{\mathbf{X}}_n\right]$, then the platoon's closed-loop dynamics can be presented as the following state-space models. In the case that vehicles are not identical, we have

$$\dot{\tilde{\mathbf{X}}}_t = \tilde{\mathbf{A}}_t\tilde{\mathbf{X}}_t = \begin{bmatrix} \mathbf{A}^*_{11} & \mathbf{A}^*_{12} & \dots & \mathbf{A}^*_{1n} \\ \\ \mathbf{A}^*_{21} & \mathbf{A}^*_{22} & \dots & \mathbf{A}^*_{2n} \\ \vdots & \dots & \ddots & \vdots \\ \mathbf{A}^*_{n1} & \mathbf{A}^*_{n2} & \dots & \mathbf{A}^*_{nn} \end{bmatrix} \tilde{\mathbf{X}}_t \tag{7.9}$$

where $\tilde{\mathbf{A}}_t$ is the overall closed-loop system matrix such that for $i = 0, \ldots, n-1$, we have ($\kappa = i + 1$, $j = 1, \ldots, n$)

$$\begin{cases} \mathbf{A}^*_{\kappa\kappa} \triangleq \mathbf{A}_\kappa - \mathbf{B}_\kappa \mathbf{K}_\kappa \\ \mathbf{A}^*_{\kappa j} \triangleq (z^j_\kappa \otimes \mathbf{I}_3)\mathbf{B}_\kappa \mathbf{K} \end{cases} \tag{7.10}$$

where $\mathbf{K}_\kappa \triangleq |\mathbb{I}_\kappa|\mathbf{K}$, and $\mathbf{A}_\kappa$ and $\mathbf{B}_\kappa$ are according to (7.2). Note that we use $z^j_\kappa = 1$ if the κ^{th} follower receives information from the j^{th} follower, and $z^j_\kappa = 0$ if it does not. Also, $|\mathbb{I}_\kappa|$ denotes the cardinality of the set $\mathbb{I}_\kappa$.

7.1.5 Communication Topologies (CTs)

CTs determine the structure under which vehicles communicate witch each other in the platoon. We split communication topologies into three categories (will be elaborated on later) such that any communication topology can neatly fit in one the following categories.

Typical Unidirectional CTs (UCTs)

In UCTs, all followers receive information only from vehicles ahead. Figs. 7.2 shows typical UCTs, in each of which there is a certain practice in the communication between vehicles. For instance, in Two-Predecessor-Following (TPF) topology, each follower vehicle receives information from two vehicles ahead.

Typical Bidirectional CTs (BCTs)

In BCTs, contrary to the UCTs, all followers also receive information from vehicles behind. Figs. 7.3 shows typical BCTs, in each of which there is a certain pattern in the communication between vehicles. For instance, in Two-Predecessor-Single-Following (TPSF) topology, each follower receives information from two vehicles ahead and one vehicle behind.

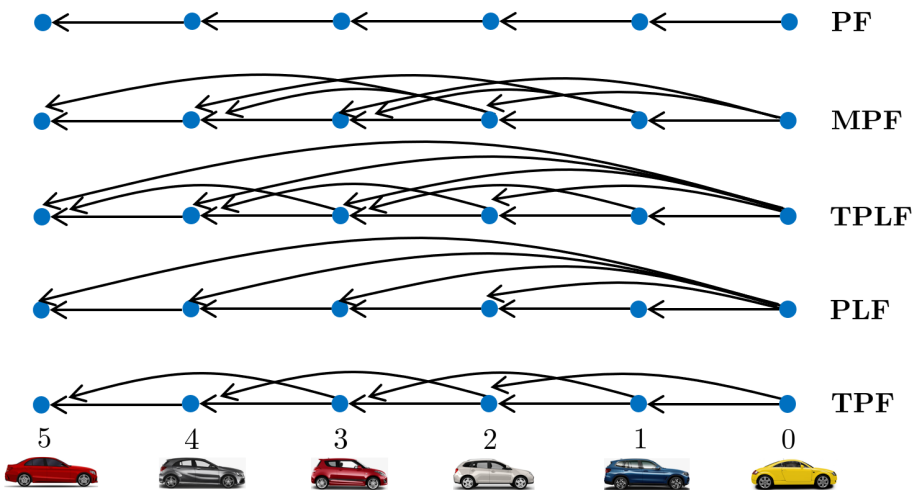

Figure 7.2: Some typical UCTs between vehicles.

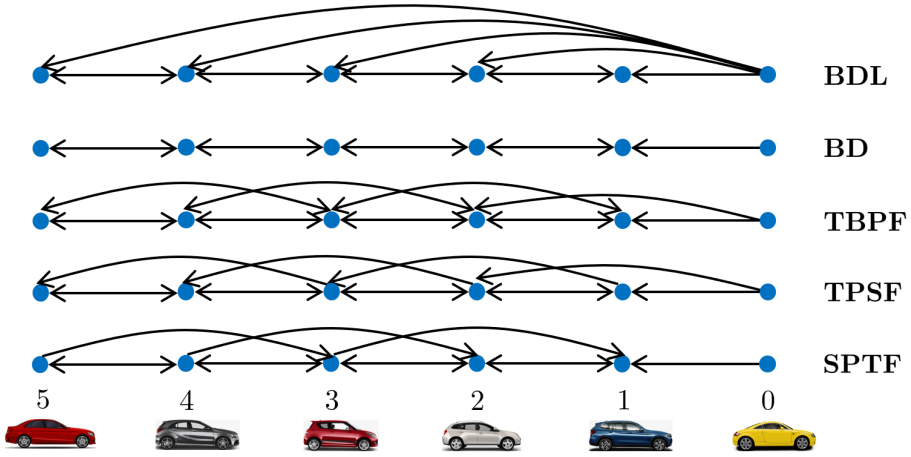

Figure 7.3: Some typical BCTs between vehicles.

Nontypical CTs

In nontypical CTs, there is no specific pattern in the communication between vehicles. Fig. 7.4 depicts some arbitrary nontypical CTs.

Remark 31 *Fig. 7.5 shows the possible connection types between the adjacent vehicles, using which we define the parameter* ζ_i^{i+1} *as needs to be rephrased no longer uzed*

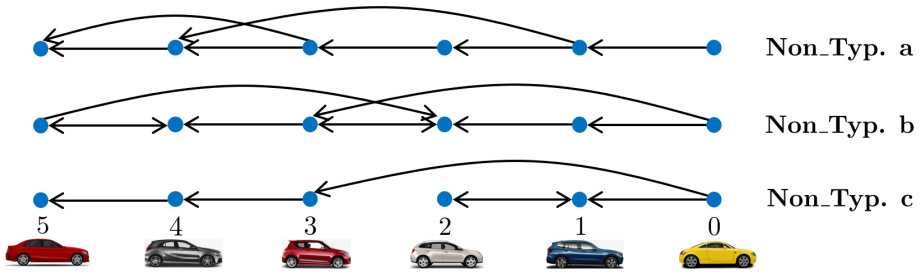

Figure 7.4: Some arbitrary nontypical CTs.

in the formulas

$$\zeta_i^{i+1} = \begin{cases} 0 & \text{if} \quad z_i^{i+1} = 0 \text{ and } z_{i+1}^i = 1 \\ z_i^{i+1} & \text{if} \quad z_i^{i+1} = 1 \text{ and } z_{i+1}^i = 1 \\ 0 & \text{if} \quad z_i^{i+1} = 0 \text{ and } z_{i+1}^i = 0 \\ z_i^{i+1} & \text{if} \quad z_i^{i+1} = 1 \text{ and } z_{i+1}^i = 0 \end{cases} \tag{7.11}$$

in which, for instance, $z_i^{i+1} = 1$ *and* $z_i^{i+1} = 0$ *denote that the* i^{th} *vehicle does/doesn't receive information from the* $(i+1)^{th}$ *vehicle, respectively.*

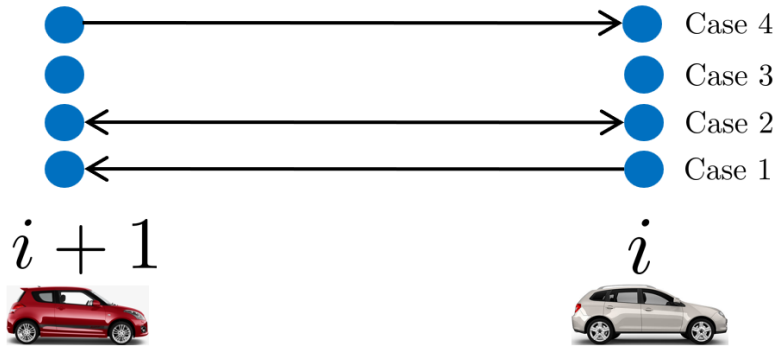

Figure 7.5: Connection types between neighboring vehicles.

Remark 32 *For any CT, for the pair* $(i, i+1)$*, let define the following coupled control gains*

$$\begin{aligned} \bar{k}_i^{i+1} &\triangleq \left(\frac{1}{\tau_{i+1}} |\mathbb{I}_{i+1}^{\leq i}| + \frac{1}{\tau_i} |\mathbb{I}_i^{\geq i+1}| \right) k \\ \bar{b}_i^{i+1} &\triangleq \left(\frac{1}{\tau_{i+1}} |\mathbb{I}_{i+1}^{\leq i}| + \frac{1}{\tau_i} |\mathbb{I}_i^{\geq i+1}| \right) b \\ \bar{h}_i^{i+1} &\triangleq \left(\frac{1}{\tau_{i+1}} |\mathbb{I}_{i+1}^{\leq i}| + \frac{1}{\tau_i} |\mathbb{I}_i^{\geq i+1}| \right) h + \frac{1}{\tau_{i+1}} \end{aligned} \tag{7.12}$$

where the sets $\mathbb{I}_{i+1}^{\leq i}$ *and* $\mathbb{I}_{i}^{\geq i+1}$ *are defined as* $\mathbb{I}_{i+1}^{\leq i} \triangleq \{j | j \in \mathbb{I}_{i+1} \ \& \ j \leq i\}$ *and* $\mathbb{I}_{i}^{\geq i+1} \triangleq \{j | j \in \mathbb{I}_{i} \ \& \ j \geq i+1\}$*, respectively. The notation* $|.|$ *shows the cardinality of the relevant set.*

7.1.6 Internal Stability

Given (7.9), the determinant of the block matrix $s\mathbf{I}_n - \tilde{\mathbf{A}}_t$ offers the characteristic polynomial of the platoon, roots of which are the eigenvalues of the system matrix $\tilde{\mathbf{A}}_t$. Note that $\mathbf{I}_n$ is the identity matrix of size n, and the closed-loop system would be stable if and only if eigenvalues of $\tilde{\mathbf{A}}_t$ are all negative.

7.2 Coupled Dynamics Between Neighboring Vehicles

To find the novel dynamic model (DM), which we name it distance dynamic model (DDM), first we split the platoon into successive pairs of neighboring vehicles, i.e., pairs $(0,1)$, $(1,2)$, $\ldots$, $(n-1,n)$, and extract coupled dynamics between the adjacent vehicles. For $i = 0, \ldots, n-1$, let the position, velocity, acceleration, and jerk errors between neighboring vehicles defined as $\tilde{p}_i^{i+1} \triangleq \tilde{x}_i - \tilde{x}_{i+1}$, $\tilde{v}_i^{i+1} \triangleq \dot{\tilde{x}}_i - \dot{\tilde{x}}_{i+1}$, $\tilde{a}_i^{i+1} \triangleq \ddot{\tilde{x}}_i - \ddot{\tilde{x}}_{i+1}$, and $\tilde{\mathfrak{J}}_i^{i+1} \triangleq \dddot{\tilde{x}}_i - \dddot{\tilde{x}}_{i+1}$, respectively. Thus, it is possible to define the state error between neighboring vehicles as

$$\begin{aligned} \tilde{\mathbf{X}}_i^{i+1} &\triangleq \tilde{\mathbf{X}}_i - \tilde{\mathbf{X}}_{i+1} \triangleq \left[\tilde{p}_i^{i+1}; \tilde{v}_i^{i+1}; \tilde{a}_i^{i+1}\right] \\ \dot{\tilde{\mathbf{X}}}_i^{i+1} &\triangleq \dot{\tilde{\mathbf{X}}}_i - \dot{\tilde{\mathbf{X}}}_{i+1} \triangleq \left[\tilde{v}_i^{i+1}; \tilde{a}_i^{i+1}; \tilde{\mathfrak{J}}_i^{i+1}\right] \end{aligned} \tag{7.13}$$

Note that, from now on, we will refer to $\tilde{p}_i^{i+1}(.)$, $\tilde{v}_i^{i+1}(.)$, $\tilde{a}_i^{i+1}(.)$ (in time-domain or Laplace-domain) as intervehicle distance error, velocity error, and acceleration error between vehicles i and $i+1$, respectively. Furthermore, for $j \in \{i, i+1\}$ and having $0 < \Delta t \ll 1$ as a quite small sampling-time, we will have $\tilde{\mathbf{X}}_j(t + \Delta t) = \tilde{\mathbf{X}}_j(t) + \Delta t \dot{\tilde{\mathbf{X}}}_j(t)$, using which and (4.13), it is obvious that

$$\lim_{\Delta t \to 0} \frac{\tilde{\mathbf{X}}_i^{i+1}(t + \Delta t) - \tilde{\mathbf{X}}_i^{i+1}(t)}{\Delta t} = \dot{\tilde{\mathbf{X}}}_i^{i+1}(t) \tag{7.14}$$

Theorem 33 *Given* (7.13) *and Remarks 31-32, defining* $\tilde{y}_i^{i+1} \triangleq \tilde{a}_i^{i+1}$, *for* $i = 0, \ldots, n-1$, *the state-space presentation of the coupled dynamics between the adjacent and heterogeneous vehicles* i *and* $i+1$ *within any CT is according to*

$$\dot{\tilde{\mathbf{X}}}_i^{i+1} = \underbrace{\begin{bmatrix} 0 & 1 & 0 \\ 0 & 0 & 1 \\ -\bar{k}_i^{i+1} & -\bar{b}_i^{i+1} & -\bar{h}_i^{i+1} \end{bmatrix}}_{\triangleq \mathbf{A}_i^{i+1}} \tilde{\mathbf{X}}_i^{i+1} + \underbrace{\begin{bmatrix} 0 \\ 0 \\ 1 \end{bmatrix}}_{\triangleq \mathbf{B}_i^{i+1}} \tilde{u}_i^{i+1} \tag{7.15}$$

in which $\tilde{u}_i^{i+1}$ *is according to*

$$\begin{aligned} \tilde{u}_i^{i+1} = & \frac{1}{\tau_i} \sum_{j \in \mathbb{R}_i^{<i}} \sum_{\kappa=j}^{i-1} \mathbf{K} \tilde{\mathbf{X}}_\kappa^{\kappa+1} - \frac{1}{\tau_i} \sum_{j \in \mathbb{R}_i^{>i+1}} \sum_{\kappa=i+1}^{j-1} \mathbf{K} \tilde{\mathbf{X}}_\kappa^{\kappa+1} \\ & + \frac{1}{\tau_{i+1}} \sum_{j \in \mathbb{R}_{i+1}^{>i+1}} \sum_{\kappa=i+1}^{j-1} \mathbf{K} \tilde{\mathbf{X}}_\kappa^{\kappa+1} - \frac{1}{\tau_{i+1}} \sum_{j \in \mathbb{R}_{i+1}^{<i}} \sum_{\kappa=j}^{i-1} \mathbf{K} \tilde{\mathbf{X}}_\kappa^{\kappa+1} - \frac{1}{\tau_i} \boldsymbol{\tau}_i^{i+1} \sum_{\kappa=0}^{i-1} \tilde{\mathbf{X}}_\kappa^{\kappa+1} \end{aligned} \tag{7.16}$$

where $\boldsymbol{\tau}_i^{i+1} = \left[0, 0, \frac{\tau_i - \tau_{i+1}}{\tau_{i+1}}\right]$, *and for the pair* $(i, i+1) = (0, 1)$, $\mathbb{R}_i^{<i} = \mathbb{R}_i^{>i+1} = \mathbb{R}_{i+1}^{<i} = \emptyset$ *in which* $\emptyset$ *denotes the empty set.*

Proof. First, let define $\tilde{\mathbf{X}}_j^i \triangleq \tilde{\mathbf{X}}_j - \tilde{\mathbf{X}}_i$ and $\tilde{\mathbf{X}}_{i+1}^j \triangleq \tilde{\mathbf{X}}_{i+1} - \tilde{\mathbf{X}}_j$. Now, for $i = 1, \ldots, n-1$ and using (7.7), we have

$$\begin{cases} \dddot{\tilde{x}}_i = -\frac{1}{\tau_i} \mathbb{K}_i \tilde{\mathbf{X}}_i + \frac{1}{\tau_i} \sum_{j \in \mathbb{I}_i} \mathbf{K} \tilde{\mathbf{X}}_j \\ \dddot{\tilde{x}}_{i+1} = -\frac{1}{\tau_{i+1}} \mathbb{K}_{i+1} \tilde{\mathbf{X}}_{i+1} + \frac{1}{\tau_{i+1}} \sum_{j \in \mathbb{I}_{i+1}} \mathbf{K} \tilde{\mathbf{X}}_j \end{cases} \tag{7.17}$$

Therefore, for $\tilde{\mathbb{J}}_i^{i+1} \triangleq \dddot{\tilde{x}}_i - \dddot{\tilde{x}}_{i+1}$, we get

$$\tilde{\mathbb{J}}_i^{i+1} = -\frac{1}{\tau_i} \mathbb{K}_i \tilde{\mathbf{X}}_i^{i+1} - \left(\frac{1}{\tau_i} \mathbb{K}_i - \frac{1}{\tau_{i+1}} \mathbb{K}_{i+1}\right) \tilde{\mathbf{X}}_{i+1} + \sum_{j \in \mathbb{I}_i} \frac{1}{\tau_i} \mathbf{K} \tilde{\mathbf{X}}_j - \sum_{j \in \mathbb{I}_{i+1}} \frac{1}{\tau_{i+1}} \mathbf{K} \tilde{\mathbf{X}}_j \tag{7.18}$$

Since $-\left(\frac{\mathbb{K}_i}{\tau_i} - \frac{\mathbb{K}_{i+1}}{\tau_{i+1}}\right) = \frac{\boldsymbol{\tau}_i^{i+1}}{\tau_i} + \sum_{j \in \mathbb{I}_{i+1}} \frac{\mathbf{K}}{\tau_{i+1}} - \sum_{j \in \mathbb{I}_i} \frac{\mathbf{K}}{\tau_i}$, then (7.18) can be rewritten as

$$\tilde{\mathbb{J}}_i^{i+1} = -\frac{1}{\tau_i} \left(\mathbb{K}_i + \boldsymbol{\tau}_i^{i+1}\right) \tilde{\mathbf{X}}_i^{i+1} + \sum_{j \in \mathbb{I}_i} \frac{1}{\tau_i} \mathbf{K} \tilde{\mathbf{X}}_j^{i+1} - \sum_{j \in \mathbb{I}_{i+1}} \frac{1}{\tau_{i+1}} \mathbf{K} \tilde{\mathbf{X}}_j^{i+1} - \frac{1}{\tau_i} \boldsymbol{\tau}_i^{i+1} \sum_{\kappa=0}^{i-1} \tilde{\mathbf{X}}_\kappa^{\kappa+1} \tag{7.19}$$

which obtained using the fact that $\tilde{\mathbf{X}}_0 = [0;0;0]$. Thus

$$\frac{\boldsymbol{\tau}_i^{i+1}}{\tau_i}\tilde{\mathbf{X}}_{i+1} = -\frac{\boldsymbol{\tau}_i^{i+1}}{\tau_i}\left(\tilde{\mathbf{X}}_0 - \tilde{\mathbf{X}}_{i+1}\right) = -\frac{\boldsymbol{\tau}_i^{i+1}}{\tau_i}\sum_{j=0}^{i}\tilde{\mathbf{X}}_j^{j+1} \tag{7.20}$$

Now, having $\tilde{\mathbf{X}}_j - \tilde{\mathbf{X}}_{i+1} = \tilde{\mathbf{X}}_j - \tilde{\mathbf{X}}_i + \tilde{\mathbf{X}}_i - \tilde{\mathbf{X}}_{i+1}$, (7.19) becomes

$$\tilde{\mathbb{J}}_i^{i+1} = -\left(\bar{\boldsymbol{\tau}}_i^{i+1} + \frac{|\mathbb{I}_{i+1}|}{\tau_{i+1}}\mathbf{K}\right)\tilde{\mathbf{X}}_i^{i+1} + \sum_{j\in\mathbb{I}_i}\frac{1}{\tau_i}\mathbf{K}\tilde{\mathbf{X}}_j^i - \sum_{j\in\mathbb{I}_{i+1}}\frac{1}{\tau_{i+1}}\mathbf{K}\tilde{\mathbf{X}}_j^i - \frac{1}{\tau_i}\boldsymbol{\tau}_i^{i+1}\sum_{\kappa=0}^{i-1}\tilde{\mathbf{X}}_\kappa^{\kappa+1} \tag{7.21}$$

in which $\bar{\boldsymbol{\tau}}_i^{i+1} = \left[0, 0, \frac{1}{\tau_{i+1}}\right]$. Note that $\bar{\boldsymbol{\tau}}_i^{i+1} + \frac{|\mathbb{I}_{i+1}|}{\tau_{i+1}}\mathbf{K} = \frac{1}{\tau_{i+1}}\mathbb{K}_{i+1}$ (see (7.8)). Now, depending on how the connection is between the neighboring vehicles i and $i+1$ (see Remark 31), (7.21) can be reformulated as

$$\tilde{\mathbb{J}}_i^{i+1} = -\frac{1}{\tau_{i+1}}\left(\mathbb{K}_{i+1} + \frac{\zeta_i^{i+1}\tau_{i+1}}{\tau_i}\mathbf{K}\right)\tilde{\mathbf{X}}_i^{i+1} + \sum_{j\in\mathbb{R}_i}\frac{1}{\tau_i}\mathbf{K}\tilde{\mathbf{X}}_j^i - \sum_{j\in\mathbb{R}_{i+1}}\frac{1}{\tau_{i+1}}\mathbf{K}\tilde{\mathbf{X}}_j^i - \frac{1}{\tau_i}\boldsymbol{\tau}_i^{i+1}\sum_{\kappa=0}^{i-1}\tilde{\mathbf{X}}_\kappa^{\kappa+1} \tag{7.22}$$

Splitting $j \in \mathbb{R}_i$ and $j \in \mathbb{R}_{i+1}$ in parts $j < i$ and $j > i+1$, and using the fact that for part $j > i+1$, we have $\mathbf{X}_j - \tilde{\mathbf{X}}_i = \mathbf{X}_j - \tilde{\mathbf{X}}_{i+1} - \left(\tilde{\mathbf{X}}_i - \tilde{\mathbf{X}}_{i+1}\right)$, then (7.22) can be reformulated as

$$\begin{aligned}\tilde{\mathbb{J}}_i^{i+1} = &\underbrace{\left(-\frac{1}{\tau_{i+1}}\mathbb{K}_{i+1} - \frac{z_i^{i+1}}{\tau_i}\mathbf{K} - \frac{1}{\tau_i}\sum_{j\in\mathbb{R}_i^{>i+1}}\mathbf{K} + \frac{1}{\tau_{i+1}}\sum_{j\in\mathbb{R}_{i+1}^{>i+1}}\mathbf{K}\right)}_{\triangleq\mathbf{A}_{i,i+1}^{31}}\tilde{\mathbf{X}}_i^{i+1} \\ &+ \sum_{j\in\mathbb{R}_i^{<i}}\frac{1}{\tau_i}\mathbf{K}\tilde{\mathbf{X}}_j^i - \sum_{j\in\mathbb{R}_{i+1}^{<i}}\frac{1}{\tau_{i+1}}\mathbf{K}\tilde{\mathbf{X}}_j^i + \sum_{j\in\mathbb{R}_{i+1}^{>i+1}}\frac{1}{\tau_{i+1}}\mathbf{K}\tilde{\mathbf{X}}_{i+1}^j \\ &- \sum_{j\in\mathbb{R}_i^{>i+1}}\frac{1}{\tau_i}\mathbf{K}\tilde{\mathbf{X}}_{i+1}^j - \frac{1}{\tau_i}\boldsymbol{\tau}_i^{i+1}\sum_{\kappa=0}^{i-1}\tilde{\mathbf{X}}_\kappa^{\kappa+1}\end{aligned} \tag{7.23}$$

in which $\mathbf{A}_{i,i+1}^{31}$ is equivalent to

$$\mathbf{A}_{i,i+1}^{31} = -\frac{1}{\tau_{i+1}}\mathbb{K}_{i+1}^{j\leq i} - \frac{1}{\tau_i}\mathbf{K}_i^{j\geq i+1} = -\left[\bar{k}_i^{i+1}, \bar{b}_i^{i+1}, \bar{h}_i^{i+1}\right] \tag{7.24}$$

Now using the fact that $\tilde{\mathbf{X}}_j^i$ and $\tilde{\mathbf{X}}_{i+1}^j$ can be rewritten in the following form:

$$\begin{cases}\tilde{\mathbf{X}}_j^i = \sum_{\kappa=j}^{i-1}\tilde{\mathbf{X}}_\kappa^{\kappa+1}; j < i \\ \tilde{\mathbf{X}}_{i+1}^j = \sum_{\kappa=i+1}^{j-1}\tilde{\mathbf{X}}_\kappa^{\kappa+1}; j > i+1\end{cases} \tag{7.25}$$

then (7.23) becomes

$$\begin{aligned}\tilde{\mathfrak{J}}_i^{i+1} &= \left(-\frac{1}{\tau_{i+1}}\mathbb{K}_{i+1}^{j\leq i} - \frac{1}{\tau_i}\mathbf{K}_i^{j\geq i+1}\right)\tilde{\mathbf{X}}_i^{i+1} - \frac{1}{\tau_i}\boldsymbol{\tau}_i^{i+1}\sum_{\kappa=0}^{i-1}\tilde{\mathbf{X}}_\kappa^{\kappa+1} \\ &+ \frac{1}{\tau_i}\sum_{j\in\mathbb{R}_i^{<i}}\sum_{\kappa=j}^{i-1}\mathbf{K}\tilde{\mathbf{X}}_\kappa^{\kappa+1} - \frac{1}{\tau_i}\sum_{j\in\mathbb{R}_i^{>i+1}}\sum_{\kappa=i+1}^{j-1}\mathbf{K}\tilde{\mathbf{X}}_\kappa^{\kappa+1} \\ &+ \frac{1}{\tau_{i+1}}\sum_{j\in\mathbb{R}_{i+1}^{>i+1}}\sum_{\kappa=i+1}^{j-1}\mathbf{K}\tilde{\mathbf{X}}_\kappa^{\kappa+1} - \frac{1}{\tau_{i+1}}\sum_{j\in\mathbb{R}_{i+1}^{<i}}\sum_{\kappa=j}^{i-1}\mathbf{K}\tilde{\mathbf{X}}_\kappa^{\kappa+1}\end{aligned} \tag{7.26}$$

Now, let us study for $i = 0$ or to be exact for the pair $(0, 1)$. Given that $\tilde{\mathbf{X}}_0 = 0$, using (7.17) yields

$$\begin{aligned}\tilde{\mathfrak{J}}_i^{i+1} &= \frac{1}{\tau_{i+1}}\mathbb{K}_{i+1}\tilde{\mathbf{X}}_{i+1} - \frac{1}{\tau_{i+1}}\sum_{j\in\mathbb{R}_{i+1}}\mathbf{K}\tilde{\mathbf{X}}_j \\ &= -\frac{1}{\tau_{i+1}}\mathbb{K}_{i+1}\tilde{\mathbf{X}}_i^{i+1} + \frac{1}{\tau_{i+1}}\sum_{j\in\mathbb{R}_{i+1}}\mathbf{K}\left(\tilde{\mathbf{X}}_i^{i+1} + \tilde{\mathbf{X}}_{i+1}^{j}\right) \\ &= -\frac{1}{\tau_{i+1}}\mathbb{K}_{i+1}^{j\leq i}\tilde{\mathbf{X}}_i^{i+1} + \frac{1}{\tau_{i+1}}\sum_{j\in\mathbb{R}_{i+1}^{>i+1}}\mathbf{K}\tilde{\mathbf{X}}_{i+1}^{j}\end{aligned} \tag{7.27}$$

which given (7.25) and the fact that the leader does not receive any information, then (7.27) can be rewritten as

$$\tilde{\mathfrak{J}}_i^{i+1} = -\frac{1}{\tau_{i+1}}\mathbb{K}_{i+1}^{j\leq i}\tilde{\mathbf{X}}_i^{i+1} + \frac{1}{\tau_{i+1}}\sum_{j\in\mathbb{R}_{i+1}^{>i+1}}\sum_{\kappa=i+1}^{j-1}\mathbf{K}\tilde{\mathbf{X}}_\kappa^{\kappa+1} \tag{7.28}$$

Now, for the pair $(0, 1)$, since the sets $\mathbb{R}_i^{<i}$, $\mathbb{R}_i^{>i+1}$, and $\mathbb{R}_{i+1}^{<i}$ are all empty sets, and the leader does not receive any information, then (7.26) is valid for the pair $(0, 1)$ as well, and is equal to (7.28). Therefore, using (7.26), noting that $d/dt\{\tilde{p}_i^{i+1}\} = \tilde{v}_i^{i+1}$, $d/dt\{\tilde{v}_i^{i+1}\} = \tilde{a}_i^{i+1}$, and $\tilde{y}_i^{i+1} = \tilde{a}_i^{i+1}$, the state-space presentation (7.15) holds true. Thus, the proof completed. ■

Remark 34 *It is crucial, obvious and worth emphasizing that in* (7.15)*,* $\tilde{u}_i^{i+1}$ *is totally independent of* $\tilde{\mathbf{X}}_i^{i+1}$*. In other words, in* (7.16)*, always we have* $\kappa \neq i$*.*

Remark 35 *Let initial values of the coupled-dynamics states, associated with positions, velocities and accelerations of the adjacent vehicles* i *and* $i + 1$*, be defined as*

ϱ_i^{i+1}, ν_i^{i+1}, *and* φ_i^{i+1}, *respectively, such that* $\varrho_i^{i+1} \triangleq \tilde{p}_i^{i+1}(0)$, $\nu_i^{i+1} \triangleq \tilde{v}_i^{i+1}(0)$ *and* $\varphi_i^{i+1} \triangleq \tilde{a}_i^{i+1}(0)$ *and accordingly the initial state vector is defined as* $\boldsymbol{\Xi}_i^{i+1} \triangleq [\varrho_i^{i+1}; \nu_i^{i+1}; \varphi_i^{i+1}]$. *Therefore, for* $i = 0, \ldots, n-1$, *in Laplacian domain, we have*

$$\tilde{\mathbf{X}}_i^{i+1}(s) = \underbrace{\begin{bmatrix} \frac{1}{s^2} \\ \frac{1}{s} \\ 1 \end{bmatrix}}_{\triangleq \mathbf{T}_1} \tilde{a}_i^{i+1}(s) + \underbrace{\begin{bmatrix} \frac{1}{s} & \frac{1}{s^2} & 0 \\ 0 & \frac{1}{s} & 0 \\ 0 & 0 & 0 \end{bmatrix}}_{\triangleq \mathbf{T}_2} \boldsymbol{\Xi}_i^{i+1} \tag{7.29}$$

using which (7.16) *can be explored in Laplacian domain as*

$$\tilde{u}_i^{i+1}(s) = \mathbf{K}\mathbf{T}_1 \Pi_i^{i+1}(s) - \frac{1}{\tau_i} \boldsymbol{\tau}_i^{i+1} \mathbf{T}_1 \mathcal{M}_i^{i+1}(s) + \frac{\Theta_i^{i+1} s + \Gamma_i^{i+1}}{s} \tag{7.30}$$

where $\mathcal{M}_i^{i+1}(s) = \sum_{\kappa=0}^{i-1} \tilde{a}_\kappa^{\kappa+1}(s)$ *and*

$$\begin{aligned} \Pi_i^{i+1}(s) \triangleq & \frac{1}{\tau_i} \left[\sum_{j \in \mathbb{R}_i^{<i}} \sum_{\kappa=j}^{i-1} \tilde{a}_\kappa^{\kappa+1}(s) - \sum_{j \in \mathbb{R}_i^{>i+1}} \sum_{\kappa=i+1}^{j-1} \tilde{a}_\kappa^{\kappa+1}(s) \right] \\ & + \frac{1}{\tau_{i+1}} \left[\sum_{j \in \mathbb{R}_{i+1}^{>i+1}} \sum_{\kappa=i+1}^{j-1} \tilde{a}_\kappa^{\kappa+1}(s) - \sum_{j \in \mathbb{R}_{i+1}^{<i}} \sum_{\kappa=j}^{i-1} \tilde{a}_\kappa^{\kappa+1}(s) \right] \end{aligned} \tag{7.31}$$

Also, $\Theta_i^{i+1} = k\varrho_t^{i,i+1} + b\nu_t^{i,i+1}$ *and* $\Gamma_i^{i+1} = k\nu_t^{i,i+1}$ *in which*

$$\begin{cases} \varrho_t^{i,i+1} \triangleq \frac{1}{\tau_i} \left[\sum_{j \in \mathbb{R}_i^{<i}} \sum_{\kappa=j}^{i-1} \varrho_\kappa^{\kappa+1} - \sum_{j \in \mathbb{R}_i^{>i+1}} \sum_{\kappa=i+1}^{j-1} \varrho_\kappa^{\kappa+1} \right] \\ \qquad + \frac{1}{\tau_{i+1}} \left[\sum_{j \in \mathbb{R}_{i+1}^{>i+1}} \sum_{\kappa=i+1}^{j-1} \varrho_\kappa^{\kappa+1} - \sum_{j \in \mathbb{R}_{i+1}^{<i}} \sum_{\kappa=j}^{i-1} \varrho_\kappa^{\kappa+1} \right] \\ \nu_t^{i,i+1} \triangleq \frac{1}{\tau_i} \left[\sum_{j \in \mathbb{R}_i^{<i}} \sum_{\kappa=j}^{i-1} \nu_\kappa^{\kappa+1} - \sum_{j \in \mathbb{R}_i^{>i+1}} \sum_{\kappa=i+1}^{j-1} \nu_\kappa^{\kappa+1} \right] \\ \qquad + \frac{1}{\tau_{i+1}} \left[\sum_{j \in \mathbb{R}_{i+1}^{>i+1}} \sum_{\kappa=i+1}^{j-1} \nu_\kappa^{\kappa+1} - \sum_{j \in \mathbb{R}_{i+1}^{<i}} \sum_{\kappa=j}^{i-1} \nu_\kappa^{\kappa+1} \right] \end{cases} \tag{7.32}$$

It is worth reminding that, for the pair $(i, i+1) = (0, 1)$, $\mathbb{R}_i^{<i} = \mathbb{R}_i^{>i+1} = \mathbb{R}_{i+1}^{<i} = \emptyset$ *in which* $\emptyset$ *denotes the empty set.*

Remark 36 *Given Remark 35, it is worth noting that* $\Psi_i^{i+1}(s)$ *is shown up in* (7.30) *as a consequence of the heterogeneity of the neighboring vehicles* i *and* $i+1$*. Furthermore, the scalar values* Θ_i^{i+1} *and* Γ_i^{i+1} *are because of initial state differences between adjacent vehicles of those other than the the pair* $(i, i+1)$*, see* (7.32) *where* $\kappa \neq i$*.*

Remark 37 *Given* (7.15)*, the transfer function, let be denoted by* $\mathcal{G}_i^{i+1}(s)$*, between the input and output of the coupled dynamics would be*

$$\mathcal{G}_i^{i+1}(s) = \mathbf{C}_i^{i+1}\left(s\mathbf{I}_3 - \mathbf{A}_i^{i+1}\right)^{-1}\mathbf{B}_i^{i+1} = s^2\Upsilon_i^{i+1}(s) \tag{7.33}$$

where $\Upsilon_i^{i+1}(s) \triangleq \left(s^3 + \bar{h}_i^{i+1}s^2 + \bar{b}_i^{i+1}s + \bar{k}_i^{i+1}\right)^{-1}$*.*

Theorem 38 *Given Remark 35, the coupled intervehicle acceleration;* $\tilde{a}_i^{i+1}(s)$*, velocity;* $\tilde{v}_i^{i+1}(s)$*, and distance;* $\tilde{p}_i^{i+1}(s)$*, between the adjacent vehicles* i *and* $i+1$ *are according to*

$$\tilde{a}_i^{i+1}(s) = \underbrace{\mathbf{K}\mathbf{T}_1\Pi_i^{i+1}(s)\mathcal{G}_i^{i+1}(s)}_{\text{out of the coupled states of the other pairs}} \underbrace{-\frac{1}{\tau_i}\boldsymbol{\tau}_i^{i+1}\mathbf{T}_1\mathcal{M}_i^{i+1}(s)\mathcal{G}_i^{i+1}(s)}_{\text{out of the heterogeneity of the pair } (i,i+1)} \underbrace{+\mathcal{H}_{i,i+1}^a(s)\Upsilon_i^{i+1}(s)}_{\text{out of the initial conditions including the pair } (i,i+1)} \tag{7.34}$$

$\tilde{v}_i^{i+1}(s) = \frac{1}{s}\left(\tilde{a}_i^{i+1}(s) + \nu_i^{i+1}\right)$*, and* $\tilde{p}_i^{i+1}(s) = \frac{1}{s}\left(\tilde{v}_i^{i+1}(s) + \varrho_i^{i+1}\right)$*, respectively, where* $\mathcal{H}_{i,i+1}^a(s) \triangleq \Lambda_{2,a}^{i,i+1}s^2 + \Lambda_{1,a}^{i,i+1}s + \Lambda_{0,a}^{i,i+1}$ *such that the scalar values* $\Lambda_{2,a}^{i,i+1}$*,* $\Lambda_{1,a}^{i,i+1}$*, and* $\Lambda_{0,a}^{i,i+1}$ *are*

$$\begin{cases} \Lambda_2^{i,i+1} \triangleq \varphi_i^{i+1} \\ \Lambda_1^{i,i+1} \triangleq \Theta_i^{i+1} - \varrho_i^{i+1}\bar{k}_i^{i+1} - \nu_i^{i+1}\bar{b}_i^{i+1} \\ \Lambda_0^{i,i+1} \triangleq \Gamma_i^{i+1} - \nu_i^{i+1}\bar{k}_i^{i+1} \end{cases} \tag{7.35}$$

Proof. Defining $\tilde{y}_i^{i+1} \triangleq \tilde{a}_i^{i+1}$ as the output of the coupled dynamics (7.15), we have $\tilde{y}_i^{i+1} = \mathbf{C}_i^{i+1}\tilde{\mathbf{X}}_i^{i+1}$ such that $\mathbf{C}_i^{i+1} \triangleq [0, 0, 1]$. Therefore, $\tilde{a}_i^{i+1}(s)$, for $i = 0, \ldots, n-1$, would be the summation of zero-state ($\boldsymbol{\Xi}_i^{i+1} = [0; 0; 0]$) response and zero-input ($\tilde{u}_i^{i+1} = 0$) response. As such, given (7.15), the zero-input response, let be denoted as $\tilde{a}_{i,zi}^{i+1}(s)$, is according to

$$\tilde{a}_{i,zi}^{i+1}(s) = \mathbf{C}_i^{i+1}\left(s\mathbf{I}_3 - \mathbf{A}_i^{i+1}\right)^{-1}\boldsymbol{\Xi}_i^{i+1} = \mathbf{K}_{i,i+1}^{ini}\mathbf{T}_1\mathcal{G}_i^{i+1}(s) \tag{7.36}$$

where $\mathbf{K}_{i,i+1}^{ini} \triangleq \left[-\nu_i^{i+1}\bar{k}_i^{i+1}, -\varrho_i^{i+1}\bar{k}_i^{i+1} - \nu_i^{i+1}\bar{b}_i^{i+1}, \varphi_i^{i+1}\right]$, and $\mathbf{I}_3$ is the identity matrix of size 3. Also, given (7.33), the zero-state response, let be denoted by $\tilde{a}_{i,zs}^{i+1}(s)$, would be $\tilde{a}_{i,zs}^{i+1}(s) = \mathcal{G}_i^{i+1}(s)\tilde{u}_i^{i+1}(s)$ which considering (7.30) and (7.33), it is obtained as

$$\tilde{a}_{i,zs}^{i+1}(s) = \mathbf{K}\mathbf{T}_1\Pi_i^{i+1}(s)\mathcal{G}_i^{i+1}(s) - \frac{1}{\tau_i}\boldsymbol{\tau}_i^{i+1}\mathbf{T}_1\mathcal{M}_i^{i+1}(s)\mathcal{G}_i^{i+1}(s) + s\left(\Theta_i^{i+1}s + \Gamma_i^{i+1}\right)\Upsilon_i^{i+1}(s) \tag{7.37}$$

Now, since $\tilde{a}_i^{i+1}(s) = \tilde{a}_{i,zi}^{i+1}(s) + \tilde{a}_{i,zs}^{i+1}(s)$, using (7.36) and (7.37), and noting that $\mathcal{G}_i^{i+1}(s) = s^2\Upsilon_i^{i+1}(s)$ results in (7.34). Therefore, the proof completed. ■

Remark 39 *Defining* $\Psi_{i,i+1}^a(s) \triangleq \mathcal{H}_{i,i+1}^a(s)\Upsilon_i^{i+1}(s)$ *and calculating* (7.34) *for* $i = 0, \ldots, n-1$ *and stacking them together, a mapping between initial conditions and coupled intervehicle accelerations can be found as follows.*

$$\tilde{\mathbf{a}}(s) = \mathbf{Q}^{-1}(s)\boldsymbol{\Psi}_a(s) \tag{7.38}$$

where $\boldsymbol{\Psi}_a(s) \triangleq \left[\Psi_{0,1}^a(s); \Psi_{1,2}^a(s); \ldots; \Psi_{n-1,n}^a(s)\right]$, $\tilde{\mathbf{a}}(s) \triangleq \left[\tilde{a}_0^1(s); \tilde{a}_1^2(s); \ldots; \tilde{a}_{n-1}^n(s)\right]$, *and* $\mathbf{Q}(s) \in \mathbb{C}^{n\times n}$ *whose elements are based on* $(j, \kappa = 1, \ldots, n)$

$$Q_{j\kappa}(s) = \begin{cases} -\mathbf{K}_{j-1,j}^{\kappa-}\mathbf{T}_1\mathcal{G}_{j-1}^j(s) & if \quad j > \kappa \\ 1 & if \quad j = \kappa \\ -\mathbf{K}_{j-1,j}^{\kappa+}\mathbf{T}_1\mathcal{G}_{j-1}^j(s) & if \quad j < \kappa \end{cases} \tag{7.39}$$

in which

$$\begin{cases} \mathbf{K}_{j-1,j}^{\kappa-} \triangleq \dfrac{1}{\tau_{j-1}}|\mathbb{R}_{\bar{j}-1}^{\leq\kappa-1}|\mathbf{K} - \dfrac{1}{\tau_j}|\mathbb{R}_{\bar{j}}^{\leq\kappa-1}|\mathbf{K} - \dfrac{1}{\tau_{j-1}}\boldsymbol{\tau}_{j-1}^j \\ \mathbf{K}_{j-1,j}^{\kappa+} \triangleq \dfrac{1}{\tau_j}|\mathbb{R}_{\bar{j}}^{\geq\kappa}|\mathbf{K} - \dfrac{1}{\tau_{j-1}}|\mathbb{R}_{\bar{j}-1}^{\geq\kappa}|\mathbf{K} \end{cases} \tag{7.40}$$

where $\mathbb{R}_{\bar{j}-1}^{\leq\kappa-1} \triangleq \{\epsilon|\epsilon \in \mathbb{R}_{j-1} \ \& \ \epsilon \leq \kappa - 1\}$, $\mathbb{R}_{\bar{j}}^{\leq\kappa-1} \triangleq \{\epsilon|\epsilon \in \mathbb{R}_j \ \& \ \epsilon \leq \kappa - 1\}$, $\mathbb{R}_{\bar{j}}^{\geq\kappa} \triangleq \{\epsilon|\epsilon \in \mathbb{R}_j \ \& \ \epsilon \geq \kappa\}$, *and* $\mathbb{R}_{\bar{j}-1}^{\geq\kappa} \triangleq \{\epsilon|\epsilon \in \mathbb{R}_{j-1} \ \& \ \epsilon \geq \kappa\}$.

Remark 40 *Given* (7.38) *and noting that for* $i = 0, \ldots, n-1$ *we have* $\tilde{v}_i^{i+1}(s) = \frac{1}{s}\left(\tilde{a}_i^{i+1}(s) + \nu_i^{i+1}\right)$ *and* $\tilde{p}_i^{i+1}(s) = \frac{1}{s}\left(\tilde{v}_i^{i+1}(s) + \varrho_i^{i+1}\right)$, *yields*

$$\begin{cases} \tilde{\mathbf{v}}(s) = \dfrac{1}{s}(\tilde{\mathbf{a}}(s) + \boldsymbol{\nu}) \\ \tilde{\mathbf{p}}(s) = \dfrac{1}{s}(\tilde{\mathbf{v}}(s) + \boldsymbol{\varrho}) = \dfrac{1}{s^2}\tilde{\mathbf{a}}(s) + \dfrac{1}{s^2}\boldsymbol{\nu} + \dfrac{1}{s}\boldsymbol{\varrho} \end{cases} \tag{7.41}$$

where $\tilde{\mathbf{v}}(s) \triangleq \left[\tilde{v}_0^1(s); \tilde{v}_1^2(s); \ldots; \tilde{v}_{n-1}^n(s)\right]$, $\boldsymbol{\nu} \triangleq \left[\nu_0^1; \nu_1^2; \ldots; \nu_{n-1}^n\right]$, $\boldsymbol{\varrho} \triangleq \left[\varrho_0^1; \varrho_1^2; \ldots; \varrho_{n-1}^n\right]$, *and* $\tilde{\mathbf{p}}(s) \triangleq \left[\tilde{p}_0^1(s); \tilde{p}_1^2(s); \ldots; \tilde{p}_{n-1}^n(s)\right]$.

Remark 41 *Given* (7.38) *and* (7.41)*, for* $j = 1, \ldots, n$*, we get we get*

$$\tilde{\mathbf{p}}(s) = \frac{1}{s^2}\mathbf{Q}^{-1}(s)\mathbf{\Psi}_a(s) + \frac{1}{s^2}\boldsymbol{\nu} + \frac{1}{s}\varrho \tag{7.42}$$

Therefore, if $\bar{\mathbf{Q}}(s) \triangleq \mathbf{Q}^{-1}(s)$*, then one can conclude that*

$$\tilde{p}^j_{j-1}(s) = \frac{1}{s}\varrho^j_{j-1} + \frac{1}{s^2}\left(\nu^j_{j-1} + \sum_{\kappa=1}^{n} Q^{-1}_{j\kappa}(s)\Psi^a_{\kappa-1,\kappa}(s)\right) \tag{7.43}$$

where $\tilde{p}^j_{j-1}(s)$*, or* $\tilde{p}^{i+1}_i(s)$*;* $i = 0, \ldots, n-1$*, is the coupled intervehicle distance between neighboring vehicles in the Laplacian domain, and* $Q^{-1}_{j\kappa}(s)$ *are the elements of the matrix* $\mathbf{Q}^{-1}(s)$*. Therefore, it is possible to obtain* $\tilde{p}^{i+1}_i(t)$ *as the impulse response of the system* $\tilde{p}^{i+1}_i(s)$*. For any given* $\mathbf{K} = [k, b, h]$*, if* $\tilde{p}^{i+1}_i(t) > -d^{i+1}_i$*;* $i = 0, 1, \ldots, n-1$*, where* d^{i+1}_i *is the desired distance between the adjacent vehicles, then we would have a non-colliding platoon. Similarly, if* $\tilde{p}^{i+1}_i(t) > -\left(d^{i+1}_i - d^s_{i,i+1}\right)$ *in which* $d^s_{i,i+1}$ *is a preset safe-distance between the neighboring vehicles, then the distance between consecutive vehicles would be always higher than* $d^s_{i,i+1}$*.*

Remark 42 *Given* (7.4) *and splitting* $\mathbb{I}_{i+1}$ *into the sets* $\mathbb{I}^{>i+1}_{i+1}$ *and* $\mathbb{I}^{<i+1}_{i+1}$ *where, for instance,* $\mathbb{I}^{>i+1}_{i+1} \triangleq \{j | j \in \mathbb{I}_{i+1}\ \&\ j > i+1\}$*, it is possible to get*

$$u_{i+1} = -\mathbf{K}\left(\sum_{j\in\mathbb{I}^{>i+1}_{i+1}}\sum_{\kappa=i+1}^{j-1}\tilde{\mathbf{X}}^{\kappa+1}_{\kappa} - \sum_{j\in\mathbb{I}^{<i+1}_{i+1}}\sum_{\kappa=j}^{i}\tilde{\mathbf{X}}^{\kappa+1}_{\kappa}\right) \tag{7.44}$$

Defining $\tilde{\mathbf{X}}^t(s) \triangleq \left[\tilde{\mathbf{X}}^1_0(s);\ \tilde{\mathbf{X}}^2_1(s);\ \ldots;\ \tilde{\mathbf{X}}^n_{n-1}(s)\right]$ *and regarding* (7.29)*, we get*

$$\tilde{\mathbf{X}}^t(s) = \left(\mathbf{I}_n \otimes \mathbf{T}_1\right)\tilde{\mathbf{a}}(s) - \left(\mathbf{I}_n \otimes \mathbf{T}_2\right)\mathbf{\Xi}_t \tag{7.45}$$

in which $\mathbf{\Xi}_t \triangleq \left[\mathbf{\Xi}^1_0; \mathbf{\Xi}^2_1; \ldots; \mathbf{\Xi}^n_{n-1}\right]$*. Now, substituting* (7.38) *into* (7.45)*, we get*

$$\tilde{\mathbf{X}}^t(s) = \left(\mathbf{I}_n \otimes \mathbf{T}_1\right)\mathbf{Q}^{-1}(s)\mathbf{\Psi}_a(s) - \left(\mathbf{I}_n \otimes \mathbf{T}_2\right)\mathbf{\Xi}_t \tag{7.46}$$

using which and defining $\mathbf{I}^\kappa \in R^{3\times 3n}$ *as the matrix comprised of* $(3(\kappa+1)-2)^{th}$ *till* $(3(\kappa+1))^{th}$ *rows of the matrix* $\mathbf{I}_{3n}$*, then for* $\kappa = 0, \ldots, n-1$ *one can conclude that* $\tilde{\mathbf{X}}^{\kappa+1}_{\kappa}(s) = \mathbf{I}^\kappa\tilde{\mathbf{X}}^t(s)$*, plugging which into* (7.44)*, for* $i = 1 \ldots, n$*, we get*

$$u_i(s) = -\mathbf{K}\left(\sum_{j\in\mathbb{I}^{>i+1}_{i+1}}\sum_{\kappa=i+1}^{j-1}\mathbf{I}^\kappa\tilde{\mathbf{X}}^t(s) - \sum_{j\in\mathbb{I}^{<i+1}_{i+1}}\sum_{\kappa=j}^{i}\mathbf{I}^\kappa\tilde{\mathbf{X}}^t(s)\right) \tag{7.47}$$

Note that $\mathbf{I}_{3n} \in R^{3n \times 3n}$ *is the identity matrix of size* $3n$.

7.3 Simulation Results

In the simulation, we examine a platoon consisting of one leader vehicle and four follower vehicles, employing various common communication topologies as illustrated in Figures 7.2 and 7.3. The presumed desired distances between consecutive vehicles are set at 5 meters, denoted as d_i^{i+1} for i ranging from 0 to 3. Each vehicle's length is fixed at 4 meters, represented as L_i for i in the same range. Unlike previous chapters, in this study, we introduce non-zero initial velocity and acceleration differences between neighboring vehicles. The simulations are conducted with a sampling interval of 0.01 seconds. A safe following distance of 3 meters is considered between vehicles, labeled as $d_{i,s}^{i+1} = 3$ meters. We specify the engine time constants as $\tau_1 = 0.7$, $\tau_2 = 0.6$, $\tau_3 = 1$, and $\tau_4 = 0.9$. To create this scenario in the simulations, all vehicles initially

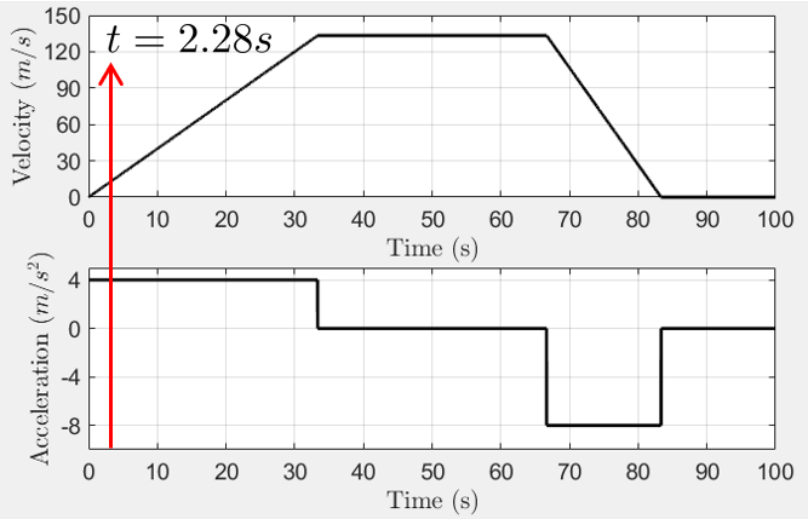

Figure 7.6: Leader's velocity and acceleration.

start from a stationary state. As they begin to move, they gradually assume different speeds and accelerations at various distances from each other. The platooning process commences when the vehicles are at these varying states, forming different distances, velocities, and accelerations. To facilitate this, we design a velocity trajectory for

the leader vehicle, as depicted in Figure 7.6. This trajectory allows vehicles to start moving, with each follower changing their position, speed, and acceleration to move in the leader vehicle's movement. After a period, we trigger the platooning at $t = 2.28$ seconds, bringing the vehicles closer together. Figure 7.7 provides a visual representation of this scenario. As a result of these distinct initial conditions, combined with

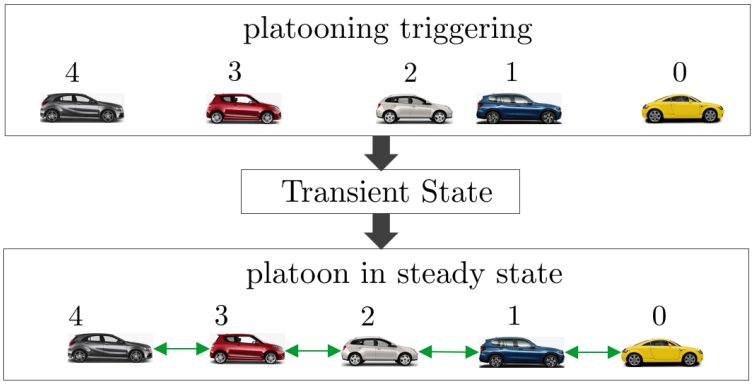

Figure 7.7: Initial velocity and acceleration differences are not zero.

various communication topologies and control parameters, different scenarios for the inter-vehicle distances may emerge. These scenarios will be explored and discussed in the following section.

7.3.1 Intervehicle Distances under Various Communication Topologies

To extract the effect of communication topologies, we consider a platoon with one leader and four followers. The vehicles are considered to be different such that $\tau_1 = 0.7$, $\tau_1 = 0.6$, $\tau_1 = 1$, and $\tau_1 = 0.9$. The lengths of vehicle are considered to be identical and equal to 4 meters. The initial coupled states are assumed to be $\tilde{p}_0^1(0) = 1.7064m$, $\tilde{p}_1^2(0) = 6.7185m$, $\tilde{p}_2^3(0) = 0.5503m$, $\tilde{p}_3^4(0) = 6.0885m$, $\tilde{v}_0^1(0) = -3.6585m/s$, $\tilde{v}_1^2(0) = -1.2465m/s$, $\tilde{v}_2^3(0) = -4.1251m/s$, $\tilde{v}_3^4(0) = -1.0198m/s$, $\tilde{a}_0^1 = -0.1351m/s^2$, $\tilde{a}_1^2 = -0.7847m/s^2$, $\tilde{a}_2^3 = -0.0594m/s^2$, and $\tilde{a}_3^4 = -1.3249m/s^2$, where they are calculated based on the following initial states of the vehicles:

Vehicle	Initial position	Initial velocity	Initial acceleration
Leader	10.3968 m	9.1200 m/s	4 m/s^2
Follower 1	-0.3096 m	12.7785 m/s	4.1351 m/s^2
Follower 2	-16.0281 m	14.0250 m/s	4.9197 m/s^2
Follower 3	-25.5784 m	18.1501 m/s	4.9792 m/s^2
Follower 4	-40.6669 m	19.1699 m/s	6.3040 m/s^2

Table 7.1: Initial states of vehicles: x_i, v_i and a_i; $i = 0, \ldots, 4$

Let $h = 4$ and control gains k and b vary between values 0.1 and 19.6 by 0.5 incremental. Any $\mathbf{K} = [k, b, 4]$ that does not satisfy stability conditions is considered as an unstable control gain, otherwise a stable $\mathbf{K}$. Thus, for $i = 0, \ldots, n-1$ and a given stable $\mathbf{K}$, using Remark 41, if $-5m < \tilde{p}_i^{i+1}(t) < -2m$ then $\mathbf{K}$ is a stable-non-collision control gain. Similarly, if $\tilde{p}_i^{i+1}(t) < -5m$, then we name $\mathbf{K}$ a stable-collision control gain. Furthermore, if $\tilde{p}_i^{i+1}(t) > -2m$, then $\mathbf{K}$ is named a stable-safe control gain which implies that the intervehicle distances are always larger than $3m$ which is assumed as the safe distance between neighboring vehicles. The results using the mentioned scenarios are provided in Fig. 7.8 in which unstable, stable-collision, stable-non-collision, and stable-safe gains are presented with red, yellow, blue, and green colors, respectively.

Effects of forward/backward communications

From Fig. 7.8, some important implications can be drawn as follows:

1. Comparing BD/BDL, PF/PLF and TPF/TPLF topologies: it is apparent that broadcasting the leader's state to the follower vehicles has starkly improved the performance of the platoon.

2. SPTF has the smallest stable area, the smallest stable-safe area, the biggest stable-collision area, the smallest positive-velocity area, and the biggest larger-settling-time

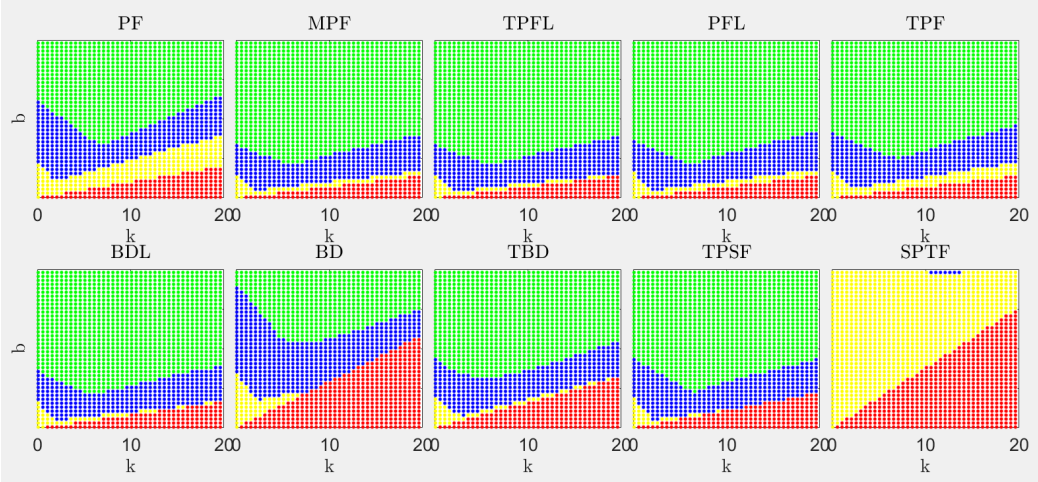

Figure 7.8: Unstable (red), stable-collision (yellow), stable-non-collision (blue) and stable-safe (green) control gains $\mathbf{K} = [k, b, 4]$. The collision distance is $5m$, therefore the control gains that result in $\tilde{p}_i^{i+1}(t) > -5m$ are called stable-non-collision gains. Also, the safe distance is $3m$, thus the control gains that result in $\tilde{p}_i^{i+1}(t) > -2m$ are called stable-safe gains.

area.

3. Comparing PF/BD, and BD/SPTF topologies: under BD and SPTF topologies and in comparison with PF and BD topologies respectively, the followers receive information from one more vehicle behind which degrades the performance of the platoon under BD and SPTF topologies when compared to those of PF and BD topologies, respectively.

4. Comparing BD/TPSF, and SPTF/TBPF topologies: under BD/SPTF topologies, follower vehicles receive information from one/two vehicles behind and one/one vehicle ahead respectively, and under TPSF/TBPF they receive from one/two vehicles behind and two/two vehicles ahead. Getting more information from vehicles ahead improves the platoon performance under TPSF/TBPF with respect to those of BD/SPTF topologies, respectively.

5. Comparing PLF/TPF, and BDL/TPSF topologies: the performance of PLF and BDL are comparable to those of TPF and TPSF, respectively. However, it sounds that if the additional information from vehicles ahead is actually from the leader ve-

hicle, then the performance would be slightly better.

6. Comparing TPLF, PLF, and nontypical CT d: there are subtle differences between performances which imply that when followers are of "look-ahead" type, and receive information from the leader, the leader's data outweighs those of the other followers. In other words, the information followers receive from other non-leader vehicles may be redundant which can be exploited to accomplished some other performance specifications. This issue needs more research.

7.3.2 Effect of Broadcasting Leader Vehicle's State in Platoon Scalability

As previously discussed, the performance of PLF is comparable to that of TPF, and BDL's performance closely matches that of TPSF. However, it appears that if the supplementary information obtained from vehicles ahead originates specifically from the leader vehicle, there is a slight improvement in performance. To further investigate this matter, this section aims to explore the impact of broadcasting the leader vehicle's state on platoon scalability.

In order to demonstrate this effect, the simulation in this section involves increasing the platoon size to 11 vehicles, consisting of one leader vehicle followed by ten others. In order to demonstrate this effect, the simulation in this section involves increasing the platoon size to 11 vehicles, consisting of one leader vehicle followed by ten others. The parameters are as follows: $\tau_1 = 0.7$, $\tau_2 = 0.6$, $\tau_3 = 1$, $\tau_4 = 0.9$, $\tau_5 = 0.7$, $\tau_6 = 0.6$, $\tau_7 = 1$, $\tau_8 = 0.9$, $\tau_9 = 0.6$, $\tau_{10} = 0.7$, and initial coupled states of neighboring vehicles are summarized in Table 7.2.

Following the guidelines provided in Remark 41, with $h = 4$ and varying the control gains k and b with increments of 0.5 between 0.1 and 19.6, the results are presented in Figure 7.9. An analysis of Figure 7.9 reveals that platoons operating under communication topologies where the leader vehicle's state is broadcast to all following vehicles demonstrate robustness when increasing the platoon size.

Pair	$\tilde{p}_i^{i+1}(0)$	$\tilde{v}_i^{i+1}(0)$	$\tilde{a}_i^{i+1}(0)$
$(0,1)$	1.7064 m	-3.6585 m/s	-0.1351 m/s^2
$(1,2)$	6.7185 m	-1.2465 m/s	-0.7847 m/s^2
$(2,3)$	0.5503 m	-4.1251 m/s	-0.0594 m/s^2
$(3,4)$	6.0885 m	-1.0198 m/s	-1.3249 m/s^2
$(4,5)$	1.7064 m	-3.6585 m/s	-0.1351 m/s^2
$(5,6)$	6.7185 m	-1.2465 m/s	-0.7847 m/s^2
$(6,7)$	0.5503 m	-4.1251 m/s	-0.0594 m/s
$(7,8)$	6.0885 m	-1.0198 m/s	-1.3249 m/s^2
$(8,9)$	1.70641 m	-3.6585 m/s	-0.1351m/s^2
$(9,10)$	6.7185 m	-1.2465 m/s	-0.7847 m/s^2

Table 7.2: Initial coupled states of neighboring vehicles.

Consequently, it is observed that under TPFL, PFL, and BDL topologies, even with the platoon size almost tripling, the platoon maintains a performance similar to what was achieved with five vehicles, as shown in the previous Figure 7.8.

7.3.3 Comparison Between Average Energy of Control Inputs

Based on (7.47), we define average energy of control inputs for four followers, out of stable control gains and under different communication topologies (CTs) as follows.

$$E_{CT} = \frac{1}{\#\mathbf{K}_{stable}^{CT}} \left(\sum_{\mathbf{K}_{stable}^{CT}} \left(\frac{1}{4} \left(\sum_{i=1}^{4} \int_{t_0}^{t_{end}} u_i^2(t) dt \right) \right) \right) \tag{7.48}$$

in which t_0 is platooning triggering time, t_{end} is simulation time, and $\#\mathbf{K}_{stable}$ is the number of stable control gains under the given communication topology (CT). The results are shown in Fig. 7.10, in Which TPFL has the best performance while PF the worst performance.

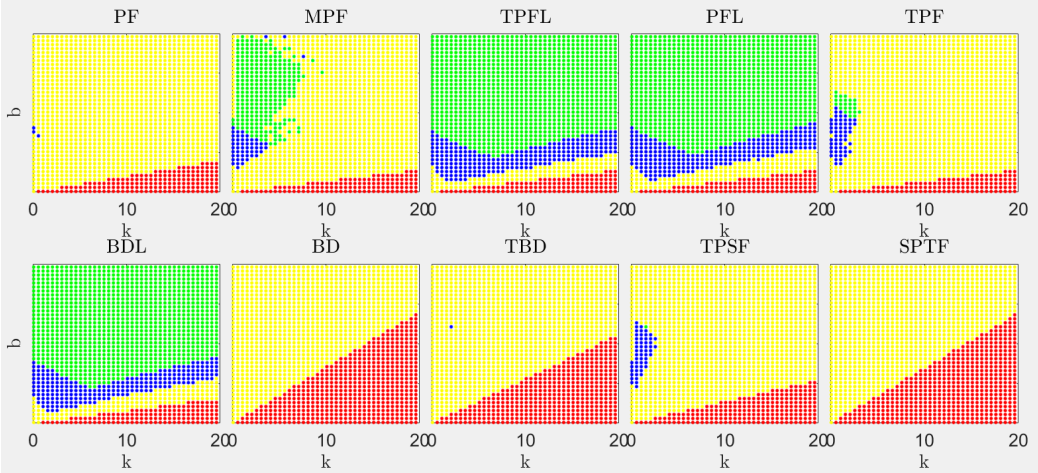

Figure 7.9: Unstable (red), stable-collision (yellow), stable-non-collision (blue) and stable-safe (green) control gains $\mathbf{K} = [k, b, 4]$. The collision distance is $5m$, therefore the control gains that result in $\tilde{p}_i^{i+1}(t) > -5m$ are called stable-non-collision gains. Also, the safe distance is $3m$, thus the control gains that result in $\tilde{p}_i^{i+1}(t) > -2m$ are called stable-safe gains.

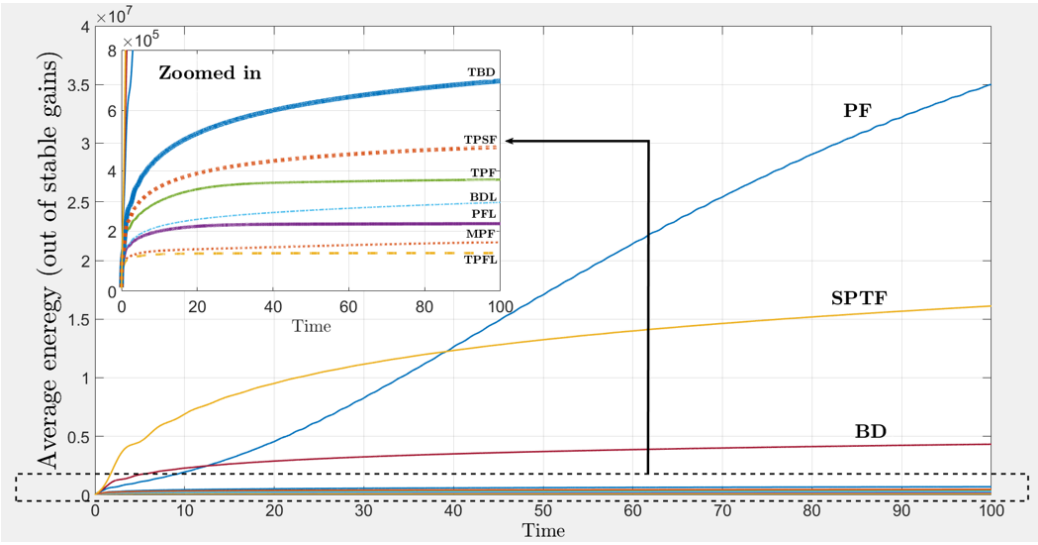

Figure 7.10: Average energy of control inputs of four follower vehicles, out of stable control gains.

7.4 Conclusion

In summary, this chapter has delved into two key aspects of heterogeneous platoon dynamics. First, it has thoroughly examined the impact of communication topologies

on intervehicle distances, even when platoons begin with highly diverse initial conditions. Secondly, it emphasizes the pivotal role of broadcasting the leader vehicle's state in elevating platoon scalability.

Through our exploration, we expanded the platoon to include 11 vehicles, comprising one leader and ten followers. Notably, this expansion did not compromise the platoon's robustness, especially under specific communication topologies such as TPFL, PFL, and BDL. Even as the platoon's size nearly tripled, it maintained its efficiency, resembling the performance levels achieved with smaller platoons.

This underscores the immense potential for enhancing platoon performance through the dissemination of the leader's state information. In essence, this chapter has shed light on the critical dynamics of platoon behavior, offering insights into how communication topologies and leader information can contribute to the robustness and scalability of heterogeneous platoons.

Chapter 8

Conclusions, Recommendations, & Future Work

8.1 Conclusions

In this thesis, we have embarked on a comprehensive exploration of the complex dynamics and stability of heterogeneous platoons, with a particular emphasis on the interplay between communication topologies and platoon behavior. The culmination of our research efforts has yielded valuable insights into the intricacies of platoon dynamics, stability, and scalability. In the following section, we summarize the key contributions and overarching themes from each of the preceding chapters, weaving together a holistic conclusion that advances our understanding of heterogeneous platoons.

Chapter 3 presented an innovative approach to stability analysis for heterogeneous platoons. By employing a decentralized linear feedback controller with non-identical gains and accommodating various Information Flow Topologies (IFTs), we developed a state-space model that enables the determination of stability conditions for platoons of any size. Our simulation results for a two-followers platoon underscored the significance of increased inter-vehicle communication, facilitated by various IFTs, in enhancing platoon stability. Additionally, we highlighted the substantial benefits of incorporating feedback signals from the leader into both followers' controllers. These findings emphasize the pivotal role of communication in platoon stability.

Chapter 4 shifted our focus to the dynamics of a homogeneous platoon, introducing a closed-loop distance dynamic model that allowed for a detailed investigation of inter-vehicle distances (IDs). We derived IDs from initial conditions, providing valuable insights into platoon behavior. By imposing constraints on collision and safe distance limits, as well as feasible-velocity limits for the followers, we comprehensively examined the platoon's performance under various Communication Topologies (CTs). This chapter deepened our understanding of platoon dynamics and highlighted the importance of constraints and communication in shaping platoon behavior.

Chapter 5 further delved into achieving both internal stability and favorable transient dynamics in inter-vehicle distances. The closed-loop distance dynamic model and analytical distance trajectory determination provided a deeper understanding of system stability and transient inter-vehicle distance analysis. We scrutinized the strengths and weaknesses of different bidirectional communication topologies (BD-CTs) and found that receiving information from vehicles further ahead could enhance transient inter-vehicle distances, while broadcasting the leader's state could elevate overall platoon performance. The findings from this chapter reinforced the importance of communication topology in platoon dynamics.

Chapter 6 extended our research beyond traditional internal stability considerations, emphasizing the formulation of a coupled distance dynamic model for platoons. We conducted a comprehensive examination of how control parameters and initial conditions impact platoon stability and inter-vehicle distance errors. The methodology presented in this chapter ensured both stable and safe behaviors for vehicles within a platoon. High-fidelity simulations further validated the effectiveness of our control strategies, emphasizing the importance of safety and stability in heterogeneous platoons.

Chapter 7 explored the impact of communication topologies on inter-vehicle distances in larger platoons, highlighting the potential for scalability while maintaining efficiency. The dissemination of the leader's state information played a pivotal role

in enhancing platoon performance, even as the platoon size increased. This chapter reinforced the idea that communication topologies and leader information are critical factors contributing to the robustness and scalability of heterogeneous platoons.

In conclusion, this thesis has advanced the field of heterogeneous platoon dynamics by elucidating the intricate interplay between communication topologies, stability, and scalability. Our findings emphasize that effective communication strategies and the dissemination of leader information can significantly enhance platoon performance and safety. These insights are invaluable for the development of future transportation systems, autonomous vehicles, and the optimization of platoon behavior in real-world scenarios. As we move forward, the knowledge generated from this research can serve as a foundation for further exploration and innovation in the field of platoon dynamics.

8.2 Future Work

While this thesis has made significant strides in advancing our understanding of heterogeneous platoon dynamics and stability, it also opens the door to several promising avenues for future research. In the scope of our research on intelligent vehicle platooning, our primary focus has been on the longitudinal dynamics and state deviations, specifically addressing aspects related to longitudinal control within the platoon. Our goal was to achieve a thorough understanding and effective control of longitudinal behaviors, such as acceleration, braking, and inter-vehicle spacing, to ensure stable and efficient platoon operation.

In our research on intelligent vehicle platooning, we deliberately directed our attention towards the nuanced intricacies of longitudinal dynamics and state deviations. The decision to prioritize longitudinal control was a strategic choice aimed at achieving a focused and in-depth analysis within the constraints of available resources and time. While lateral dynamics, covering critical elements such as lane keeping, turning maneuvers, and responses to environmental disturbances, are undoubtedly essential in ensuring overall platoon stability and safety, we acknowledge their significance.

It is crucial to note that the exclusion of explicit consideration for lateral dynamics should not be interpreted as a dismissal of their importance. On the contrary, we recognize the vital role that lateral control plays in real-world scenarios. Therefore, we intentionally left lateral dynamics as a part of potential future work. This strategic approach allows us to incrementally expand our research scope, with the intention to investigate and integrate lateral control mechanisms in subsequent phases, thus providing a more holistic solution for intelligent vehicle platooning. Lateral control in platooning can be effectively explored through prospective methods such as Model Predictive Control (MPC) and game theory. These approaches offer the potential to develop iterative predictive strategies for optimizing platoon lateral control.

The primary focus in this work was on continuous braking to lay the groundwork for understanding platoon behavior within communication constraints. Anti-lock braking system (ABS) is an integral to vehicles, as it prevents wheel lockup during intense braking and ensures the retention of steering control. Therefore, it plays a crucial role in real-world scenarios, preventing wheel lockup and influencing braking behavior and vehicle stability. Recognizing the significance of ABS in practical applications, It is beneficial to extend the current work to incorporate ABS activation and its impact on platoon dynamics as a future research direction. By modeling ABS dynamics and integrating them into the problem formulation, and utilizing proper controllers, the aim would be to enhance the realism of the braking system and address potential consequences such as unrealistic behavior, loss of stability, and limited applicability in diverse driving environments.

The following section outlines other potential directions for future work, building upon the foundations established in this study:

1. Enhancing Simulation Toolbox for Vehicle Platoons: To further aid researchers and practitioners in the field, future work can focus on developing an enhanced simulation toolbox specifically tailored for vehicle platoons operating under distributed linear controls. This toolbox could incorporate advanced modeling techniques and

real-time simulation capabilities, allowing for more intricate and comprehensive analysis of platoon behavior.

2. Dynamic Communication Topologies: The investigation of dynamic communication topologies is an area with substantial potential. Future research can explore the dynamic adaptation of communication structures in response to varying traffic conditions, network constraints, and platoon goals. Implementing self-organizing communication networks within platoons could enhance their adaptability and efficiency.

3. Data Loss and Delay Analysis: The effect of data loss and communication delay remains a critical aspect of platoon dynamics. Future studies could delve deeper into this domain, exploring mechanisms for mitigating the impact of data loss and delay, and designing robust control strategies that are resilient to these challenges. This work might involve advanced error-correction techniques, communication protocol optimizations, and novel control algorithms.

4. Leveraging AI for Online Control Tuning: The integration of artificial intelligence, particularly reinforcement learning, to online control tuning is an exciting avenue for future research. Developing intelligent control systems that can adapt and optimize control gains in real-time, considering the dynamic environment and platoon-specific conditions, could significantly improve platoon performance and stability.

5. Incorporating Control Input Optimization into Safe Distance Analysis:** Extending the concept of safe distance analysis to include optimization of control inputs is a critical direction for future work. Integrating control input optimization within the safe distance analysis framework can enhance safety and efficiency simultaneously. This might involve dynamic adjustments of control inputs to minimize energy consumption or reduce traffic congestion.

6. Multimodal and Heterogeneous Platoons: Investigating platoons that consist of various vehicle types, including autonomous and non-autonomous vehicles, as well

as those with different propulsion systems, is an emerging field. Future research can explore the challenges and benefits of managing heterogeneous platoons and develop control strategies that can accommodate a wide range of vehicle characteristics.

7. Real-world Implementations: Taking theoretical findings from this thesis and implementing them in real-world scenarios is crucial. Conducting field trials with actual vehicle platoons and assessing the practicality and scalability of the proposed methodologies will be instrumental in advancing the field and achieving safe and efficient platoon operations.

8. Policy and Standardization: Collaborating with policymakers and regulatory bodies to establish guidelines and standards for platoon operations is essential. Future work can focus on contributing to the development of legal frameworks, safety regulations, and certification processes for platooning technologies to facilitate their widespread adoption.

9. Human-Machine Interaction: As platoons become more common on the road, understanding the interaction between human-driven and autonomous vehicles within platoons will be vital. Future research could explore how to improve the coexistence and cooperation between human and automated drivers in mixed traffic environments.

10. Environmental Considerations: Investigating the environmental impact of vehicle platooning, including its potential to reduce fuel consumption and greenhouse gas emissions, is an area that requires further exploration. Future research can quantify the environmental benefits and challenges of platooning and develop strategies for optimizing its ecological footprint.

In summary, the potential for future research in the field of heterogeneous platoon dynamics is vast. This thesis has laid a strong foundation, and the research community has numerous exciting opportunities to explore, advancing the safety, efficiency, and sustainability of platoon-based transportation systems. These future works hold the promise of shaping the future of transportation and contributing to the development of intelligent and adaptive traffic systems.

Bibliography

[1] A. Alam, B. Besselink, V. Turri, J. Mårtensson, and K. H. Johansson, "Heavy-duty vehicle platooning for sustainable freight transportation: A cooperative method to enhance safety and efficiency," *IEEE Control Systems Magazine*, vol. 35, no. 6, pp. 34–56, 2015.

[2] C. Bonnet and H. Fritz, "Fuel consumption reduction in a platoon: Experimental results with two electronically coupled trucks at close spacing," SAE Technical Paper, Tech. Rep., 2000.

[3] S. E. Shladover, D. Su, and X.-Y. Lu, "Impacts of cooperative adaptive cruise control on freeway traffic flow," *Transportation Research Record*, vol. 2324, no. 1, pp. 63–70, 2012.

[4] F.-Y. Wang, "Parallel control and management for intelligent transportation systems: Concepts, architectures, and applications," *IEEE Transactions on Intelligent Transportation Systems*, vol. 11, no. 3, pp. 630–638, 2010.

[5] M. Seraj, J. Li, and Z. Qiu, "Modeling microscopic car-following strategy of mixed traffic to identify optimal platoon configurations for multiobjective decision-making," *Journal of Advanced Transportation*, vol. 2018, 2018.

[6] J. Tan, T. Yang, Y. Zhang, and T. Z. Qiu, "Evaluation of vehicles' platooning on expressways based on v2x," in *2019 5th International Conference on Transportation Information and Safety (ICTIS)*, IEEE, 2019, pp. 369–375.

[7] J. Li, C. Qiu, M. Seraj, L. Peng, and T. Z. Qiu, "Platoon priority visualization modeling and optimization for signal coordination in the connected vehicle environment," *Transportation research record*, vol. 2673, no. 5, pp. 36–48, 2019.

[8] C. Zhai, Y. Liu, and F. Luo, "A switched control strategy of heterogeneous vehicle platoon for multiple objectives with state constraints," *IEEE Trans. Intell. Transp. Syst*, vol. 20, no. 5, pp. 1883–1896, 2018.

[9] L. Xu, W. Zhuang, G. Yin, and C. Bian, "Energy-oriented cruising strategy design of vehicle platoon considering communication delay and disturbance," *Transp. Res. Part C Emerg. Technol.*, vol. 107, pp. 34–53, 2019.

[10] S. E. Li, X. Qin, K. Li, J. Wang, and B. Xie, "Robustness analysis and controller synthesis of homogeneous vehicular platoons with bounded parameter uncertainty," *IEEE/ASME Transactions on Mechatronics*, vol. 22, no. 2, pp. 1014–1025, 2017.

[11] A. Elahi, A. Alfi, and H. Modares, "H consensus of homogeneous vehicular platooning systems with packet dropout and communication delay," *IEEE Transactions on Systems, Man, and Cybernetics: Systems*, vol. 52, no. 6, pp. 3680–3691, 2021.

[12] Y. Wu, S. E. Li, J. Cortés, and K. Poolla, "Distributed sliding mode control for nonlinear heterogeneous platoon systems with positive definite topologies," *IEEE Transactions on Control Systems Technology*, vol. 28, no. 4, pp. 1272–1283, 2019.

[13] G. Feng, D. Dang, and Y. He, "Robust coordinated control of nonlinear heterogeneous platoon interacted by uncertain topology," *IEEE Transactions on Intelligent Transportation Systems*, vol. 23, no. 6, pp. 4982–4992, 2020.

[14] P. A. Ioannou and C.-C. Chien, "Autonomous intelligent cruise control," *IEEE Transactions on Vehicular technology*, vol. 42, no. 4, pp. 657–672, 1993.

[15] D. Swaroop and J. K. Hedrick, "Constant spacing strategies for platooning in automated highway systems," 1999.

[16] J. Zhou and H. Peng, "Range policy of adaptive cruise control vehicles for improved flow stability and string stability," *IEEE Transactions on intelligent transportation systems*, vol. 6, no. 2, pp. 229–237, 2005.

[17] G. Orosz, "Connected cruise control: Modelling, delay effects, and nonlinear behaviour," *Vehicle System Dynamics*, vol. 54, no. 8, pp. 1147–1176, 2016.

[18] B. Besselink and K. H. Johansson, "String stability and a delay-based spacing policy for vehicle platoons subject to disturbances," *IEEE Transactions on Automatic Control*, vol. 62, no. 9, pp. 4376–4391, 2017.

[19] K. Santhanakrishnan and R. Rajamani, "On spacing policies for highway vehicle automation," *IEEE Trans. Intell. Transp. Syst*, vol. 4, no. 4, pp. 198–204, 2003.

[20] J. Ploeg, N. Van De Wouw, and H. Nijmeijer, "Lp string stability of cascaded systems: Application to vehicle platooning," *IEEE Trans. Control Syst. Technol.*, vol. 22, no. 2, pp. 786–793, 2013.

[21] D. Swaroop and J. K. Hedrick, "String stability of interconnected systems," *IEEE Trans. Autom. Control*, vol. 41, no. 3, pp. 349–357, 1996.

[22] P. Seiler, A. Pant, and K. Hedrick, "Disturbance propagation in vehicle strings," *IEEE Transactions on automatic control*, vol. 49, no. 10, pp. 1835–1842, 2004.

[23] S. Feng, Y. Zhang, S. E. Li, Z. Cao, H. X. Liu, and L. Li, "String stability for vehicular platoon control: Definitions and analysis methods," *Annual Reviews in Control*, vol. 47, pp. 81–97, 2019.

[24] S. S. Stankovic, M. J. Stanojevic, and D. D. Siljak, "Decentralized overlapping control of a platoon of vehicles," *IEEE Transactions on Control Systems Technology*, vol. 8, no. 5, pp. 816–832, 2000.

[25] S. E. Li *et al.*, "Dynamical modeling and distributed control of connected and automated vehicles: Challenges and opportunities," *IEEE Intelligent Transportation Systems Magazine*, vol. 9, no. 3, pp. 46–58, 2017.

[26] S. E. Li, Y. Zheng, K. Li, and J. Wang, "An overview of vehicular platoon control under the four-component framework," in *2015 IEEE Intelligent Vehicles Symposium (IV)*, IEEE, 2015, pp. 286–291.

[27] Y. Zheng, S. E. Li, J. Wang, D. Cao, and K. Li, "Stability and scalability of homogeneous vehicular platoon: Study on the influence of information flow topologies," *IEEE Transactions on intelligent transportation systems*, vol. 17, no. 1, pp. 14–26, 2015.

[28] S. Badnava *et al.*, "Platoon transitional maneuver control system: A review," *IEEE Access*, 2021.

[29] R. Rajamani, "Introduction to longitudinal control," in *Vehicle Dynamics and Control*. Boston, MA: Springer US, 2012, pp. 113–139, ISBN: 978-1-4614-1433-9. DOI: 10.1007/978-1-4614-1433-9_5. [Online]. Available: https://doi.org/10.1007/978-1-4614-1433-9_5.

[30] C. Hong *et al.*, "A joint design of platoon communication and control based on lte-v2v," *IEEE Trans. Veh. Technol.*, vol. 69, no. 12, pp. 15 893–15 907, 2020.

[31] J. Lan, D. Zhao, and D. Tian, "Data-driven robust predictive control for mixed vehicle platoons using noisy measurement," *IEEE Trans. Intell. Transp. Syst*, 2021.

[32] P. Wang, H. Deng, J. Zhang, L. Wang, M. Zhang, and Y. Li, "Model predictive control for connected vehicle platoon under switching communication topology," *IEEE Transactions on Intelligent Transportation Systems*, 2021.

[33] Y. Zheng, S. E. Li, K. Li, F. Borrelli, and J. K. Hedrick, "Distributed model predictive control for heterogeneous vehicle platoons under unidirectional topologies," *IEEE Trans. Control Syst. Technol.*, vol. 25, no. 3, pp. 899–910, 2016.

[34] K. Li, Y. Bian, S. E. Li, B. Xu, and J. Wang, "Distributed model predictive control of multi-vehicle systems with switching communication topologies," *Transportation Research Part C: Emerging Technologies*, vol. 118, p. 102 717, 2020.

[35] F. Gao, X. Hu, S. E. Li, K. Li, and Q. Sun, "Distributed adaptive sliding mode control of vehicular platoon with uncertain interaction topology," *IEEE Transactions on Industrial Electronics*, vol. 65, no. 8, pp. 6352–6361, 2018.

[36] M. Di Bernardo, A. Salvi, and S. Santini, "Distributed consensus strategy for platooning of vehicles in the presence of time-varying heterogeneous communication delays," *IEEE Trans. Intell. Transp. Syst*, vol. 16, no. 1, pp. 102–112, 2014.

[37] Y. Li, C. Tang, K. Li, S. Peeta, X. He, and Y. Wang, "Nonlinear finite-time consensus-based connected vehicle platoon control under fixed and switching communication topologies," *Transp. Res. Part C Emerg. Technol.*, vol. 93, pp. 525–543, 2018.

[38] Y. Li, C. Tang, K. Li, X. He, S. Peeta, and Y. Wang, "Consensus-based cooperative control for multi-platoon under the connected vehicles environment," *IEEE Trans. Intell. Transp. Syst*, vol. 20, no. 6, pp. 2220–2229, 2018.

[39] Y. Li, C. Tang, S. Peeta, and Y. Wang, "Nonlinear consensus-based connected vehicle platoon control incorporating car-following interactions and heterogeneous time delays," *IEEE Trans. Intell. Transp. Syst*, vol. 20, no. 6, pp. 2209–2219, 2018.

[40] V. S. Dolk, J. Ploeg, and W. M. H. Heemels, "Event-triggered control for string-stable vehicle platooning," *IEEE Transactions on Intelligent Transportation Systems*, vol. 18, no. 12, pp. 3486–3500, 2017.

[41] H. Zhang, J. Liu, Z. Wang, H. Yan, and C. Zhang, "Distributed adaptive event-triggered control and stability analysis for vehicular platoon," *IEEE Trans. Intell. Transp. Syst*, vol. 22, no. 3, pp. 1627–1638, 2020.

[42] S. Feng, H. Sun, Y. Zhang, J. Zheng, H. X. Liu, and L. Li, "Tube-based discrete controller design for vehicle platoons subject to disturbances and saturation constraints," *IEEE Trans. Control Syst. Technol.*, vol. 28, no. 3, pp. 1066–1073, 2019.

[43] X. Ge, S. Xiao, Q.-L. Han, X.-M. Zhang, and D. Ding, "Dynamic event-triggered scheduling and platooning control co-design for automated vehicles over vehicular ad-hoc networks," *IEEE/CAA Journal of Automatica Sinica*, vol. 9, no. 1, pp. 31–46, 2021.

[44] S. Xiao, X. Ge, Q.-L. Han, and Y. Zhang, "Secure distributed adaptive platooning control of automated vehicles over vehicular ad-hoc networks under denial-of-service attacks," *IEEE Transactions on Cybernetics*, 2021.

[45] Y. Liu, D. Yao, H. Li, and R. Lu, "Distributed cooperative compound tracking control for a platoon of vehicles with adaptive nn," *IEEE Transactions on Cybernetics*, 2021.

[46] G. Yu, P. K. Wong, W. Huang, J. Zhao, X.-B. Wang, and Z.-X. Yang, "Distributed adaptive consensus protocol for connected vehicle platoon with heterogeneous time-varying delays and switching topologies," *IEEE Trans. Intell. Transp. Syst*, 2022.

[47] A. Liu, T. Li, Y. Gu, and H. Dai, "Cooperative extended state observer based control of vehicle platoons with arbitrarily small time headway," *Automatica*, vol. 129, p. 109 678, 2021.

[48] X. Ge, Q.-L. Han, J. Wang, and X.-M. Zhang, "Scalable and resilient platooning control of cooperative automated vehicles," *IEEE Transactions on Vehicular Technology*, vol. 71, no. 4, pp. 3595–3608, 2022.

[49] Y. Zhu *et al.*, "Joint sliding-mode controller and observer for vehicle platoon subject to disturbance and acceleration failure of neighboring vehicles," *IEEE Transactions on Intelligent Vehicles*, 2022.

[50] Q. Luo, A.-T. Nguyen, J. Fleming, and H. Zhang, "Unknown input observer based approach for distributed tube-based model predictive control of heterogeneous vehicle platoons," *IEEE Trans. Veh. Technol.*, vol. 70, no. 4, pp. 2930–2944, 2021.

[51] J. Lan, D. Zhao, and D. Tian, "Safe and robust data-driven cooperative control policy for mixed vehicle platoons," *International Journal of Robust and Nonlinear Control*, 2022.

[52] M. Li, Z. Cao, and Z. Li, "A reinforcement learning-based vehicle platoon control strategy for reducing energy consumption in traffic oscillations," *IEEE Trans. Neural Netw. Learn. Syst.*, vol. 32, no. 12, pp. 5309–5322, 2021.

[53] S. E. Li, X. Qin, Y. Zheng, J. Wang, K. Li, and H. Zhang, "Distributed platoon control under topologies with complex eigenvalues: Stability analysis and controller synthesis," *IEEE Transactions on Control Systems Technology*, vol. 27, no. 1, pp. 206–220, 2017.

[54] Y. Zheng, S. E. Li, K. Li, and L.-Y. Wang, "Stability margin improvement of vehicular platoon considering undirected topology and asymmetric control," *IEEE Trans. Control Syst. Technol.*, vol. 24, no. 4, pp. 1253–1265, 2015.

[55] A. Ghasemi, R. Kazemi, and S. Azadi, "Stable decentralized control of a platoon of vehicles with heterogeneous information feedback," *IEEE Trans. Veh. Technol.*, vol. 62, no. 9, pp. 4299–4308, 2013.

[56] D. Huang, S. Li, Z. Zhang, Y. Liu, and B. Mi, "Design and analysis of longitudinal controller for the platoon with time-varying delay," *IEEE Trans. Intell. Transp. Syst*, 2022.

[57] S. Wen and G. Guo, "Sampled-data control for connected vehicles with markovian switching topologies and communication delay," *IEEE Trans. Intell. Transp. Syst*, vol. 21, no. 7, pp. 2930–2942, 2019.

[58] C. P. Bechlioulis and G. A. Rovithakis, "Robust adaptive control of feedback linearizable mimo nonlinear systems with prescribed performance," *IEEE Transactions on Automatic Control*, vol. 53, no. 9, pp. 2090–2099, 2008. DOI: 10.1109/TAC.2008.929402.

[59] X. Bu, "Prescribed performance control approaches, applications and challenges: A comprehensive survey," *Asian Journal of Control*, vol. 25, no. 1, pp. 241–261, 2023.

[60] C. K. Verginis, C. P. Bechlioulis, D. V. Dimarogonas, and K. J. Kyriakopoulos, "Robust distributed control protocols for large vehicular platoons with prescribed transient and steady-state performance," *IEEE Trans. Control Syst. Technol.*, vol. 26, no. 1, pp. 299–304, 2017.

[61] W. Wang, X. Gao, T. Li, Y. Wang, and C. L. P. Chen, "Observer-based platoon formation control with prescribed performance guarantees for unmanned surface vehicles in presence of nonsmooth input characteristics," *IEEE Transactions on Circuits and Systems II: Express Briefs*, pp. 1–1, 2023. DOI: 10.1109/TCSII.2023.3315733.

[62] Z. Sun, Z. Gao, G. Guo, and S. Wen, "Finite-time control of vehicular platoons with global prescribed performance and actuator nonlinearities," *IEEE Transactions on Intelligent Vehicles*, pp. 1–12, 2023. DOI: 10.1109/TIV.2023.3292393.

[63] Z. Gao, Y. Zhang, and G. Guo, "Adaptive fixed-time prescribed performance control of vehicular platoons with unknown dead-zone and actuator saturation," *International Journal of Robust and Nonlinear Control*, vol. 33, no. 2, pp. 1231–1253, 2023.

[64] P. Liu, A. Kurt, and U. Ozguner, "Distributed model predictive control for cooperative and flexible vehicle platooning," *IEEE Trans. Control Syst. Technol.*, vol. 27, no. 3, pp. 1115–1128, 2018.

[65] I. Karafyllis, D. Theodosis, and M. Papageorgiou, "A novel nonlinear adaptive cruise controller for vehicular platoons," in *2021 European Control Conference (ECC)*, IEEE, 2021, pp. 1814–1821.

[66] Z. Yang, J. Huang, Z. Hu, D. Yang, and Z. Zhong, "Safety-guaranteed constraint-oriented modelling and control for bidirectional vehicular platoons," *IET Control Theory & Applications*, vol. 14, no. 19, pp. 3116–3127, 2020.

[67] J. Ligthart, E. Semsar-Kazerooni, J. Ploeg, M. Alirezaei, and H. Nijmeijer, "Controller design for cooperative driving with guaranteed safe behavior," in *2018 IEEE Conference on Control Technology and Applications (CCTA)*, IEEE, 2018, pp. 1460–1465.

[68] J. Lunze, "Adaptive cruise control with guaranteed collision avoidance," *IEEE Trans. Intell. Transp. Syst*, vol. 20, no. 5, pp. 1897–1907, 2018.

[69] S. Magdici and M. Althoff, "Adaptive cruise control with safety guarantees for autonomous vehicles," *IFAC-PapersOnLine*, vol. 50, no. 1, pp. 5774–5781, 2017.

[70] X. Guo, J. Wang, F. Liao, and W. Xiao, "Adaptive platoon control for nonlinear vehicular systems with asymmetric input deadzone and inter-vehicular spacing constraints," in *2017 IEEE 56th Annual Conference on Decision and Control (CDC)*, IEEE, 2017, pp. 393–398.

[71] J. Huang, Q. Huang, Y. Deng, and Y.-H. Chen, "Toward robust vehicle platooning with bounded spacing error," *IEEE Transactions on Computer-Aided Design of Integrated Circuits and Systems*, vol. 36, no. 4, pp. 562–572, 2016.

[72] S. Xiao, X. Ge, Q.-L. Han, and Y. Zhang, "Secure and collision-free multi-platoon control of automated vehicles under data falsification attacks," *Automatica*, vol. 145, p. 110 531, 2022.

[73] Y. Zhu and F. Zhu, "Barrier-function-based distributed adaptive control of nonlinear cavs with parametric uncertainty and full-state constraint," *Transportation Research Part C: Emerging Technologies*, vol. 104, pp. 249–264, 2019.

[74] Y. Li, Y. Zhao, and S. Tong, "Adaptive fuzzy control for heterogeneous vehicular platoon systems with collision avoidance and connectivity preservation," *IEEE Transactions on Fuzzy Systems*, vol. 31, no. 11, pp. 3934–3943, 2023. DOI: 10.1109/TFUZZ.2023.3271904.

[75] J. Han *et al.*, "Prescribed-time performance recovery fault tolerant control of platoon with nominal constraints guarantee," *IEEE Transactions on Intelligent Transportation Systems*, vol. 24, no. 3, pp. 3501–3513, 2023. DOI: 10.1109/TITS.2022.3232818.

[76] M. Amoozadeh *et al.*, "Security vulnerabilities of connected vehicle streams and their impact on cooperative driving," *IEEE Communications Magazine*, vol. 53, no. 6, pp. 126–132, 2015.

[77] F. Acciani, P. Frasca, A. Stoorvogel, E. Semsar-Kazerooni, and G. Heijenk, "Cooperative adaptive cruise control over unreliable networks: An observer-based approach to increase robustness to packet loss," in *2018 European Control Conference (ECC)*, IEEE, 2018, pp. 1399–1404.

[78] K. Fitch and N. E. Leonard, "Information centrality and optimal leader selection in noisy networks," in *52nd IEEE Conference on Decision and Control*, IEEE, 2013, pp. 7510–7515.

[79] M. Pirani, E. M. Shahrivar, B. Fidan, and S. Sundaram, "Robustness of leader–follower networked dynamical systems," *IEEE Transactions on Control of Network Systems*, vol. 5, no. 4, pp. 1752–1763, 2017.

[80] B. Bamieh, M. R. Jovanovic, P. Mitra, and S. Patterson, "Coherence in large-scale networks: Dimension-dependent limitations of local feedback," *IEEE Transactions on Automatic Control*, vol. 57, no. 9, pp. 2235–2249, 2012.

[81] H. J. LeBlanc, H. Zhang, X. Koutsoukos, and S. Sundaram, "Resilient asymptotic consensus in robust networks," *IEEE Journal on Selected Areas in Communications*, vol. 31, no. 4, pp. 766–781, 2013.

[82] S. Öncü, J. Ploeg, N. Van de Wouw, and H. Nijmeijer, "Cooperative adaptive cruise control: Network-aware analysis of string stability," *IEEE Transactions on Intelligent Transportation Systems*, vol. 15, no. 4, pp. 1527–1537, 2014.

[83] H. Hao, P. Barooah, and J. Veerman, "Effect of network structure on the stability margin of large vehicle formation with distributed control," in *49th IEEE Conference on Decision and Control (CDC)*, IEEE, 2010, pp. 4783–4788.

[84] H. Xing, J. Ploeg, and H. Nijmeijer, "Compensation of communication delays in a cooperative acc system," *IEEE Transactions on Vehicular Technology*, vol. 69, no. 2, pp. 1177–1189, 2019.

[85] M. Pirani, E. Hashemi, J. W. Simpson-Porco, B. Fidan, and A. Khajepour, "Graph theoretic approach to the robustness of k-nearest neighbor vehicle platoons," *IEEE Transactions on Intelligent Transportation Systems*, vol. 18, no. 11, pp. 3218–3224, 2017.

[86] M. Pirani, S. Baldi, and K. H. Johansson, "Impact of network topology on the resilience of vehicle platoons," *IEEE Trans. Intell. Transp. Syst*, 2022.

[87] T. Ruan, H. Wang, L. Zhou, Y. Zhang, C. Dong, and Z. Zuo, "Impacts of information flow topology on traffic dynamics of cav-mv heterogeneous flow," *IEEE Trans. Intell. Transp. Syst*, 2022.

[88] S Huang and W. Ren, "Longitudinal control with time delay in platooning," *IEE Proceedings-Control Theory and Applications*, vol. 145, no. 2, pp. 211–217, 1998.

[89] A. Zakerimanesh, T. Qiu, and M. Tavakoli, "Heterogeneous vehicular platooning with stable decentralized linear feedback control," in *2021 IEEE Int. Conf. on Auton. Syst. (ICAS)*, IEEE, 2021, pp. 1–5.

[90] P. D. Powell, "Calculating determinants of block matrices," *arXiv preprint arXiv:1112.4379*, 2011.

[91] B. Van Arem, C. J. Van Driel, and R. Visser, "The impact of cooperative adaptive cruise control on traffic-flow characteristics," *IEEE Trans. Intell. Transp. Syst*, vol. 7, no. 4, pp. 429–436, 2006.

[92] K. C. Dey *et al.*, "A review of communication, driver characteristics, and controls aspects of cooperative adaptive cruise control (cacc)," *IEEE Trans. Intell. Transp. Syst*, vol. 17, no. 2, pp. 491–509, 2015.

[93] J. Axelsson, "Safety in vehicle platooning: A systematic literature review," *IEEE Trans. Intell. Transp. Syst*, vol. 18, no. 5, pp. 1033–1045, 2016.

[94] K.-Y. Liang, J. Mårtensson, and K. H. Johansson, "Heavy-duty vehicle platoon formation for fuel efficiency," *IEEE Trans. Intell. Transp. Syst*, vol. 17, no. 4, pp. 1051–1061, 2015.

[95] C. Zhai, F. Luo, Y. Liu, and Z. Chen, "Ecological cooperative look-ahead control for automated vehicles travelling on freeways with varying slopes," *IEEE Trans. Veh. Technol.*, vol. 68, no. 2, pp. 1208–1221, 2018.

[96] C. Zhai, F. Luo, and Y. Liu, "Cooperative power split optimization for a group of intelligent electric vehicles travelling on a highway with varying slopes," *IEEE Trans. Intell. Transp. Syst*, 2020.

[97] W. B. Dunbar and D. S. Caveney, "Distributed receding horizon control of vehicle platoons: Stability and string stability," *IEEE Trans. Autom. Control*, vol. 57, no. 3, pp. 620–633, 2011.

[98] D. Zhang, Y.-P. Shen, S.-Q. Zhou, X.-W. Dong, and L. Yu, "Distributed secure platoon control of connected vehicles subject to dos attack: Theory and application," *IEEE Transactions on Systems, Man, and Cybernetics: Systems*, vol. 51, no. 11, pp. 7269–7278, 2020.

[99] H. Chehardoli and A. Ghasemi, "Adaptive centralized/decentralized control and identification of 1-d heterogeneous vehicular platoons based on constant time headway policy," *IEEE Trans. Intell. Transp. Syst*, vol. 19, no. 10, pp. 3376–3386, 2018.

[100] L. Güvenç *et al.*, "Cooperative adaptive cruise control implementation of team mekar at the grand cooperative driving challenge," *IEEE Trans. Intell. Transp. Syst*, vol. 13, no. 3, pp. 1062–1074, 2012.

[101] Y. Zheng, S. E. Li, K. Li, and W. Ren, "Platooning of connected vehicles with undirected topologies: Robustness analysis and distributed h-infinity controller synthesis," *IEEE Trans. Intell. Transp. Syst*, vol. 19, no. 5, pp. 1353–1364, 2017.

[102] F. Ma *et al.*, "Distributed control of cooperative vehicular platoon with non-ideal communication condition," *IEEE Trans. Veh. Technol.*, vol. 69, no. 8, pp. 8207–8220, 2020.

[103] I. G. Jin and G. Orosz, "Optimal control of connected vehicle systems with communication delay and driver reaction time," *IEEE Trans. Intell. Transp. Syst*, vol. 18, no. 8, pp. 2056–2070, 2016.

[104] W. B. Qin, M. M. Gomez, and G. Orosz, "Stability and frequency response under stochastic communication delays with applications to connected cruise control design," *IEEE Trans. Intell. Transp. Syst*, vol. 18, no. 2, pp. 388–403, 2016.

[105] R. Liu, Y. Ren, H. Yu, Z. Li, and H. Jiang, "Connected and automated vehicle platoon maintenance under communication failures," *Vehicular Communications*, vol. 35, p. 100 467, 2022.

[106] Z. Shen, Y. Liu, Z. Li, and M. H. Nabin, "Cooperative spacing sampled control of vehicle platoon considering undirected topology and analog fading networks," *IEEE Trans. Intell. Transp. Syst*, 2022.

[107] L. Xu, X. Jin, Y. Wang, Y. Liu, W. Zhuang, and G. Yin, "Stochastic stable control of vehicular platoon time-delay system subject to random switching topologies and disturbances," *IEEE Trans. Veh. Technol.*, 2022.

[108] Y. Toor, P. Muhlethaler, A. Laouiti, and A. De La Fortelle, "Vehicle ad hoc networks: Applications and related technical issues," *IEEE communications surveys & tutorials*, vol. 10, no. 3, pp. 74–88, 2008.

[109] H. Zhang, J. Liu, Z. Wang, C. Huang, and H. Yan, "Adaptive switched control for connected vehicle platoon with unknown input delays," *IEEE Transactions on Cybernetics*, 2021.

[110] W.-D. Xu, X.-G. Guo, J.-L. Wang, W.-W. Che, and Z.-G. Wu, "Nonlinear disturbance observer-based fault-tolerant sliding-mode control for 2-d plane vehicular platoon with utvfd and anas," *IEEE Transactions on Cybernetics*, 2022.

[111] S. Xiao, X. Ge, Q.-L. Han, and Y. Zhang, "Dynamic event-triggered platooning control of automated vehicles under random communication topologies and various spacing policies," *IEEE Transactions on Cybernetics*, vol. 52, no. 11, pp. 11 477–11 490, 2021.

[112] G. Fiengo, D. G. Lui, A. Petrillo, S. Santini, and M. Tufo, "Distributed robust pid control for leader tracking in uncertain connected ground vehicles with v2v communication delay," *IEEE/ASME Trans. Mechatron.*, vol. 24, no. 3, pp. 1153–1165, 2019.

[113] Z. Liu, H. Wang, Y. Wang, and H. Wang, "Cooperative platoon control of automated industrial vehicles: A synchronization approach and real-world experiments," *IEEE/ASME Trans. Mechatron.*, 2022.

[114] J. Wang, X. Deng, J. Guo, Y. Luo, and K. Li, "A fully distributed anti-windup control protocol for intelligent-connected electric vehicles platooning with switching topologies and input saturation," *IEEE/ASME Trans. Mechatron.*, 2022.

Appendix A: Details on Table 6.1

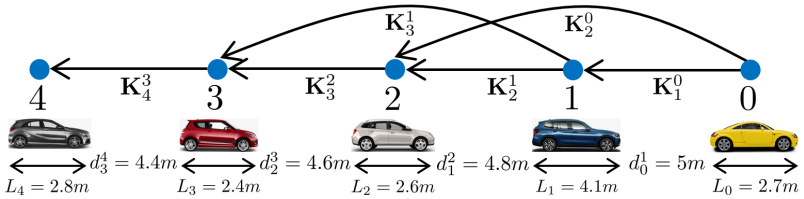

Figure A.1: A look-ahead topology in a heterogeneous platoon with 1 leader and 4 follower vehicles.

Based on equations (6.22)-(6.24), for $i = 0, \ldots, 3$, we have:

For the pair (0,1):

$$\begin{cases} \Theta_0^1 = \Gamma_0^1 = 0 \\ H_0^1(s) = \tau_1 \left(\tau_1 s^3 + (1 + h_1^0)s^2 + b_1^0 s + k_1^0\right)^{-1} \\ \psi_0^1(s) = \frac{\beta}{\tau_1} \left(\tau_1 s^2 + (1 + h_1^0)s + b_1^0\right) H_0^1(s) \end{cases}$$

For the pair (1,2):

$$\begin{cases} \Theta_1^2 = \frac{h_1^0}{\tau_1} - \frac{\tau_1 - \tau_2}{\tau_1 \tau_2} - \frac{h_2^0}{\tau_2} \\ \Gamma_1^2 = \frac{b_1^0}{\tau_1} - \frac{b_2^0}{\tau_2} \\ H_1^2(s) = \tau_2 \left(\tau_2 s^3 + (1 + h_2^1 + h_2^0)s^2 + (b_2^1 + b_2^0)s + (k_2^1 + k_2^0)\right)^{-1} \\ \psi_1^2(s) = \frac{\beta}{\tau_2} \left(\tau_2 s^2 + (1 + h_2^1 + 2h_2^0 - \frac{\tau_2}{\tau_1} h_1^0 + \frac{\tau_1 - \tau_2}{\tau_1})s + b_2^1 + 2b_2^0 - \frac{\tau_2}{\tau_1} b_1^0\right) H_1^2(s) \end{cases}$$

For the pair (2,3):

$$\begin{cases} \Theta_2^3 = \frac{2h_2^0}{\tau_2} + \frac{h_2^1}{\tau_2} - \frac{2(\tau_2 - \tau_3)}{\tau_2 \tau_3} - \frac{h_3^1}{\tau_3} \\ \Gamma_2^3 = \frac{2b_2^0}{\tau_2} + \frac{b_2^1}{\tau_2} - \frac{b_3^1}{\tau_3} \\ H_2^3(s) = \tau_3 \left(\tau_3 s^3 + (1 + h_3^2 + h_3^1)s^2 + (b_3^2 + b_3^1)s + (k_3^2 + k_3^1)\right)^{-1} \\ \psi_2^3(s) = \frac{\beta}{\tau_3} \left(\tau_3 s^2 + (1 + h_3^2 + 2h_3^1 - \frac{2\tau_3}{\tau_2} h_2^0 - \frac{\tau_3}{\tau_2} h_2^1 + \frac{2(\tau_2 - \tau_3)}{\tau_2})s + b_3^2 + b_3^1 - \frac{2\tau_3}{\tau_2} b_2^0 - \frac{\tau_3}{\tau_2} b_2^1 + b_3^1\right) H_2^3(s) \end{cases}$$

For the pair (3,4):

$$\begin{cases}\Theta_3^4=\frac{2h_3^1}{\tau_3}+\frac{h_3^2}{\tau_3}-\frac{3(\tau_3-\tau_4)}{\tau_3\tau_4}\\ \Gamma_3^4=\frac{2b_3^1}{\tau_3}+\frac{b_3^2}{\tau_3}\\ H_3^4(s)=\tau_4\left(\tau_4s^3+(1+h_4^3)s^2+b_4^3s+k_4^3\right)^{-1}\\ \psi_3^4(s)=\frac{\beta}{\tau_4}\left(\tau_4s^2+(1+h_4^3-\frac{2\tau_4}{\tau_3}h_3^1-\frac{\tau_4}{\tau_3}h_3^2+\frac{3(\tau_3-\tau_4)}{\tau_3})s+b_4^3-\frac{2\tau_4}{\tau_3}b_3^1-\frac{\tau_4}{\tau_3}b_3^2\right)H_3^4(s)\end{cases}$$

Having the above calculations, we can form the vector $\mathbf{\Psi}(s)=[\psi_0^1(s);\psi_1^2(s);\psi_2^3(s);\psi_3^4(s)]$. Also, based on the equation (6.30) of the manuscript which is $\tilde{\mathbf{P}}(s)=\mathbf{Q}^{-1}(s)\mathbf{\Psi}(s)$, to have the vector $\tilde{\mathbf{P}}(s)=[\tilde{p}_0^1(s);\tilde{p}_1^2(s);\tilde{p}_2^3(s);\tilde{p}_3^4(s)]$, we need to find the matrix $\mathbf{Q}^{-1}(s)$ as well. Based on the equation (31) of the manuscript which is

$$Q_{(i+1)\kappa}(s)=\begin{cases}-\mathbf{K}_{i,i+1}^{\kappa}\mathbf{T}_1H_i^{i+1}(s) & \text{if } \ i+1>\kappa\\ 1 & \text{if } \ i+1=\kappa\\ 0 & \text{if } \ i+1<\kappa\end{cases}$$

where $i=0,\ldots,n-1$ and $\kappa=1,\ldots,n$, the matrix $\mathbf{Q}(s)$ can be obtained as

$$\mathbf{Q}(s)=\begin{bmatrix}Q_{11}&Q_{12}&Q_{13}&Q_{14}\\ Q_{21}&Q_{22}&Q_{23}&Q_{24}\\ Q_{31}&Q_{32}&Q_{33}&Q_{34}\\ Q_{41}&Q_{42}&Q_{43}&Q_{44}\end{bmatrix}=\begin{bmatrix}1&0&0&0\\ -\mathbf{K}_{1,2}^1\mathbf{T}_1H_1^2(s)&1&0&0\\ -\mathbf{K}_{2,3}^1\mathbf{T}_1H_2^3(s)&-\mathbf{K}_{2,3}^2\mathbf{T}_1H_2^3(s)&1&0\\ -\mathbf{K}_{3,4}^1\mathbf{T}_1H_3^4(s)&-\mathbf{K}_{3,4}^2\mathbf{T}_1H_3^4(s)&-\mathbf{K}_{3,4}^3\mathbf{T}_1H_3^4(s)&1\end{bmatrix}$$

in which $\mathbf{T}_1\triangleq[1;\ s;\ s^2]$, and based on (6.32), $\mathbf{K}_{i,i+1}^{\kappa}\triangleq\frac{1}{\tau_i}\sum_{j_\kappa}\mathbf{K}_i^j-\frac{1}{\tau_{i+1}}\sum_{j_\kappa^+}\mathbf{K}_{i+1}^j-\frac{1}{\tau_i}\boldsymbol{\tau}_i^{i+1}$, we have:

$$\begin{cases}\mathbf{K}_{1,2}^1=\frac{1}{\tau_1}\mathbf{K}_1^0-\frac{1}{\tau_2}\mathbf{K}_2^0-\frac{1}{\tau_1}\boldsymbol{\tau}_1^2\\ \mathbf{K}_{2,3}^1=\frac{1}{\tau_2}\mathbf{K}_2^0-\frac{1}{\tau_2}\boldsymbol{\tau}_2^3\\ \mathbf{K}_{2,3}^2=\frac{1}{\tau_2}(\mathbf{K}_2^1+\mathbf{K}_2^0)-\frac{1}{\tau_3}\mathbf{K}_3^1-\frac{1}{\tau_2}\boldsymbol{\tau}_2^3\\ \mathbf{K}_{3,4}^1=-\frac{1}{\tau_3}\boldsymbol{\tau}_3^4\\ \mathbf{K}_{3,4}^2=\frac{1}{\tau_3}\mathbf{K}_3^1-\frac{1}{\tau_3}\boldsymbol{\tau}_3^4\\ \mathbf{K}_{3,4}^3=\frac{1}{\tau_3}(\mathbf{K}_3^2+\mathbf{K}_3^1)-\frac{1}{\tau_3}\boldsymbol{\tau}_3^4\end{cases}$$

Finally, since $\bar{\mathbf{Q}}(s)\triangleq\mathbf{Q}^{-1}(s)$, we have $\tilde{\mathbf{P}}(s)=\bar{\mathbf{Q}}(s)\mathbf{\Psi}(s)$ or to be exact:

$$\tilde{\mathbf{P}}(s)=\begin{bmatrix}1&0&0&0\\ -Q_{21}&1&0&0\\ Q_{21}*Q_{32}-Q_{31}&-Q_{32}&1&0\\ -Q_{21}*Q_{32}*Q_{43}+Q_{21}*Q_{42}+Q_{31}*Q_{43}-Q_{41}&Q_{32}*Q_{43}-Q_{42}&-Q_{43}&1\end{bmatrix}\mathbf{\Psi}(s)$$

in which

$$\begin{bmatrix} 1 & 0 & 0 & 0 \\ -Q_{21} & 1 & 0 & 0 \\ Q_{21}*Q_{32}-Q_{31} & -Q_{32} & 1 & 0 \\ -Q_{21}*Q_{32}*Q_{43}+Q_{21}*Q_{42}+Q_{31}*Q_{43}-Q_{41} & Q_{32}*Q_{43}-Q_{42} & -Q_{43} & 1 \end{bmatrix} = \bar{\mathbf{Q}}(s)$$

Now, for simplicity, if we show $\bar{\mathbf{Q}}(s)$ as

$$\bar{\mathbf{Q}}(s) = \begin{bmatrix} 1 & 0 & 0 & 0 \\ \bar{Q}_{21} & 1 & 0 & 0 \\ \bar{Q}_{31} & \bar{Q}_{32} & 1 & 0 \\ \bar{Q}_{41} & \bar{Q}_{42} & \bar{Q}_{43} & 1 \end{bmatrix}$$

then using the relation obtained for $\tilde{\mathbf{P}}(s)$ above, we have

$$\begin{cases} \tilde{p}_0^1(s) = \psi_0^1(s) \\ \tilde{p}_1^2(s) = \bar{Q}_{21}\psi_0^1(s) + \psi_1^2(s) \\ \tilde{p}_2^3(s) = \bar{Q}_{31}\psi_0^1(s) + \bar{Q}_{32}\psi_1^2(s) + \psi_2^3(s) \\ \tilde{p}_3^4(s) = \bar{Q}_{41}\psi_0^1(s) + \bar{Q}_{42}\psi_1^2(s) + \bar{Q}_{43}\psi_2^3(s) + \psi_3^4(s) \end{cases} \tag{A.1}$$

which is exactly the relation (6.33) of the manuscript. Note that

$$\begin{cases} \bar{Q}_{21} = -Q_{21} \\ \bar{Q}_{31} = Q_{21}*Q_{32}-Q_{31} \\ \bar{Q}_{32} = -Q_{32} \\ \bar{Q}_{41} = -Q_{21}*Q_{32}*Q_{43}+Q_{21}*Q_{42}+Q_{31}*Q_{43}-Q_{41} \\ \bar{Q}_{42} = Q_{32}*Q_{43}-Q_{42} \\ \bar{Q}_{43} = -Q_{43} \end{cases}$$

The relation (A.1) shows the mapping in Laplace domain. Therefore, the relation in time-domain would be

$$\begin{cases} \tilde{p}_0^1(t) = \mathcal{L}^{-1}\{\psi_0^1(s)\} \\ \tilde{p}_1^2(t) = \mathcal{L}^{-1}\{\bar{Q}_{21}\psi_0^1(s) + \psi_1^2(s)\} \\ \tilde{p}_2^3(t) = \mathcal{L}^{-1}\{\bar{Q}_{31}\psi_0^1(s) + \bar{Q}_{32}\psi_1^2(s) + \psi_2^3(s)\} \\ \tilde{p}_3^4(s) = \mathcal{L}^{-1}\{\bar{Q}_{41}\psi_0^1(s) + \bar{Q}_{42}\psi_1^2(s) + \bar{Q}_{43}\psi_2^3(s) + \psi_3^4(s)\} \end{cases} \tag{A.2}$$

where $\mathcal{L}^{-1}$ signifies the inverse Laplace transform operator. Considering the relations we illustrated for $\tilde{p}_i^{i+1}(t)$; $i = 0, \ldots, 3$, in the following table the impact of control gains and other parameters on the stability and intervehicle distances for the platoon is shown.

Table A.1: The effect of control gains, initial conditions, and engine time constants on intervehicle distance (ID) errors. The symbol ✓implies that the corresponding parameter affects the ID error or platoon stability, and the symbol × indicates that the relevant parameter does not affect the ID error or platoon stability.

	$\mathbf{K}_1^0$	$\mathbf{K}_2^1$	$\mathbf{K}_2^0$	$\mathbf{K}_3^2$	$\mathbf{K}_3^1$	$\mathbf{K}_4^3$	τ_1	τ_2	τ_3	τ_4	β
$\tilde{p}_0^1(t)$	✓	×	×	×	×	×	✓	×	×	×	✓
$\tilde{p}_1^2(t)$	✓	✓	✓	×	×	×	✓	✓	×	×	✓
$\tilde{p}_2^3(t)$	✓	✓	✓	✓	✓	×	✓	✓	✓	×	✓
$\tilde{p}_3^4(t)$	✓	✓	✓	✓	✓	✓	✓	✓	✓	✓	✓
Platoon Stability	✓	✓	✓	✓	✓	✓	✓	✓	✓	✓	×

We observe that the initial conditions have an impact on safety and intervehicle distances, the initial conditions β affect all intervehicle distances. However, initial conditions do not affect the internal stability of the platoon which is affected by all control gains and vehicles' engine-time-constants. It is worth pointing out that the intervehicle distance between follower vehicles three and four is affected by all control gains, initial conditions, and vehicles' engine-time-constants.

Appendix B: Details on (4.6)

We present (B.1), which describes the dynamics of each follower vehicle as follows:

$$\dot{a}_{i+1} = -\frac{1}{\tau}a_{i+1} + \frac{1}{\tau}u_{i+1} \tag{B.1}$$

Here, $\dot{a}_{i+1} = \dddot{x}_{i+1}$ and $a_{i+1} = \ddot{x}_{i+1}$. Additionally, we introduce (B.2), defining desired states for each follower vehicle:

$$x^*_{i+1} \triangleq x_0 - \sum_{\kappa=0}^{i}(L_\kappa + d_\kappa^{\kappa+1}), \quad \dot{x}^*_{i+1} = v_0, \text{ and } \quad \ddot{x}^*_{i+1} = a_0 \tag{B.2}$$

Given (B.2), we can derive $\dddot{x}^*_{i+1} = \dot{a}_0$, where $\dot{a}_0$ represents the derivative of the acceleration of the leader vehicle. Consequently, we have $\dddot{x}_{i+1} = \dddot{\tilde{x}}_{i+1} + \dddot{x}^*_{i+1} = \dddot{\tilde{x}}_{i+1} + \dot{a}_0$ and $\ddot{x}_{i+1} = \ddot{\tilde{x}}_{i+1} + \ddot{x}^*_{i+1} = \ddot{\tilde{x}}_{i+1} + a_0$. We also describe the controller based on (B.3):

$$u_{i+1} = -\sum_{j\in\mathbb{I}_{i+1}} \mathbf{K}\tilde{\mathbf{X}}_{i+1} + \sum_{j\in\mathbb{I}_{i+1}} \mathbf{K}\tilde{\mathbf{X}}_j \tag{B.3}$$

Substituting (B.3) into (B.1) and utilizing the aforementioned facts; $\dddot{x}_{i+1} = \dddot{\tilde{x}}_{i+1} + \dot{a}_0$ and $\ddot{x}_{i+1} = \ddot{\tilde{x}}_{i+1} + a_0$, we obtain:

$$\dddot{\tilde{x}}_{i+1} + \dot{a}_0 = -\frac{1}{\tau}(\ddot{\tilde{x}}_{i+1} + a_0) - \frac{1}{\tau}\sum_{j\in\mathbb{I}_{i+1}} \mathbf{K}\widetilde{\mathbf{X}}_{i+1} + \frac{1}{\tau}\sum_{j\in\mathbb{I}_{i+1}} \mathbf{K}\widetilde{\mathbf{X}}_j$$

Notably, we express $\tilde{\mathbf{X}}_{i+1}$ as $\tilde{\mathbf{X}}_{i+1} \triangleq [\tilde{x}_{i+1};\ \dot{\tilde{x}}_{i+1};\ \ddot{\tilde{x}}_{i+1}]$. Consequently, we can rewrite $\ddot{\tilde{x}}_{i+1}$ as $\ddot{\tilde{x}}_{i+1} = [0, 0, 1]\tilde{\mathbf{X}}_{i+1}$. Substituting this into the previous equation, we arrive at:

$$\begin{aligned}\dddot{\widetilde{x}}_{i+1} &= -\frac{1}{\tau}[0,0,1]\widetilde{\mathbf{X}}_{i+1} - \frac{1}{\tau}\sum_{j\in\mathbb{I}_{i+1}}\mathbf{K}\tilde{\mathbf{X}}_{i+1} + \frac{1}{\tau}\sum_{j\in\mathbb{I}_{i+1}}\mathbf{K}\tilde{\mathbf{X}}_{j} - \frac{1}{\tau}a_0 - \dot{a}_0 \\ &= -\frac{1}{\tau}\mathbb{K}_{i+1}\tilde{\mathbf{X}}_{i+1} + \sum_{j\in\mathbb{I}_{i+1}}\frac{1}{\tau}\mathbf{K}\tilde{\mathbf{X}}_{j} + \epsilon_{i+1}\end{aligned}$$

This equation corresponds precisely to (4.6) in the manuscript where $\mathbb{K}_{i+1} \triangleq [\mathbf{k}_{i+1}, \mathbf{b}_{i+1}, 1 + \mathbf{h}_{i+1}]$ such that $\mathbf{k}_{i+1} = \sum_{j\in\mathbb{I}_{i+1}} k$, $\mathbf{b}_{i+1} = \sum_{j\in\mathbb{I}_{i+1}} b$, and $\mathbf{h}_{i+1} = 1 + \sum_{j\in\mathbb{I}_{i+1}} h$. Therefore, in case that $|\mathbb{I}_{i+1}| = 1$ then $\mathbb{K} = [k, b, 1 + h]$ which exhibits itself in (4.30) of the manuscript.